

051

[2005LEMA1099]

**A STUDY OF NON-CATALYTIC HYDROGENATION OF
NATURAL RUBBER**

JAREERAT SAMRAN

**A THESIS SUBMITTED IN PARTIAL FULFILLMENT
OF THE REQUIREMENTS FOR
THE DEGREE OF DOCTOR OF PHILOSOPHY
(POLYMER SCIENCE AND TECHNOLOGY)
FACULTY OF GRADUATE STUDIES
MAHIDOL UNIVERSITY
BANGKOK, THAILAND**

and

**LE GRADE DE DOCTEUR DE L'UNIVERSITÉ DU MAINE
FACULTÉ DES SCIENCES ET TECHNIQUES
(PHYSIQUE-SCIENCE DES MATERIAUX)
UNIVERSITÉ DU MAINE
LE MANS, FRANCE**

2005

**ISBN 974-04-6163-8
COPYRIGHT OF MAHIDOL UNIVERSITY**

BIBLIOTHEQUE UNIVERSITAIRE DU MANS



M049048



Thesis
Entitled

**A STUDY OF NON-CATALYTIC HYDROGENATION OF
NATURAL RUBBER**

Jareerat Samran

Miss Jareerat Samran
Candidate

Pranee Phinyocheep

Assoc.Prof.Pranee Phinyocheep
Doctorat de l'Université du Maine
Major-Advisor

Philippe Daniel

Prof.Philippe Daniel
Doctorat de l'Université du Maine
Co-Advisor

T. Amornsakchai

Assoc.Prof.Taweechai Amornsakchai
Ph.D.
Co-Advisor

Rassmidara Hoonsawat

Assoc.Prof.Rassmidara Hoonsawat
Ph.D.
Dean
Faculty of Graduate Studies

T. Amornsakchai


Assoc.Prof.Taweechai Amornsakchai
Ph.D.
Chair
Doctor of Philosophy Programme in
Polymer Science and Technology
Faculty of Science

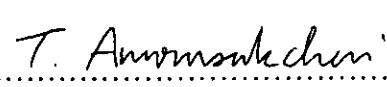


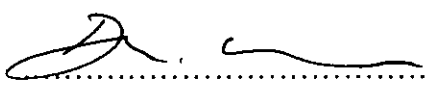
Thesis
Entitled

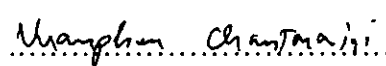
**A STUDY OF NON-CATALYTIC HYDROGENATION OF
NATURAL RUBBER**

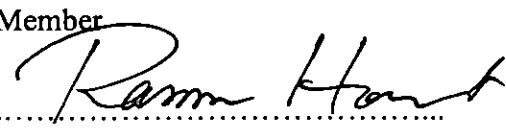
was submitted to the Faculty of Graduate Studies, Mahidol University,
Bangkok, Thailand
for the degree of Doctor of Philosophy (Polymer Science and Technology)
and
for Faculté des Sciences et Techniques, Université du Maine, le Mans, France
Le grade de Docteur de l' Université du Maine (Physique-Science des Matériaux)
on
May 25, 2005

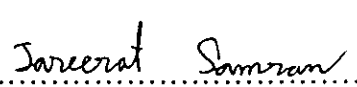

.....
Mr. Daniel Derouet,
Doctorat d'État
Member

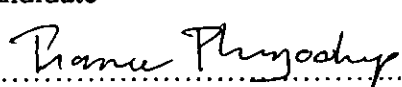

.....
Assoc.Prof.Tawechai Amornsakchai
Ph.D.
Member

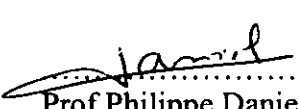

.....
Assoc.Prof.Dhirayos Wititsuwannakul
Ph.D.
Member



.....
Assoc.Prof.Nuanphun Chantarasiri
Ph.D.
Member

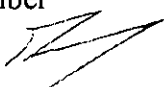

.....
Assoc.Prof.Rassmidara Hoonsawat
Ph.D.
Dean
Faculty of Graduate Studies
Mahidol University



.....
Miss Jareerat Samran
Candidate


.....
Assoc.Prof.Pranee Phinyocheep
Doctorat de l'Université du Maine
Chair


.....
Prof.Philippe Daniel
Doctorat de l'Université du Maine
Member


.....
Prof.Jean-Yves Buzaré
Doctorat d'État
Member


.....
Prof.Émeritus Jean-Claude Brosse
Doctorat d'État
Member


.....
Prof.Amaret Bhumiratana
Ph.D.
Dean
Faculty of Science
Mahidol University



ACKNOWLEDGEMENTS

The success of this challenge project can be attributed to valuable guidance and the warmest assistance of my great supervisor, Assoc.Prof.Pranee Phinyocheep. I equally express my sincere gratitude and great appreciation to my co-advisor, Prof.Philippe Daniel for his kind supervision and constructive guidance and also for his kindness in taking care during my stay at l'Université du Maine, France. I am extremely grateful to Assoc.Prof. Tawechai Amornsakchai for his kindness and advice for completion my thesis.

I feel deeply thank Prof.Jean-Yves Burazé and Dr. Daniel Derouet l'Université du Maine for their kind supervision, noteworthy guidance and helpful discussion. My appreciation is also given to Prof. Emeritus Jean Claude Brosse, l'Université du Maine for his powerful advice and providing suggestion for my research, and who was the external examiner of the thesis defense.

I would like to thank Assoc.Prof.Dhirayos Wititsuwannakul for his kindness providing fresh NR latex and suggestion and who was the external examiner of the thesis defense.

I am also gratefulness to Assoc.Prof.Nuanphun Chantarasiri, Faculty of Science, Chulalongkorn University for her kind's helpful suggestions and comments of completion of my thesis and who was the external examiner of the thesis defense.

I also would thank Prof. Jean L Leblanc for carrying out rheological measurement and suggestion for the discussion.

I gratefully acknowledge the University Development Committee Scholarship, Ministry of Education Thailand and the Université du Maine au Mans (Relations Internationales) France for providing me the scholarship and a marvelous opportunity to conduct my research at Université du Maine, France and for the expense of work presentation abroad.

I am thankful to the Department of Chemistry, Faculty of Science, Mahidol University, Laboratoire de Physique de l'Etat Condensé (UMR CNRS n° 6087) and LCOM-Chimie des Polymères (UMR CNRS UCO2M n° 6011) Université du Maine for the laboratory facilities.

I am also greatly indebted to all technicians in Department of Chemistry, Mahidol University for their assistance of analyzing the NMR, DSC and TGA.

Finally, I would like to thank Dr. Polphat Ruamcharoen, for the English grammar correction in this thesis and continuously valuable encouragement during my study.

Thanks also go to my gorgeous family especially for my lovely parents.



A STUDY OF NON-CATALYTIC HYDROGENATION OF NATURAL RUBBER

JAREERAT SAMRAN 4337511 SCPO/D

Ph.D.(POLYMER SCIENCE AND TECHNOLOGY)

THESIS ADVISORS: PRANEE PHINYOCHEEP, Doctorat de l'Université du Maine,
PHILIPPE DANIEL, Doctorat de l'Université du Maine, TAWEECHAI AMORNSAKCHAI,
Ph.D.**ABSTRACT**

Hydrogenation is one of the most efficient methods to alter and improve the physical properties of unsaturated polymers and to produce a new material. The aim of this research is to transform partially the unsaturated part of natural rubber (NR) into saturated moiety in order to improve its thermal and oxidative properties and to widen its area of applications. In this study, non-catalytic hydrogenation process was applied by using diimide generated *in situ* from two types of hydrogenating agent i.e. thermal decomposition of *p*-toluenesulfonylhydrazide (TSH) and oxidation of hydrazine (N_2H_4) by hydrogen peroxide (H_2O_2). The chemical structure of the hydrogenated rubbers was analyzed by vibrational and resonance spectroscopies i.e. FTIR, Raman, 1H - and ^{13}C -NMR.

First, the hydrogenation of NR and its modified form as epoxidized NR (ENR) was performed by using TSH in xylene solution at $135^\circ C$. The molar ratio of $[TSH]:[C=C]$ equal to 2 was used for hydrogenation of NR and four different types of ENR i.e. ENR-10, ENR-22, ENR-30 and ENR-40, containing 10, 22, 30 and 40% mole of epoxide content, respectively. The quantitative measurements on fraction of saturated units determined by Raman, 1H -NMR in liquid state and ^{13}C -NMR in solid state gave similar results which indicated that percent hydrogenation increased with increasing reaction time and about 80-89 % hydrogenation was obtained at 8h. While in the case of ENRs, the percent hydrogenation is approximately 93-98%. *Cis-trans* isomerization was also observed by 1H -NMR in liquid state and ^{13}C -NMR both in liquid and solid state. Some side reaction occurred i.e. chain degradation of both NR and ENRs which might be due to a relatively high temperature process. In the case of hydrogenation of ENRs, formation of furan structure and fixation of *p*-toluenesulfinic acid (TSOH) by-product were detected by FTIR.

For hydrogenation using (N_2H_4) and (H_2O_2), NR in the original form of latex was used. Various parameters affecting the hydrogenation reaction were investigated i.e. reaction time and temperature, amount of reactants, and dry rubber content. The hydrogenation progress could be monitored by means of NMR in liquid state as function of reaction condition. The results indicated that the best result was obtained when equimolar ratio of (N_2H_4) and (H_2O_2) was used. With addition of varying hydrazine and hydrogen peroxide contents, the best condition of diimide reduction is achieved when their content is 1.5 times the amount $C=C$ of the rubber.

Molecular characteristics in the NR, ENR-10 and the hydrogenated rubbers were investigated by Raman and ^{13}C -NMR in solid state techniques. The relative variation force constant as analyzed by Raman spectroscopy tends to increase with the hydrogenation level. It might be suggested that the higher stiffness of the rubber chains upon hydrogenation is correlated to the increased relative variation force constants. In cross-polarization (CP) experiment of HNR and HENR, it was found that the rate of cross polarization of methyl carbon in HENR-30(8) is highest with respect to methyl carbon in HNR(8) and HENR-10(8). It is clear that the methyl carbon of HENR-30(8) has the least mobility due to more furan units and chemical fixation of TSOH on the rubber chains.

Thermal properties studied by a differential scanning calorimetry revealed thermal improvement after hydrogenation, both in solution and in aqueous systems. Comparison of the thermal stability using thermogravimetric analyzer, under air and nitrogen atmosphere, showed the decomposition temperature of HNR in air is lower than that in nitrogen atmosphere. The thermal stability of ENR was also enhanced after hydrogenation. Rheological properties of HNR samples measured using RPA rheometer exhibited the storage and loss moduli of HNR97 sample with the highest value compared to HNR38 and HNR69 samples. For instance, the fully hydrogenated NR has a significant increment in the loss and storage moduli of the samples. By using Raman mapping technique, it revealed that the hydrogenation of NR is a random process at the micron level.

KEY WORDS: NATURAL RUBBER / NON-CATALYTIC HYDROGENATION /
DIIMIDE MOLECULE / HYDROGENATED RUBBER

288 P. ISBN 974-04-6163-8



CONTRIBUTION A L'ETUDE DE L'HYDROGENATION DU CAOUTCHOUC NATUREL PAR VOIE NON CATALYTIQUE

JAREERAT SAMRAN 4337511 SCPO/D

Ph.D.(POLYMER SCIENCE AND TECHNOLOGY)

THESIS ADVISORS: PRANEE PHINYOCHEEP, Doctorat de l'Université du Maine,
PHILIPPE DANIEL, Doctorat de l'Université du Maine, TAWEECHAI AMORNSAKCHAI,
Ph.D.**RÉSUMÉ**

Cette étude aborde l'hydrogénation du caoutchouc naturel dans un but de développement et de valorisation de cette substance largement produite dans le sud-est asiatique et en particulier en Thaïlande. En effet, ce composé est un polymère insaturé bien connu, possédant d'excellentes propriétés élastiques, mais sa résistance en température est nettement inférieure aux élastomères synthétiques. Dans ce travail, l'hydrogénation a été menée par voie non catalytique, en utilisant un agent intermédiaire de type diimide généré in-situ à partir de deux types de composés, à savoir i) la décomposition thermique du p-toluensulfonnylhydrazide (TSH) ainsi que ii) la réaction de l'hydrazine (N_2H_4) et l'hydroperoxyde (H_2O_2) en présence d'un catalyseur. La structure des caoutchoucs hydrogénés a été analysée par différentes méthodes spectroscopiques : absorption infrarouge, diffusion Raman, RMN en phase liquide et solide.

L'hydrogénation du caoutchouc naturel et de sa forme époxyde a été réalisée à l'aide de TSH dans une solution de xylène à $135^\circ C$. Un ratio molaire [TSH] : [C=C] de 2 a été choisi pour l'hydrogénation du caoutchouc naturel et de 4 formes époxydes contenant respectivement 10, 22, 30 et 40% d'époxyde. Les mesures quantitatives menées par les différentes techniques spectroscopiques sont toutes concordantes et indiquent une augmentation du taux d'hydrogénation avec le temps de réaction pour atteindre des valeurs limites proches de 90% pour un temps de réaction égal à 8h. L'isomérisation *cis-trans* a été observée par RMN en phase liquide et solide. En outre des réactions secondaires peuvent apparaître, dues aux températures élevées des protocoles utilisés.

Dans le cas de l'utilisation de N_2H_4 et de H_2O_2 , l'hydrogénation a été réalisée directement sur la forme latex du caoutchouc naturel, avec étude de l'influence de divers paramètres : temps de réaction, température, taux des réactifs. Le suivi du taux d'hydrogénation par RMN liquide montre que les meilleurs résultats sont obtenus pour des rapports équimolaires de N_2H_4 et de H_2O_2 .

Les caractéristiques moléculaires du caoutchouc naturel, de la forme époxyde à 10% et des différents composés hydrogénés a été complètement étudiée par diffusion Raman et RMN du carbone ^{13}C . La diffusion Raman montre l'augmentation de la constante de force associée à la double liaison C=C en fonction du taux d'hydrogénation, qu'il est possible d'associer à un accroissement de la rigidité de la structure d'ensemble.

L'étude thermique effectuée par DSC révèle une amélioration des propriétés des échantillons après hydrogénation tant en solution que pour les systèmes en phase aqueuse. La comparaison des propriétés de stabilité thermique des caoutchoucs naturels hydrogénés, par analyse thermogravimétrique, sous air ou sous atmosphère d'azote montre que la décomposition en température est plus faible sous air. De même les propriétés thermiques des formes époxydes ont été améliorées après hydrogénation. L'ensemble des matériaux a également fait l'objet d'une étude rhéologique complète. Enfin la technique d'imagerie Raman révèle que l'hydrogénation est un processus aléatoire au moins à l'échelle micrométrique.

288 P. ISBN 974-04-6163-8



การศึกษาปฏิกิริยาการเติมไฮโดรเจนแบบไม่ใช้ตัวเร่งบนโมเลกุลยางธรรมชาติ (A STUDY OF NON-CATALYTIC HYDROGENATION OF NATURAL RUBBER)

จรรยาวัจน์ สาราญ 4337511 SCPO/D

ปร.ค. (วิทยาศาสตร์และเทคโนโลยีพอลิเมอร์)

คณะกรรมการควบคุมวิทยานิพนธ์ : ปรานี ภิญญูชีพ Doctorat de l'Université du Maine, PHILIPPE DANIEL, Doctorat de l'Université du Maine, ทวีชัย อมรศักดิ์ชัย, Ph.D.

บทคัดย่อ

ปฏิกิริยาการเติมไฮโดรเจนเป็นวิธีทางเคมีที่มีประสิทธิภาพมาก ในการเปลี่ยนและปรับปรุงสมบัติทางกายภาพของพอลิเมอร์ชนิดไม่อิ่มตัวและเพื่อผลิตวัสดุพอลิเมอร์ชนิดใหม่ เป้าหมายของงานวิจัยนี้เพื่อเปลี่ยนยางธรรมชาติที่ไม่อิ่มตัวไปเป็นยางที่อิ่มตัวบางส่วน เพื่อปรับปรุงสมบัติทางความร้อนและทนการเกิดปฏิกิริยาออกซิเดชันสำหรับเพิ่มการนำไปใช้งานให้มากขึ้น ในการศึกษากระบวนการเติมไฮโดรเจนแบบไม่ใช้ตัวเร่งได้นำมาประยุกต์ใช้กับยางธรรมชาติ โดยใช้ไดออกไซด์ซึ่งได้มาจากสารตั้งต้น 2 ชนิด คือจากปฏิกิริยาการสลายตัวของความร้อนของพาราโทลูอินซิลฟีนีลไฮดรอกไซด์ (TSH) และปฏิกิริยาออกซิเดชันของไฮโดรคาร์บอนด้วยไฮโดรเจนเปอร์ออกไซด์ โครงสร้างทางเคมีของยางไฮโดรจิเนต ได้วิเคราะห์โดยใช้เทคนิคที่เกี่ยวข้องกับการสั่นและเรโซแนนซ์สเปกโตรสโกปี ซึ่งได้แก่ อินฟราเรดสเปกโตรสโกปี (FTIR) รามาน (Raman) นิวเคลียร์แมกเนติกเรโซแนนซ์ (^1H และ ^{13}C -NMR)

ในส่วนแรก ได้ศึกษาปฏิกิริยาการเติมไฮโดรเจนของยางธรรมชาติและยางธรรมชาติอีพอกซีไดซ์ โดยใช้ TSH ในไซลีน (xylene) ที่ 135°C อัตราส่วนโดยโมลของ TSH ต่อปริมาณพันธะคู่เท่ากับ 2 ในกรณียางธรรมชาติอีพอกซีไดซ์ ได้ทำการศึกษาเกี่ยวกับตัวอย่าง 4 ชนิด ที่มีปริมาณร้อยละโดยโมลของหมู่เอพอกไซด์เป็น 10, 22, 30 และ 40 ในการวิเคราะห์ปริมาณของสัดส่วนที่ถูกไฮโดรจิเนตทำโดยเทคนิค Raman ^1H -NMR ในสภาวะสารละลาย และ ^{13}C -NMR ในสภาวะของแข็ง ทั้งสามเทคนิคให้ผลการทดลองในลักษณะคล้ายคลึงกัน ซึ่งบ่งบอกถึงเปอร์เซ็นต์การเติมไฮโดรเจนที่เพิ่มขึ้นกับเวลาในการทำปฏิกิริยา พบว่าที่ 8 ชั่วโมง ได้ประมาณ 80-89% ส่วนกรณียางธรรมชาติอีพอกซีไดซ์ พบว่าเปอร์เซ็นต์การเติมไฮโดรเจนได้ประมาณ 93-98 จากการศึกษา ^1H -NMR ในสภาวะของเหลวและ ^{13}C -NMR ทั้งในสภาวะของเหลวและของแข็งพบหลักฐานของการเกิดปฏิกิริยา ซิส-ทรานส์ ไอโซเมอร์ไรเซชัน และปฏิกิริยาข้างเคียง เช่น การแตกสลายของโมเลกุลทั้งในยางธรรมชาติและยางธรรมชาติอีพอกซีไดซ์ ทั้งนี้อาจเนื่องมาจากการทำปฏิกิริยาที่อุณหภูมิสูง นอกจากนั้นเทคนิค FTIR ได้แสดงให้เห็นว่า มี โครงสร้างของฟิวเรน และ การติดเพิ่มของ กรด พาราโทลูอินซิลฟีนิก (TSOH) บนสายโซ่ของยางธรรมชาติอีพอกซีไดซ์ (ENR)

ยางธรรมชาติในรูปของน้ำยางได้ถูกนำมาใช้สำหรับการเติมไฮโดรเจนโดยใช้ไฮโดรคาร์บอนและไฮโดรเจนเปอร์ออกไซด์ ปัจจัยที่มีผลต่อปฏิกิริยาการเติมไฮโดรเจนซึ่งได้แก่ ระยะเวลาในการทำปฏิกิริยา อุณหภูมิ ปริมาณของสารตั้งต้น และปริมาณเนื้อยางได้ถูกศึกษา โดยใช้เทคนิค NMR สภาวะของเหลวในการติดตามปฏิกิริยาการเติมไฮโดรเจนเป็นฟังก์ชันกับสภาวะของการเกิดปฏิกิริยา และพบว่าการใช้สัดส่วนของไฮโดรคาร์บอนและไฮโดรเจนเปอร์ออกไซด์ในปริมาณที่เท่ากันจะให้ผลการทดลองที่ดีที่สุด และจากการแปรสัดส่วนของปริมาณไฮโดรคาร์บอนและไฮโดรเจนเปอร์ออกไซด์พบว่าสภาวะที่ดีที่สุดของปฏิกิริยาการเติมไฮโดรเจน ได้แก่การใช้ไฮโดรคาร์บอนและไฮโดรเจนเปอร์ออกไซด์เป็น 1.5 เท่าของปริมาณพันธะคู่ของยางธรรมชาติ

ลักษณะเฉพาะโมเลกุลของยางธรรมชาติ ยางอีพอกซีไดซ์ซึ่งมีปริมาณ 10%(ENR-10)และยางไฮโดรจิเนตได้ถูกตรวจสอบโดยใช้เทคนิค Raman และ ^{13}C -NMR ในสภาวะของแข็ง ค่าความผันแปรของแรง (variation force constant) ซึ่งได้จากเทคนิค Raman นั้น เพิ่มขึ้นเมื่อปริมาณการเติมไฮโดรเจนเพิ่มขึ้น ซึ่งจากการทดลองนี้ สามารถบอกได้ว่ายางไฮโดรจิเนตมีความแข็งแรงเพิ่มขึ้นเนื่องจาก ค่าความผันแปรของแรงเพิ่มขึ้น

สำหรับการทดลองของ cross polarization (CP) ใน ^{13}C -NMR พบว่าอัตราของ cross polarization ของหมู่เมทิลใน HENR-30 นั้นสูงที่สุดเมื่อเทียบกับคาร์บอนของเมทิลใน HNR(8) และ HENR-10(8) จะสามารถเห็นได้อย่างชัดเจนว่าคาร์บอนของหมู่เมทิลของ HENR-30(8) นั้นมีการเคลื่อนไหวได้น้อยที่สุดเนื่องจากมี หมู่ฟิวเรนและการยึดติดของ TSOH บนสายโซ่ของยางมากกว่ายางธรรมชาติ

ในการศึกษาสมบัติทางความร้อน โดยใช้เทคนิค DSC พบว่าเพิ่มขึ้นหลังปฏิกิริยาการเติมไฮโดรเจนทั้งในสภาวะสารละลายและในน้ำ และ ในการใช้เทคนิค TGA พบว่าความเสถียรต่อความร้อนของยางธรรมชาติ ภายใต้บรรยากาศของไนโตรเจนดีกว่าภายใต้อากาศ ส่วนยางอีพอกซีไดซ์ความเสถียรต่อความร้อนนั้นเพิ่มขึ้นหลังจากผ่านกระบวนการเกิดปฏิกิริยาการเติมไฮโดรเจนแล้ว ในส่วนของสมบัติการไหลของยางไฮโดรจิเนต ได้ศึกษาโดยใช้เครื่อง RPA พบว่าค่า storage และ loss modulus ของ ยางไฮโดรจิเนต ที่ 97% มีค่าสูงกว่าที่ 38%และ 69% ในการใช้เทคนิค Raman mapping พบว่าปฏิกิริยาการเติมไฮโดรเจนของยางธรรมชาตินั้นเป็นกระบวนการแบบสุ่มในระดับโมโครน



CONTENTS

	Page
ACKNOWLEDGEMENT	iii
ABSTRACT (in English)	iv
ABSTRACT (in French)	v
ABSTRACT (in Thai)	vi
LIST OF TABLES	xii
LIST OF FIGURES	xvii
LIST OF ABBREVIATIONS	xxviii
PUBLICATIONS	xxx
CHAPTER	
1 INTRODUCTION	1
2 OBJECTIVES	5
3 LITERATURE REVIEW	7
3.1 General Description of Natural Rubber	7
3.1.1 Natural Rubber Latex.....	7
3.1.2 Manufacturing of NR Latex	11
3.2 Chemical Modification of Natural Rubber	12
3.2.1 Bond Rearrangement Reaction.....	12
3.2.2 Attachment of Pendant Groups.....	15
3.2.3 Graft Copolymer.....	18
3.2.4 Degradation Reaction.....	18
3.3 Hydrogenation Method.....	19
3.3.1 Catalytic Hydrogenation.....	19
3.3.2 Non-Catalytic Hydrogenation.....	21
3.3.2.1 Diimide Reduction in Organic System.....	22
3.3.2.2 Diimide Reduction in Aqueous System.....	25
3.4 Principle of Methods for Characterization.....	



CONTENTS (continued)

	Page
3.4.1 Vibrational Spectroscopy.....	28
3.4.1.1 Classical Electromagnetism Theory of Vibration Spectroscopy	29
3.4.1.2 Experimental Analysis of Infrared and Raman Spectroscopy.....	34
3.4.2 Nuclear Magnetic Resonance Spectroscopy.....	38
3.4.2.1 Theoretical Analysis	38
3.4.2.2 Experimental Analysis	40
3.4.3 Mathematical Techniques for Processing Spectra....	48
3.5 Thermal Analysis.....	50
3.5.1 Differential Scanning Calorimetry (DSC)	50
3.5.2 Thermal Gravimetric Analysis (TGA).....	53
3.6 Rheology Behavior.....	55
3.6.1 Theoretical Analysis of Rheological Behavior	55
3.6.2 Measurement of Rheological Properties.....	56
3.6.3 Basic Principle of Fourier Transform Rheology.....	58
3.6.4 Factors Affecting the Rheological Properties.....	59
3.6.5 Rheological Properties of Hydrogenated Rubbers....	61
4 MATERIALS AND METHODS.....	63
4.1 Materials.....	63
4.2 Instruments.....	64
4.3 Experiment Flow Chart.....	65
4.4 Hydrogenation of Unsaturated Units by <i>p</i> -Toluenesulfo- nylhydrazide (TSH).....	66
4.4.1 Hydrogenation of Model Molecule.....	66
4.4.2 Hydrogenation of NR and ENRs.....	66
4.5 Hydrogenation of Unsaturated Units by Hydrazine and Hydrogen Peroxide.....	67
4.5.1 Hydrogenation of Synthetic Polyisoprene (PI) latex..	67



CONTENTS (continued)

	Page
4.5.2 Hydrogenation of Natural Rubber (NR) Latex...	68
4.6 Chemical Structure Characterization.....	71
4.6.1 FT-IR Spectroscopy.....	71
4.6.2 Raman Spectroscopy.....	71
4.6.3 NMR Spectroscopy in Solution.....	73
4.6.4 NMR Spectroscopy in Solid State.....	73
4.7 Evaluation of the Microstructure.....	74
4.7.1 Determination of Percentage of <i>Cis</i> and <i>Trans</i> Microstructures.....	74
4.7.2 Determination of Epoxidation Level.....	76
4.7.3 Determination of Percentage of Hydrogenation	77
4.8 Average Molar Mass and Particle Size Measurement.....	81
4.8.1 Dilute Solution Viscosity Measurement.....	81
4.8.2 Particle Size Analysis.....	82
4.9 Thermal Analysis.....	82
4.9.1 Raman Spectroscopy.....	82
4.9.2 Differential Scanning Calorimetry (DSC).....	83
4.9.3 Thermalgravimetric Analysis (TGA).....	83
4.10 Rheological Measurement.....	84
5 RESULTS AND DISCUSSION.....	85
Part I: Hydrogenation by <i>p</i> -Toluenesulfonylhydrazide (TSH)..	86
5.1 Hydrogenation of 4-Methyl-4-octene.....	86
5.1.1 Structural Analysis.....	87
5.1.2 Evolution of Microstructures and Hydrogenation....	92
5.1.3 Side Reaction.....	95
5.2 Hydrogenation of NR.....	96
5.2.1 Microstructure Analysis of NR and Hydrogenated NR.....	96



CONTENTS (continued)

	Page
5.2.2 Evaluation of Percent Hydrogenation of NR.....	120
5.2.3 Side Reactions.....	126
5.3 Hydrogenation of ENR.....	131
5.3.1 Structural Analysis of ENR and Hydrogenated ENR	131
5.3.2 Evaluation of Percent Hydrogenation of ENR.....	145
5.3.3 Side Reactions.....	150
Part II: Hydrogenation by Hydrazine and Hydrogen Peroxide..	153
5.4 Hydrogenation of Synthetic Polyisoprene (PI) latex.....	153
5.4.1 Evidence of Diimide Hydrogenation of Polyisoprene	154
5.4.2 Percentage of Hydrogenation and Microstructures	158
5.4.3 Proposed Reaction Mechanism.....	160
5.4.4 Side Reaction.....	161
5.5 Hydrogenation of NR in Latex form.....	161
5.5.1 Evidence of Hydrogenation of NR	163
5.5.2 Parameters Affecting on Hydrogenation Reaction....	165
5.5.3 Side Reactions.....	191
5.5.4 Kinetic Study of Diimide Hydrogenation of NR Latex.....	193
Part III: Molecular Characteristic and Physical Properties of Hydrogenated NR.....	196
5.6 Molecular Dynamic Characteristic Analysis.....	196
5.6.1 By Raman Spectroscopy.....	196
5.6.2 By Solid State NMR Spectroscopy.....	203
5.7 Thermal Behaviors.....	225
5.7.1 By Raman Spectroscopy.....	225
5.7.2 By Differential Scanning Calorimetry (DSC).....	232
5.7.2.1 Effect of Scanning Rate on the Thermal Transition of NR and HNR Samples.....	



CONTENTS (continued)

	Page
5.7.2.2 Effect of Hydrogenation Content on Thermal Transition.....	234
5.7.3 By Thermal Gravimetric Analysis (TGA).....	239
5.7.3.1 Thermal Stability of Hydrogenated NR Carried out in Organic Media.....	239
5.7.3.2 Thermal Stability of HNR Carried out in Latex Form.....	244
5.7.3.3 Thermal stability of ENR and HENR.....	245
5.8 Rheological Properties.....	250
5.8.1 Results on HNR Samples Using RPA.....	250
5.8.2 Results on HNR Samples Using Fourier Transform	256
Rheometry.....	
5.9 Correlation of the Molecular Characteristic with Physical Properties of NR, ENR and their Hydrogenated Samples.	261
5.10 Raman Microscopic Study of the Homogeneties of the Hydrogenated Rubbers.....	265
6 CONCLUSIONS.....	269
REFERENCES.....	274
APPENDIX	283
BIOGRAPHY.....	290



LIST OF TABLES

Table		Page
3.1	Typical composition of fresh natural rubber latex.....	8
4.1	Instruments used in the experiment for characterization	64
4.2	Reaction conditions used for the preparation of hydrogenated rubbers in organic media.....	67
4.3	Recipe used for the hydrogenation of PI latex.....	68
4.4	Various conditions used for the hydrogenation of NR in latex (20% DRC) at 60°C, using CuSO ₄ .5H ₂ O as a catalyst.....	69
4.5	Various reaction temperatures and dry rubber contents used for the hydrogenation of NR latex.....	69
4.6	Various amount of reagents used for the hydrogenation of NR latex (20%DRC) at 60°C.....	70
4.7	Various types of NR latex used in the hydrogenation reaction at 60°C.....	70
4.8	RPA test conditions and protocols.....	84
5.1	The assignment of proton and carbon signals of 4-methyl-4-octene (MO).....	90
5.2	Influence of the reaction time on the hydrogenation of MO.....	93
5.3	Character table of point group C _s	98
5.4	Wavenumber (cm ⁻¹) and assignment of bands observed in Infrared and Raman spectra of NR	102
5.5	Wavenumber (cm ⁻¹) and assignment of bands observed in Infrared and Raman spectra of hydrogenated NR	106



LIST OF TABLES (continued)

Table		Page
5.6	The assignment of Raman spectrum of TSH	108
5.7	The assignment of ^1H - and ^{13}C -NMR resonances of NR spectra in liquid state.....	112
5.8	The assignment of ^1H - and ^{13}C -NMR resonances of the hydrogenated NR in liquid state.....	112
5.9	The assignment of carbon positions of 2,6,10,15,19,23-hexamethyltetracosane obtained from NMR software	115
5.10	The results of chemical shift, peak widths and areas obtained from resolving ^{13}C -NMR spectrum of NR in solid state	119
5.11	The results of chemical shift, peak widths and areas obtained from resolving ^{13}C -NMR spectrum of HNR in solid state.....	119
5.12	The percent hydrogenation of NR at various reaction times as determined by Raman, ^1H -NMR and ^{13}C -NMR	124
5.13	The percent hydrogenation of NR and DPNR at various reaction times as determined by ^1H -NMR.....	125
5.14	The percent of <i>cis</i> and <i>trans</i> isomers of HNR as determined by ^1H -NMR in liquid state and ^{13}C -NMR in solid state	127
5.15	Intrinsic viscosity data at different hydrogenation levels.....	130
5.16	The assignment of vibration modes of Infrared and Raman spectra of ENR and the hydrogenated ENR.....	135
5.17	The assignment of ^1H - and ^{13}C -NMR resonances of the partially epoxidizedNR.....	138
5.18	The assignment of ^1H -NMR and ^{13}C -NMR resonance of the hydrogenated ENR in liquid state.....	141
5.19	The assignment of chemical shift of ENR and HENR spectra of HD/MAS technique in solid state	144
5.20	The percent hydrogenation of ENRs at various reaction times as determined by Raman and ^1H -NMR techniques	



LIST OF TABLES (continued)

Table		Page
5.21	The amount of hydrogenation content, residual 1,4-PI and 3,4-PI determined by ¹ H-NMR.....	159
5.22	Hydrogenation level taken place without and with CuSO ₄ .5H ₂ O and surfactant.....	170
5.23	Effect of amount of CuSO ₄ .5H ₂ O on the percent hydrogenation of NR	172
5.24	The percent hydrogenation of NR latex at various reaction times and temperatures as determined by ¹ H-NMR.....	176
5.25	The percentage of <i>cis</i> and <i>trans</i> -polyisoprene units determined by ¹ H-NMR obtained during hydrogenation reaction at various temperatures.....	178
5.26	Influence dry rubber contents on the hydrogenation of NR in latex phase using molar ratio of [C=C]:[N ₂ H ₄]:[H ₂ O ₂] = 1:1:1 at 60°C	179
5.27	Influence of amount of hydrazine on the degree of hydrogenation in NR latex molar ratio of [C=C]:[H ₂ O ₂] = 1 at 60°C.....	182
5.28	Influence of amount of hydrogen peroxide on the degree of hydrogenation in NR latex using molar ratio of [C=C]:[N ₂ H ₄] = 1 at 60°C	184
5.29	Effect of the molar ratio of [N ₂ H ₄]:[C=C] on the percent hydrogenation at 60°C by keeping the equal molar ratio of [N ₂ H ₄] and [H ₂ O ₂].....	186
5.30	Results of percent hydrogenation of different types of NR latex obtained at various reaction times using molar ratio of [C=C]:[N ₂ H ₄]:[H ₂ O ₂] = 1:1:1 at 60°C.....	189
5.31	Average particle size of NR latex at various types.....	190
5.32	The percent gel content of the hydrogenated products obtained from various reaction temperatures.....	192



LIST OF TABLES (continued)

Table		Page
5.33	The rate constant (k) and $\ln k$ of hydrogenation reaction at different temperatures.....	194
5.34	Raman shift, square of wavenumber ($\bar{\nu}^2$), estimated force constant ($\approx k_f$) and relative variation force constant (Δk_f) of the characteristic peak of C=C stretching mode of the HNRs at various hydrogenation levels.....	200
5.35	Raman shift, square of wavenumber ($\bar{\nu}^2$), estimated force constant ($\approx k_f$) and relative variation force constant (Δk_f) of the characteristic peak of C=C stretching mode of the HENR-10.....	202
5.36	The line widths of NMR peaks of hydrogenated rubber at various hydrogenation levels	206
5.37	The spin-lattice relaxation time ($T_{1\rho}^H$) and cross-polarized time (T_{CH}) obtained from the fitting kinetic CP curve in all carbon resonances of HNR (85%).....	211
5.38	The line widths of the NMR lines at 60 and 64 ppm in ENR with various epoxidation levels.....	214
5.39	The spin-lattice relaxation time ($T_{1\rho}^H$) and cross-polarized time (T_{CH}) obtained from the simulation of kinetic CP curve of carbon signal of HENR-10(8).....	220
5.40	The spin-lattice relaxation time ($T_{1\rho}^H$) and and cross-polarized time (TCH) obtained from the simulation of kinetic CP curve of carbon signal of HENR-30(8).....	223
5.41	Effect of scanning rate on the onset temperature and glass transition temperature of NR, HNR38 and HNR97.....	233



LIST OF TABLES (continued)

Table		Page
5.42	Glass transition temperature values of NR and the HNR obtained at different percent hydrogenations with scanning rate 20°C/min.....	235
5.43	Glass transition temperature values of ENR containing various epoxide contents and HENR obtained at 8 h of reaction time	237
5.44	The results of TGA of NR and their hydrogenated rubbers under air atmosphere.....	243
5.45	The results of TGA of NR and their hydrogenated rubbers under nitrogen atmosphere.....	243
5.46	The results of TGA of NR and their hydrogenated rubbers prepared in latex stage under nitrogen atmosphere.....	245
5.47	The results of TGA of ENR-10 and their hydrogenated rubbers obtained at various reaction times under nitrogen atmosphere.....	246
5.48	Results of TGA of ENR and their hydrogenated rubbers obtained at 8 h of reaction time in N ₂ atmosphere	249
5.49	Effect of strain amplitude on third harmonic component; fit parameters obtained by sigmoidal model	259
5.50	Correlation between relative variation force constant, glass transition (T _g) and maximum degradation temperatures (T ^P ₂) of the HNR at various hydrogenation level.....	262
5.51	Correlation between relative variation force constant and maximum degradation temperatures of the HENR-10 at various hydrogenation levels	262
5.52	Correlation between line widths, glass transition temperature and hydrogenation level.....	263
5.53	Correlation between line widths and glass transition temperature of the ENR at different epoxidation levels	264



LIST OF FIGURES

Figure		Page
3.1	Three major zones of fresh NR latex obtained by using ultracentrifugation.....	8
3.2	<i>Cis-trans</i> isomerization of NR by sulfur dioxide	13
3.3	Cyclization of NR via the carbonium ion mechanism forming monocyclic (I), bicyclic (II) and tricyclic (III) structures	14
3.4	Hydrochlorination reaction of NR.....	15
3.5	Mechanism of ene reaction.....	16
3.6	Maleation reaction of NR by ene reaction.....	16
3.7	Epoxidation reaction of NR by peracid.....	17
3.8	Graft copolymerization of NR.....	18
3.9	Decomposition of <i>p</i> -toluenesulfonylhydrazide (TSH) by thermal treatment	22
3.10	<i>Syn</i> -addition of hydrogen molecule of diimide onto the carbon - carbon double bond of unsaturated unit	22
3.11	The energy levels of elastic (Rayleigh) and inelastic (Raman) scattering lines.....	31
3.12	Quantized energy of nuclei in a magnetic field.....	39
3.13	Chemical shift anisotropy patterns for (a) axially symmetric and (b) nonaxially symmetric atoms.....	43
3.14	Macroscopic sample rotation at an angle to the applied magnetic field B_0	44
3.15	Pulse sequence diagram for cross-polarization.....	46
3.16	Typical DSC thermogram.....	52
3.17	Typical ITGA thermogram.....	54
3.18	RPA dynamic torsional rheometer and testing principle	57



LIST OF FIGURES (continued)

Figure		Page
3.19	Complex torque (S^*), elastic torque (S') and viscous torque (S'') responses from a sinusoidal strain.....	58
4.1	Flow chart of hydrogenation of NR and ENRs in this research.....	65
4.2	Picture of Raman spectrometer	72
4.3	Schematic diagram for performing Raman mapping.....	73
4.4	Picture of Solid state NMR spectrometer.....	74
4.5	Typical curve fitting of solid state ^{13}C -NMR spectrum of hydrogenated NR (pseudo voigt line shape).....	76
4.6	Typical curve fitting of Raman spectrum of natural rubber (Lorentzian shape).....	80
5.1	The decomposition of <i>p</i> -toluenesulfonylhydrazide (TSH) by thermal treatment at 135°C and disproportionation of diimide intermediate.....	86
5.2	^1H -NMR (a) and ^{13}C -NMR (b) spectra of 4-methyl-4-octene (MO).....	89
5.3	^1H -NMR (a) and ^{13}C -NMR (b) spectra of the hydrogenated MO obtained at 24 h of reaction time.....	91
5.4	HPLC chromatogram of hydrogenated MO obtained at 4h of reaction time.....	92
5.5	The percent microstructures of MO as function of reaction time; <i>cis</i> (■), <i>trans</i> (□) and hydrogenation (●).....	93
5.6	Hydrogenation of MO in <i>cis</i> (upper) and <i>trans</i> (lower) units	94
5.7	Schematic representation of the addition of <i>p</i> -toluenesulfinic acid, followed by hydrolysis.....	95
5.8	The addition of hydrogen molecule from diimide onto double bond of <i>cis</i> -1,4 polyisoprene units.....	96
5.9	Infrared (a) and Raman (b) spectra of NR.....	101



LIST OF FIGURES (continued)

Figure		Page
5.10	Infrared (a) and Raman (b) spectra of hydrogenated rubber obtained at 8 h of reaction time.....	105
5.11	Raman spectrum of <i>p</i> -toluenesulfonylhydrazide (TSH).....	108
5.12	¹ H-NMR (a) and ¹³ C-NMR (b) spectra of NR in liquid state.....	111
5.13	¹ H-NMR (a) and ¹³ C-NMR (b) spectra of the hydrogenated NR in liquid state after 8h of reaction time.....	113
5.14	¹ H-NMR spectrum of 2,6,10,15,19,23-hexamethyltetracosane (C ₃₀ H ₆₂).....	114
5.15	¹³ C-NMR solid state spectra of NR (a) and the hydrogenated NR after 8h of the hydrogenation (b).....	118
5.16	Comparison between the Raman spectra of NR and hydrogenated NR samples taken at reaction time 4 and 8h.....	121
5.17	¹ H-NMR spectra of NR and hydrogenated NR samples taken at 4 and 8h analyzed in liquid state.....	122
5.18	¹³ C-NMR spectra of NR and hydrogenated NR samples taken at 2, 4, 6 and 8h analyzed in solid state	123
5.19	The percent hydrogenation at various reaction times of NR determined by ¹ H-NMR in solution (○), Raman scattering (Δ) and ¹³ C-NMR in solid state (□).	124
5.20	Progress of <i>cis-trans</i> isomerization rate during hydrogenation of NR determined by ¹ H-NMR in solution (a) and ¹³ C-NMR in solid state (b) as symbolized of the % <i>cis</i> (■) and % <i>trans</i> (□).....	128
5.21	<i>Cis-trans</i> isomerization of <i>cis</i> -1,4 polyisoprene.....	129
5.22	Infrared spectra of ENR-22 containing 22 mol% epoxy group (ENR-22) (a) and the hydrogenated ENR-22 after 8h (HENR-22(8)) reaction time (b).....	133
5.23	Raman spectra of ENR-22 containing 22 mol% epoxy group (ENR-22) (a) and the hydrogenated ENR-22 after 8h (HENR-22(8)) reaction time	

LIST OF FIGURES (continued)

Figure		Page
5.24	¹ H-NMR (a) and ¹³ C-NMR (b) of ENR-22 containing 22 mol% epoxy group.....	137
5.25	¹ H-NMR (a) and ¹³ C-NMR (b) spectra of the hydrogenated ENR-22 after 8h (HENR-22(8)) reaction time as analyzed in liquid state.....	140
5.26	HD/MAS ¹³ C-NMR spectra of ENR-22 (a) and HENR-22(8) containing 22 mol% epoxy content.....	143
5.27	Stack plots of HD/MAS/CP ¹³ C-NMR spectra of HENR-22(8) and HENR-40(8) containing 22 and 40 mol% epoxy content.....	145
5.28	Comparison between the Raman spectra of ENR-22 containing 22% epoxide content and the hydrogenated ENR samples taken at various reaction times.....	146
5.29	¹ H-NMR spectra of epoxidized NR containing 22% epoxide content (ENR-22) and hydrogenated ENR samples taken at 4h (HENR-22(4))and 8h (HENR-22(8)).....	147
5.30	%Hydrogenation of epoxidized natural rubber containing 10, 22, 30 and 40 % epoxy content at various reaction times as determined by Raman (a) and ¹ H-NMR (b).....	149
5.31	Schematic of furanization reaction of partial epoxidized polyisoprene after hydrogenation by TSH.....	152
5.32	FT-IR spectra of synthetic polyisoprene (PI) (a) and hydrogenated PI (b) prepared by using 10% dry rubber content, molar ratio of [C=C]=[N ₂ H ₄]=[H ₂ O ₂] = 1 at 45°C for 24h.....	155
5.33	¹ H-NMR spectra of synthetic polyisoprene (PI) (a) and hydrogenated PI (b) prepared by using 10% dry rubber content, molar ratio of [C=C]:[N ₂ H ₄]:[H ₂ O ₂] = 1:1:1 at 45°C for 24h.....	157



LIST OF FIGURES (continued)

Figure		Page
5.34	Percentage hydrogenation of synthetic PI and microstructures versus reaction times prepared by using 10% dry rubber content with the molar ratio of $[C=C]:[N_2H_4]:[H_2O_2]$ equal to 1 at 45°C...	159
5.35	Proposed mechanism of diimide reduction of NR in latex phase using N_2H_2/H_2O_2	160
5.36	Diimide reduction of 3,4-PI units of synthetic PI.....	160
5.37	FT-IR spectra of NR (a) and hydrogenated NR (b) prepared by using 20% dry rubber content, molar ratio of $[C=C]:[N_2H_4]:[H_2O_2] = 1:1:1$ at 60 °C for 24h.....	162
5.38	1H -NMR (a) and ^{13}C -NMR (b) spectra of HNR prepared by using 20% dry rubber content, molar ratio of $[C=C]:[N_2H_4]:[H_2O_2] = 1:1:1$ at 60°C for 24h.....	164
5.39	FT-IR spectra of NR (a) and hydrogenated NR obtained from: (b) without sodium dodecyl sulfate (SDS, (c) with 4.00×10^{-3} mmol of $CuSO_4 \cdot 5H_2O$ and (d) with SDS and 4.00×10^{-3} mmol of $CuSO_4 \cdot 5H_2O$ using molar ratio of $[C=C]:[N_2H_4]:[H_2O_2] = 1$ at 60°C.....	167
5.40	1H -NMR spectrum of hydrogenated rubber obtained from the presence of $CuSO_4 \cdot 5H_2O$ (a) and $CuSO_4 \cdot 5H_2O$ and SDS as a surfactant (b) using molar ratio of $[C=C]:[N_2H_4]:[H_2O_2] = 1:1:1$ at 60°C.....	168
5.41	Effect of $CuSO_4 \cdot 5H_2O$ and surfactant on the hydrogenation rate: (\square) without SDS, (\blacksquare) with SDS, (\bullet) with 4.00×10^{-3} mmol of $CuSO_4 \cdot 5H_2O$ and (\circ) with 4.00×10^{-3} mmol of $CuSO_4 \cdot 5H_2O$ and SDS using molar ratio of $[C=C]:[N_2H_4]:[H_2O_2] = 1:1:1$ at 60°C....	170



LIST OF FIGURES (continued)

Figure		Page
5.42	The percent hydrogenation of NR in latex phase with the presence SDS as a surfactant (■), SDS and 2.40×10^{-3} mmol of $\text{CuSO}_4 \cdot 5\text{H}_2\text{O}$ (□), and SDS and 4.00×10^{-3} mmol of $\text{CuSO}_4 \cdot 5\text{H}_2\text{O}$ (●) using molar ratio of $[\text{C}=\text{C}]:[\text{H}_2\text{N}_4]:[\text{H}_2\text{O}_2] = 1:1:1$ at 60°C	172
5.43	FT-IR spectra of NR (a) and HNR obtained from various reaction temperatures: 30 (b), 60 (c), and 80°C (f) using molar ratio of $[\text{C}=\text{C}]:[\text{N}_2\text{H}_4]:[\text{H}_2\text{O}_2] = 1$	174
5.44	^1H -NMR spectrum of the hydrogenated NR obtained from 60°C using molar ratio of $[\text{C}=\text{C}]:[\text{N}_2\text{H}_4]:[\text{H}_2\text{O}_2] = 1:1:1$ at 24h.....	174
5.45	Effect of reaction time and temperature on hydrogenation of NR in latex phase varied at 30°C (□), 45°C (■), 60°C (▲), 70°C (Δ) and 80°C (●) by using 20% dry rubber content, molar ratio of $[\text{C}=\text{C}]:[\text{N}_2\text{H}_4]:[\text{H}_2\text{O}_2] = 1:1:1$	177
5.46	Influence of dry rubber contents on diimide reduction of NR in latex phase using molar ratio of $[\text{C}=\text{C}]:[\text{N}_2\text{H}_4]:[\text{H}_2\text{O}_2] = 1:1:1$; %10DRC (■), %20DRC (▲) and %30DRC (●).....	180
5.47	Influence of hydrazine concentration on the hydrogenation level of NR latex at various amount of N_2H_4 ; (■) 0.5mol, (□) 1.0mol, (●) 1.5mol and (○) 2.0mol carried out using 20 %DRC and the molar ratio of $[\text{C}=\text{C}]:[\text{H}_2\text{O}_2] = 1$ at 60°C	182
5.48	Influence of hydrogen peroxide concentration on the hydrogenation level of NR latex at various amount; (■) 0.5mol, (□) 1.0mol, (●) 1.5mol and (○) 2.0mol carried out using 20 %DRC and the molar ratio of $[\text{C}=\text{C}]:[\text{N}_2\text{H}_4] = 1$ at 60°C	185
5.49	Influence of molar ratio of $[\text{N}_2\text{H}_4]:[\text{C}=\text{C}]$ on the percent hydrogenation at 60°C by keeping the equal molar ratio of $[\text{N}_2\text{H}_4]$ and $[\text{H}_2\text{O}_2]$, using 20 %DRC at 60°C	187



LIST OF FIGURES (continued)

Figure		Page
5.50	The percent hydrogenation of different types of NR latex obtained at various reaction times using 20% DRC with molar ratio of $[C=C]:[N_2H_4]:[H_2O_2] = 1:1:1$ at $60^\circ C$	189
5.51	Particle size distribution of various types of rubber latex: (■) NR, (▲) DPNR(TER), (Δ) DPNR(SDS), (●) SFNR, (○) CFNR, (◆) LNR and (◇) UNR.....	190
5.52	Formation mechanism of <i>cis-trans</i> isomerization occurred in diimide reduction in latex form.....	191
5.53	Proposed crosslinking reaction during diimide hydrogenation of NR in the presence of hydrogen peroxide.....	193
5.54	Plots of $\ln k$ and $1/T$ from diimide hydrogenation of NR latex.....	195
5.55	Characteristic of Raman shift of $C=C$ bond at 1664 cm^{-1} of NR and HNR samples.....	199
5.56	The plot of the relative variation force constant versus the hydrogenation level of the HNR samples.....	200
5.57	Characteristics of Raman shift of the $C=C$ bond at 1664 cm^{-1} of HENR-10 samples.....	202
5.58	The plot of the relative variation force constant versus the hydrogenation level of the HENR-10.....	203
5.59	A stack plot of solid state HD/MAS ^{13}C -NMR spectra of NR and the HNR samples obtained at 2, 4, 6 and 8h.....	205
5.60	The plot of line widths of solid state HD/MAS ^{13}C -NMR spectra of the HNRs obtained at various hydrogenation levels: (■) C-1, (●) C-5, (▲) C-6 and C-8, (□) C-4, (○) C-7, (Δ) C-9 and (◇) C-10.....	206



LIST OF FIGURES (continued)

Figure		Page
5.61	A Stack plot of solid state ^{13}C -NMR spectra of the hydrogenated NR (85%) at various contact times in the chemical shift range of 15- 40 ppm.....	207
5.62	Variation of the magnetization with contact time in a CP experiment for HNR (85%) of carbon positions at C-10 (a), C-9 (b), C-7 (c) and C-6, C-8 (d).....	210
5.63	A stack plot of MAS and HD/MAS ^{13}C -NMR spectra of ENR-22 containing 22 mol% epoxy content.....	212
5.64	Stack plots of HD/MAS ^{13}C -NMR spectra of NR, ENR-10, ENR-15, ENR-22 and ENR-40 containing 10, 15, 22, and 40 mol% epoxy content, respectively.....	213
5.65	Line widths of the characteristic of oxirane units with extent of epoxidation: (□) quaternary carbon at 60 ppm and (■) methine carbon at 64 ppm.....	214
5.66	HD/MAS ^{13}C -NMR spectra of ENR containing 10 mol% epoxy content and their hydrogenated ENR (HENR-10(8)) obtained at 8h.....	215
5.67	Stack plots of HD/MAS ^{13}C -NMR spectra of HENR-10(8), HENR-15(8), HENR-22(8), HENR-30(8) and HENR-40(8) containing 10, 15, 22, 30 and 40 mol% epoxy content obtained at 8h of reaction time.....	216
5.68	Stack plots of HD/MAS/CP ^{13}C -NMR spectra of HENR-10(8), HENR-15(8), HENR-22(8), HENR-30(8) and HENR-40(8) containing 10, 15, 22, 30 and 40 mol% epoxy content obtained at 8h of reaction time.....	217
5.69	Stack plots of HD/MAS ^{13}C -NMR spectra of HNR(8), HENR-10(8) and HENR-30(8) containing 10 and 30 mol% epoxy content, respectively, obtained at 8h of reaction time.....	218



LIST OF FIGURES (continued)

Figure		Page
5.70	Stack plots of solid state ^{13}C -NMR spectra of HENR-10(8) at various contact times in the chemical shift range of 0-60 ppm.....	219
5.71	Variation of the magnetization with contact time in a CP experiment for HENR-10 sample of carbon positions at C-10 (a), C-9 (b), C-7 (c) and C-6, C-8 (d).....	221
5.72	Stack plots of solid state ^{13}C -NMR spectra of HENR-30 at various contact times in the chemical shift range of 0-60 ppm.....	222
5.73	Variation of the magnetization with contact time in a CP experiment for the HENR-30(8) sample of carbon positions at C-10 (a), C-9 (b), C-7 (c) and C-6, C-8 (d).....	224
5.74	Stack plots of Raman spectra of NR as a function of temperature.	226
5.75	Raman shift of C=C bond of NR as a function of temperature.....	227
5.76	Raman spectra of partially hydrogenated NR (HNR(6)) obtained from reaction time 6h as a function of temperature.....	228
5.77	Raman shift of C=C bond of the HNR(6) as a function of temperature.....	229
5.78	Raman shift of epoxidized NR containing 10 mol% epoxide content as a function of temperature.....	230
5.79	Raman shift of C=C bond of ENR-10 as a function of temperature.....	230
5.80	Raman shift of HENR-10(4) at 4h as a function of temperature...	231
5.81	The relationship between glass transition temperature and scanning rate of NR, HNR38 and HNR97.....	233
5.82	The relationship between the glass transition temperature and the epoxidation level of ENR (a) and of HENRs (b) containing 10, 22, 30 and 40 % epoxide content.....	238
5.83	TG (a) and DTG (b) thermograms of natural rubber (NR) and their hydrogenated products (HNR) in air atmosphere.....	



LIST OF FIGURES (continued)

Figure		Page
5.84	TG (a) and DTG (b) thermograms of natural rubber (NR) and their hydrogenated products (HNR) in nitrogen atmosphere.....	242
5.85	TG and DTG thermograms of natural rubber (NR) and their hydrogenated products (HNRs) obtained in latex at various percent hydrogenations under nitrogen atmosphere.....	244
5.86	TG and DTG curves of ENR containing 10 mol% epoxy content and hydrogenated ENR obtained at 2, 4, 6 and 8h.....	246
5.87	TG and DTG thermograms of ENR (a) containing 10, 22, 30 and 40 mol% epoxy content and their hydrogenated products (b) obtained at 8h.....	248
5.88	¹³ C-NMR spectra of hydrogenated rubbers containing 38, 69 and 97 mol% hydrogenation content.....	251
5.89	Strain sweep tests on HNR38 sample; RPA built-in data treatment.....	253
5.90	Strain sweep tests on HNR69 sample; RPA built-in data treatment.....	254
5.91	Strain sweep tests on HNR97 sample; RPA built-in data treatment.....	255
5.92	Main torque components detected from Fourier transform treatment of strain sweep tests on HNR38, HNR69 and HNR97 samples.....	257
5.93	Relative third harmonic component versus strain (%) of the samples fit without constraint on parameters (a) HNR38, (b) HNR69 and (c) HNR97.....	260
5.94	Raman spectra of NR and the hydrogenated rubbers obtained from 2 and 6h: HNR(2), and HNR(6) containing 39 and 79 % hydrogenation level.....	267



LIST OF FIGURES (continued)

Figure		Page
5.95	Micro-Raman mapping of NR (a), the hydrogenated rubbers obtained from 2 and 6h: HNR(2) (b), and HNR(6) (c) containing 39 and 79 % hydrogenation level at area $2\ \mu\text{m} \times 2\ \mu\text{m}$	268



LIST OF ABBREVIATIONS

NR	Natural rubber
HNBR	Hydrogenated nitrile butadiene rubber
HBR	Hydrogenated butadiene rubber
HSBR	Hydrogenated styrene butadiene rubber
HSIR	Hydrogenated styrene isoprene rubber
HSIS	Hydrogenated styrene isoprene styrene
TSH	<i>p</i> -toluenesulfonylhydrazide
ENR	Epoxidized natural rubber
EPDM	Ethylene-propylene diene rubber
IR	Infrared spectroscopy
¹ H-NMR	Proton Nuclear Magnetic Resonance
¹³ C-NMR	Carbon Nuclear Magnetic Resonance
HPLC	High performance liquid chromatography
C-serum	Cytoplasm serum
BF	Bottom fraction
HANR	High ammonia natural rubber
DPNR	Deproteinized natural rubber
SDS	Sodium dodecyl sulfate
PB	Polybutadiene
NBR	Nitrile butadiene rubber
SBR	Styrene butadiene rubber
T _g	Glass transition temperature
TGA	Thermalgravimetric analyzer
TSOH	<i>p</i> -Toluenesulfonic acid
PI	Polyisoprene
GPC	Gel permeation chromatography
MWD	Molecular weight distribution



LIST OF ABBREVIATIONS (continued)

NRL	Natural rubber latex
μ	Dipole moment
E	Electric field
α	Polarizability
E_o	Equilibrium electric field strength
ν	Frequency
A_i	Number of vibration mode
R	Symmetry operator
$k(R)$	Number of elements in each class
$\chi(R)$	Symmetry operator (R)
γ	Magnetogyric ratio
T_2	Spin-spin relaxation time
CP	Cross polarization
MAS	Magic angle spinning
H_o	Applied magnetic field
$T_{1\rho}({}^1\text{H})$	Proton spin-lattice relaxation time in the rotating frame



PUBLICATIONS



Spectroscopic Study of Di-Imide Hydrogenation of Natural Rubber

Jareerat Samran,¹ Pranee Phinyocheep,*^{1,2} Philippe Daniel,³ Daniel Derouet,⁴ Jean-Yves Buzare³

¹ Department of Chemistry, Faculty of Science, Mahidol University, Rama VI Road, Payathai, Bangkok, 10400, Thailand

² Institute of Science and Technology for Research and Development, Mahidol University, Salaya Campus, Puthamonthon, Nakornpathom, 73170, Thailand

E-mail: scppo@mahidol.ac.th

³ Laboratoire de Physique de l'Etat Condensé LPEC (UMR CNRS n° 6087), Université du Maine, Avenue Olivier Messiaen, 72085 Le Mans Cedex 9, France

⁴ L.C.O.M. Chimie des Polymères (UMR du CNRS LCO2M n° 6011), Université du Maine, Avenue Olivier Messiaen, 72085 Le Mans Cedex 9, France

Summary: The diimide hydrogenation of natural rubber (NR) was studied by using *p*-toluenesulfonylhydrazide (TSH) as a diimide-releasing agent. The microstructure and the percentage of hydrogenation were studied by Raman, ¹H-NMR and ¹³C-NMR spectroscopic techniques. Quantitative measurements on fraction of hydrogenated part gave the results in good agreement by using these techniques. The results indicated that percent hydrogenation increased with increasing of reaction time and about 80-85 % hydrogenation was achieved when a two-fold excess of TSH was used. The vibrational characteristic of C=C bond of NR is strongly Raman active and noted at 1663 cm⁻¹. The decrease of this signal was clearly observed during the progress of hydrogenation but the vibrational frequency of the *cis* and *trans* structures of the trisubstituted olefin unit of NR can not be differentiated by this technique. While ¹H- and ¹³C-NMR analysis showed that *cis-trans* isomerization of carbon-carbon unsaturation of NR occurred during hydrogenation.

Keywords: diimide hydrogenation; FT-IR; natural rubber; NMR; Raman spectroscopy

Introduction

Chemical modification of unsaturated polymers via hydrogenation is one of the most important methods for altering and optimizing the physical and mechanical properties of the macromolecules. The hydrogenation is also a potential method offering a polymer that can



not be prepared by a simple conventional polymerization reaction. An example is the preparation of poly(ethylene-alt-propylene) which can be potentially obtained by fully hydrogenation of 1,4-polyisoprene.^[1] Diimide (N_2H_2) is an inorganic reducing agent which has been progressively used for hydrogenation of unsaturated molecules.^[2,3] It is considered as a noncatalytic reaction and found to be a convenient hydrogenation method since it can be performed under atmospheric pressure with relatively simple apparatus and procedure. In contrary, catalytic hydrogenation using hydrogen gas in the presence of a noble metal catalyst is rather difficult in handling the reaction, usually involving high pressure and temperature.^[1,4]

Natural rubber (NR) which has been known as highly *cis*-1,4 polyisoprenic structure, has a primary drawback in thermal and oxidative stabilities and poor oxygen and ozone resistance. This is due to the presence of the unsaturation along the molecular chain. Therefore, reduction of the unsaturated units of NR should overcome some of these drawbacks. N.K. Singha *et al* reported that catalytic hydrogenation of NR using $RhCl(PPh_3)$ catalyst increased the thermal stability of the resulting product without affecting its glass transition temperature.^[1] Utilization of a diimide hydrogenating agent generated from thermal decomposition of *p*-toluenesulfonylhydrazide (TSH) for hydrogenation of polybutadiene and polyisoprene has been reported.^[2,3] In both cases, an excess amount of TSH is required if complete hydrogenation is expected. The evidence of hydrogenation was examined by IR and NMR spectroscopy.

Generally, spectroscopic techniques i.e. Raman, infrared, 1H - and ^{13}C -NMR can be used for characterization of the microstructure of the chemically modified products.^[5,6] Hydrogenation of NR can be therefore extensively investigated by vibrational (i.e. Raman and infrared) and resonance spectroscopic techniques (i.e. 1H - and ^{13}C -NMR) since the characteristic signal of the C=C bond of polyisoprene is very sensitive to its environment.^[7,8] However, only a few work has been analyzed by Raman scattering and solid state NMR, including the quantification of the unsaturated units of NR. Therefore, these two techniques have been used for such purposes in this present work and compared to other spectroscopic technique i.e. 1H -NMR in solution.

This article describes the hydrogenation of NR by using diimide as a reducing agent generated from the *in situ* decomposition of TSH. The progress of reaction was observed by



Raman, FT-IR and NMR both in solution and solid state spectroscopic techniques. The percentage of hydrogenation was determined by Raman, $^1\text{H-NMR}$ in solution and $^{13}\text{C-NMR}$ in solid state. The evidence of *cis-trans* isomerization as hydrogenation progress was also investigated by $^1\text{H-}$ and $^{13}\text{C-NMR}$.

Experimental

Hydrogenation

Hydrogenation of NR was carried out as follows; about 1.0 g of rubber was dissolved in 100 ml of xylene (JT Baker). Two folds of *p*-toluenesulfonylhydrazide (TSH, Fluka) as compared to rubber unsaturated units ($[\text{TSH}]/[\text{C}=\text{C}] = 2$) was added to the solution. The mixture was then stirred and heated to 135°C under nitrogen atmosphere. Samples were taken at various reaction times and precipitated in methanol. The hydrogenated product was purified by dissolving in hexane and reprecipitating in methanol. Finally, the product was dried in vacuum at room temperature before analysis.

Characterization

Raman Spectroscopy

Raman spectra of all samples were recorded with a T64000 Jobin-Yvon multichannel spectrometer adjusted either in simple spectrograph configuration with a 600 lines/mm grating or in triple subtractive configuration for high resolution experiments. Samples were illuminated with a Coherent Argon-Krypton Ion Laser selecting the 647.1 nm lines in order to minimize luminescence contribution to spectra. To improve the signal/noise ratio, each spectrum was accumulated 20 times during 30 sec. The frequency range selected was 500-3200 cm^{-1} . Calibration of the spectrometer was precisely checked on the 520.2 cm^{-1} silicon band and the resolution of the spectra was estimated to be smaller than 1 cm^{-1} . All experiments were performed under microscope using an x 50 long work distance objective (Olympus B x 40 microscope).



FT-IR Spectroscopy

FT-IR spectra were carried out by using Perkin-Elmer system 2000 spectrometer by casting thin film of the sample on NaCl plate. All samples were recorded at 16 scans in the range of 500-4000 cm^{-1} with 4 cm^{-1} spectra resolution in order to obtain a good signal-noise ratio.

Nuclear Magnetic Resonance Spectroscopy in Solution

^1H -NMR and ^{13}C -NMR (Bruker DPX-300 NMR spectrometer) spectra were obtained from the samples dissolved in CDCl_3 using tetramethylsilane (TMS) as an internal reference.

Nuclear Magnetic Resonance Spectroscopy in Solid State

High resolution solid state experiments were recorded on a Bruker MSL 300 spectrometer operating at 75.47 MHz. The instrument is equipped with a high-power amplifier for proton decoupling. The experiments were carried out using a pulse width of 90° (4 μs) with a repetition time of 4 s. A spectral width of 20 kHz and 16 K data points were used for data collection. The spinning speed of MAS technique was applied at 10 kHz.

Results and Discussion

The diimide molecule (N_2H_2) is generated *in situ* from the thermal decomposition of *p*-toluenesulfonylhydrazide (TSH) as shown in equation (1) in Figure 1. It can then release a hydrogen molecule directly to the carbon-carbon double bonds of isoprene units as represented in equation (2) in Figure 1.

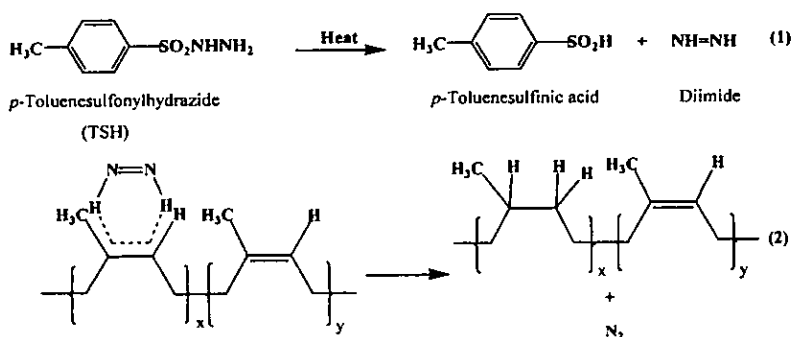


Figure 1. Hydrogenation of NR by using diimide generated from *p*-toluenesulfonylhydrazide.

Microstructure Analysis of Hydrogenated Rubber

Vibrational Spectroscopy

Non catalytic hydrogenation of NR in this study was carried out by using 2 moles of TSH as compared to the isoprene units. When one molecule of diimide reacted with the NR, one unit of the C=C should be disappeared as shown in Figure 1. The vibrational characteristic of the C=C of the isoprene unit can therefore be examined by Raman and Infrared (IR) spectroscopy. A comparison between the Raman spectra of the starting NR and that of hydrogenated NR (HNR) samples taken during hydrogenation at various reaction times is given in Figure 2. As hydrogenation reaction proceeded, the decrease of absorption band at 1664 cm^{-1} assigned to the C=C stretching modes can be clearly detected with increasing of the vibrational intensity of the band at 1432 cm^{-1} , attributed to the $-\text{CH}_2-$ deformation vibration. No alteration of the band at 1452 cm^{-1} which belongs to an asymmetric vibration of $-\text{CH}_3$ group in Raman spectra was noted after hydrogenation.

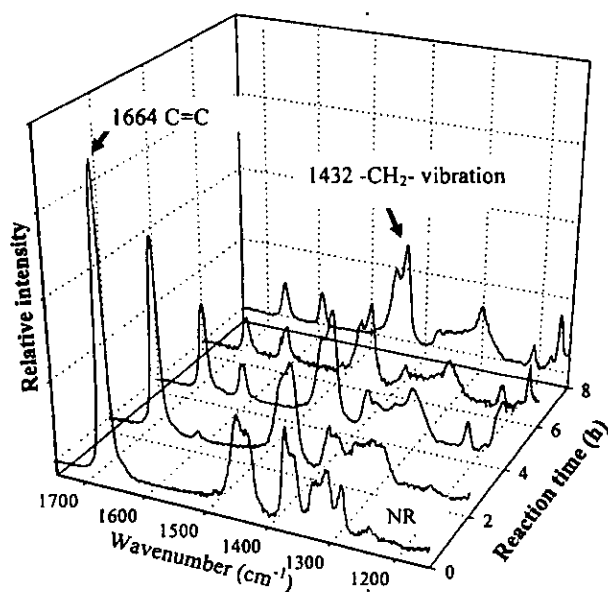


Figure 2. Raman spectra of natural rubber (NR) and hydrogenated rubbers at different reaction times.

It is not surprising that after 8 h of reaction the total disappearance of the peak at 1664 cm^{-1} is not observed as it has been reported that the complete reduction of unsaturation of butadiene polymers and of polyisoprene can be obtained with a five-fold excess of TSH.^[2,3]

For IR analysis of the hydrogenated rubber, the decrease of two important characteristic peaks at 1665 and 836 cm^{-1} , attributing to C=C stretching and the C-H out of plane deformation of the trisubstituted olefin of polyisoprene, respectively, were observed as shown in Figure 3. The signal at 1375 cm^{-1} assigning to the C-H deformation and the signal at 735 cm^{-1} , being due to sequences of three continuous methylene units occurred after hydrogenation were also detected. It can be seen that the vibrational absorption modes obtained from IR spectrum is not as powerful as Raman mode. The intensity of the C=C absorption peaks at 1665 and 836 cm^{-1} are not strong for quantitative analysis of the percent of hydrogenation.

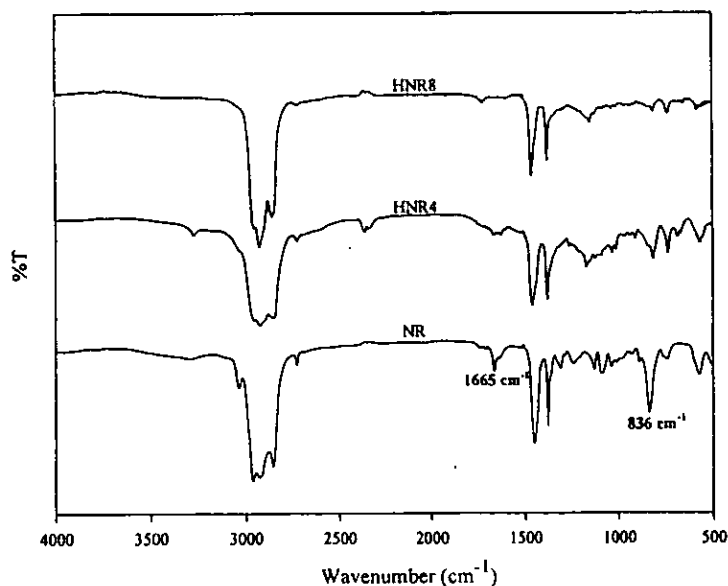


Figure 3. FTIR spectra of natural rubber (NR) and hydrogenated rubbers at 4h (HNR4) and 8h (HNR8) reaction times.

Resonance Spectroscopy

$^1\text{H-NMR}$ analysis of NR in Figure 4 shows three main characteristic signals of proton adjacent to $\text{C}=\text{C}$, methylene and methyl protons of the unsaturated unit at 5.12, 2.03 and 1.67 ppm, respectively. $^1\text{H-NMR}$ spectra of the products of hydrogenation after 4 and 8 h of the reaction, symbolized as HNR4 and HNR8, respectively are also shown in Figure 4. The figure indicates that the intensity of proton signal adjacent to $\text{C}=\text{C}$ bonds at 5.12 ppm decreases with the increased reaction time, as well as the decrease of signal at 1.67 ppm characteristic of methyl proton of *cis*-1,4 polyisoprenic units of NR. The methyl and methylene proton signals observed at 0.84 and 1.1-1.3 ppm, respectively showed a strong increment due to the transformation of double bonds into saturation moieties. The hydrogenation levels can be therefore determined by comparison of the integrals of signal at 5.12 ppm with the integrals for proton signal of saturated units.

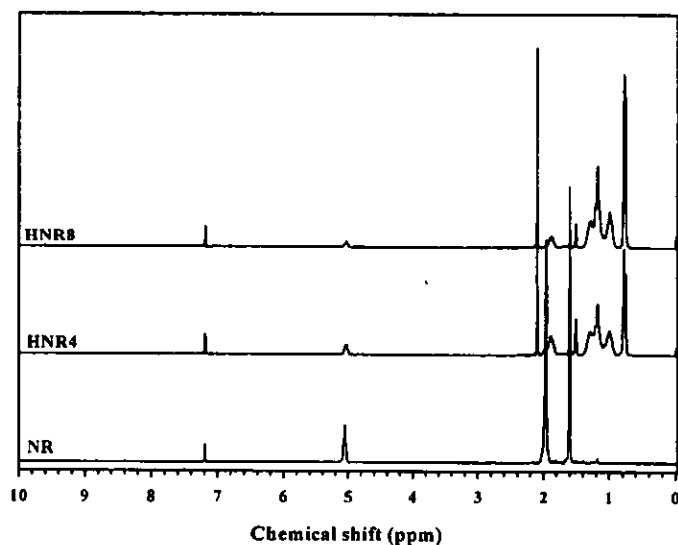


Figure 4. $^1\text{H-NMR}$ spectra of natural rubber (NR) and hydrogenated NRs at 4h (HNR4) and 8 h (HNR8) reaction times.

In the case of ^{13}C -NMR analysis in solution, the carbon signals of $\text{C}=\text{C}$ of *cis*-structure of isoprene units of NR are positioned at 135.2 and 125.5 ppm. Three signals characteristic of methyl and two methylene carbons of the unsaturated unit were found at 23.4, 26.4 and 32.2 ppm, respectively. The extra peaks at 19.5, 33 and 37.1 ppm assigning to the methyl, methine and methylene carbons of saturated units in the hydrogenated rubbers are observed. The detected chemical shifts are in good agreement with those reported in the literatures.^[1,9] The ^{13}C -NMR spectrum of the partially hydrogenated product reveals the evidence of the *cis-trans* isomerization of isoprene unit in the polymer chains as the signal at 134.9 and 124.7 ppm, corresponding to olefinic carbons of *trans*-polyisoprenic structure are detected for HNR.

The ^{13}C -NMR study in solid state of natural rubber and hydrogenated rubbers was carried out at room temperature, which is the temperature far above their glass transition temperatures (T_g). Under this condition, the dipolar interactions and chemical shift anisotropy that lead to line broadening are partially averaged by chain motion, and sharp lines are observed with high power decoupling and magic angle spinning. The motional averaging is such that high resolution signals of NR and HNR can be observed with spinning, and peak assignments can be established using the traditional solution methods (Figure 5).

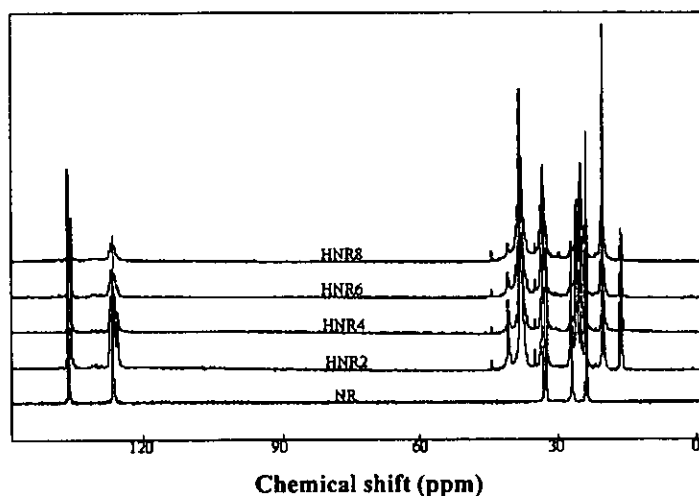


Figure 5. Solid state ^{13}C -NMR spectra of natural rubber (NR) and hydrogenated NR at 2h (HNR2), 4h (HNR4), 6h (HNR6) and 8 h (HNR8) reaction times.

The dominant peaks of NR spectrum at 23.6, 26.7, 32.5, 134.8 and 125 ppm observed were related to the five carbon atoms of the *cis*-1,4 polyisoprenic units, similar to the assignments using ^{13}C -NMR in solution. These characteristic peaks can be seen to diminish as the hydrogenation reaction proceeded. Then the significant peaks at 20.4, 33.3 and 38.1 ppm are found. Based on literature and by making comparison with the NMR spectra in liquid state, these peaks are assigned to the carbon signal of methyl, methine and methylene types, respectively.^[1] Figure 5 shows also the characteristic *trans*-1,4-polyisoprene located at 16, 27 and 40 ppm, assigning to methyl and two methylene carbons.^[10] This is the confirmation of *cis-trans* isomerization occurred simultaneously with hydrogenation. The extra resonances of *trans*-structural units allowed us to evaluate the amount of *trans*-isomer as increasing the reaction time.

Determination of Percent Hydrogenation

With the Raman scattering technique, it is possible to monitor the progress of saturated units in NR during hydrogenation. The percent hydrogenation of each sample can be estimated from the ratio of band areas arising from the stretching mode of C=C bond and the bending mode of CH₂, since each addition of hydrogen molecule on C=C bond gives rise to one new CH₂ unit.^[11] The repeating unit of polyisoprene already presents two CH₂ groups. The CH₂ bending band appears to be moderately active near 1432 cm⁻¹ as shown in Figure 2. The band intensity in Raman spectra can be roughly considered as proportional to the concentration of each species in the following:

$$\begin{aligned} A(\text{C}=\text{C}) &= k_1[\text{C}=\text{C}] \\ A(\text{CH}_2) &= k_2[\text{CH}_2] \end{aligned}$$

where $A(\text{C}=\text{C})$ is the integrated intensity area of the band located between 1645 and 1685 cm⁻¹ assigned to the C=C stretching vibrational band, $A(\text{CH}_2)$ is the integrated intensity area of the CH₂ bending band between 1415 and 1440 cm⁻¹, k_1 and k_2 are proportional constants associated with the considered C=C and CH₂ vibrational modes. If the starting rubber is composed of 100 repeating units, 100 C=C and 200 CH₂ units are then present, hence

$$k_1/k_2 = 2A_0(\text{C}=\text{C})/A_0(\text{CH}_2)$$

Then, the ratio k_1/k_2 can be determined from the Raman spectrum of NR in Figure 2.

X is assigned for the concentration or number of the unit disappeared or formed, when X



C=C units disappear during hydrogenation, it can be noted that X of CH₂ units are created. For a partially hydrogenated product, X or the hydrogenation rate can then be calculated from the following equation :

$$X = 100 [(K - 2\alpha)/(K + \alpha)]$$

where $K = k_1/k_2$ and $\alpha = A_0(\text{C}=\text{C})/A_0(\text{CH}_2)$ of the partially hydrogenated compound.

From ¹H-NMR spectroscopy, the integrated areas of the signal at 5.12 and 0.84 ppm, corresponding to the proton adjacent to olefinic unit and methyl proton of saturated unit, respectively, were used for the determination of percentage of hydrogenation. The progress of hydrogenation by solid state ¹³C-NMR was obtained by using the integrated areas of the signals of saturated methyl carbon at 20.4 ppm comparing to the methyl carbon of both *cis*- and *trans*-unsaturated units at 23.6 and 16 ppm, respectively. The results of percentage of hydrogenation at various reaction times of NR determined by different techniques are illustrated in Figure 6. It was found that the hydrogenation increased with the increase of reaction time. The maximal percentage of hydrogenation approximately 80-85 % was found by using all three techniques when a two-fold excess of TSH was used. Several publications reported that complete hydrogenation was obtained when 4-5 moles of TSH per mole of polyisoprene units were utilized for hydrogenation of homopolymer or copolymer containing polyisoprene units.^[11,12] It was described that not only the *syn* form of the generated diimide can react with the C=C bonds of polyisoprene units, but it can also undergo disproportionation, giving nitrogen molecule and hydrazine.

***Cis-trans* Isomerization**

It was reported that utilization of TSH as a diimide releasing agent for hydrogenation of *cis*-polybutadiene resulted in *cis-trans* isomerization.^[13] Unfortunately, the *cis-trans* isomerization of the unsaturated units of NR during hydrogenation can not be detected by Raman spectroscopy as the vibrational frequency of the *cis* and *trans* structures of trisubstituted olefinic unit in Raman scattering are very close. While the ¹H-NMR spectra of the hydrogenated rubber exhibit the signal of methyl proton of the *cis*- and *trans*-1,4 polyisoprenic units at 1.67 and 1.60 ppm, respectively. The percentage of the remaining double bonds in *cis*- and *trans*- configurations of the hydrogenated samples at various reaction times can then be calculated and the results are shown in Figure 7 (a).



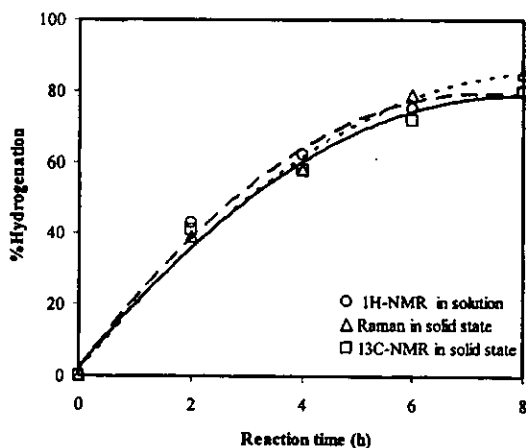


Figure 6. Results of percentage of hydrogenation at various reaction times of NR determined by ^1H -NMR in solution, Raman scattering and ^{13}C -NMR in solid state.

The ^{13}C -NMR spectrum in solution of the partial hydrogenated product reveals the evidence of the *cis-trans* isomerization. The carbon signals of *cis*-structure were located at 135.2 and 125.5 ppm while the signals at 134.9 and 124.7 ppm, corresponding to olefinic carbons of 1,4-*trans* polyisoprenic units were also detected for hydrogenated NR.

For solid state ^{13}C -NMR spectra, the signal of methyl carbon of *cis*- and *trans*- polyisoprenic structure can be clearly seen at 23.6 and 16 ppm, respectively. The results of the percentage of *cis*- and *trans*- isomers at various reaction times are illustrated in Figure 7(b). It seems likely that in this system the *cis-trans* isomerization is a reversible process. The thermal decomposition of TSH generates a diimide acted as a hydrogen-donor molecule as well as *p*-toluenesulfonic acid by-product. The formation of unstable complex between the double bonds and the *p*-toluenesulfonic acid by-product may be responsible for the *cis-trans* isomerization reaction.⁽¹³⁾ No signal of the addition of the by-product onto the hydrogenated rubber was detected.

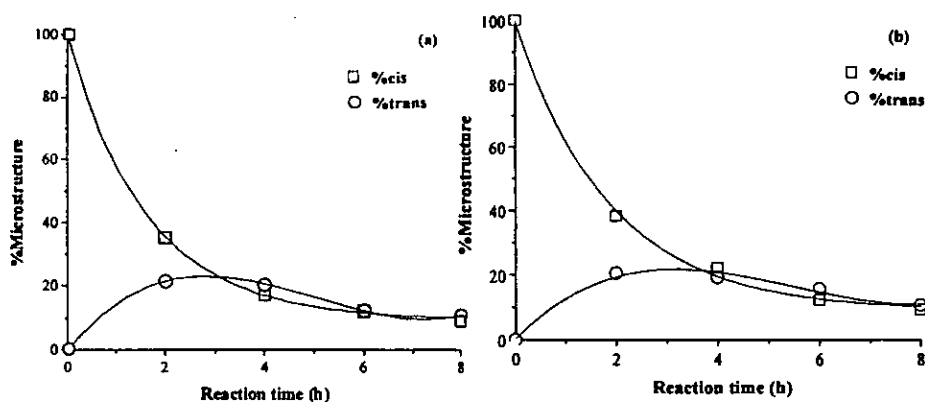


Figure 7. Progress of *cis-trans* isomerization rate during hydrogenation of NR determined by $^1\text{H-NMR}$ in solution (a) and $^{13}\text{C-NMR}$ in solid state (b).

Conclusion

Natural rubber (NR) was partially hydrogenated using two-fold moles of *p*-toluenesulfonylhydrazide (TSH) compared to the unsaturated unit. The microstructure of the hydrogenated products can be observed by using spectroscopic techniques i.e. Raman, FT-IR, $^1\text{H-}$ and $^{13}\text{C-NMR}$. The quantitative measurements on fraction of hydrogenated part at different reaction times determined by Raman, $^1\text{H-}$ and $^{13}\text{C-NMR}$ gave similar results which indicated that percent hydrogenation increased with increasing of reaction time and about 80-85 % hydrogenation were obtained at 8h. $^1\text{H-NMR}$ and $^{13}\text{C-NMR}$ gave the evidence of the *cis-trans* isomerization during hydrogenation. These techniques were also used to monitor the progress of the isomerization.

Acknowledgement

The scholarship from the Ministry of the University Affairs, Thailand to J. Samran is greatly appreciated.

- [1] N. K. Singha, P. P. De, S. J. Sivaram, *J. Appl. Polym. Sci.* **1997**, *66*, 1647.
- [2] L. A. Mango, R. W. Lenz, *Makromol. Chem.* **1973**, *163*, 13.
- [3] H. J. Harwood, D. B. Russell, J. A. Verthe, J. Zymonas, *Makromol. Chem.* **1973**, *163*, 1.
- [4] G. Rempel, N. Mohammadi, *Macromolecules* **1987**, *20*, 2362.
- [5] J. L. Koenig, *Spectroscopy of Polymers*; American Chemical Society, Washington, USA, **1992**, 115-252.
- [6] K. D. O. Jackson, M. J. R. Loadman, C. H. Jones, G. Ellis, *Spectrochim. Acta.* **1990**, *46A*, 217.
- [7] P. J. Hendra, K. D. O. Jackson, *Spectrochim. Acta.* **1994**, *50A*, 1987.
- [8] S. J. Bunce, H. G. M. Edwards, A. F. Johnson, I. R. Lewis, *Spectrochim. Acta.* **1993**, *49A*, 775.
- [9] Y. A. Shahab, R. A. Basheer, *J Polym Sci Polym Chem Ed* **1979**, *17*, 919.
- [10] J. Y. Buzaré, G. Silly, J. Emery, G. Boccaccio, E. Rouault, *Eur. Polym. J.* **2001**, *37*, 85.
- [11] J. Podesva, P. Spacek, C. Konak, *J. Appl. Polym. Sci.* **1992**, *44*, 527.
- [12] P. Phinyocheep, S. Pasiri, O. Tavichai, *J. Appl. Polym. Sci.* **2003**, *87*, 76.
- [13] S. Poshyachinda, V. Kaniathanon, *Spectrochimica Acta.* **1994**, *50A*, 2011.



Raman spectroscopic study of non-catalytic hydrogenation of unsaturated rubbers

Jareerat Samran,¹ Pranee Phinyocheep,^{1,2*} Philippe Daniel,^{3,4} Daniel Derouet^{4,5} and Jean-Yves Buzaré^{3,4}

¹ Department of Chemistry, Faculty of Science, Mahidol University, Rama VI Road, Phayathai, Bangkok 10400, Thailand

² Institute of Science and Technology for Research and Development, Mahidol University, Salaya Campus, Puthamonthon, Nakompathom 73170, Thailand

³ Laboratoire de Physique de l'Etat Condensé (UMR CNRS No. 6087), Université du Maine, Avenue Olivier Messiaen, 72085 Le Mans Cedex 9, France

⁴ Institut de Recherche en Ingénierie Moléculaire et Matériaux Fonctionnels IRIM2F FR CNRS No. 2575, Université du Maine, Avenue Olivier Messiaen, 72085 Le Mans Cedex 9, France

⁵ LCOM – Chimie des Polymères (UMR CNRS UCO2M No. 6011), Université du Maine, Avenue Olivier Messiaen, 72085 Le Mans Cedex 9, France

Received 3 May 2004; Accepted 20 July 2004

The non-catalytic hydrogenation of natural rubber (NR) and two epoxidized NRs (ENRs) i.e. ENR-22 and ENR-40 containing 22 and 40 mol% of epoxide, respectively, was carried out using *p*-toluenesulfonylhydrazide (TSH) as a hydrogenating agent. A two-fold molar excess of TSH compared with unsaturated units of the rubber was used. The evidence of hydrogenation is a decrease in the intensity of the characteristic signal of the carbon–carbon double bond stretching vibration of the rubber in both the Raman and FT-IR spectra. The percentage hydrogenation was successfully determined by Raman spectroscopy since the vibrational mode of the carbon–carbon unsaturation is strongly Raman active. The progress of the hydrogenation could be monitored by means of the techniques mentioned above as a function of reaction time. The maximum degree of hydrogenation of NR is ~89% whereas in the case of ENR-22 and ENR-40 it reaches 94 and 96%, respectively. Solid-state ¹³C NMR spectroscopy was also used to confirm the microstructure characteristics of the hydrogenated rubbers. ¹³C NMR analysis showed that *cis*–*trans* isomerization of carbon–carbon unsaturations occur during hydrogenation. Copyright © 2004 John Wiley & Sons, Ltd.

KEYWORDS: diimide hydrogenation; epoxidized natural rubber; non-catalytic hydrogenation; unsaturated rubber

INTRODUCTION

Hydrogenation is an important method for improving and modifying the properties of unsaturated elastomers. Two methods of hydrogenation can be applied for these polymers, i.e. catalytic and non-catalytic.^{1–3} Catalytic hydrogenation requires a high pressure of hydrogen and the presence of a suitable metal catalyst such as Ni or Rh. In non-catalytic hydrogenation, an organic molecule which can generate a diimide intermediate is employed. The diimide molecule can provide a hydrogen molecule to the carbon–carbon double bonds without the use of a catalyst. Therefore, non-catalytic hydrogenation using diimide is a more convenient method since it can be easily performed under atmospheric pressure with simpler apparatus and procedure than used for catalytic hydrogenation.

*Correspondence to: Pranee Phinyocheep, Department of Chemistry, Faculty of Science, Mahidol University, Rama VI Road, Phayathai, Bangkok 10400, Thailand. E-mail: scppo@mahidol.ac.th

Natural rubber (NR) has been widely used in automotive applications. However, owing to its high *cis*-1,4-polyisoprene structure, its primary drawback is its low thermal and oxidation stability. Epoxidized natural rubber (ENR), which is one of the polar-modified forms of NR (see Fig. 1), shows similar disadvantages caused by the presence of residual double bonds in the macromolecular chains. Therefore, attempts to reduce the number of carbon–carbon double bonds in NR and ENR by means of hydrogenation reactions have been explored.^{4–6} Singha *et al.*⁴ studied the catalytic hydrogenation of NR using hydrogen gas and RhCl(PPh₃)₃ as a catalyst. They used IR and ¹H and ¹³C NMR spectroscopy and the iodine value to characterize the hydrogenated NR, while the kinetics of hydrogenation were studied by measuring the decrease in hydrogen pressure applied at various reaction times. Gan *et al.*⁵ used ¹H NMR spectroscopy to measure the extent of hydrogenation in NR using catalytic hydrogenation. Bhattacharjee *et al.*⁶ studied the hydrogenation of NR and ENR by using hydrogen gas



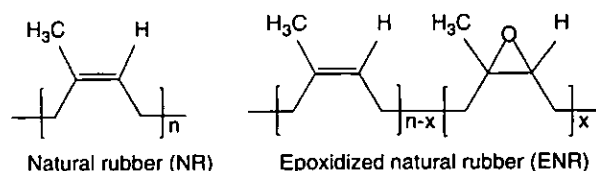


Figure 1. Structures of natural rubber and epoxidized natural rubber.

and palladium acetate as a catalyst, and found that the rate constant of hydrogenation decreases when the epoxide content in the rubber is increased.

Generally, IR and ^1H and ^{13}C NMR spectroscopy have been employed to determine the microstructure of elastomers and the modified forms such as epoxidized and hydrogenated elastomers.^{7–10} More often, the IR technique has been used for qualitative analysis whereas the determination of the degree of modification has mostly been studied by NMR techniques. The characterization of elastomers by Raman spectroscopy has long been used as $\nu(\text{C}=\text{C})$ is sensitive to its environment in a similar but much clearer way than in IR spectroscopy. This technique has been successfully used for the study the microstructure of elastomers and hydrogenated polybutadienes.^{11–14} However, only a few studies have been carried out to characterize the unsaturated units in natural rubber after modification by Raman scattering.

In this work, hydrogenation of NR and two ENRs with 22 and 40 mol% epoxide contents was studied using *p*-toluenesulfonylhydrazide (TSH) as a hydrogenating agent. During hydrogenation, the hydrogenated rubbers were characterized by the decrease in their $\text{C}=\text{C}$ unsaturations and the increase in the number of methylene groups in the macromolecular chain of the original polymer. The changes in the structure of NR and ENRs can be quantitatively detected by using Raman spectroscopy since $\nu(\text{C}=\text{C})$ shows strong intensity. FT-IR and solid-state ^{13}C NMR methods were also used to confirm the microstructure characteristics of the hydrogenated rubbers.

EXPERIMENTAL

Hydrogenation

Natural rubber (NR) was purchased from Thai Rubber Latex. Epoxidized natural rubbers (ENRs) were prepared by epoxidation of NR in latex form using hydrogen peroxide and formic acid as described in the literature.⁹ Two types of ENR were prepared, i.e. ENR-22 (containing 22 mol% epoxide) and ENR-40 (containing 40 mol% epoxide).

Hydrogenation of unsaturated rubbers (NR or ENRs) was carried out as follows. About 2.0 g of rubber were dissolved in 100 ml of xylene (J. T. Baker). A twofold molar excess of *p*-toluenesulfonylhydrazide (TSH, Fluka) compared with rubber unsaturated units ($[\text{TSH}]/[\text{C}=\text{C}] = 2$) was then added to the rubber solution. The mixture was stirred under a nitrogen atmosphere in a thermostated bath at

135 °C. Samples were taken at various reaction times and precipitated in methanol. The hydrogenated rubbers were purified by dissolution in hexane and reprecipitated in methanol. Finally, the product was dried under vacuum at room temperature.

Raman spectroscopy

Raman spectra of all samples were recorded with a Jobin-Yvon T64000 multichannel spectrometer adjusted in a simple spectrograph configuration with a 600 lines mm^{-1} grating and in the triple subtractive configuration for high-resolution experiments. Samples were illuminated with a Coherent argon–krypton ion laser selecting the red 647.1 nm line in order to minimize the contribution of luminescence to the spectra. To improve the signal-to-noise ratio, each spectrum was accumulated 20 times during 30 s. The wavenumber range selected was 500–3200 cm^{-1} . Calibration of the spectrometer was precisely checked on the 520.2 cm^{-1} silicon band and the resolution of the spectra was estimated to be better than 1 cm^{-1} . All experiments were performed at room temperature under a microscope using a $\times 50$ long work distance objective.

FT-IR spectroscopy

FT-IR spectra were measured by using a Perkin-Elmer System 2000 spectrophotometer by casting a thin film of the sample on a NaCl cell. All spectra were recorded in the range 500–4000 cm^{-1} with 4 cm^{-1} spectral resolution.

NMR spectroscopy in the liquid state

^1H NMR data recorded on a Bruker DPX-300 NMR spectrometer were obtained from the samples dissolved in CDCl_3 using tetramethylsilane (TMS) as an internal reference.

NMR spectroscopy in the solid state

High-resolution solid-state ^{13}C NMR experiments were conducted on a Bruker Avance 300 spectrometer operating at 75.47 MHz with a 4 mm cross-polarization magic angle spinning (CP/MAS) probe. The instrument was equipped with a high-power amplifier for proton decoupling. Single pulse experiments combining MAS and ^1H decoupling were carried out using a pulse width of 90° (4 μs) with a repetition time of 4 s. A spectral width of 20 kHz and 16K data points were used for data collection. The MAS technique was applied at 10 kHz. The decoupling radiofrequency was 60 kHz.

RESULTS AND DISCUSSION

The thermal decomposition (135 °C) of TSH as shown in Fig. 2 provides the diimide (N_2H_2) molecule, used to hydrogenate the carbon–carbon double bond of the unsaturated polymer, and *p*-toluenesulfonic acid (TSH) as

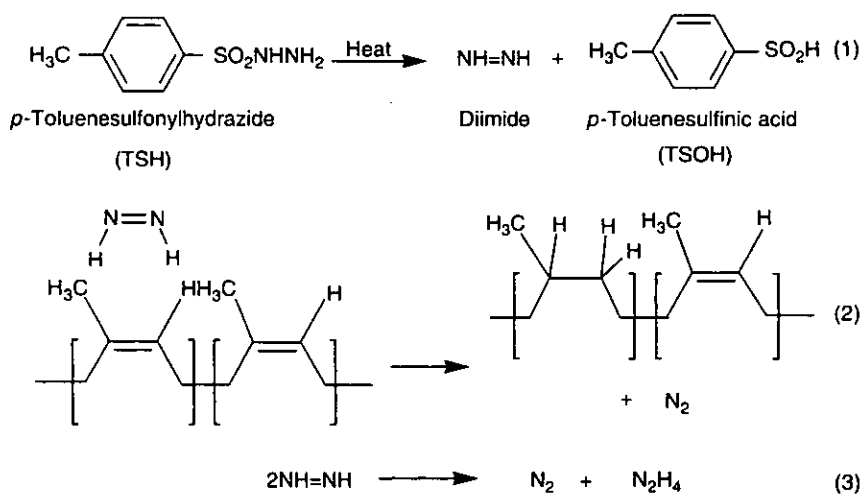


Figure 2. Hydrogenation of *cis*-1,4-polyisoprene units by using the diimide intermediate generated from thermolysis of TSH.

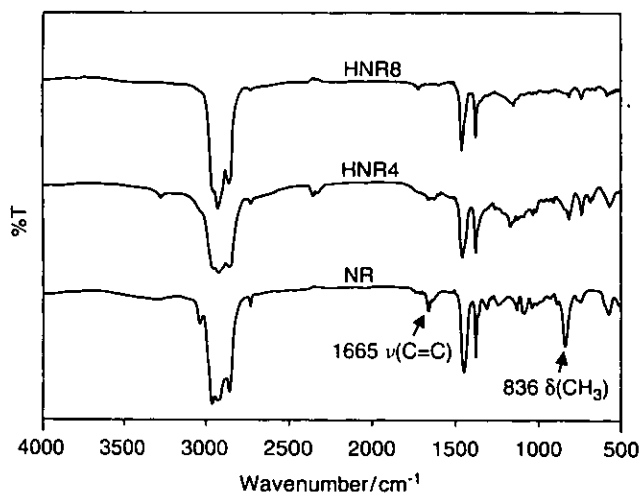


Figure 3. FT-IR spectra of NR and hydrogenated NR after reaction times of 4 h (HNR4) and 8 h (HNR8).

by-product.¹ This hydrogenation procedure, so-called non-catalytic hydrogenation, was performed without the aid of a catalyst.

Generally, 1 mol of TSH produces 1 mol of diimide under suitable conditions, which may give a fully hydrogenated product. It was found in several cases that an excess of about a 4–5-fold excess of diimide compared with the unsaturated units was needed for complete hydrogenation of polyisoprene in homo- and copolymers.^{1,10,15} In our case, a twofold excess of TSH was used to hydrogenate the unsaturated units of NR and ENRs. The FT-IR spectra of NR and ENRs show mainly two characteristic peaks at 1665 and 836 cm⁻¹, attributing to the ν(C=C) and the C–H out-of-plane deformation of the trisubstituted carbon–carbon double bonds of polyisoprene units, respectively. Figure 3 exhibits the decrease in intensity of the 1665 cm⁻¹ line of hydrogenated NRs at various reaction times of diimide

hydrogenation. The disappearance of the C=C signal does not totally occur after 8 h of reaction, because not only does the *syn* form of the generated diimide react with the C=C bonds of polyisoprene units [Eqn (2) in Fig. 2], but also the diimide can undergo disproportionation, leading to the formation of a nitrogen molecule and hydrazine [Eqn (3) in Fig. 2].¹⁵ Similar results were also obtained in the case of hydrogenation of ENRs.

Raman spectroscopic analysis

It is well known that NR possesses a highly regular structure, entirely composed of linear sequences of *cis*-1,4-polyisoprene units. On the basis of the NR structure, the *cis*-1,4-polyisoprene unit possesses a low symmetry point group, probably identical with C_s symmetry of the single unit. This point group was then considered to analyze the number of vibration modes of NR. It is assumed that the CH₃ group of the *cis*-1,4-polyisoprene units is spherical and lies in the same plane with the main-chain atoms and hydrogen. According to classical group theory analysis, the determination of the number of vibration modes was performed and the distribution of the normal modes among the irreducible representations for point group C_s is given by Γ_{vib} = 26A' + 13A". Because of the low symmetry of the unit without any symmetry centre, all the vibrations are both Raman and IR active. A typical recorded Raman spectrum of NR is illustrated in Fig. 4. It can be noted that the number of vibration modes experimentally observed in the Raman spectrum (31 modes) is lower than that predicted by group theory (39 modes).

The observed wavenumbers of the NR can be assigned on the basis of several literature reports on isostructural compounds exhibiting the same kinds of entities or molecular bonds, and are illustrated in Table 1.^{11–13,16,17} The CH₂ and CH₃ stretching vibrations in both symmetric and asymmetric modes typically appear in the 2800–3000 cm⁻¹ range. The strong emission band observed at 1664 cm⁻¹ assigned to



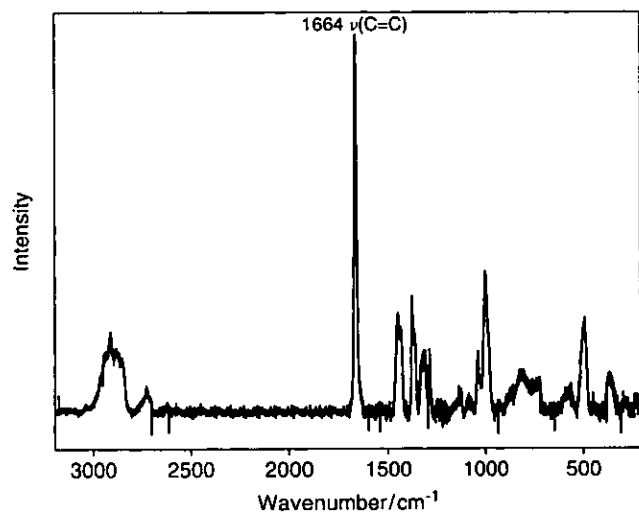


Figure 4. Typical Raman spectrum of NR.

$\nu(\text{C}=\text{C})$ is in good agreement with the literature as $\nu(\text{C}=\text{C})$ is particularly clear and sensitive to its environment. The bands at 1452 and 1432 cm^{-1} are attributed to the C–H deformation of methyl and methylene groups, respectively. The medium bands at 1327 and 1286 cm^{-1} can be attributed to the =C–H deformation in-plane and CH bending mode, respectively.

A comparison between the Raman spectra of the starting NR and hydrogenated NR samples taken at various hydrogenation times is given in Fig. 5. As the hydrogenation reaction progresses, the decrease in intensity of the $\nu(\text{C}=\text{C})$ mode is obviously evidenced together with an increase in the vibrational intensity of the band at 1432 cm^{-1} , which is attributed to the CH_2 deformation vibration. On the other hand, there is no alteration of the intensity of the 1452 cm^{-1} band, which belongs to the asymmetric vibration of CH_3 in the Raman spectrum during hydrogenation. An extra peak at 2925 cm^{-1} corresponding to the C–H stretching vibration of a saturated unit after hydrogenation was also detected. In addition, Raman spectra of hydrogenated rubber products exhibit new characteristic bands at 1299 and 939 cm^{-1} , assigned to the $-(\text{CH}_2)_n-$ in-plane twisting and symmetrical stretching of $-\text{C}-\text{C}-\text{C}-$ modes in the rubber chains.¹⁶

In the case of ENR, the repeating units containing epoxide and isoprene units are randomly arranged in the molecular chains as reported in the literature.¹⁶ Therefore, the number of vibrational modes cannot be determined by group theory. Hydrogenation was performed on two ENRs containing 22 mol% (ENR-22) and 40 mol% (ENR-40) of epoxidized units. Similar results were obtained in both cases. Figure 6 shows the Raman spectra of ENR-22 and hydrogenated samples at various reaction times. Similarly to the hydrogenation of NR, the band at 1664 cm^{-1} corresponding to the C=C bond of ENR significantly decreases during the hydrogenation process. The band at

1452 cm^{-1} due to an asymmetric vibration of the CH_3 group does not change, whereas the intensity of the CH_2 deformation at 1432 cm^{-1} increases with the reaction time. On the other hand, the differences are related to the band characteristics of the epoxide functions of ENR which were identified in the Raman spectra by a weak band at 1248 cm^{-1} associated with another weak line at 833 cm^{-1} assigned to the C–O–C ring vibration of epoxide groups. As a result of hydrogenation, the bands associated with the C–O–C ring vibration of epoxide groups disappeared. Additionally, two distinct extra bands at 1152 and 1592 cm^{-1} are observed and can be assigned to the symmetric $-\text{C}-\text{SO}_2-\text{C}-$ vibration mode and the C=C bond stretching mode of the aromatic ring of the TSOH by-product, respectively, as found by Edwards *et al.*¹⁹ Epoxide ring opening of the ENR was confirmed by the disappearance of the signals in the IR spectrum at 870 and 1250 cm^{-1} characteristic of the C–O–C vibrations of epoxide groups. The band at 3460 cm^{-1} assigned to the O–H stretching of the hydroxy group was also detected as shown in Fig. 7.

The ^1H NMR spectrum of the hydrogenated ENR also gives information to confirm the signal of the aromatic ring of TSOH found at 7.7 ppm. These signals still appear after several purifications by dissolution in hexane and precipitation in methanol. This evidence supports for the chemical fixation of TSOH on the ENR backbone which could occur from the reaction of TSOH with the oxirane ring of epoxidized units during the hydrogenation.

The thermal behavior of the hydrogenated NR and ENR samples was investigated using thermogravimetric analysis (TGA). It was found that the decomposition temperatures of the hydrogenated products of NR and ENR obtained from TGA are higher than those of the starting rubbers by about 60–70 °C. This indicates that the hydrogenation of NR and ENR can improve their thermal stability.

Determination of percentage hydrogenation

In the present study, Raman scattering was demonstrated to be a good technique for monitoring the progress of saturated units in NR and ENR during hydrogenation. The degree of hydrogenation of each sample can be estimated from the ratio of the integrated intensities of the band arising from the stretching mode of the C=C bond at 1664 cm^{-1} and the bending mode of CH_2 at 1432 cm^{-1} , since each addition of a hydrogen molecule to the C=C bond gives rise to one new CH_2 unit as shown in Eqn (2) in Fig. 2. The repeating polyisoprene unit in the rubber already includes two CH_2 groups. The CH_2 bending mode near 1432 cm^{-1} appears to be moderately active, as shown in Fig. 5.

As a first approach, the band intensity in Raman spectra can be roughly considered as proportional to the concentration of each species as follows:

$$A(\text{C}=\text{C}) = k_1[\text{C}=\text{C}]$$

$$A(\text{CH}_2) = k_2[\text{CH}_2]$$

Table 1. Wavenumbers (cm⁻¹) and assignment of bands observed in the Raman spectrum of natural rubber

Literature ^{11-13,16,17}	Experimental ^a	Assignment
3032	3033 vw	=C-H stretching
2962	2965 m	CH ₃ asymmetric stretching
2931	2940 m	CH ₂ asymmetric stretching
2912	2911 s	CH ₃ symmetric stretching
2885	2881 m	— ^d
2854	2850 m	CH ₂ symmetric stretching
2727	2725 vw	— ^d
1666	1664 vs	C=C stretching
1452	1452 m	CH ₃ asymmetric stretching
1440	1432 m	CH ₂ deformation
1375	1371 m	— ^d
1363	1357 m	CH ₂ deformation
1325	1327 m	=C-H in-plane deformation
1311	1314 m	CH ₂ twisting
1287	1286 m	CH bending
1243	1243 w	CH ₂ twisting
1208	— ^c	=C-H in-plane bending
1143	1147 vw	C-H out-of-plane of <i>cis</i> -C(CH ₃)=CH wagging
1131	1130 w	CH ₂ wagging
1040	1039 m	CH ₃ rocking
1000	1000 m	C-CH ₂ stretching
— ^b	983 m	C-CH ₃ stretching
— ^b	840 w	=CH out-of-plane bending
820	815 m	CH wagging
— ^b	788	CH ₂ rocking
— ^b	759 m	CH ₂ rocking
724	729	— ^d
— ^b	596 w	C-C in plane bending
572	569	— ^d
492	491	=CC ₂ rocking and scissoring
428	— ^c	CC ₂ rocking
367	372 w	CC ₂ rocking
— ^b	223 vw	CH ₃ torsion

^a s, Strong; m, medium; w, weak; v, very.

^b Not mentioned in the literature.

^c Not detected in this experiment.

^d No assignment in the literature.

where $A(\text{C}=\text{C})$ is the integrated intensity of the band located between 1645 and 1685 cm⁻¹ assigned to the C=C stretching vibrational mode, $A(\text{CH}_2)$ is the integrated intensity area of the CH₂ bending band between 1415 and 1440 cm⁻¹ and k_1 and k_2 are proportionality constants associated with the C=C and CH₂ vibrational modes, respectively. For NR, it was observed that the CH₂ bending mode was overlapped by the CH₃ bending one at 1452 cm⁻¹. The standard Peakfit software (Jandel Scientific) was then used to resolve areas of $\delta_a(\text{CH}_2)$ band required for the calculation as shown, for instance, in Fig. 8. A Lorentzian shape was assumed to simulate the

Raman bands and the integrated intensities were determined by subtraction of a nearly constant background.

In the case of NR, if 100 repeating units of the starting rubber are considered, 100 C=C and 200 CH₂ units are present, then

$$k_1/k_2 = 2A_0(\text{C}=\text{C})/A_0(\text{CH}_2)$$

where the subscript 0 represents the starting natural rubber. Then, $K = k_1/k_2$ can be determined from the Raman spectrum of NR (see Fig. 4).

If X represents the concentration or the number of the units disappeared or formed, when X C=C units disappear



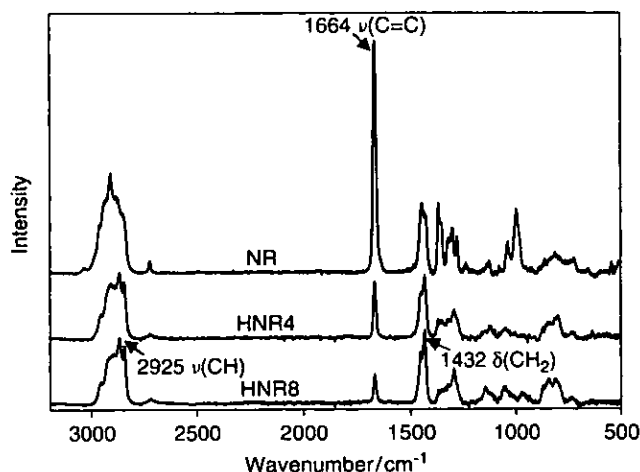


Figure 5. Comparison between the Raman spectra of NR and hydrogenated NR samples taken at 4 h (HNR4) and 8 h (HNR8).

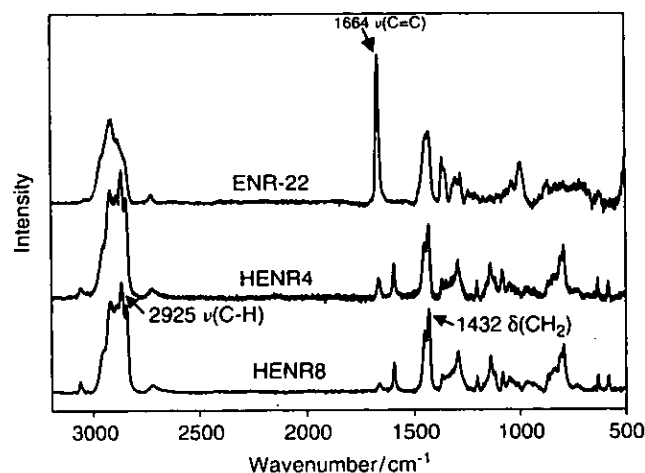


Figure 6. Comparison between the Raman spectra of epoxidized NR containing 22% epoxide (ENR-22) and hydrogenated ENR samples taken at 4 h (HENR4) and 8 h (HENR8).

during the hydrogenation process, it results that X CH_2 units are created. Therefore, for a partially hydrogenated product, X , which is the percentage hydrogenation, can be related to the integrated intensities according to

$$A(\text{C}=\text{C}) = (100 - X)k_1[\text{C}=\text{C}]$$

$$A(\text{CH}_2) = (200 + X)k_2[\text{CH}_2]$$

If we denote $\alpha = A(\text{C}=\text{C})/A(\text{CH}_2)$ of the partially hydrogenated compound, we can easily deduce that

$$X = 100[(K - 2\alpha)/(K + \alpha)]$$

The percentage hydrogenation obtained at various reaction times of NR and ENR hydrogenation is shown in Table 2 and Fig. 9. It was found that the percentage hydrogenation

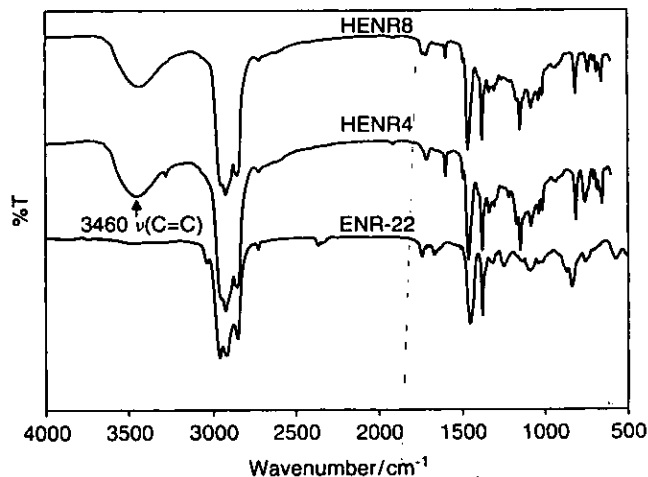


Figure 7. FT-IR spectra of epoxidized natural rubber (ENR-22) and hydrogenated ENR-22 after 4 h (HENR4) and 8 h (HENR8) reaction times.

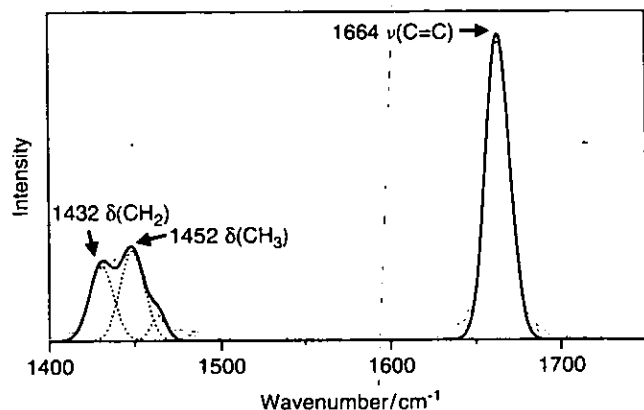


Figure 8. Typical curve fitting of Raman spectrum of natural rubber (Lorentzian shape).

Table 2. Calculation of percentage hydrogenation in hydrogenated rubbers coming from NR, ENR-22 and ENR-40 at various reaction times, by using Raman scattering

Reaction time/h	Hydrogenation/%		
	NR	ENR-22	ENR-40
0	0	0	0
2	43.1	43	84.9
4	73.1	86.5	94.5
6	83.8	95.9	94.2
8	88.5	93.9	95.8

increases with increasing reaction time. The maximum percentage hydrogenation of NR was found to be 89% whereas in the case of ENR-22 and ENR-40 it reached 94% and 96%, respectively. It can be noted that the hydrogenation of ENR is very fast at the early stage of the reaction. It seems likely

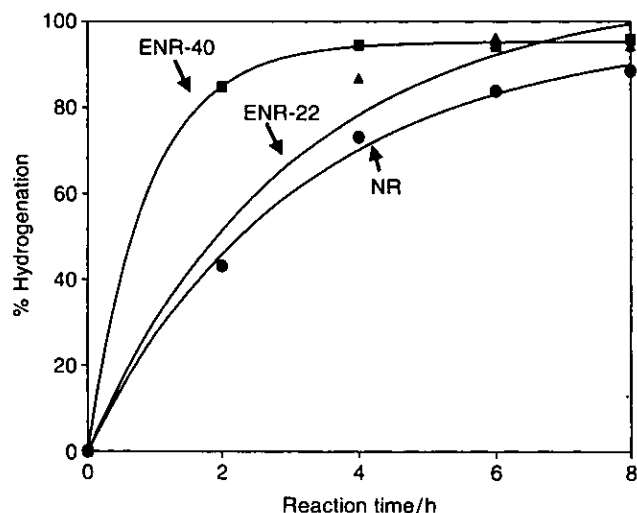


Figure 9. Percentage hydrogenation determined by Raman spectroscopy versus reaction times for NR (●), epoxidized NR containing 22 mol% epoxide (ENR-22) (▲) and 40 mol% epoxide (ENR-40) (■).

that the rate of hydrogenation also increases when the epoxidation level of the rubber is increased and is faster than the hydrogenation of NR. This may be due to the addition of the diimide to the C=C of ENR being less disturbed by the *cis-trans* isomerization, which will be discussed in the next section, than in the case of NR. On the other hand, whatever the rubber considered, the yield of hydrogenation reaches very high values, but the complete hydrogenation of the polyisoprene units could not be obtained in this study. However, complete hydrogenation may be achieved if a larger amount of TSH is employed.

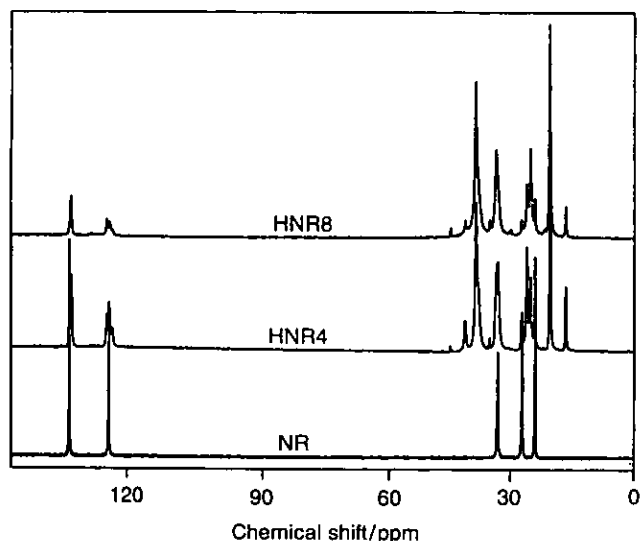


Figure 10. Solid-state ^{13}C NMR spectra of NR and hydrogenated NR after reaction times of 4 h (HNR4) and 8 h (HNR8).

Cis-trans isomerization

It was reported previously that hydrogenation of polybutadiene by using the diimide procedure, resulting in *cis-trans* isomerization, can be clearly identified by FT-Raman spectroscopy.¹⁴ However, the unsaturated units of synthetic *cis*-1,4-polyisoprene and *trans*-1,4-polyisoprene are very difficult to differentiate by Raman spectroscopy because the *cis* and *trans* structures of trisubstituted alkenes give very close wavenumbers in Raman spectra.¹⁷ In our case, this *cis-trans* modification may be suggested by a very weak additional peak close to the 1664 cm^{-1} C=C Raman wavenumber. However, no definitive analysis can be established by Raman spectroscopy for this *cis-trans* isomerization process. In order to check the occurrence of *cis-trans* isomerization in the case of diimide hydrogenation of NR and ENRs, ^{13}C NMR in the solid state was used. Figure 10 shows the ^{13}C NMR spectra of NR and hydrogenated NR obtained after 4 and 8 h of hydrogenation. The dominant peaks of the five carbon atoms of *cis*-1,4-polyisoprene units in NR are noted at δ 23.6, 26.7, 32.5, 134.8 and 125 ppm. With the progress of NR hydrogenation, these characteristic peaks decrease, and in the same time the extra peaks at δ 19.5, 32.8 and 37.1 ppm are observed in the spectra of the hydrogenated NR samples. These signals are assigned to the carbon of the methyl (19.5), methylene (32.8) and methine (37.1 ppm) of saturated units. The observed chemical shifts are in good agreement with those reported in the literature.⁴ Figure 10 also indicates the presence of *trans*-1,4-polyisoprene units located at δ 16, 27 and 40 ppm, assigned to methyl and two methylene carbons, respectively.²⁰ This appears to provide confirmation of *cis-trans* isomerization occurring simultaneously with hydrogenation. It seems likely that in this system the *cis-trans* isomerization is a reversible process. The thermal decomposition of TSH generates a diimide acting as a hydrogen-donor molecule and TSOH as a by-product. The formation of an unstable complex between the carbon-carbon double bonds and the TSOH generated could be responsible for the *cis-trans* isomerization.¹⁰ No signal of the addition of the by-product to the hydrogenated NR was detected.

In the case of hydrogenation of ENRs, an increase in reaction time leads to a decrease in the signal characteristic of the carbon-carbon double bond in the ^{13}C NMR spectrum of *cis*-1,4-polyisoprene, similarly to the hydrogenation of NR. The carbon signal of *trans*-1,4-polyisoprene units was slightly observed. This may be because the TSOH could not play a perfect role in *cis-trans* isomerization as it reacted with the epoxide group of the ENR as detected and mentioned earlier.

CONCLUSIONS

The hydrogenation of NR and its epoxidized derivative ENR was performed by using diimide generated *in situ* from the thermal decomposition of TSH. The progress of



the hydrogenation was followed by FT-IR and Raman spectroscopy. The Raman technique was successfully used to determine the percentage hydrogenation versus reaction times because the characteristic carbon-carbon double bond vibration is strongly Raman active. The microstructure of the hydrogenated product was also followed by ^{13}C NMR spectroscopy. Raman scattering appears to be a highly efficient tool for the determination of the percentage hydrogenation in NR and ENRs. However, the *cis-trans* isomerization of carbon-carbon unsaturation of the hydrogenated NR could be identified only by solid-state ^{13}C NMR spectroscopy.

Acknowledgement

A scholarship from the Ministry of the University Affairs, Thailand, to J. Samran is greatly appreciated.

REFERENCES

- Mango LA, Lenz RW. *Die Makromol. Chem.* 1973; **163**: 13.
- Schulz DN, Turner SR, Golub MA. *Rubber Chem. Technol.* 1982; **55**: 809.
- Singha NK, Bhattacharjee S, Sivaram S. *Rubber Chem. Technol.* 1997; **70**: 309.
- Singha NK, De PP, Sivaram S. *J. Appl. Polym. Sci.* 1997; **66**: 1647.
- Gan SN, Subramaniam N, Yahya R. *J. Appl. Polym. Sci.* 1996; **59**: 63.
- Bhattacharjee S, Bhowmick AK, Avasthi BN. *Polymer* 1993; **34**: 5168.
- Shahab YA, Basheer RA. *J. Polym. Sci., Polym. Chem. Ed.* 1979; **16**: 2667.
- Luo Y. *J. Appl. Polym. Sci.* 1995; **56**: 721.
- Phinyocheep P, Duangthong S. *J. Appl. Polym. Sci.* 2000; **78**: 1478.
- Phinyocheep P, Pasiri S, Tavichai O. *J. Appl. Polym. Sci.* 2003; **87**: 76.
- Jackson KDO, Loadman MJR, Jones CH, Ellis G. *Spectrochim. Acta, Part A* 1990; **46**: 217.
- Koenig JL. *Spectroscopy of Polymers*. American Chemical Society: Washington, DC, 1992; 115.
- Hendra PJ, Jackson KDO. *Spectrochim. Acta, Part A* 1994; **50**: 1987.
- Poshyachinda S, Kanitthanon V. *Spectrochim. Acta, Part A* 1994; **50**: 2011.
- Hahn SF. *J. Polym. Sci., Part A* 1992; **30**: 397.
- Lin-Vien D, Colthup NB, Fateley WG, Grasselli JG. *The Handbook of Infrared and Raman Characteristic Frequencies of Organic Molecules*. Academic Press: London, 1991; 9.
- Bunce SJ, Edwards HGM, Johnson AF, Lewis IR. *Spectrochim. Acta, Part A* 1993; **49**: 775.
- Bradbury JH, Perera MCS. *J. Appl. Polym. Sci.* 1985; **30**: 3347.
- Edwards HGM, Johnson AF, Lewis IR, Maitland DJ, Webb N. *J. Mol. Struct.* 1992; **268**: 363.
- Buzaré JY, Silly G, Emery J, Boccaccio G, Rouault E. *Eur. Polym. J.* 2001; **37**: 85.



Hydrogenation of Unsaturated Rubbers Using Diimide as a Reducing Agent

J. Samran,¹ P. Phinyocheep,^{1,2} P. Daniel,³ S. Kittipoom²

¹Department of Chemistry, Faculty of Science, Mahidol University, Rama VI Road, Payathai, Bangkok 10400, Thailand

²Institute of Science and Technology for Research and Development, Mahidol University, Salaya Campus, Puthamonthon, Nakornpathom, 73170 Thailand

³Laboratoire de Physique de l'Etat Condensé LPEC (UMR CNRS no. 6087) Université du Maine, Avenue Olivier Messiaen, 72085 Le Mans Cedex 9, France

Received 16 October 2003; accepted 14 April 2004

DOI 10.1002/app.20811

Published online in Wiley InterScience (www.interscience.wiley.com).

ABSTRACT: The hydrogenation of natural rubber (NR) and various epoxidized natural rubbers (ENR) was investigated by using diimide generated *in situ* from the thermal decomposition of *p*-toluenesulfonylhydrazide (TSH) in *o*-xylene solution at 135°C. ¹H-NMR analysis indicated that approximately 85–95% of hydrogenation was performed with a twofold excess of TSH. FT-IR and Raman spectroscopy were employed to confirm the microstructure characteristics of the hydrogenated rubbers. The *cis*–*trans* isomerization was also observed by ¹H- and ¹³C-NMR. The signal in ¹H-NMR of the epoxide group of the ENR disappears after hydrogenation while the signal of the opened epoxide

ring product was detected. This may be due to the epoxide ring opening reaction caused by the *p*-toluenesulfonic acid by-product. The high temperature of the reaction condition leads to chain degradation in both NR and ENR. Thermal behaviors of the hydrogenated rubbers characterized by differential scanning calorimetry showed that the glass transition temperatures of the hydrogenated rubbers were increased about 10–20°C compared with the starting rubbers. © 2004 Wiley Periodicals, Inc. *J Appl Polym Sci* 95: 16–27, 2005

Key words: elastomers; hydrogenation; isomerization; modification; NMR

INTRODUCTION

Chemical modification of existing polymers has been an active field of research as it leads to polymers with altered and improved properties or production of new materials. Unsaturated polymers, especially diene rubbers, are useful targets for chemical modification, because the double bonds in the polymer chains are prone to chemical reactions such as epoxidation, halogenation, and maleinization.¹ However, the polymers containing olefinic units have a tendency to be low-heat-resistant materials. Hydrogenation is a useful method for the reduction of unsaturation in diene rubbers.^{2,3} It improves the thermal and oxidative stability of their parent polymers. For instance, hydrogenated nitrile butadiene rubber (HNBR) has been known to be a new oil-resistant elastomer with superior abrasion resistance at elevated temperatures. These properties provide more applications for HNBR in the automotive, military, and aerospace industries. Hydrogenated butadiene rubber (HBR) has good aging, heat and abrasion resistance, and improved dy-

amic properties, therefore HBR is part of the rubber formulation for tire treads.⁴

The hydrogenation of unsaturated polymers can be performed with elemental hydrogen in the presence of a transition metal catalyst or by a noncatalytic method, using an inorganic reagent such as diimide (N₂H₂).^{1,4} Special equipment is normally required to perform catalytic hydrogenation because the reaction is carried out at a high temperature under high pressure. Additionally, various factors influence the catalytic hydrogenation, such as types of catalyst that affect the selectivity of hydrogenation and solvents that influence not only the solubility of reactants and resulting products but also the activity of catalysts.

Hydrogenation of polyisoprene is a rather complicated case of unsaturated polymers. The isopropenyl groups constituting the rubber chains are trisubstituted ethylene derivatives; they should be hydrogenated with a lower rate than mono- and disubstituted ethylenes. The process is even more complicated by virtue of the high molecular mass of polyisoprene obtained from natural rubber, due to its poor segmental mobility. Unfortunately, this condition has an adverse effect on product because increasing chain stiffness causes even greater restriction of chain mobility. Therefore, the use of catalytic hydrogenation of polyisoprene requires high temperatures and high pressures and considerable amounts of catalyst, and longer reaction

Correspondence to: P. Phinyocheep (scppo@mahidol.ac.th).



times.⁵ The severe conditions of catalytic hydrogenation, i.e., high pressure and high temperature, may cause degradation and difficulty in removing residual catalysts. Therefore, a moderate condition using other mild reducing agents has been explored and is preferred. Diimide used to hydrogenate the unsaturated rubbers can be conveniently prepared at atmospheric pressure with relatively simple apparatus and procedures. It is considered a noncatalytic hydrogenation process and has become increasingly popular. Diimide can be generated from various chemicals via the oxidation of hydrazine, the decarboxylation of potassium azodicarboxylate, and the thermal treatment of arenesulfonylhydrazides.⁵⁻⁷ Among these reducing agents, the thermal decomposition of *p*-toluenesulfonylhydrazide has been widely used to hydrogenate the unsaturated unit in diene rubbers. Mango and Lenz employed noncatalytic hydrogenation to convert BR, IR, and SBR copolymers to high-heat-resistance polymers.⁶ Hardwood *et al.*³ reported the hydrogenation of unsaturated polymers, i.e., polybutadiene and polyisoprene by using diimide as a reducing agent. They found that the complete reduction could be obtained when five moles of TSH per mole of double bonds of butadiene or isoprene units was employed. Similar results were obtained in the case of isoprene-styrene diblock copolymers.⁸

Natural rubber (NR) and epoxidized natural rubber (ENR) are unsaturated rubbers with excellent elastic properties. The ENR also has good oil resistance upon epoxidation. However, both NR and ENR have primary drawbacks of poor thermal and oxidative resistances due to the unsaturated unit on the backbone. Singha *et al.*⁹ reported that catalytic hydrogenation of NR using RhCl(PPh₃) catalyst increased the thermal stability of the resulting product without affecting its glass transition temperature. The hydrogenation of NR using a homogeneous catalyst prepared from nickel 2-ethylhexanoate and triisobutylaluminum can lead to 100% hydrogenation under optimum reaction conditions.¹⁰ For ENR, the presence of the epoxy group should influence the reaction condition of hydrogenation and properties of the resulting rubbers. A few studies have been conducted on catalytic hydrogenation of ENR. Bhattacharjee *et al.*¹¹ hydrogenated the NR and ENR by using a homogeneous palladium-macrocyclic catalyst and found that the rate constant of hydrogenation decreases with an increase in the epoxide content of the rubber. This article describes the hydrogenation of NR and different epoxide levels of ENR by using the diimide reducing agent generated from the decomposition of *p*-toluenesulfonylhydrazide (TSH). The progress of the reaction determined by ¹H-NMR, IR, and Raman techniques is reported including the *cis-trans* isomerization evidence.

EXPERIMENTAL

Materials

Natural rubber latex was procured from Thai Rubber Latex Corporation (Thailand) Public Company Limited. The NR for hydrogenation was obtained from precipitation of the NR latex in methanol and it was then dried under vacuum at room temperature. Different types of ENR were prepared in latex form by using *in situ* performic acid generated from hydrogen peroxide and formic acid, according to the procedure outlined in the literature.¹² ENR22, ENR33, and ENR40 represent ENR containing 22, 33, and 40% epoxide levels, respectively, determined by ¹H-NMR. *p*-Toluenesulfonylhydrazide, which is a practical grade product from Fluka, and *o*-xylene, which is a product from JT Baker, were used as purchased.

Hydrogenation procedure

Hydrogenation of unsaturated rubbers (NR or ENR) was carried out in a 250-ml three-necked round-bottomed flask, equipped with a magnetic stirring, a reflux condenser, and a nitrogen inlet tube. A solution of 1% (w/v) rubber in *o*-xylene was used with a molar ratio of TSH to unsaturated unit ([TSH]/[C=C]) equal to 2. The reaction took place at 135°C under nitrogen atmosphere. The solution was sampled at various reaction times and precipitated in methanol. The hydrogenated product was purified by dissolution in hexane and reprecipitation in methanol. Finally, the product was dried under vacuum at room temperature.

Characterization of products

FT-IR spectroscopy

The chemical structure of the rubber samples was investigated by FT-IR (Perkin-Elmer System 2000 Fourier transform infrared spectrometer) spectroscopy. The samples were dissolved in distilled chloroform and then cast onto a NaCl cell. All samples were taken at 16 scans in the range of 4,000–600 cm⁻¹ with 4 cm⁻¹ resolution of spectra to obtain a good signal-to-noise ratio.

Raman spectroscopy

The Raman spectra of all samples were recorded on a T64000 Jobin-Yvon multichannel spectrometer adjusted to be a simple spectrograph configuration with a 600 line/nm grating. Samples were illuminated with a Coherent Argon-Krypton Ion Laser using the 647.1 nm line to avoid luminescence bands. To improve the ratio of signal/noise, each spectrum was accumulated 20 times during 30 s. The frequency range collected was 500–3,200 cm⁻¹. Calibration of the spectrometer was



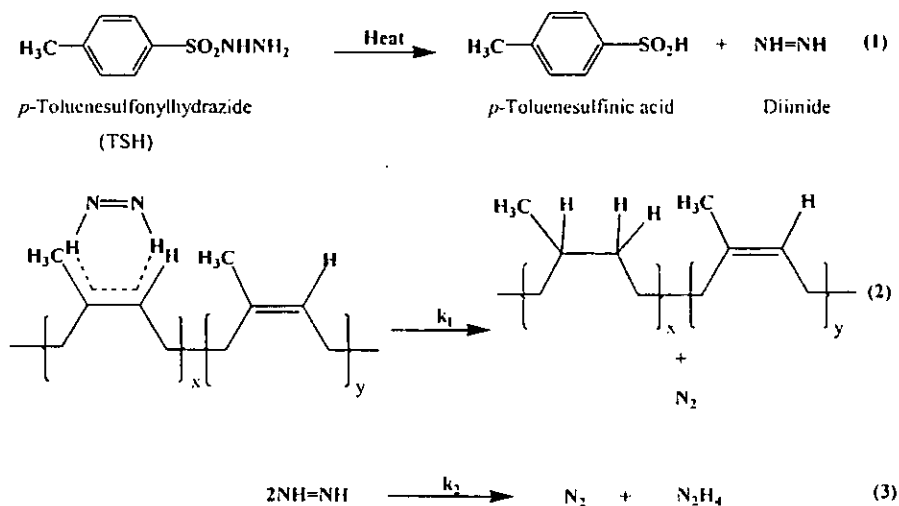


Figure 1 Hydrogenation of polyisoprene unit by *p*-toluenesulfonylhydrazide (TSH): (1) decomposition of TSH by thermal treatment, (2) reaction of diimide and polyisoprene unit, and (3) disproportionation of diimide.

precisely checked on the 520.2 cm^{-1} silicon band and the resolution of spectra can be estimated to be smaller than 2 cm^{-1} .

Nuclear magnetic resonance spectroscopy

$^1\text{H-NMR}$ and $^{13}\text{C-NMR}$ (Bruker DPX-300 NMR spectrometer) were used to identify the chemical structure of the rubbers before and after hydrogenation. NMR spectra were obtained from the samples dissolved in CDCl_3 using tetramethylsilane (TMS) as an internal reference.

Determination of molecular weight by viscometry

The intrinsic viscosity, $[\eta]$, of samples was measured using an Ubbelohde viscometer at 30°C . The viscosity average molecular weight $[M_v]$ was evaluated by the Mark-Houwink equation as shown below

$$[\eta] = KM_v^a$$

The Mark-Houwink constants, $K = 33.1 \times 10^{-3}$ and $a = 0.71$, were used to estimate the M_v in toluene at 30°C .¹³

Differential scanning calorimeter (DSC)

The thermal behavior of the rubber sample was made on a DSC (Perkin Elmer DSC 7) under the scanning temperature from -100 to 150°C at a heating rate of $10^\circ\text{C}/\text{min}$ with the sample mass of 10 mg encapsulated in aluminium pans. The glass transition temperatures (T_g) of hydrogenated products were measured from a DSC thermogram.

Thermogravimetric analysis (TGA)

The thermal stability of all samples was investigated by using TGA (Perkin-Elmer thermogravimetric analyzer 2000) in an atmosphere of nitrogen. The sample weight was 7–10 mg. The heating rate was $10^\circ\text{C}/\text{min}$ and the temperature range was 30 – 500°C .

RESULTS AND DISCUSSION

Noncatalytic hydrogenation of NR and three types of epoxidized natural rubbers (ENR22, ENR33, and ENR40) was carried out by using 2 moles of TSH compared to the unsaturated unit. In principle, 1 mole of TSH generates 1 mole of diimide molecule under suitable condition [eq. (1) in Fig. 1]. The reduction could be conducted to highly specific hydrogen addition in a syn configuration [eq. (2) in Fig. 1]. Therefore, a 1 : 1 molar ratio should give complete hydrogenation. Several authors reported that 4 to 5 moles of hydrazide per mole of isoprene units are required for complete hydrogenation of homopolymers or copolymers containing a polyisoprene segment.^{6,8} In our case, the molar ratio TSH/[C=C] of 2 : 1 was used to hydrogenate the unsaturated unit of NR and ENR. Partial hydrogenation is expected to occur in both cases. As described in the literature, the diimide could undergo disproportionation giving nitrogen and hydrazine as shown in eq. (3) of Figure 1. In addition, the rate of disproportionation (k_2) was reported to be faster than that of the reaction between diimide and double bonds of diene polymers (k_1).¹⁴

Hydrogenation of NR

The microstructure of HNR can be investigated by $^1\text{H-NMR}$ as the signal of the proton adjacent to the



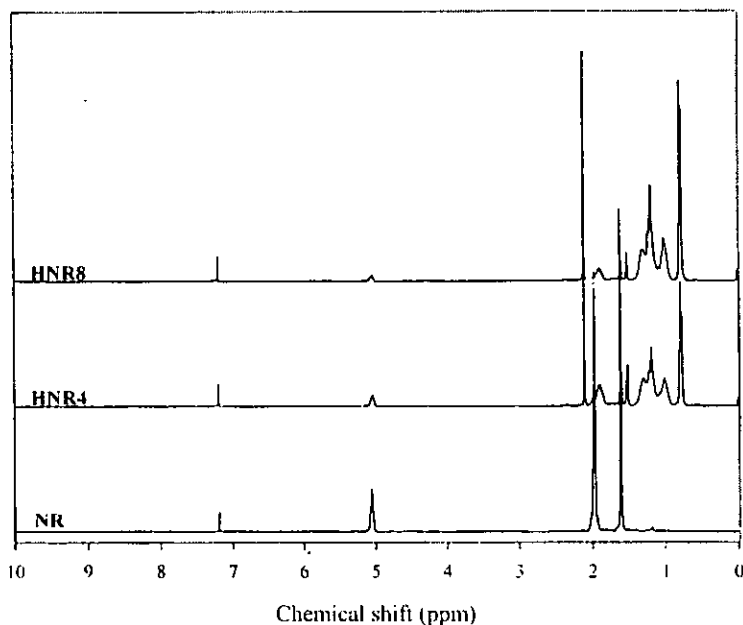


Figure 2 $^1\text{H-NMR}$ spectra of natural rubber (NR) and hydrogenated NR obtained at 4 (HNR4) and 8 h (HNR8).

double bond decreases as the hydrogenation proceeds. Figure 2 shows the $^1\text{H-NMR}$ spectra of NR and the products of hydrogenation after 4 and 8 h of the reaction, symbolized as HNR4 and HNR8, respectively. It can be seen that the signal of the proton adjacent to the unsaturated unit of the hydrogenated NR at 5.12 ppm decreases with the increase of reaction time, as well as the decrease of signal at 1.67 ppm characteristic of the methyl proton of *cis*-1,4 polyisoprenic (PI) structure of NR. The appearance of the signals at 0.84 and 1.1–1.3 ppm, which represent methyl and methylene protons of the saturated unit, confirms the hydrogenation reaction.¹⁰ The integrated areas of the signal at 5.12 and 0.84 ppm, corresponding to the olefinic unit and methyl proton of saturated unit, respectively, were used for the determination of the percentage of hydrogenation. The results of hydrogenation up to 8 h of reaction times are displayed in Table I. It can be seen that as the reaction time increased, the degree of hydrogenation increased. The $^1\text{H-NMR}$ spectrum of the hydrogenated rubber also exhibits another extra signal at 1.60 ppm, which can be assigned to the methyl proton of *trans*-1,4-polyisoprenic unit. The percentage of the remaining double bonds in *cis* and *trans* structures of the hydrogenated samples at various reaction times is shown in Table I. The results demonstrate that, after 2 h of hydrogenation, *cis*–*trans* isomerization occurs and the concentration of the *trans* units increases at longer reaction times (4 h). However, at longer reaction times (6 h), the *trans* structure converts into the *cis* structure as the concentrations of the *cis* and *trans* units become equal. After a further increase in reaction time to 8 h, percent

hydrogenation increases and the *trans* unit obtained is slightly higher than the *cis* unit. It is proposed that in this system the *cis*–*trans* isomerization is reversible. The evidence of *cis*–*trans* isomerization is similar to polybutadiene and isoprene–styrene diblock copolymer, reported in the literature.^{8,15} The formation of an unstable complex between the double bond and the *p*-toluenesulfonic acid by-product may cause the *cis*–*trans* isomerization reaction.⁸ No fixation of the by-product on the rubber molecule was detected by $^1\text{H-NMR}$.

$^{13}\text{C-NMR}$ spectra of the HNR and NR are compared in Figure 3. The extra peaks at 19.5, 32.8, and 37.1 ppm are observed in the HNR sample. These signals correspond to the carbon of the methyl, methylene, and methine of the saturated unit. The observed chemical shifts are in good agreement with those reported in

TABLE I
Results of % Hydrogenation and *cis* and *trans*
Microstructures of Hydrogenated Rubbers at Various
Reaction Times

Reaction time (h)	Hydrogenation ^a (%)	<i>Cis</i> structure ^b (%)	<i>Trans</i> structure ^b (%)
0	0	100	0
2	44.4	33.8	21.8
4	67.4	15	17.6
6	78.6	10.7	10.7
8	84.4	6.8	7.8
10	87.5	6.5	6.9

^a Determined by $^1\text{H-NMR}$.

^b Remaining double bonds in *cis* and *trans* configurations, i.e., % *cis* + % *trans* = 100 – % hydrogenation.



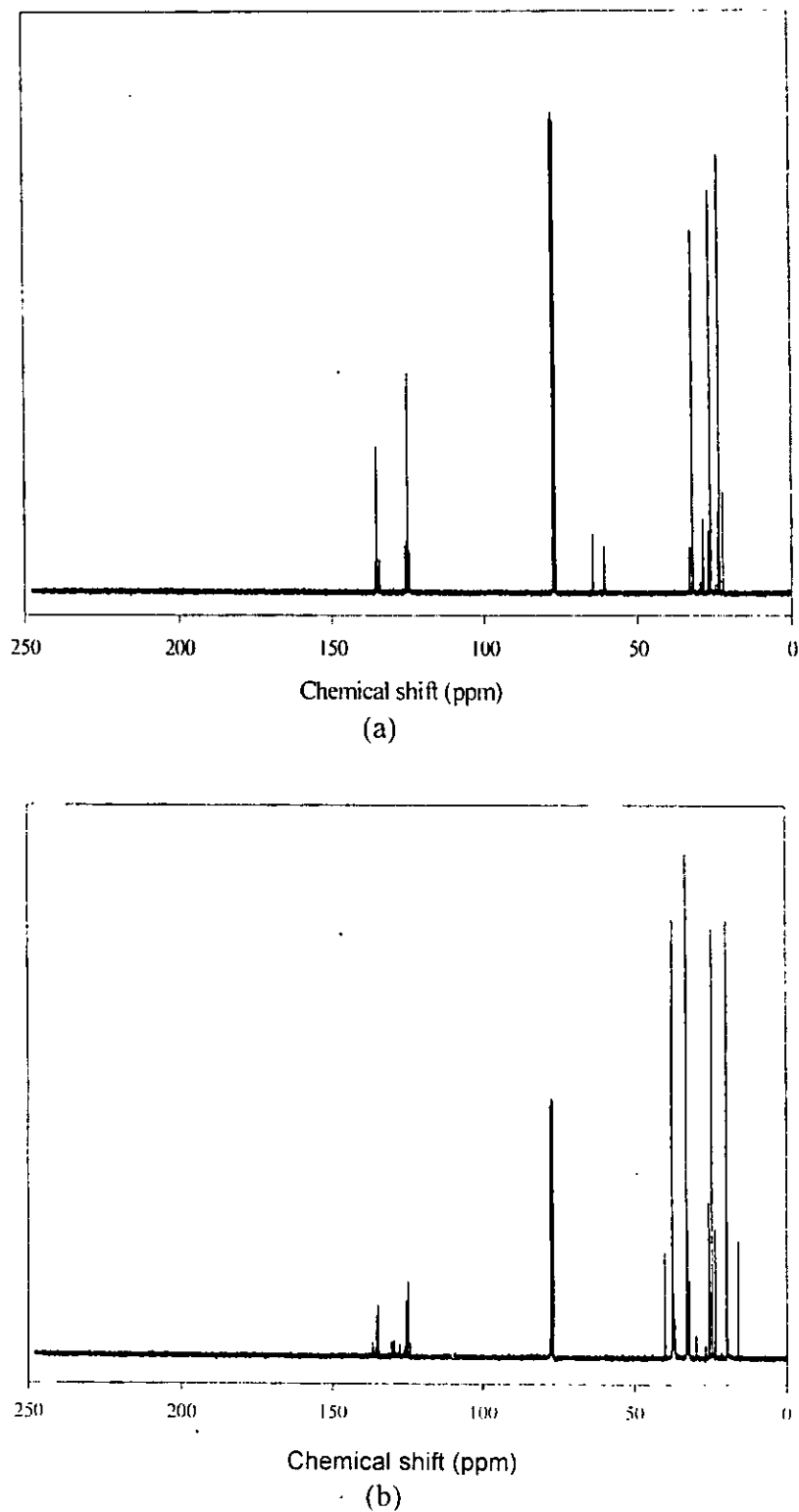


Figure 3 ^{13}C -NMR spectra of (a) natural rubber and (b) hydrogenated NR obtained at 8 h.

the literature.^{9,16} The ^{13}C -NMR spectrum of the partially hydrogenated product reveals evidence of the *cis-trans* isomerization of the isoprene unit in polymer chains. The carbon signals of the *cis* structure are positioned at 135.2 and 125.5 ppm while the signal at

134.9 and 124.7 ppm, corresponding to olefinic carbons of the *trans*-polyisoprenic structure, are also detected for HNR.

IR spectra of NR and HNR are depicted in Figure 4. The IR spectrum of NR exhibits two important char-



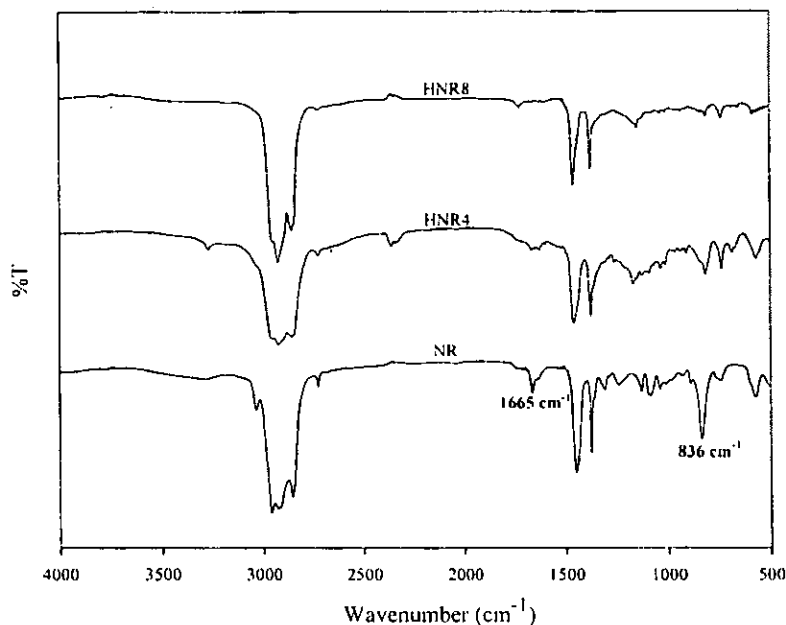


Figure 4 IR spectra of natural rubber and hydrogenated rubbers (HNR4 after 4 h and HNR8 after 8 h of reaction time).

acteristic peaks at $1,665$ and 836 cm^{-1} , attributing to the C=C stretching mode and the C-H out of plane deformation of the trisubstituted olefinic of polyisoprene, respectively. As the hydrogenation reaction proceeds, the intensity of the peaks at $1,665$ and 836 cm^{-1} are gradually decreased. Moreover, the appearance of peak at 735 cm^{-1} , assigned to the $-(\text{CH}_2)-$ groups of the hydrogenated products, is clearly observed.

Raman scattering technique can be used to follow the evolution of the hydrogenation reaction at various reaction times. The C=C stretching vibration is strongly active in Raman spectroscopy. The strong signal of C=C of NR is observed at $1,663\text{ cm}^{-1}$ as shown in Figure 5. Upon hydrogenation, the decrease of this signal is clearly detected with the appearance of the signal at $1,430\text{ cm}^{-1}$, attributed to the $-\text{CH}_2-$ deformation vibration. No alteration of the peak at $1,452\text{ cm}^{-1}$ belonging to an asymmetric vibration of the $-\text{CH}_3$ group in the Raman spectrum is illustrated after hydrogenation. Unfortunately, the *cis-trans* isomerization of the unsaturated unit of NR during hydrogenation cannot be detected, as the vibration frequency of the *cis* and *trans* structures of trisubstituted olefin in Raman spectrum is very close.¹⁷

Hydrogenation of ENR

Figure 6 shows the typical $^1\text{H-NMR}$ spectra before and after hydrogenation of ENR, containing 22 mol % of epoxidation level. Major peaks of ENR are observed in the aliphatic region at 1.6–2.03 ppm and the olefinic region at 5.12 ppm, while the oxirane group is ob-

served at 2.70 ppm. With the progress of hydrogenation, the area of the olefinic peak of hydrogenated ENR (HENR) decreases considerably compared with the starting rubber. Concurrently, a peak at 0.84 ppm assigned to the signal of the methyl proton of the saturated unit increases with the addition of reaction time. The results of hydrogenation of the three types of ENR at various reaction times are shown in Table II.

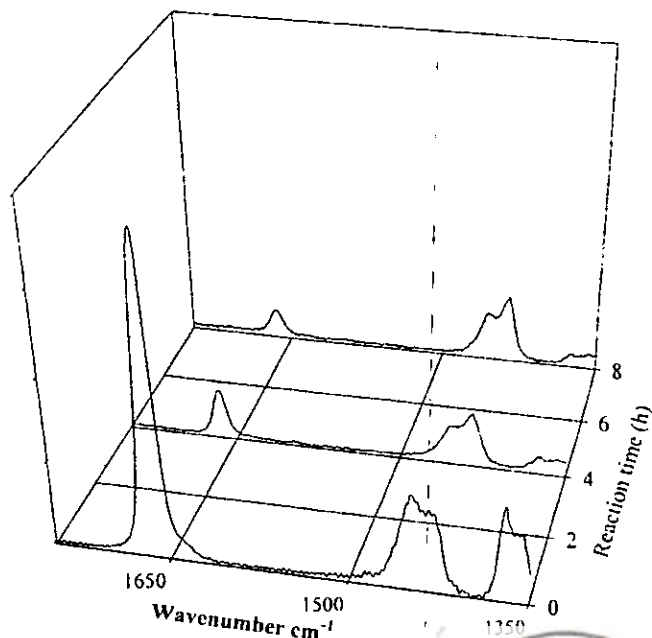


Figure 5 Raman spectra of natural rubber and hydrogenated rubbers obtained at 4 and 8 h.

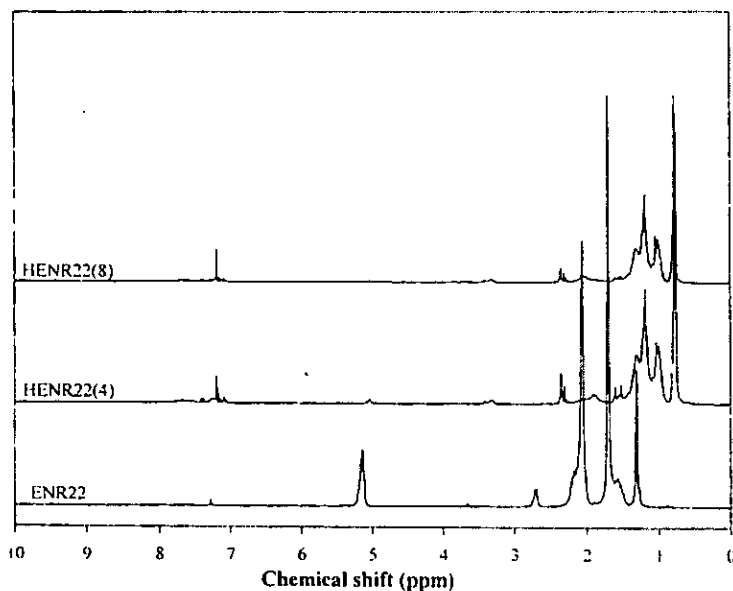


Figure 6 $^1\text{H-NMR}$ spectra of ENR22 and hydrogenated ENR22 samples obtained at 4 and 8 h reaction times [HENR22(4) and HENR22(8)].

It can be observed that the hydrogenation of ENR is very fast at the early stage of the reaction. It seems likely that the rate of hydrogenation increases with increasing epoxide levels and much faster than the hydrogenation of NR. These results are in contrast to the work reported by Bhattacharjee *et al.*¹¹ using a homogeneous palladiumacetate catalyst for hydrogenation of ENR. In their case, they explained that the presence of the epoxide group might coordinate with the metal center, which competed with the coordination of the metal-hydride complex with the carbon-carbon double bond of the rubber, hence decreasing the rate of hydrogenation when the amount of the epoxide group increased. But in our case, the diimide generated from the decomposition of TSH directly react with the double bond of the polyisoprenic unit, which is preferably at the *cis* structure. In the case of NR, there was *cis-trans* isomerization, which might be due to the formation of an unstable complex between

the double bond and *p*-toluenesulfonic acid by-product. But in the case of ENR, the formation of the epoxide ring-opened product and the addition of *p*-toluenesulfonic acid on the rubber chain were found, which will be discussed later in this section. Therefore, it can be proposed that the by-product might not interfere much at the double bond during hydrogenation reaction but rather it goes to the epoxide group on the molecular chain. Therefore, by increasing the epoxide content, the possibility that the *p*-toluenesulfonic acid encounters the epoxide unit increases, resulting in a decrease in the interference at the double bond of the rubber chain, therefore the hydrogenation reaction of ENR is much faster than that of NR. It was found that the signal of the proton at 5.12 ppm almost disappears at the 6-h reaction time in all cases of ENR. It may be postulated that the degree of hydrogenation is about 100% at this duration.

It is also noted in Figure 6 that the signal of the proton at 2.7 ppm disappears in all HENRs. The observation of extra signals in $^1\text{H-NMR}$ at 1.83, 3.40, and 3.87 ppm can be assigned to signals of a methylene proton of a large membered ring, a proton at the α -position of the hydroxyl group, and a methine proton. The epoxide ring-opened product may occur by the influence of *p*-toluenesulfonic acid by-product, followed by the furanization process as schematized in Figure 7. The epoxide ring is protonated, followed by the formation of the ring-opened product containing carbocationic intermediate. The epoxide ring at the adjacent unit then reacts with the carbocationic intermediate forming a furan unit. Propagation of furanization then proceeds with the other epoxide groups. A termina-

TABLE II
Results of % Hydrogenation of Various Types of Epoxidized Natural Rubbers^a at Various Reaction Times

Reaction time (h)	Hydrogenation (%)		
	ENR22 ^a	ENR33 ^a	ENR40 ^a
0	0	0	0
2	71.3	78.0	89.0
4	92.9	89.2	95.9
6	96.2	96.0	98.3
8	97.7	97.4	99.3

^a Contain 22, 33, and 40 mole % epoxide groups, respectively.



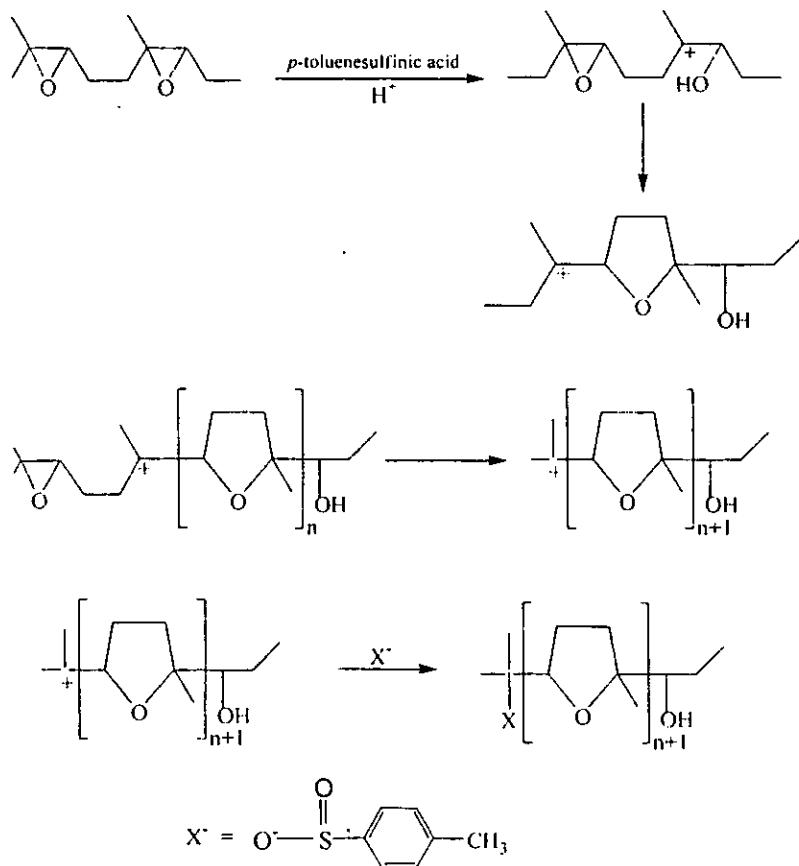


Figure 7 Schematic representation of the furanization of epoxidized 1,4-polyisoprene.

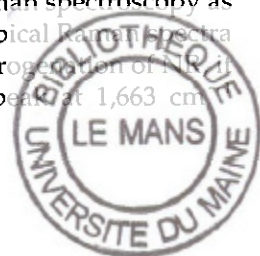
tion reaction can then occur by the fixation of the *p*-toluenesulfinate anionic group, resulting in the fixation of *p*-toluenesulfonic acid by-product onto the rubber chain. The formation of secondary epoxide ring-opened product so-called furanization also occurred on the preparation of epoxidized natural rubber when high concentrations of peroxyacid and elevated temperatures were employed.^{18,19} The ¹H-NMR spectrum of the hydrogenated ENR reveals the signal at 7.70 ppm, corresponding to the signal of aromatic ring of *p*-toluenesulfonic group.³ This signal is not observed in the case of HNR.

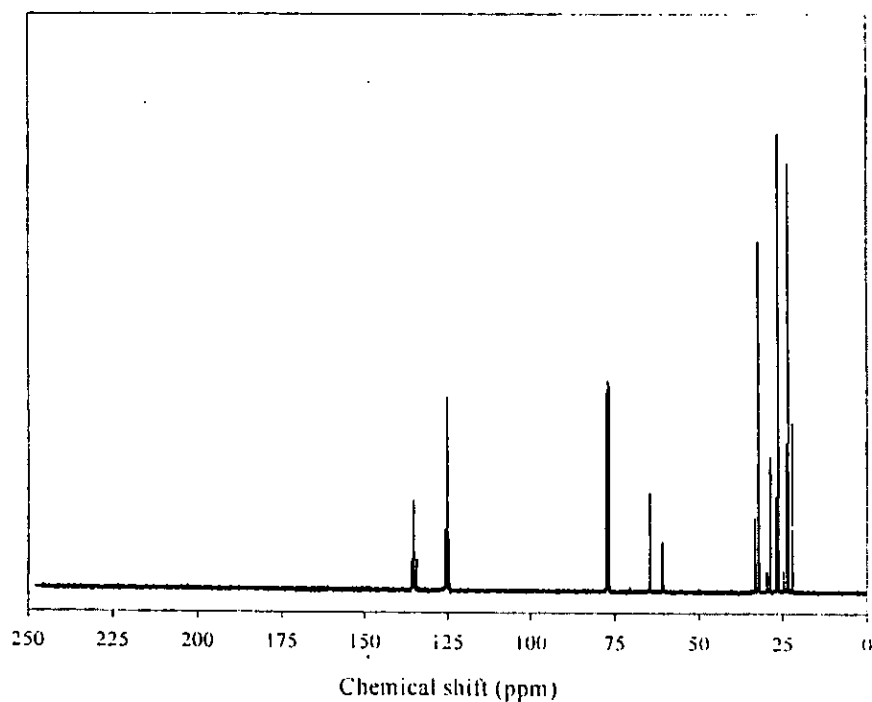
The ¹³C-NMR spectrum of partially epoxidized natural rubber is shown in Figure 8(a). The characteristics of ENR are observed at 60.8 and 64.5 ppm, attributed to the methine carbon and the quaternary carbon resonances of the oxirane ring, respectively. The peaks at 126 and 135 ppm are the olefinic double-bond carbons in the unmodified polyisoprene units. Similar to HNR, the ¹³C-NMR spectrum of HENR in Figure 8(b) exhibits signals at 37.5, 32.8, and 19.7 ppm. These results are assigned to the methine carbon of the saturated unit and carbons of methyl and methylene, respectively. The ¹³C-NMR spectrum of HENR also supports evidence of furan ring formation at 82 ppm.²⁰

Infrared spectra of ENR and HENR were recorded in the wavenumber range of 500–3,500 cm⁻¹, as

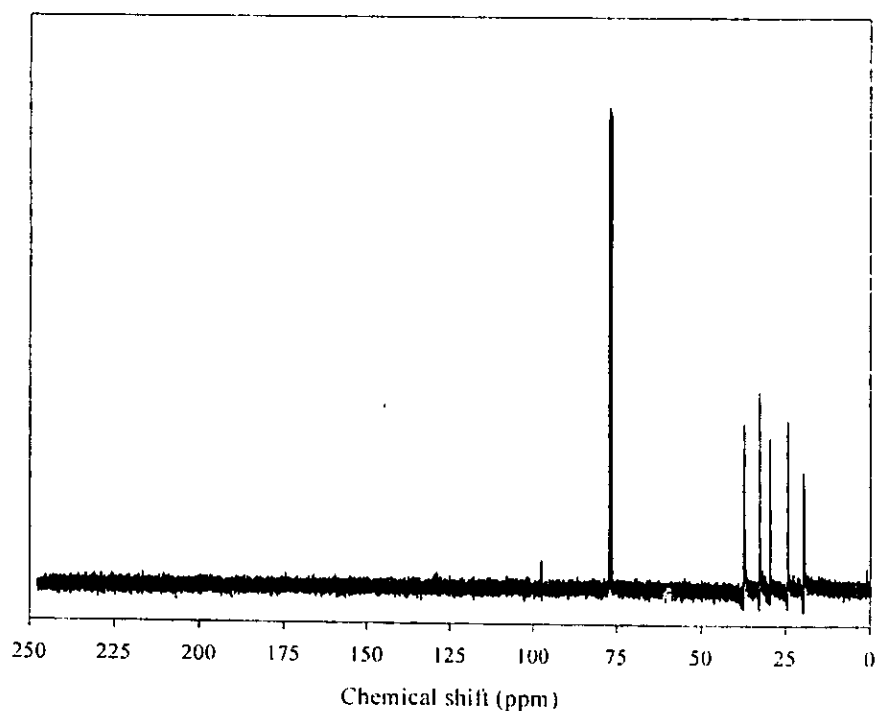
shown in Figure 9. The –CH₂ deformation vibration is exhibited in the region of 1,452 cm⁻¹. A sharp peak appears at 1,377 cm⁻¹ due to the deformation vibration of the –CH₃ group. Two distinct peaks for the C–O–C of epoxy group are observed at 870 and 1,250 cm⁻¹ of ENR while the out of plane deformation of *cis* double bond is positioned at 836 cm⁻¹. The IR spectrum of HENR reveals the decrease of signals at 1,665 and 836 cm⁻¹, contributing to the C=C bond and the characteristic of *cis*-polyisoprene in the backbone. The characteristic of the oxirane ring in IR spectra also disappears after hydrogenation, as a result of ring opening during hydrogenation as proposed earlier. The strong absorption band at 3,450 cm⁻¹ is the O–H stretching of the hydroxy group. The IR spectrum of HENR also contains the signal contributing to SO₂ asymmetric and symmetric stretching at 1,334 and 1,145 cm⁻¹, respectively. These signals are not eliminated after several precipitations in nonsolvent. This evidence supports the fixation of *p*-toluenesulfonic acid on the ENR backbone. The peaks at 811 and 1,035 cm⁻¹ correspond to the *p*-tolyl aromatic ring.²¹

The characterization of microstructures of ENR and HENR was also carried out by Raman spectroscopy as shown in Figure 10. This shows typical Raman spectra of ENR and HENR. Similar to hydrogenation of ENR, it can be obviously seen that the peak at 1,663 cm⁻¹





(a)



(b)

Figure 8 ^{13}C -NMR spectra of (a) ENR22 and (b) hydrogenated ENR22.

corresponding to the C=C bond of ENR decreases significantly after hydrogenation, while the peak at $1,452\text{ cm}^{-1}$ belonging to an asymmetric vibration of

the CH_3 -group did not alter after hydrogenation. From Raman scattering, the bands at $1,350$ and $1,152\text{ cm}^{-1}$ are depicted as asymmetric and symmetric -C-



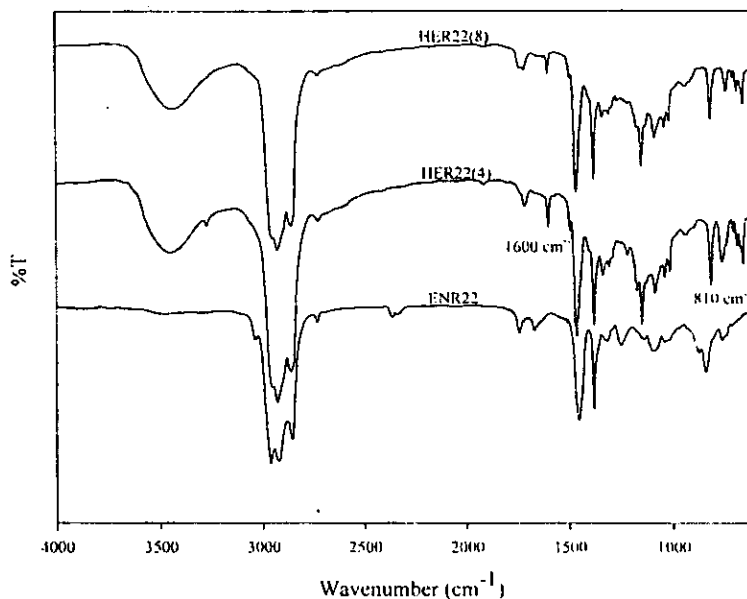


Figure 9 IR spectra of ENR22 and hydrogenated ENR22 samples obtained at 4 and 8 h.

SO₂-C-vibration, respectively. The appearance of the band at 1,592 cm⁻¹, assigned to the C=C stretching mode of aromatic ring, may confirm that *p*-toluenesulfonic acid attacks the rubber backbone of ENR.

Side reactions

Beside the *cis-trans* isomerization of C=C in the case of NR, the treatment of NR with TSH at 135°C causes the

chain cleavage as the percent hydrogenation increases. The decrease of viscosity average molecular weight of the HNR is observed as shown in Table III. Similar results of chain degradation are obtained in the case of hydrogenation of ENR by TSH. The *cis-trans* isomerization cannot be observed for HENR. The *p*-toluenesulfonic acid by-product of the decomposition of TSH induced the epoxide ring-opening reaction of ENR, leading to formation of furan and the fixation of the by-product on the rubber chain as described by IR, ¹H-NMR, and Raman spectroscopy.

Thermal behavior

TGA of NR, ENR, and the hydrogenated derivatives was measured under nitrogen atmosphere. TGA thermograms of NR and HNR are illustrated in Figure 11. The HNR begins to lose its weight starting from

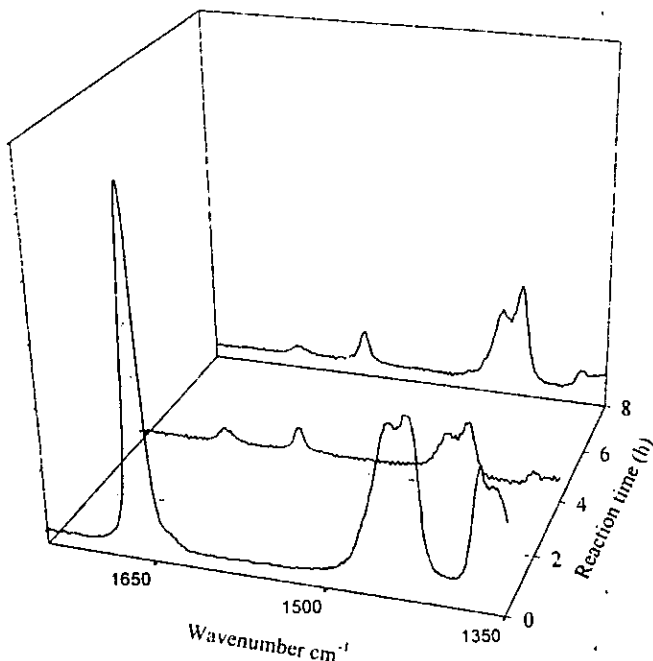


Figure 10 Raman spectra of ENR22 and hydrogenated ENR22 samples obtained at 4 and 8 h.

TABLE III
Results of Glass Transition Temperature and Decomposition Temperature of NR, ENR, and Hydrogenated Rubbers

Sample	M _v	Hydrogenation (%)	T _g (°C)	T _d (°C)
NR	912,000	—	-66.1	377
HNR8	288,000	86.7	-42.7	449
ENR22	—	—	-40	381
HENR22(8) ^a	—	97.7	-31.1	450
ENR33	—	—	-37.6	390
HENR33(8) ^a	—	97.4	-14.4	449
ENR40	—	—	—	368
HENR40(8) ^a	—	99.3	—	415

^a Hydrogenation was carried out during 8 h.



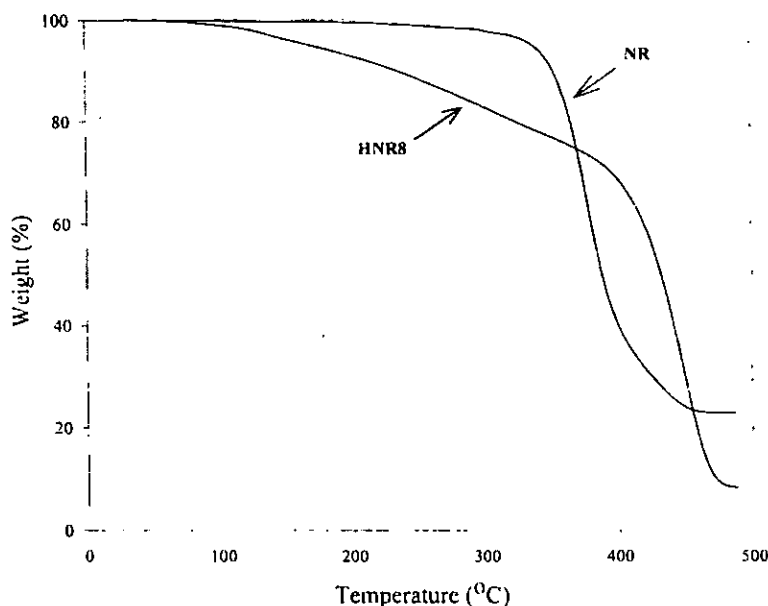


Figure 11 TGA thermograms of natural rubber (NR) and hydrogenated natural rubber (HNR).

around 100°C at about 20%, the complete decomposition temperature of HNR is around 450°C, which is higher than that of the NR (about 350°C). One reason may be the M_v of the HNR ($M_v = 288,000$) is much lower than that of the NR ($M_v = 912,000$). For another reason, the HNR is the partial hydrogenation product of NR, therefore the residual unsaturated units that are located in a random manner in the molecular chain might be degraded in the first place, while the rigid part obtained after hydrogenation can resist the high temperature applied for a longer time. The decomposition temperatures (T_d) of the hydrogenated products of ENR are higher than those of the starting rubbers by about 60–70°C (Table III).

The heat required for molecular deformation of polymers, i.e., glass transition temperature (T_g), was recorded on DSC. T_g of the HNR and HENR are shown in Table III. It was found that the T_g of the rubber is increased by 20–30°C after hydrogenation. The increase in T_g results from the higher amount of saturated units, that is, the segmental mobility decreases. In addition, the *trans* microstructure obtained by *cis-trans* isomerization of residual double bonds may also result in the enhancement of T_g in the case of the hydrogenated NR. For HENR, T_g increases with higher epoxide contents in the starting sample. The result shows that T_g of HENR based on 40 mol % of epoxide content is higher than that of HENR (22 and 30 mol % of epoxide level). This might be because the rigid part in the rubber chains of HENR40 after hydrogenation contains a higher amount of the furan ring structure, which leads to less segmental mobility of the molecular chain.

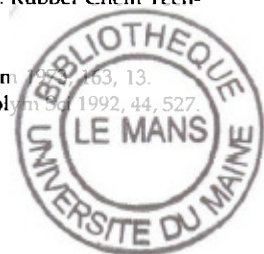
CONCLUSION

The hydrogenation of natural rubber and various epoxidized natural rubbers were investigated by using diimide generated *in situ* from the thermal decomposition of *p*-toluenesulfonylhydrazide in *o*-xylene solution at 135°C. The percentage hydrogenation was determined by $^1\text{H-NMR}$ technique. The microstructure of the hydrogenated product was observed by IR, ^1H , and $^{13}\text{C-NMR}$ as well as Raman techniques. The *cis-trans* isomerization was also observed from $^1\text{H-NMR}$ and $^{13}\text{C-NMR}$ spectra in the case of hydrogenated NR, while furanization and addition of *p*-toluenesulfinic acid on the HENR were obviously detected. Thermal behaviors of the hydrogenated rubbers characterized by differential scanning calorimetry showed that the glass transition temperatures of the hydrogenated rubbers were increased about 10–20°C compared with the starting rubbers.

The scholarship from the Ministry of the University Affairs, Thailand, to J. Samran is greatly appreciated.

References

- Schulz, D. N.; Turner, S. R.; Golub, M. A. *Rubber Chem Technol* 1982, 55, 809.
- Rempel, G.; Mohammadi, N. *Macromolecules* 1987, 20, 2362.
- Harwood, H. J.; Russell, D. B.; Verthe, J. A.; Zymonas, J. *Makromol Chem* 1973, 163, 1.
- Singha, N. K.; Bhattacharjee, S.; Sivaram, S. *Rubber Chem Technol* 1997, 70, 309.
- Luo, Y. *J Appl Polym Sci* 1995, 56, 721.
- Mango, L. A.; Lenz, R. W. *Makromol Chem* 1971, 163, 13.
- Podesva, J.; Spacek, P.; Konak, C. *J Appl Polym Sci* 1992, 44, 527.



8. Phinyocheep, P.; Pasiri, S.; Tavichai, O. *J Appl Polym Sci* 2003, 87, 76.
9. Singha, N. K.; De, P. P.; Sivaram, S. *J Appl Polym Sci* 1997, 66, 1647.
10. Gan, S. N.; Subramaniam, N.; Yahya, R. *J Appl Polym Sci* 1996, 59, 63.
11. Bhattacharjee, S.; Bhowmick, A. K.; Avasthi, B. N. *Polymer* 1993, 34, 5168.
12. Phinyocheep, P.; Duangthong, S. *J Appl Polym Sci* 2000, 78, 1478.
13. Subramaniam, A. *Rubber Chem Technol* 1972, 45, 346.
14. Hahn, S. F. *J Polym Sci Part A: Polym Chem* 1992, 30, 397.
15. Poshyachinda, S.; Kanitthanon, V. *Spectrochim Acta* 1994, 50A, 2011.
16. Shahab, Y. A.; Basheer, R. A. *J Polym Sci Polym Chem Ed* 1979, 17, 919.
17. Bunce, S. J.; Edwards, H. G. M.; Johnson, A. F.; Lewis, I. R. *Spectrochim Acta* 1993, 49A, 775.
18. Perera, M. C. S.; Elix, J. A.; Bradbury, J. H. *J Polym Sci Part A: Polym Chem* 1988, 26, 637.
19. Gelling, I. R. *J Nat Rubber Res* 1991, 6, 184.
20. Perera, M. C. S.; Ishiaku, U. S.; Ishak, Z. A. M. *Polym Degrad Stab* 2000, 68, 393.
21. Edwards, H. G. M.; Johnson, A. F.; Lewis, I. R.; Maitland, D. J.; Webb, N. *J Mol Struct* 1992, 268, 363.



CHAPTER 1

INTRODUCTION

Natural rubber (NR) is not only an important industrial material, particularly in the tyre industry, but is also used in the manufacture of various products including household, engineering, medical, and commercial goods. *Hevea brasiliensis*, a tropical tree, is a major source of the world's rubber [1]. Thailand has approximately 5 million acres of rubber plantations located mostly in the southern and eastern parts of the country and is the world's largest rubber producer followed by Indonesia and Malaysia with these three countries producing around 90% of the world's natural rubber.

The NR is chemically known as *cis*-1,4 polyisoprene and consists of ten thousands of linked isoprene molecules. It has a uniform microstructure that provides the material with very unique and important characteristics, namely the ability to crystallize under strain, a phenomenon known as “strain-induced crystallization” [2]. The rubber products made from NR possess very useful technical characteristics e.g. tensile strength, resilience (very low hysteresis), excellent flexibility and resistance to impact and tear, low heat-built-up, plus good “green” strength and building tack [2, 3]. However, owing to its high *cis*-1,4 polyisoprene structure containing unsaturated units, its primary drawbacks include low thermal and oxidative stability and ozone resistance. These inherent drawbacks apparently cause limitations in versatility of NR usage, particularly for technical and engineering applications. Modification of NR through chemical manipulation of the rubber chain would induce certain special properties.

Chemical modification of various commercially available polymers has been an active field of research as it leads to polymer with altering and improving the properties or production of new materials [4-7]. Unsaturated polymers, especially diene rubbers, are useful targets for chemical modification, because the double bonds in the polymer chains are prone to varieties of chemical reactions such as epoxidation



halogenation, and maleinization [5-10]. The chemical modification of NR is one of alternative methods to increase its value and to develop versatile applications of NR.

Hydrogenation is one of the most important methods for enhancement of physical and mechanical properties of the macromolecules. It is also a method offering a polymer that cannot be prepared by a simple conventional polymerization reaction. An example is the preparation of poly (ethylene-alt-propylene), which can be obtained by fully hydrogenation of synthetic polyisoprene and NR [11, 12]. The hydrogenation of unsaturated rubbers has been carried out. The hydrogenated rubbers have good resistance to oxidative and thermal degradation, improved weathering, and better processibility comparing with the unmodified rubbers [13]. For instance, hydrogenated nitrile butadiene rubber (HNBR) has been known to be an excellent heat and oil resistance combined with superior mechanical properties [14]. These properties provide more applications for HNBR in automotive industry, military and aerospace. Hydrogenated butadiene rubber (HBR) has good aging, heat and abrasion resistance and improved dynamic property, therefore, the HBR takes part in rubber formulation for tire treads. Hydrogenated styrene-butadiene (HSBR) and hydrogenated styrene-isoprene (HSIR) block copolymers were developed and used as thermoplastic elastomers [15-18]. These materials can be also used as compatibilizers and impact modifiers for various polymer blends [15-17]. The HSIR was also applied as a viscosity index improver in lubricants [18].

The hydrogenation of unsaturated rubbers can be carried out by both catalytic and non-catalytic methods [6, 11-13]. In catalytic hydrogenation, hydrogen molecules react with the double bonds of unsaturated units with the aid of a noble metal catalyst. The important aspects to be considered are the type and nature of catalyst, its activity, selectivity, occurrence of side reactions, catalyst poisoning and problems associated with recycling of catalysts. In order to avoid these problems, the non-catalytic hydrogenation has been developed. This process concerns the reduction of carbon-carbon double bond of polyisoprene using diimide molecule as a hydrogen-releasing agent. This methodology is of interest because it can be easily performed at atmospheric pressure with simple apparatus and procedure. Without the addition of a catalyst, the non-catalytic hydrogenation process become increasingly popular and it can be applied in organic solvent or aqueous medium. The hydrogenation reaction can



be carried out at room temperature or elevated temperatures (110 to 160°C) depending on the compound generating diimide molecule. *p*-Toluenesulfonylhydrazide (TSH) is one of the mostly used hydrogen-generating molecule. It undergoes decomposition at 130-140°C to form reactive diimide (N_2H_2), which subsequently releases hydrogen molecule to the carbon-carbon double bonds. The reaction is generally carried out in aromatic solvent. Partial hydrogenation of NR would provide an equivalent product of ethylene-propylene diene (EPDM) rubber, which can lead to the rubber having higher thermal and oxidative resistance and better chemical resistance than the original NR.

The oxidation of hydrazine by hydrogen peroxide is another efficient in-situ generation of diimide. The reaction is feasible in aqueous medium; therefore a new direction to hydrogenate NR in latex system can be developed. This strategy is beneficial as the reaction can be performed with the NR latex without the need to coagulate the NR and the dissolution of the NR. Potential applications of such lattices may include gloves, thin walled tubing, paints, adhesives, rust proof coatings, etc. The advantage of the hydrogenated rubbers is that it preserves the characteristic of the elastic behaviour of unsaturated part and the stiffness part of saturated fraction. Moreover, they provide thermal and oxygen stability and in extreme service environments by improving creep resistance, tear and impact strengths.

Epoxidized natural rubber (ENR), which is one of the polar-modified forms of NR, shows similar disadvantages as NR, caused by the presence of residual double bonds in the macromolecular chains. Therefore, attempts to reduce the amount of the carbon-carbon double bonds in NR and ENR by means of hydrogenation reaction have been explored [12, 19-21].

The chemical structure of rubber and its modified form has been principally observed by the vibration and resonance spectroscopy techniques. Generally, infrared spectroscopy (IR) and nuclear magnetic resonance, both 1H - and ^{13}C -NMR spectroscopies are the important techniques to characterize the microstructure of the rubber and chemically modified products [11-13, 19-22]. IR technique has been used for qualitative analysis whereas the quantitative analysis has mostly been studied by NMR spectroscopy. The characterization of elastomers by Raman spectroscopy has long been used, as the stretching vibration mode of carbon-carbon double bond is sensitive to its environment in a similar but much clearer way than by the IR [22].



This technique was successfully used for investigating the change in the microstructure particularly the carbon-carbon double bond of hydrogenated polybutadiene [25].

In this present thesis, hydrogenation of NR and epoxidized NR (ENR) were investigated by using non-catalytic process using TSH and oxidation of hydrazine by hydrogen peroxide. Vibrational (i.e. Raman and infrared) and nuclear magnetic resonance spectroscopic techniques (i.e. ^1H - and ^{13}C -NMR) were employed to investigate the chemical structure of the hydrogenated rubbers. Raman scattering, ^1H - and ^{13}C -NMR were used to quantify the degree of hydrogenation. In addition, the molecular characteristic of the rubber chain was investigated to elucidate the correlation between the molecular behavior and macroscopic property of the materials after modification.



CHAPTER 2

OBJECTIVES

The principal goal of this research is to investigate the hydrogenation of natural rubber (NR) and four types of epoxidized NR (ENR) by using non-catalytic hydrogenation. The reaction system was performed into two procedures. The first one was the study carried out in organic solvent for NR and ENR using *p*-toluenesulfonylhydrazide (TSH). The second one is the study in latex system for NR using hydrazine and hydrogen peroxide. The study of the molecular characteristic and the property of the hydrogenated products were also included.

The scope of this present thesis is divided into 3 parts.

Part I: Hydrogenation by using *p*-toluenesulfonylhydrazide (TSH)

This part concerns the study of hydrogenation of NR and ENRs in an organic solvent. The reaction was carried out in xylene solution using the amount of TSH to C=C ratio equal to 2 at 135°C.

The study of various characterization techniques to analyze the hydrogenation level and chemical structure of the hydrogenated rubber was carried out. IR and ¹H-NMR in liquid state were used in the first place to characterize the characteristic of the starting rubbers and their hydrogenated products. Then, Raman scattering and solid state ¹³C-NMR techniques were introduced for evaluation of the hydrogenation level of hydrogenated products compared with ¹H-NMR in liquid state

The study of the side reaction and by-product occurred from hydrogenation using TSH was also included.

Part II: Hydrogenation by using hydrazine and hydrogen peroxide

In this part, the study of hydrogenation of NR in latex phase was performed using diimide generated *in situ* from the reaction of hydrazine and hydrogen peroxide. The investigation of various parameters affecting the hydrogenation level of NR in



aqueous system, such as reaction time and temperature, amount of reagents, dry rubber content and type of NR were planned to be carried out.

Part III: Study the molecular characteristic and physical properties of hydrogenated NR

To examine the correlation between of hydrogenation level on the thermal and rheological properties of the hydrogenated products, various techniques will be performed.

- The investigation of the molecular characteristic of the macromolecular chains after modification will be carried out using Raman and ^{13}C -NMR in solid state.

- The effect of hydrogenation content on the thermal properties of the hydrogenated products will be investigated using DSC and TGA.

- The rheological characteristic of the hydrogenated rubber will be examined by Rubber Process Analyzer and modified torsional dynamic rheometer with Fourier transform analysis.

- To study the heterogeneity of the hydrogenated rubbers in micro-scale level, Raman mapping technique will be applied.



CHAPTER 3

LITERATURE REVIEW

3.1 General Description of Natural Rubber

Natural rubber (NR) is a high molecular weight hydrocarbon obtained from plants. It consists of 320 to 35,000 isoprene units in its molecular structure. Among the rubber producing plant species, the Brazilian rubber tree named *Hevea brasiliensis* is the only commercial source at present, due to its high rubber content and exceptional quality. *Hevea* rubber is typically high *cis*-1,4 polyisoprene with a very wide range of molecular weight distribution. The NR is what one usually calls an elastomer, that is, it recovers its shape after being stretched or deformed. Normally, the NR is treated with sulfur to give its chains having been crosslinked, which makes it better elastic behavior. Therefore, it can be applied in various rubber products such as tyre and glove.

3.1.1 Natural Rubber Latex

The *Hevea* latex contains the rubber particles accumulated in specialized cell vessels known as laticifers [26]. The latex collected by regular tapping consists of the cytoplasm expelled from the latex vessels. The opening of latex vessels by tapping cuts causes the latex flow out due to the high turgor pressure inside. The latex flow will continue for a certain period of time and subsequently stop because of coagulation of the rubber particles at incision of the bark.

Fresh NR latex is a white fluid of density between 0.975 and 0.980 g/cm³ with pH ranging from 6.5 to 7.0. The NR latex can be fractionated into three major layers by ultracentrifugation (see Figure 3.1). The top rubber layer comprises almost entirely of rubber, the middle fraction is the metabolic active aqueous phase called C-serum



and the sedimented bottom fraction (BF). The BF is mainly composed of membrane-bound organelles called lutoids. However, it has been reported in some literatures that yellowish orange layer containing Frey-Wyssling particles is found at the interface between the top rubber layer and the C-serum as seen in Figure 3.1. The Frey-Wyssling complexes are also found at the upper border of the sedimented bottom fraction in some cases. Typical components of fresh NR latex, apart from water, are summarized in Table 3.1 [27, 28].

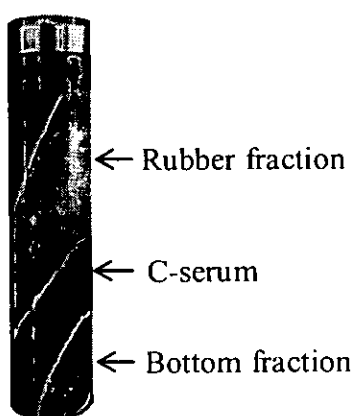


Figure 3.1 Three major zones of fresh NR latex obtained by using ultracentrifugation [27].

Table 3.1 Typical composition of fresh natural rubber latex

Component	Content (%w/v)
Rubber hydrocarbon	25-45
Proteinous substances	1-2
Carbohydrate	1-2
Lipids	0.9-1.7
Organic solutes	0.4-0.5
Inorganic substances	0.4-0.6

- Rubber phase

The top rubber phase contains mainly the rubber hydrocarbon having the chemical structure as *cis*-1,4 polyisoprene unit and it also includes some non-rubber constituents mainly proteins and lipids adsorbed as a layer on the rubber particles as well as some enzymes. The rubber hydrocarbon content is varying from 25 to 45% as dry content of latex, with a spherical shape having its size ranging from 5 nm to 3 μ m. Molecular weight analysis performed by gel permeation chromatography shows a bimodal distribution of rubber, with average values of 100-200 kDa and 1000-2500 kDa [27].

The rubber particles appear homogeneous having a uniform structure, enclosed by a thin film membrane as examined by electron microscopy [29]. It has been mentioned that the film layer surrounded the rubber particles is more opaque than the polyisoprene contained inside. The nature of film is believed to be non-rubber components such as phospholipids and proteins, together with neutral lipids. These components are distributed as colloidal charges covering the rubber particle and play a role on the stability of the latex.

-C-serum

The C-serum fraction of the centrifuged latex is the aqueous phase of laticiferous cytoplasm. The composition of C-serum phase comprises a wide variety of chemical species of many high molecular weight compounds, low molecular weight organic solutes and mineral elements. The high molecular weight compounds are proteins and specific nuclei acids. One C-serum protein presenting at the highest level is α -globulin, which has high binding affinity for adsorption onto rubber particles. Several enzymes are found in the C-serum named rubber transferase. This enzyme has an importance for the formation of rubber molecules. Low molecular weight organic compounds comprise sugars, amino acids, nucleotides, and nitrogenous bases among many others.

-Bottom fraction

The bottom fraction obtained from ultracentrifugation contains mainly luteoids and Frey-Wyssling particles. The luteoid content of latex constitutes 20% by volume.



fresh latex, whereas the rubber phase forms an average of 30-40%. Lutoid is spherical shape, and the diameter is larger than that of rubber particles. Their compositions can be considered as having two distinct components, namely the lutoid membrane and the internal contents, referred to as B-serum. Electron microscopy showed the micellar nature of the lutoid membrane structure [30]. Analysis of the membrane chemical composition indicated the phospholipids content of 37.5% by weight of proteins. The lutoids membrane has been shown to be very rich in phosphatidic acids. Thus, they play an important role in the colloidal stability of latex due to the negative charge of phosphatidic acids onto membrane layer.

Frey-Wyssling particles are the major components of the vivid yellow layer due to the presence of carotenoid. There is mostly spherical non-rubber particle, with diameter ranging from about 3 to 6 μm and slightly higher density than the rubber hydrocarbon.

- Non-rubber substances

The *Hevea* latex contains about 4-5% non-rubber constituents which are presented and distributed in all the three latex fractions. Proteineous substances and lipids are mostly found in this category. The main component of nitrogenous substances is protein, which represents about 1-2 % in the rubber latex. The protein in fresh natural rubber latex can be presented in three parts of latex as follows: 27 % is adsorbed on the surface of rubber particles, 25 % in bottom fraction, and 48 % in C-serum fraction. It has been reported that there could be more than 200 different proteins present in the latex.

Lipids are located in the rubber fraction with a small amount in the bottom fraction and Frey-Wyssling complexes. Lipids can be classified into two types namely neutral (acetone extractable) and polar lipids (glycolipids and phospholipids). The neutral lipids composed of more than 14 substances including sterols, sterol esters, and free fatty acids, which are able to dissolve into rubber particles while the polar lipids are found strongly adsorbed onto the surfaces of rubber particles.

Several inorganic components are also found in the rubber latex. Main components include potassium and magnesium. The magnesium was found to play an important role on the mechanical stability of the latex.



3.1.2 Manufacturing of NR Latex

On tapping the *Hevea brasiliensis* tree, the latex exuded contains rubbers varied between 25 to 40 %w/v. The variations depend on several factors such as the clones of rubber tree, tapping methods, soil condition and season. The latex from the small holder is preserved with ammonia (0.05-0.2%) and normally sold in its original rubber concentration. In the market, the NR latex is mostly found as high content of rubber so called high ammonia (concentrated) natural rubber (HANR) latex. Recently due to the problem of protein allergy, the NR latex is served as deproteinized form named as deproteinized natural rubber (DPNR) latex.

(a) High Ammonia Natural Rubber (HANR) Latex

The original form of NR latex contains quite high water content which makes high cost for transportation therefore centrifugation technique has been applied in the latex manufacture to reduce the amount of water practically to make the latex having about 60 % or more of dry rubber [31]. Ammonia solution (about 0.05-0.2%) is added to preserve the latex for long storage. The use of ultracentrifugation machine in latex manufacture can provide the separation of the rubber parts from the non-rubber components and water called skim latex. Skim latex is considered as a by-product of the latex concentrated production. It contains about 5-10% rubber and some non-rubbers in the serum phase.

(b) Deproteinized Natural Rubber (DPNR) Latex

As mentioned earlier that the *Hevea* latex contains some non-rubber constituents in which proteins are believed to be the cause of allergic problem to some particular persons. However, the specific type of allergic protein among more than a hundred proteins present in the latex is not known at present. Partial elimination of proteins from the *Hevea* latex has been developed for such purpose. The contribution of the proteins in the latex may be associated at the rubber particle as well as the soluble proteins in serum fraction. To eliminate the proteins from the NR latex, some researchers have applied double centrifugations, while others have used proteolytic enzyme to incubate the NR latex before applying double centrifugation technique [32, 33]. In both cases, surfactant has been employed for dispersion of the rubber fraction



into emulsion form after each centrifugation step. The latex obtained is called deproteinized NR (DPNR). It has been proposed that the proteolytic enzyme breaks down the peptide linkages selectively, while the surfactant such as sodium dodecyl sulfate (SDS) washes out the resulting oligopeptides in the course of centrifugation. Tangpakdee et. al. had reported that 0.016% w/w of the nitrogen content found in DPNR is less than that of fresh field NR latex (0.231% w/w) [33]. In addition, the gel content in the rubber from fresh field latex was reduced from 5% to 3% after deproteinization. It is believed that the deproteinization process decomposed the branch points of the rubber.

3.2 Chemical Modification of Natural Rubber

Natural Rubber (NR) known as *cis*-1,4 polyisoprene has excellent physical properties as already mentioned in previous Chapter. However, NR along with other synthetic diene rubbers like polybutadiene (PB), and styrene butadiene rubber (SBR) have disadvantages such as poor heat and oil resistance, high air permeability and low aging resistance. Chemical modifications of NR have been applied not only to overcome these drawbacks but also to diversify the use of NR. Some examples of the chemical modification of NR are as the followings.

3.2.1 Bond Rearrangement Reaction

In this category, there is normally no major addition of any foreign atoms into the molecular chain but it involves the rearrangement of the molecular structure resulting in modifying the property of the original NR.

(a) *Cis-trans* Isomerization

The distinct characteristic of NR is its highly *cis*-1,4 polyisoprenic structure. The transformation of the *cis*-structure into the *trans*-form will certainly affect on the properties of NR. The *cis-trans* isomerization of the 1,4-polyisoprenic structure of the NR can be achieved by treating it with selenium, thiol acids, disulfides, sulfur dioxide, butadiene sulfone, and related materials [4, 6]. In commercial practice, butadiene



sulfone, which produces sulfur dioxide (SO_2) *in situ* from its thermal decomposition, is used. The *cis-trans* transformation is assumed to involve the reversible addition of SO_2 to the carbon-carbon double bonds, forming an unstable complex as seen in Figure 3.2. The SO_2 -catalyzed isomerization at 140°C has been found to result in an equilibrium *cis/trans* ratio of polyisoprene of 43/57 [6]. The reaction with SO_2 does not involve free radicals and probably proceeds by an “on-off” reaction at the double bonds as shown in Figure 3.2.

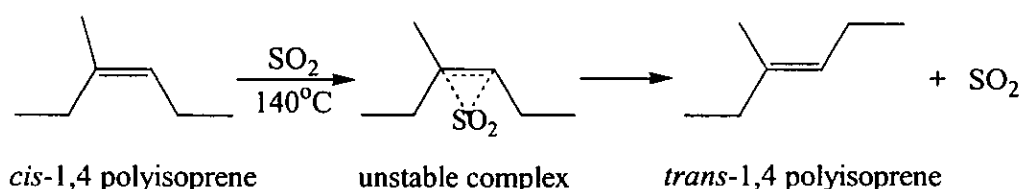


Figure 3.2 *Cis-trans* isomerization of NR by sulfur dioxide.

It was reported that increasing the *trans* content in the isomerized NR affected on various properties. The processing characteristic differs from that of NR because far less breakdown occurs on cold mastication. The distinct advantage of isomerized rubber is the decrease of the rate of low temperature crystallization to less than that of NR [34]. Thus, the isomerized rubber retains its elasticity for a long time at low temperature; it has been promoted as a non-crystallizing rubber. The rate of crystallization by strain is also decreased by isomerization. Thus, the tensile strength of vulcanized rubber is progressively decreased with increasing isomerization.

(b) Cyclization Reaction

Cyclization is a process involving the conversion of a long linear macromolecule into a much shortened polymer chain comprising mono-, bi-, tri-, tetra-, and other polycyclic groups distributed randomly along the polymer backbone [35-37]. It can be carried out on NR, in solution, or even in latex form with the presence of strong acids such as sulfuric acid (H_2SO_4) and *p*-toluenesulfonic acid or Lewis acids such as titanium chloride (TiCl_4), ferric chloride (FeCl_3) etc. Cyclization reaction of NR leads to the formation of a hard, non-rubber material with much less unsaturation than



original rubber. It has been considered to involve a carbonium ion mechanism as shown in Figure 3.3. As a result of this chemical modification, cyclized rubber has a higher density, refractive index, and softening point (90-130°C), but lower intrinsic viscosity and unsaturation, than the original NR.

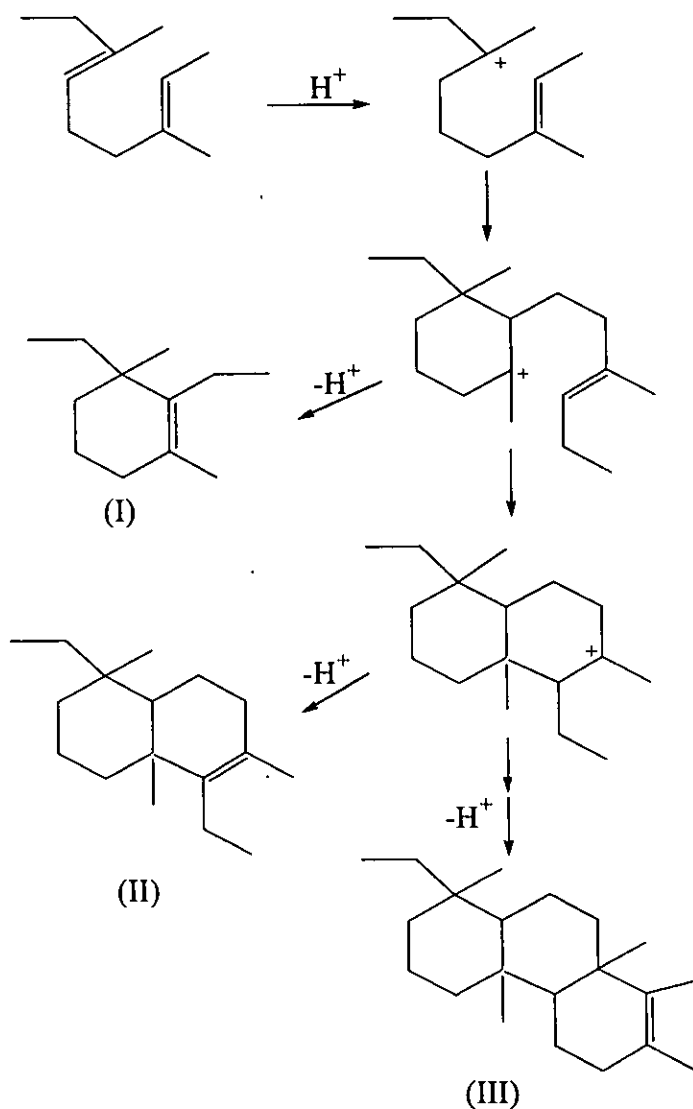


Figure 3.3 Cyclization of NR via the carbonium ion mechanism forming monocyclic (I), bicyclic (II) and tricyclic (III) structures [37].

3.2.2 Attachment of Pendant Groups

The chemical structure of the NR known as *cis*-1,4 PI is considered to be a trisubstituted olefinic structure. Therefore, attachment of pendent groups on the NR can be done by tremendous chemicals via the addition reaction at the olefin unit or substitution reaction by an appropriate chemical reagent. Some of the most interesting reactions are cited below.

(a) Hydrohalogenation Reaction

Hydrohalogenation of NR has been a subject of considerable interest in terms of chemistry and applications. The hydrochlorination involves the addition of hydrogen chloride at the carbon-carbon double bond according to Markovnikov's rule (see Figure 3.4) with a small amount of concomitant cyclized unit of rubber. The reaction is rather complex and may include addition, substitution, cyclization, crosslinking, and degradation. The hydrochlorinated rubber is a crystallizable polymer with a syndiotactic structure. It has found application in printing inks, adhesives and chemical resistant paints [6].

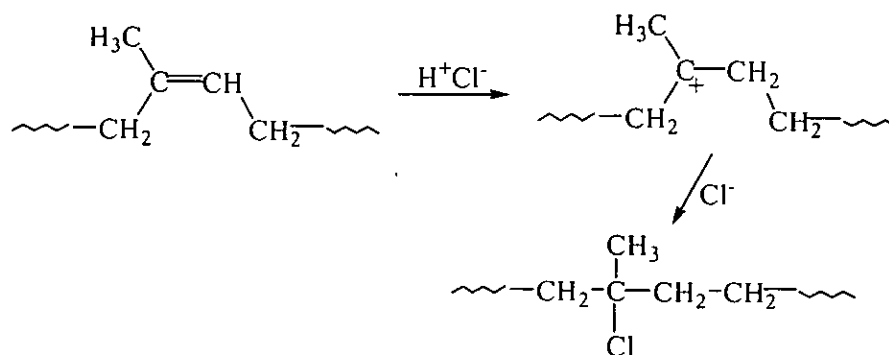


Figure 3.4 Hydrochlorination reaction of NR.

(b) Ene Addition Reaction

There are a number of reagents that can react with olefinic molecule or unsaturated unit of diene rubbers through ene mechanism (see Figure 3.5). It is also known as the dipolar addition.



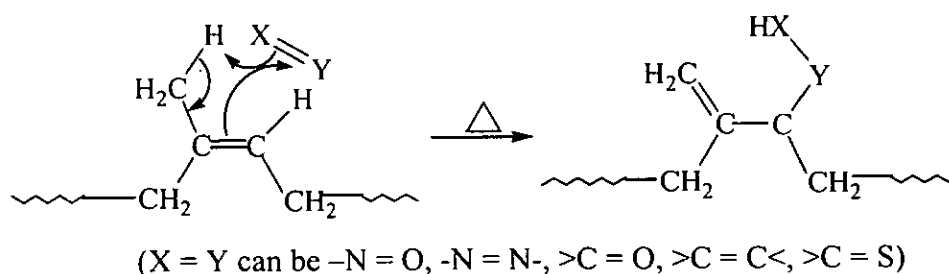


Figure 3.5 Mechanism of ene reaction.

One of dipolar additions is the reaction of maleic anhydride with the double bond of the rubber chains as seen in Figure 3.6. This process gives the resulting product not only does it provide increased polarity, but also the resulting anhydride group can act as a convenient site for subsequent functionalization.

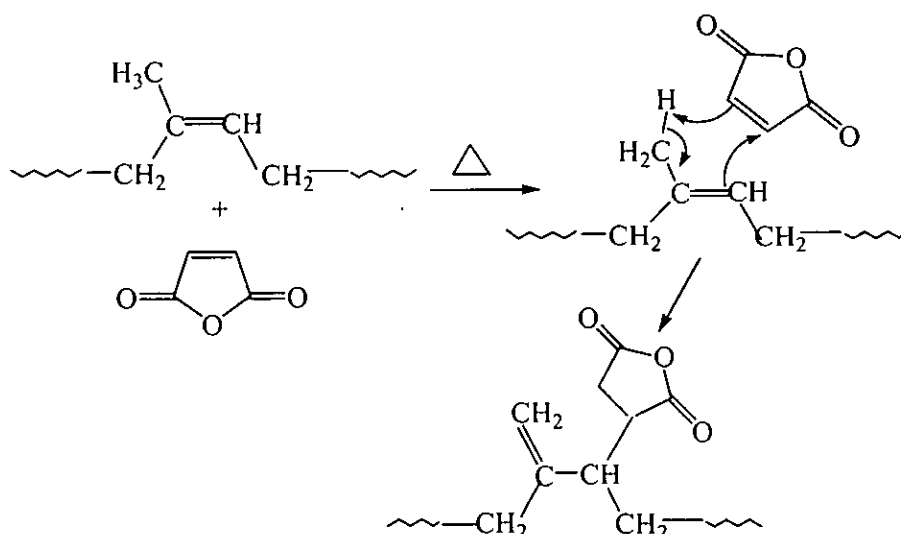


Figure 3.6 Maleation reaction of NR by ene reaction.

(c) Epoxidation Reaction

Epoxidation is another typical modification reaction of unsaturated polymers such as NR or polyisoprene, as presented in Figure 3.7. The variety of peroxides and peracids has been used to effect this transformation both in organic and aqueous systems.

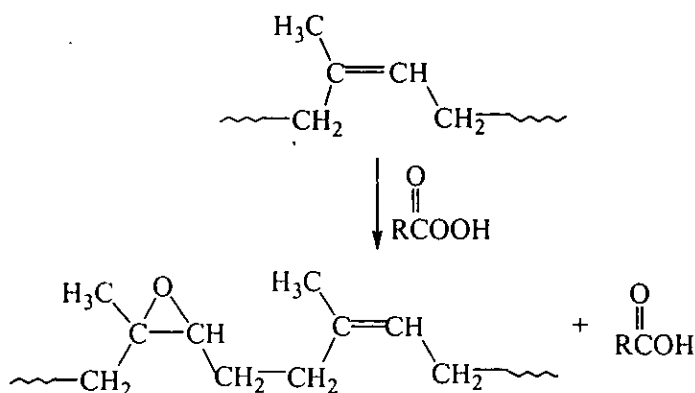


Figure 3.7 Epoxidation reaction of NR by peracid.

The epoxidized product obtained has higher polarity than the NR starting material. The epoxide functionality on the NR backbone can be deliberately converted to other functionalities by further reaction with materials containing N-, O- or S- in functional groups. Epoxidation of unsaturated rubbers results in significant changes in the physical and mechanical properties [8, 38, 39]. Epoxidation increases the T_g linearly by about 1°C for every one mole percentage of epoxide content. Increasing epoxidation level increases the damping and improves the abrasion resistance, wet traction, and hydrocarbon solvent resistance.

(d) Hydrogenation Reaction

Hydrogenation of polydienes based polymer is one of the important methods for improving and changing the properties of unsaturated rubbers toward greater stability against thermal, oxidative, and radiation-induced degradation. In addition, the complete hydrogenation of NR results in new material as an alternating copolymer of ethylene and propylene [12, 19]. The hydrogenation of unsaturated polymers can be prepared by catalytic hydrogenation with elemental hydrogen in the presence of a transition metal catalyst [12, 13, 19] or by non-catalytic method using chemical reagent such as *p*-toluenesulfonylhydrazide (TSH) generated diimide (N_2H_2) molecule [11, 13, 25]. The detail of this modification will be presented in later section.



3.2.3 Graft Copolymer

With an exceptional elastic property of NR, many attempts have been done to graft copolymerization of various vinylic monomers onto the NR. The most probable reaction is via free radical initiated polymerization. In the presence of radical initiator, free radical can be formed at the allylic position of the molecular backbone. The rubber macroradicals formed are the initiation site for polymerization of the monomer, leading to the graft copolymer. The mechanism of graft polymerization is shown in Figure 3.8.

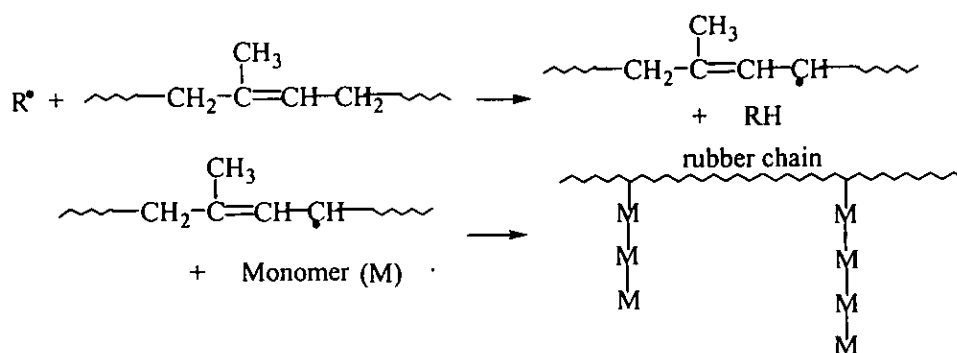


Figure 3.8 Graft copolymerization of NR.

Grafting of methyl methacrylate (MMA) onto NR has been commercialized under the name Heveaplus MG [40]. This material is considered to possess the elastic property of the rubber and the rigidity of the MMA.

3.2.4 Degradation Reaction

Another type of modification of NR is to change the high molecular weight of NR into a lower form, which is considered as liquid derivative of the NR or so called liquid natural rubber. It can be produced by oxidative degradation of NR by different process from the solid rubber by mastication or radiation, or from the latex phase by chemical reaction such as the action of phenylhydrazine/oxygen system or potassium persulfate in the presence of propanal [7, 41]. The liquid natural rubber is an attractive

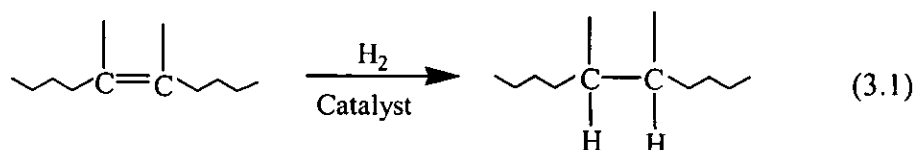
industrial application in two areas: first as a reactive plasticizer, in tire production and high hardness compounds, and second as a lubricant in the blending system of NR.

3.3 Hydrogenation Method

As mentioned in Section 3.2.2(d), hydrogenation reaction is employed to reduce the unsaturation level of diene polymers by adding hydrogen molecule onto the double bond of the unsaturated units. It is found to be a useful method for improvement of resistance to oxidative and thermal degradation of rubbers. The hydrogenation of unsaturated rubbers can be carried out by two methods i.e., catalytic and non-catalytic processes [11-13].

3.3.1 Catalytic Hydrogenation

Catalytic hydrogenation or a hydrogen transfer process is the reaction of an unsaturated substrate with transition metal-activated hydrogen as given in Equation 3.1 below:



This method can be divided into two types, homogeneous and heterogeneous reactions, depending on the feature of systems. Homogeneous hydrogenation employs a soluble transition metal complex, whereas heterogeneous system relies on an insoluble transition metal catalyst to contribute hydrogen addition to the carbon carbon double bond.

The catalysts for homogeneous system generally are the organotransition metals like cobalt (Co) and nickel (Ni) together with reducing agents like R_3Al and $n\text{-BuLi}$, which are soluble with the solvent used [13, 19, 42]. An insoluble transition-metal catalyst like palladium on calcium carbonate is used in the heterogeneous system. Unlike homogeneous hydrogenation, this technique yields high conversion without chain scission occurring. Generally, special equipment is required to perform catalytic



hydrogenation because the reaction is carried out at a high temperature under high pressure. Additionally, various factors influence on the catalytic hydrogenation, such as types of catalyst, which affect the selectivity of hydrogenation and solvents which influence not only the solubility of reactants and resulting products but also the activity of catalysts.

There are several reports of hydrogenation of polybutadiene (PB), acrylonitrile-butadiene copolymer (NBR), and styrene-butadiene copolymer (SBR) using transition metal compound catalysts [42-45]. A Ziegler-Natta type catalyst prepared with nickel acetylacetonate and *n*-BuLi has been used to hydrogenate SBR copolymer in cyclohexane [45].

Hydrogenation of polyisoprene especially NR is a rather complicated case of unsaturated polymers. The isopropenyl groups constituting the rubber chains are trisubstituted ethylene derivatives, they should be hydrogenated with a lower rate than mono- and di-substituted ethylenes. The process is even more complicated by virtue of the high molecular mass of polyisoprene obtained from natural rubber, due to its poor segmental mobility. This situation becomes worse as hydrogenation proceeded because the increase of chain stiffness restricts even more the chain mobility. Therefore, the utilization of catalytic hydrogenation of polyisoprene requires high temperature and pressure, considerable amount of catalyst, and rather long reaction time [12, 13, 19, 46]. The severe conditions of catalytic hydrogenation i.e. high pressure and high temperature may cause degradation and the difficulty of residual catalysts removal.

Natural rubber (NR) and epoxidized natural rubber (ENR) have been known as unsaturated rubbers with excellent elastic properties. The ENR has an additional good oil resistance upon epoxidation. However, both NR and ENR have primary drawbacks of poor thermal and oxidative resistances due to the unsaturated unit on the backbone. Hydrogenated NR and ENRs are expected to be more stable against thermal, oxidative, and radiation induced degradation. Singha et. al. mentioned catalytic hydrogenation of NR using $\text{RhCl}(\text{PPh}_3)$ catalyst with high pressure hydrogen gas and temperature [12]. They showed that the rate of hydrogenation increased with an increase in hydrogen pressure and concentration of the catalyst. The improvement of the thermal stability was found in the hydrogenated NR as compared with the original



NR. The hydrogenation of commercial NR using homogeneous catalyst prepared from nickel 2-ethylhexanoate and tri-isobutylaluminum can lead to 100% hydrogenation under appropriate condition [19]. Charmondusit et. al. studied the hydrogenation of *cis*-1,4 polyisoprene in the presence of various types of catalysts for example $\text{RuCl}(\text{CO})(\text{styryl})(\text{PCy}_3)_2$, $\text{OsHCl}(\text{CO})(\text{O}_2)(\text{PCy}_3)_2$, and $[\text{Ir}(\text{COD})\text{py}(\text{PCy}_3)]\text{PF}_6$ [46]. $\text{OsHCl}(\text{CO})(\text{O}_2)(\text{PCy}_3)_2$ was observed to be a very efficient catalyst for hydrogenation of *cis*-1,4 polyisoprene and the rate of hydrogenation was faster than either the $\text{RuCl}(\text{CO})(\text{styryl})(\text{PCy}_3)_2$ or $[\text{Ir}(\text{COD})\text{py}(\text{PCy}_3)]\text{PF}_6$ [46].

For ENR, the presence of epoxy group should influence on the reaction condition of hydrogenation and properties of the resulting rubbers. A few works have been done on catalytic hydrogenation of ENR. Bhattacharjee et. al. hydrogenated the NR and ENR by using homogeneous palladium catalyst, which is highly selective in reducing unsaturated part in the presence of epoxy groups [20]. They found that the rate constant of hydrogenation decreased with an increase of epoxide content of ENR.

3.3.2 Non-Catalytic Hydrogenation

For non-catalytic hydrogenation, inorganic diimide (N_2H_2) molecule has been found to be an effective intermediate for releasing a hydrogen molecule to low molecular weight olefins. It has been considered as a relatively simple procedure, which can be carried out in both organic and aqueous phase at atmospheric pressure under moderate temperature (50-140°C).

The diimide hydrogenation is an attractive method becoming popular for application to reduce the unsaturated unit of polymers. Diimide molecule can be generated from various chemicals, via the thermal treatment of arenesulfonylhydrazides, the carboxylation of potassium azodicarboxylate, the decomposition of hydroxylamine-o-sulfonic acid or chloramine, the photochemical irradiation of 1-thia-3,4-diazolidine-2,5-dione, and the oxidation of hydrazine [11, 13, 25, 47-49].



3.3.2.1 Diimide Reduction in Organic System

(a) Reaction Mechanism

Among several types of reducing agents, the diimide generated from the thermal decomposition of *p*-toluenesulfonylhydrazide (TSH) has been popularly used for the hydrogenation of the unsaturated units in diene rubbers. The decomposition reaction of TSH is presented in Figure 3.9.

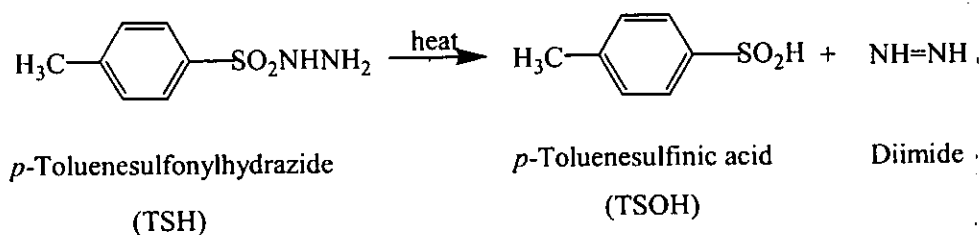


Figure 3.9 Decomposition of *p*-toluenesulfonylhydrazide (TSH) by thermal treatment [11].

Diimide reduction is unique in which the reaction is homogeneous and is highly specific with the *syn*-addition of a hydrogen molecule to the carbon-carbon double bond. The diimide may actually exist as *cis*- or *trans*- isomers; but only the *cis*-isomer serves as a reducing agent. An example of alkene reduction using diimide molecule is shown in Figure 3.10.

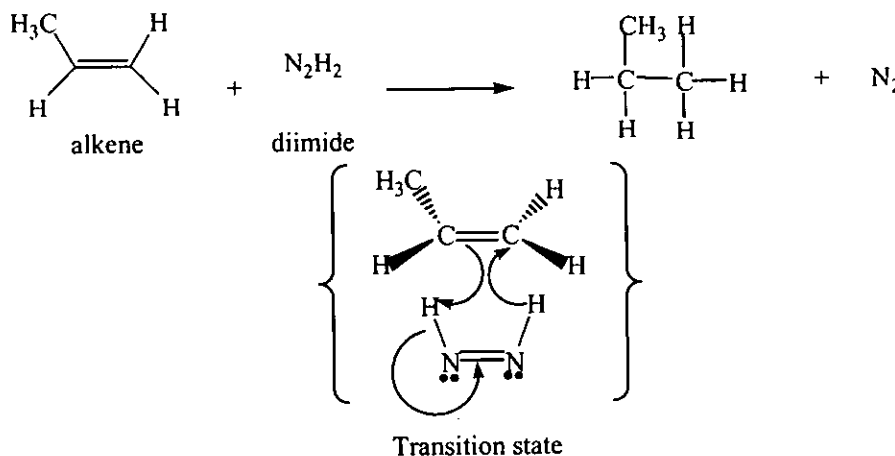


Figure 3.10 *Syn*-addition of hydrogen molecule of diimide onto the carbon-carbon double bond of unsaturated unit.

Mango and Lenz had studied the non-catalytic hydrogenation of synthetic polybutadiene (PB), polyisoprene (PI), and styrene butadiene copolymer (SBR) by using TSH and found that the thermal stability of the resulting product was improved [11] depending on the hydrogenation level. Harwood et. al. had reported the hydrogenation of PB and PI by using diimide as a reducing agent [48]. They found that complete hydrogenation could be attained when five moles of TSH per mole of unsaturated units of polybutadiene or polyisoprene were used. Similar results were obtained in the case of SIR [50, 51, 52]. Edwards et. al. [53] had investigated the diimide hydrogenation of PB by using NMR measurements to identify the incorporation of an aromatic impurity in the polymer, resulted from the side reaction during hydrogenation reaction. Poshyachinda and Kanitthanon [25] demonstrated some evidence of *cis-trans* isomerization of the diimide hydrogenation of *cis*-polybutadiene by FT-Raman spectroscopic method. They also reported that the rate of addition of hydrogen to the olefinic sites in the *cis* configuration is likely to be faster than that of the *trans* unit because of having only one side steric effect. It must be easier for the *cis* configuration to form an intermediate with the diimide, thus resulting in a more rapid addition of hydrogen molecule. Nang et. al. [52] had also studied the hydrogenation of *cis*-1,4 PI by using TSH. It was mentioned that the rate of hydrogenation increases with an increase in concentration of PI and TSH. In addition, they found that the reaction was accompanied by depolymerization and cyclization.

The rate of hydrogenation also depends on the microstructure of polymer, as reported by Mango and Lenz [11] in the hydrogenation of PI with different microstructures. It was found that vinyl segments were hydrogenated at a greater extent than either *cis*- or *trans*-1,4 units of PI. Hahn [50] also employed the diimide reduction of unsaturated part in poly(styrene-butadiene-styrene) (SBS) and poly(styrene-isoprene-styrene) (SIS). It was found that the C=C of polybutadiene and polyisoprene blocks were reduced whereas styrene parts were not affected. Additionally, Hahn had found that at the molar ratio of TSH to double bond of PB and PI equal to 2, the former was completely hydrogenated while only partial hydrogenation was obtained in the later case [50], because of the steric effect. It has generally been found that an excess amount of TSH compared with the amount of the unsaturation is to be introduced to fulfill complete hydrogenation of diene rub



because only syn form of diimide conducts to highly specific hydrogen addition to double bond and some portions can also undergo disproportionation, giving unreactive nitrogen molecule and hydrazine.

(b) Side Reactions

Several publications reported various side reactions occurred together with diimide hydrogenation such as incorporation of by-product, *cis-trans* isomerization, degradation and cyclization reactions [25, 50-52].

-*Cis-trans* isomerization

The hydrogenation of diene polymer with TSH reveals some *cis-trans* isomerization [25, 51]. For examples, the hydrogenation of *cis*-polybutadiene with TSH indicates the transformation of the *cis* unit in the backbone into the *trans* unit, detected by Raman spectroscopy. Phinyocheep et. al. [51] also mentioned that the *cis-trans* isomerization of *cis*-polyisoprene units in styrene-isoprene diblock copolymer was occurred. This side reaction was proposed to promote by the presence of sulfur containing molecule of the TSH or *p*-toluenesulfinic acid by-product.

-Addition of *p*-toluenesulfinic acid

The thermal decomposition of the TSH leads to diimide and *p*-toluenesulfinic acid (TSOH) by-product. The attachment of the by-product on the olefinic sites can be detected by various methods [11, 48, 50, 52, 53]. Hahn had investigated the hydrogenated products using FT-IR spectroscopy [50]. The presence of sulfone functionality was indicated by the IR bands at 1311 and 1148 cm^{-1} due to SO_2 asymmetric and symmetric stretching, respectively, and the located bands at 812 and 1020 cm^{-1} due to the *p*-tolyl aromatic ring. From Raman scattering, the bands at 1331 and 1152 cm^{-1} were depicted to asymmetric and symmetric $-\text{C}-\text{SO}_2-\text{C}-$ vibration and a band near 1600 cm^{-1} was claimed for benzene ring of TSH by-product [53]. According to $^1\text{H-NMR}$ spectra, resonances due to the *p*-tolyl substituent are obviously exhibited at 2.4 ppm for the para methyl and 7.7 ppm for the aryl ring protons [11, 48].



-Degradation

The changes in molecular weight (MW) and molecular weight distribution (MWD) during hydrogenation might designate the degradation of polymers, which can be normally detected by gel permeation chromatography (GPC). Hahn [50] found that the chromatograms of hydrogenated SBS did not change in MWD compared with that of the starting polymer whereas there were changes in hydrogenated products of SIS. These were unclear whether these changes were due to thermal or catalytic degradation by acid by-product.

-Cyclization

Cyclization can be another side reaction of hydrogenation as the TSOH may act as a proton-donor to the C=C unit. Nang et. al. investigated the resulting product obtained after hydrogenation of polyisoprene using FT-IR [52]. It was found that the slight shifts of the CH₃ deformation vibration at 1450 cm⁻¹ of the hydrogenated polymer were recorded and this was assumed to be the result of the cyclization reaction.

3.3.2.2 Diimide Reduction in Aqueous System

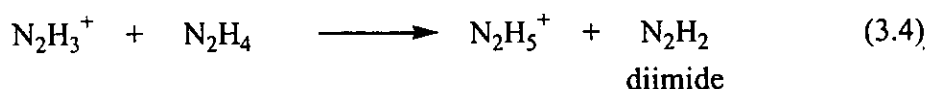
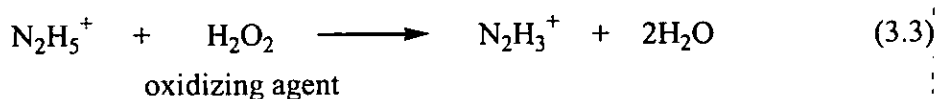
Wideman discovered that various types of rubber in latex form can be converted directly into its saturated analogue when treated with hydrazine hydrate, an oxidant, and a metal ion initiator without any requirement of pressure vessel, suitable solvent, or hydrogen gas [49]. It was later revealed by Parker et. al. that the same system could be successfully used for preparing the hydrogenated SBR latex. They also claimed that material obtained was a thermoplastic elastomer in nature [54]. This method was then used by Sarker De et. al. [55-57] for a series of studies on the hydrogenation of SBR and carboxylated SBR latex. There has not been any reports on the study of reduction of C=C bonds of natural rubber latex (NRL). It is therefore interesting to cite here some important conditions already studied concerning this method as the following.

(a) Reaction Mechanism of Diimide Formation

The generation of diimide molecule from hydrazine (N₂H₄) in the presence of hydrogen peroxide (H₂O₂) is considered as a redox system. The mechanism

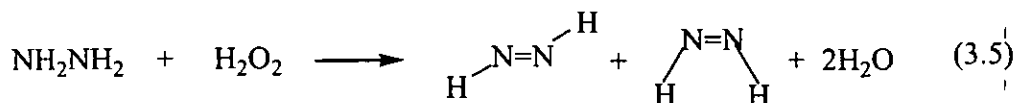


formation of diimide molecule by oxidation of hydrazine in aqueous system was demonstrated as the following [55]:



The solution of hydrazine in water is basic in nature and is postulated to form a protonated intermediate (N_2H_5^+). This reactive intermediate is then oxidized and undergone for diimide (diazene), $\text{NH}=\text{NH}$ formation. The stereospecificity of the reduction with this diimide has been attributed to the formation of a cyclic transition state as previously shown in Figure 3.10.

Almost an equal amount of *cis* and *trans* isomers of diimide can be generated during the oxidation of hydrazine as shown in Equation 3.5 but it seems likely that only the *cis* form of diimide can function as a reducing agent. Hence, the *trans* isomer is believed to be loss by the diimide decomposition reactions as shown in Equation 3.6 and 3.7.



The diimide reduction mechanism for NBR latex was also proposed by Parker et. al. [58]. This process directly converts NBR latex into hydrogenated NBR latex with the presence of carboxylated surfactant and copper sulfate as a catalyst. They proposed that the diimide-hydrogenating agent was generated at the surfaces of the rubber particles from a hydrazine/hydrogen peroxide redox system.



(b) Parameters Affecting on Hydrogenation in Latex Phase

-Latex particle size

He et. al. had studied hydrogenation of two particle sizes, i.e., 60 nm for small particle and 230 nm for large particle of SBR latex using hydrazine and hydrogen peroxide ($\text{N}_2\text{H}_4/\text{H}_2\text{O}_2$) system. They reported that the higher particle size of the rubber (total surface area was decreased) led to the decrease of percentage of hydrogenation [59]. This was probable that the reaction between N_2H_4 and H_2O_2 in the presence of copper sulfate (CuSO_4) as a catalyst generating the diimide molecule for hydrogenation had occurred at the particle surface of latex. For either the small particle or large particle system, there is the same optimum surface area density of Cu^{2+} that is 2 ions of Cu^{2+} presenting on 1000 nm^2 of rubber particle, the total number of Cu^{2+} in the large particle latex system is much less than that for the small particle latex system because of the much smaller total surface area for the latexes with the same solid content (20%). It could be one of the reasons that led to the decrease of overall degree of hydrogenation for the large particle system. Another possible factor that could influence the degree of hydrogenation is the distance for the diffusion of the diimide molecule from the surface to react with double bonds residing in the inner side of the particles. For the large particle system, the distance is longer comparing with the small particle system due to the larger particle size. The longer the diffusion distance was, the greater the lifetime was needed for the diimide before reaching the double bond and the greater the probability for the disproportionation reaction of diimide itself. The relative extents of these two competitive reactions could be decided by the local concentration of double bonds and diimide molecules, which were dependent on the rates of diffusion of both polymer chains and diimide molecules.

-Gel fractions

The diimide reduction of SBR in latex form having high (95%) and low (23%) gel fractions with nearly average particle size had carried out by He et. al. [59]. The results showed that high degree of hydrogenation was achieved in both systems, i.e., 91 and 93% for high and low gel fractions. Although the mobility of polymer chains in the latex particles for both systems is expected to be quite different, it seems that



high gel fraction does not exert much influence on the diffusion of the small diimide molecules generated at the particle surfaces. In other words, the diimide molecule is small enough to diffuse from the surface to the centre of latex particle.

(c) Side Reactions

Parker et. al. [58] studied the conversion of NBR latex to hydrogenated NBR latex by using N_2H_4/H_2O_2 redox system. They reported that the diimide reduction could induce cross-linking reaction indicated by the occurrence of gel fraction after hydrogenation. The possibility of cross-linking during hydrogenation reaction was also mentioned by Sarker De et. al. [55-57]. They found that the gel fraction of hydrogenated product increased during hydrogenation of both SBR and carboxylated SBR.

3.4 Principle of Methods for Characterization

Spectroscopic techniques used in this research are vibrational and nuclear magnetic resonance spectroscopies.

3.4.1 Vibrational Spectroscopy

A number of factors determine the selection of various spectroscopic methods for characterization of polymers. The first criterion is the nature of the spectral information relative to the problem at hand. All of the spectroscopic techniques have strengths and weaknesses in certain aspects of their applications so that no single technique is going to solve all of the problems. There are three principal methods by which the vibrations may be studied: infrared, Raman spectroscopies and inelastic neutron scattering. The first two methods are available in many laboratories, since the equipment required is relatively simple and cheap as compared with neutron scattering. The main purpose of this section will be to explain theoretical and experimental analysis and the information obtained from vibrational spectroscopy.



3.4.1.1 Classical Electromagnetism Theory of Vibration Spectroscopy

A vibrating molecule may interact in two distinctly different ways with electromagnetic (EM) radiation of appropriate frequency [22, 60-62]. If the radiation includes the same spectral component as one of the normal modes of vibration, it may be possible for the molecule to absorb the radiation. The energy absorbed will later lose by the molecule either by re-radiation or by transfer to other molecules of the material in the form of heat energy. The frequency at which any peak in the absorption spectrum appears is equal to the frequency of one of the normal molecular vibration modes of the sample. The possible vibrations of a molecule are sensitive to IR absorption if the vibration results in a change in the dipole moment, μ , of the molecule. When an electromagnetic wave in the IR wavelengths irradiates a molecule the electric field acts on the charge distribution in the molecule, i.e. the more polar the molecule the larger the effect. The oscillation of the EM field, if of the quantized frequency for absorption by a particular bond, will set the bond in motion, vibrating at the specific frequency needed for that vibrational excitation.

The second way in which electromagnetic radiation may interact with a molecule is by being scattered, with or without a change of frequency as can be seen in Figure 3.11. The scattering without change of frequency may be thought of as scattering from the equilibrium states of the molecules and is called "Rayleigh scattering". The scattering with change of frequency is called "Raman scattering" and the change in frequency corresponds to the frequency of one of the normal modes of vibration of the molecules.

Scattering can be either elastic or inelastic. The electric field, \vec{E} , of the incident light induces a dipole moment, $\vec{\mu}$, in the molecule, given by

$$\vec{\mu} = \alpha \vec{E} \quad (3.8)$$

The proportionality constant α is the polarizability of molecule, which expresses the distortion of the electron cloud of the molecule. A fluctuation of the electric field will produce a fluctuating dipole moment of the same frequency. Electromagnetic radiation generates such an electric field, which can be expressed as in Equation 3.9



$$\bar{E} = \bar{E}_o \cos 2\pi\nu_o t \quad (3.9)$$

where \bar{E}_o is the equilibrium field strength and ν_o is the angular frequency of the radiation.

Consider the particular case of a diatomic molecule, which vibrates with a frequency “ ν ”. If it performs simple harmonic vibrations, then a coordinate q along the axis of vibration at time, t , is written by:

$$q = q_o \cos 2\pi\nu t \quad (3.10)$$

Since the polarizability is modulated by the vibration, its value for small vibrational amplitude can be written by:

$$\alpha = \alpha_o + \left(\frac{\partial \alpha}{\partial q} \right)_o q \quad (3.11)$$

Substitution of Equation 3.10 in Equation 3.11 yields:

$$\alpha = \alpha_o + \left(\frac{\partial \alpha}{\partial q} \right)_o q_o \cos 2\pi\nu t \quad (3.12)$$

If incident radiation of frequency ν_o interacts with the molecule then the dipole moment can be expressed by the following:

$$\bar{\mu} = \alpha \bar{E} = \alpha \bar{E}_o \cos 2\pi\nu_o t \quad (3.13)$$

Substitution of Equation 3.12 in Equation 3.13 gives:

$$\bar{\mu} = \alpha_o \bar{E}_o \cos 2\pi\nu_o t + \left(\frac{\partial \alpha}{\partial q} \right)_o \bar{E}_o q_o \cos 2\pi\nu t \cos 2\pi\nu_o t \quad (3.14)$$

which can be rearranged as:

$$\bar{\mu} = \alpha_o \bar{E}_o \cos 2\pi\nu_o t + \left(\frac{\partial \alpha}{\partial q} \right)_o \frac{\bar{E}_o q_o}{2} [\cos 2\pi(\nu_o + \nu)t + \cos 2\pi(\nu_o - \nu)t] \quad (3.15)$$

The first term in Equation 3.15 describes the Rayleigh scattering and the second terms describe the Stokes and the anti-Stokes Raman scattering. Equation 3.15 indicates that light will be scattered with different frequencies: ν_o is Rayleigh scattering and $\nu_o \pm \nu$ is Raman scattering. In addition, the Raman scattering occurs when $(\partial\alpha/\partial q)_o$ is unequal to 0 that is, the polarizability of the molecule must change during a vibration if that vibration is to be Raman active. This vibration involves the selection rule for Raman spectroscopy.



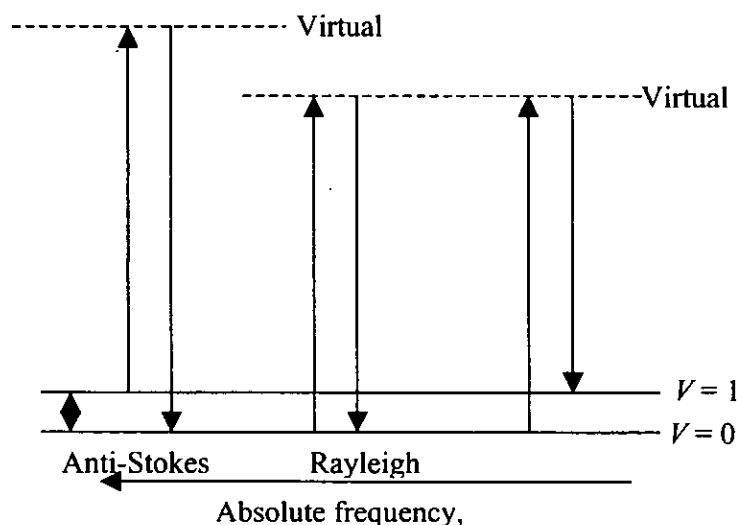


Figure 3.11 The energy levels of elastic (Rayleigh) and inelastic (Raman) scattering lines.

Raman spectroscopy is a very versatile technique where in the specimen is illuminated with a high-intensity monochromatic source (e.g. a laser) and the scattered light is investigated. As described previously a component of scattered light is inelastically scattered, i.e. it appears at a wavelength different from that of the source. The Raman scatter is very weak but can be detected readily using high sensitive optical detectors.

Molecules consist of atoms which have a certain mass and which are connected by elastic bonds. As a result, they can perform periodic motion, they have vibrational degrees of freedom. All motions of the atoms in a molecule relative to each other are a superposition of so called normal vibrations, in which all atoms are vibrating with the same phase and normal frequency. Polyatomic molecules with N atoms possess $3N-6$ vibration degrees of freedom. The six degrees of freedom subtracted from the total of $3N$ displacement degrees of freedom of N atoms are the degrees of freedom of the undistorted molecule, i.e. the translations (3) and rotations (3) of the whole molecule.

Consider a polymer molecule is composed of several repeating units. In polymer analysis, we can greatly and roughly simplify the characteristic spectrum for a chain by considering the repeating chemical groups, which occur in the chain as independently contributing to the IR and Raman spectra. The number of vibrational modes, molecular vibration and intensity of signal were described as follows.



(a) Number of Vibration Modes by Group Theory Analysis

The classically described group theory allows to simply determining the number and symmetry of the vibrational modes. Based on the matrix built on the atomic displacements, it is possible to reduce it to irreducible representations of the symmetry point group of the molecule. The usual relation used is then:

$$A_i = \frac{1}{n} \sum_R k(R) \chi_i(R) \chi(R) \quad (3.16)$$

where the group order “ n ” is the number of symmetry operators of this point group, and the summation is extended over all classes of symmetry operator “ R ”. $k(R)$ is the number of elements in each class, $\chi_i(R)$ is the character of the species (irreducible representation) i for the symmetry operator R found in the character table of the point group. $\chi(R)$ is the character of the reducible representation of the symmetry operator determined with the matrix built on atomic displacement. Point group corresponds to the symmetry elements which let invariant the elementary molecule.

When molecules possess symmetry, this symmetry restricts the types of vibrational modes that can be observed in the IR and Raman spectra. Note that for non-centered molecules as in the case of natural rubber the active modes are the same in IR and Raman spectroscopies.

(b) Molecular Vibrations

Vibrational spectra contain information about every aspect of the molecular structure. This information can be evaluated by comparing observed infrared and Raman spectra with those calculated from systematically modified model molecules until the best adjustment is achieved. However, very simple calculations may help to assign the observed bands to structure as a result of a chemical reaction. Such models usually ignore anharmonicity, they treat molecules just as simple systems of diatomic molecule having the masses of the atoms m_1 and m_2 .

It is easy to show that when the molecule is disturbed from equilibrium it will vibrate with simple harmonic motion of frequency, ν according to Equation 3.17.

$$\nu = \frac{1}{2\pi} \sqrt{\frac{k(m_1 + m_2)}{m_1 m_2}}$$



$$= \frac{1}{2\pi} \sqrt{\frac{k}{m^*}} \tag{3.17}$$

where m^* is the reduce mass of the molecule defined by $\frac{1}{m^*} = \frac{1}{m_1} + \frac{1}{m_2}$ and the quantity k is called a force constant between the two atoms and corresponded to the restoring force acting on either atom.

The displacement of atoms arises from the change of bond lengths and bond angles, resulting molecule vibration.

(c) Intensity of Vibrational Bands

In this section, the intensity of vibrational bands in normal IR and Raman spectra are presented [22, 61]. When IR radiation is absorbed by molecule, the intensity of the absorption depends on the movement of the electronic charges during the molecular vibration. Therefore, the IR intensities should provide information about the electronic charges distribution in molecules. The IR intensity A_s , is related to the molecular parameters as follows:

$$A_s = \left[\frac{8\pi^2 N_A}{3hc_s} \right] \nu_s \left| \frac{\partial \mu}{\partial Q_s} \right|^2 \tag{3.18}$$

where N_A is Avogadro's number, h is Planck's constant, c_s is the velocity of light, and ν_s is the frequency of the band center. This relationship can be expressed inversely as

$$\left| \frac{\partial \mu}{\partial Q_s} \right| = 0.03200 \left(\frac{A_s}{\nu_s} \right)^{1/2}$$

Hence, each intensity can be related to the dipole moment derivative with respect to the Q_s normal coordinate.

For Raman scattering, the total intensity of a Stoke Raman band of shift frequency, ν , scattered over a solid angle of 4π by randomly oriented molecule perturbed by electromagnetic radiation from an initial vibration state to a final state is given by:

$$I \propto I_o (\nu_o - \nu)^4 \sum_{ij} |\alpha_{ij}|^2 \tag{3.19}$$

where I_o is the incident intensity and α_{ij} represents the components of



polarizability tensor associated with the transition from an initial vibration state to a final state.

3.4.1.2 Experimental Analysis of Infrared and Raman Spectroscopy

Infrared and Raman spectrometers are the most important tools for observing vibrational spectra. Depending on the nature of the vibration, which is determined by the symmetry of the molecules, vibrations may be active or forbidden in the infrared or Raman spectrum. The following characteristics may be employed for the elucidation of the molecular structure.

(a) FTIR Spectroscopy

Infrared spectroscopy provides more useful information for identifying polymers and modified polymer. IR yields both qualitative and quantitative information concerning a polymer sample's chemical nature, i.e., structural repeating units, end group and branch units, additives and impurities. IR spectroscopy is sensitive to change in the dipole moments of vibrating groups in molecules and, accordingly, yields useful information for the identification of the polymers after modification. In practice, it is very difficult to observe the absorption intensity changes of an important characteristic of polyisoprene after modification. Then this method can be used only on qualitative mode. Generally, there are two kinds of fundamental vibrations for molecules: stretching, in which the distance between two atoms increases or decreases, but the atoms remain in the same bond axis, and bending (or deformation), in which the position of the atom changes relative to original bond axis.

The utilization of FT-IR spectroscopy investigated the microstructures of hydrogenated products of PB, SBR and NBR had been reported in several literatures [42-45, 63]. The catalytic hydrogenation of PB had been carried out by Doi et. al. [63]. They found that after 15 min of hydrogenation the band at 912 cm^{-1} is due to the vinyl group of 1,2 addition disappeared. The broad absorption band at 734 cm^{-1} due to the C=C bond of *cis*-1,4 addition disappeared after 30 min of hydrogenation, and new absorption bands appeared at 728 and 720 cm^{-1} , being attributable to the -CH₂- rocking vibrations in crystalline and amorphous fractions of poly(ethylene) segments respectively. In addition, the absorption band at 967 cm^{-1} due to the C=C



trans-1,4 addition completely disappeared at 24 h of hydrogenation. Thus, the double bonds of 1,2 and *cis*-1,4 additions were hydrogenated faster than the *trans*-1,4 addition. Harwood and co-workers reported the complete hydrogenation of PB detected by FT-IR when the molar ratio of [TSH]/[C=C] equal to 6 was used [48]. For hydrogenating NR, FT-IR spectroscopy had employed to investigate the decrease of the absorption peaks at 840 cm^{-1} corresponding to the C-H out of plane deformation of trisubstituted PI, after hydrogenation as reported by Bhattacharjee et. al. [20].

(b) Raman Spectroscopy

The choice of Raman spectroscopy for analysis of polymer structure and composition is based on the high sensitivity of the Raman effects for certain non-polar chemical groups. In polymers, these groups are primarily the nearly homonuclear single and multiple C-C bonds, of which the vibrational intensity is difficult to observe in the IR spectra. Several researches reported the study of chemical structure of rubber by Raman spectroscopy as the vibration frequency of the C=C bond is sensitive to its environment [22-25]. Raman spectroscopy can differentiate between internal and external bonds as well as *cis* and *trans* isomers in compounds with ethylenic linkages. The type of unsaturation in butadiene and isoprene rubbers can be determined from the intense Raman scattering of the C=C stretching modes. For instance, the *trans* and *cis*-1,4 polybutadiene structures scatter at 1664 cm^{-1} and 1650 cm^{-1} , respectively. The 1,2 vinyl structure of polybutadiene scatters at 1639 cm^{-1} , and this scattering is well resolved from that of the 1,2-polybutadiene structures. Jackson et. al. [23] had reviewed the application of Raman spectroscopy to investigate the chemical structure of elastomers. They studied the characteristics of the chemical structure of the raw polybutadiene (PB) and natural rubber (NR) at different commercial grades. The C=C vibrational mode of *cis*, *trans* and vinyl in PB can be seen at 1650, 1664 and 1639 cm^{-1} , respectively. For NR, its structure consists of repeating isoprene units in the *cis* configuration. Commercial grades of NR have varying amounts of impurities, such as protein, fatty acids and dirt which cause high fluorescence backgrounds or absorption of excitation source with conventional Raman spectroscopy. This makes the spectra of NR difficult to obtain. Unlike the PB, the shift between *cis* and *trans* isomers of NR is unfortunately, too small to enable the isomers to be resolved by Raman technique.



Raman spectroscopy had been employed to study NR and deproteinized NR as a function of time cold soaking reported by Jones [64]. FT-Raman spectroscopy has considerable potential for the study of the crystallization processes which are occurred in NR. It was found that the intensity of the C-H stretching peak increased with increasing cold soaking time indicating that it may be related to further crystal formation.

The integrated intensity of Raman absorption band is directly related to the concentration of the absorbing species and this spectroscopic method has been used for the assay of residual unsaturated unit of polybutadiene rubber after hydrogenation [25] as well as the quantitative analysis of the microstructure of NR.

Edwards et. al. [65] had investigated the hydrogenation of PB using Raman spectroscopic technique. Quantitative measurements of the hydrogenation by Raman spectroscopy found only 50% reduction in unsaturation since fluorescence problems from the impurity incorporation and reflection problems arising from the surface changes in the sample becoming white marked the Raman spectra.

Raman spectroscopy had been used as the preferred method to quantify the amount of the C=C bond of unsaturated units after modification in the work reported here since the C=C stretching vibration of cis units is strongly active as compared to infrared absorption technique. Additionally, the high resolution of adapted configuration possible in Raman spectroscopy making this technique favored over other spectroscopic techniques.

The principal limitation of Raman spectroscopy in the visible region is the existence of fluorescence, and Raman spectra cannot be obtained from many samples because of the curtain of fluorescence that hides them. All impure specimens, and natural rubber is such species, fluoresce. As a result, the very weak Raman scatter is swamped by fluorescence. Raman spectroscopy for studying the natural rubber having problems with fluorescence gave high background of spectra. However with an adapted incident wavelength and a classical subtraction of the background the spectra could be estimated for each spectrum with a standard fitting procedure.

Recently, Raman spectroscopy has also become important, as instrumentation has become smaller, less expensive, and more sensitive. While developments taking place in many areas of vibrational spectroscopy, this study will focus on



of imaging or mapping techniques, which are becoming important as we aim to understand the heterogeneous nature of polymer materials and polymer surface.

-Raman Mapping

Two different techniques can be used, either the samples are globally illuminated, either the mapping rebuilt from an analysis possible point. The spectrometers are usually dispersive and utilize a CCD camera. Consequently, images are collected based on individual bands selected by filters, rather than the whole spectra. Mapping is the collection of many spectra consecutively by the use of a micro-spectrometer with point illumination and a computer-controlled stage. The micro-Raman mapping was employed to assess the composition of ternary polymer blends consisting of polypropylene/polyethylene/ethene-propene copolymer [66]. Raman imaging was proved to be suitable for the characterization of heterogeneities in composition and morphology on a size scale equal to or larger than 1 μm . Liu et. al. studied the degradation of polyolefin grafted polystyrene [67]. These grafted sites of the samples can be seen from scanning electron microscopy or detected by Raman micro-spectroscopy. They found that the grafting spots detected by Raman mapping are heterogeneous as observed in SEM images.

(c) Spectral Differences between IR and Raman Spectroscopy

As a result, the information obtained from IR measurements can also be found in the Raman spectra. Some vibration mode appears only in the IR spectrum, and other modes appear only in the Raman spectrum. The differences in the vibrational spectra of IR and Raman spectroscopy can be used to a great advantage in the determination of the structure of molecules. If the molecule does not possess a symmetry center the spectra are identical by IR and Raman scattering. Generally, the more symmetric the molecule is, the greater the differences will be between the IR and Raman spectra. Strong Raman scattering arises from non-polar molecules and strong IR absorption presents when the molecule contains polar groups. In chainlike polymer molecule, the vibrations of the substituents on the carbon chain are most easily studied by using FT-IR spectroscopy, and the vibrations of the carbon chain can be studied by using Raman scattering.



3.4.2 Nuclear Magnetic Resonance Spectroscopy

Nuclear magnetic resonance (NMR) has become one of the most frequently used techniques in the investigation of organic compounds. The primary importance of NMR is the power and versatility of the technique for structural identification of diene rubbers, which are involved in chemical modification reactions as reactants, or products.

3.4.2.1 Theoretical Analysis of Resonance

This section introduces general background about NMR spectroscopy both in liquid and solid states. NMR measurements can be applied to molecules that contain atomic nuclei possessing a spin, as described by the nuclear spin number (I) [22, 68-70]. The nuclear spin corresponds to a small magnetic dipole, when a sample is placed in a homogeneous magnetic field, the dipoles will align with the lines of induction or the force of the applied magnetic field. The torque from the applied field will cause the magnetic moments to precess. The precession frequency is known as the Larmor Frequency. It is proportional to the applied magnetic field, H_0 . The Larmor frequency, ω_0 , is given by

$$\omega_0 = \gamma H_0 \quad (3.20)$$

A nucleus with a spin number of $\frac{1}{2}$ will orient itself in one of two permitted directions in the presence of an externally applied magnetic field (as in the NMR spectrometer), corresponding to two spin states at discrete, quantized energy levels as shown in Figure 3.12.

The difference between the two energy levels of the nuclei with a spin of $\frac{1}{2}$ in the presence of magnetic field is given by

$$\Delta E = \hbar \gamma H_0 \quad (3.21)$$

where γ is the magnetogyric ratio. The NMR spectrum is the result of transitions from the lower to the upper energy spin state induced by the absorption of energy from electromagnetic radiation applied at the proper frequency. When the absorption occurs, the system is said to be in resonance.



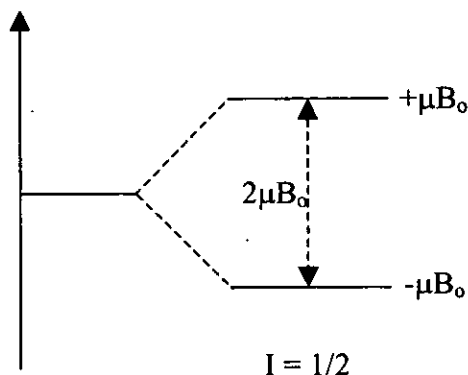


Figure 3.12 Quantized energy of nuclei in a magnetic field.

-Nuclear spin relaxation

After the resonance radiofrequency pulse has been applied, a higher energy excited state exists. This higher energy level corresponds to the nuclei that are elevated to the antiparallel position. To return to the equilibrium or ground state, this excess energy is passed to the surroundings by stimulated emission, and some of the antiparallel nuclei return to the parallel or low energy level. This decay of the magnetization proceeds to equilibrium in an exponential function known as the relaxation times. The rate of this process is determined by two external factors or relaxations: the spin-lattice relaxation time, $T_{1\rho}^H$, and the spin-spin relaxation time, T_2 [22, 68, 69].

The rate of transfer of energy between nuclei and the environment or lattice is always called the *spin-lattice relaxation time*, T_1 . This phenomenon depends on the effectiveness of energy transfer from the excited nuclei to the lattice. The T_1 is specific for each molecule and its environment and gives information about the molecular dynamics of the magnetic moments and the molecule around them. When the nuclear magnetization rotates at the Larmor frequency, local fluctuating magnetic fields, which are generated by molecular motion lead to a decay of the longitudinal spin magnetization.

The transverse magnetization decay involves the return to equilibrium by the loss of coherence of the transverse magnetization of the nuclei. The energy is transferred adiabatically between the nuclei as they are jostled between high and low energy positions. This internal adiabatic exchange occurs between two different spins.

The transverse magnetic relaxation time, T_2 , is called the *spin-spin relaxation time*. The T_2 provides information about the distribution of resonant frequencies and about the local field experienced by the magnetic moments of the nuclei. Local field is related to the structure and to the chemical nature of the environment around the nuclei. Because the local magnetic field in liquid fluctuates very rapidly and can average to zero, the internal local field is weak and yields narrow resonance lines. In solid state, the position of atoms is nearly fixed, and the internal field is significant and contributes to the rapid loss of coherence. Therefore, the T_2 in solid is very short, and the resonance lines are very broad.

3.4.2.2 Experimental Analysis

(a) ^1H and ^{13}C -NMR in Liquid State

A ^1H -NMR spectrum of a molecule consists of series of peaks corresponding to the resonance frequencies of chemically different protons in molecule. These peaks may show fine structure (splitting) due to mutual interaction with non-equivalent nuclei. The peak areas are proportional to the number of protons that resonate at the particular frequencies; the number of protons is dependent on the number of chemically equivalent protons in the molecule and on the concentration of the molecule. Peak areas are usually integrated electronically and recorded with the spectra.

The dependence of peak position on chemical environment and of peak area on the number of protons is the basis of kinetic measurements using NMR. If some of the nuclei responsible for a resonance change environments during the course of a reaction, a peak corresponding to the reactant will diminish in size and a new peak corresponding to the products will increase.

The major limitation of the NMR technique is the requirement of high sample concentrations, as previously mentioned. Furthermore, the high expense of NMR spectrometers limits their availability for lengthy kinetic measurements. The use of NMR measurements for study of concentration changes is practical for reactions with half-times of about one minute or longer. Typically, a reaction will be followed by recording and integrating the entire spectra at various time intervals when the



reactions are involved. NMR may also be used for kinetic measurements of some fast reactions at equilibrium, by studying line broadening effects.

The larger ^{13}C chemical shift range enables very subtle structural and conformational changes to be discerned. In addition, the ^{13}C spectrum may be simplified by proton decoupling which makes all the carbon resonances appear as singlet. This is in contrast to proton NMR where spectra of large molecules are complex because of homonuclear spin-spin splitting and congested because of the small proton chemical shift range.

Generally, nuclear magnetic resonance spectroscopy in solution both ^1H - and ^{13}C -NMR have been employed for studying the microstructure of elastomers and the modified forms such as epoxidized and hydrogenated elastomers [13, 22, 38].

Mohammadi and Rempel [42] carried out the homogeneous catalytic hydrogenation of polybutadiene. The microstructure of hydrogenated PB was analyzed by FTIR, ^1H -NMR and ^{13}C -NMR techniques. They found that all the characteristic bands for unsaturation disappeared, suggesting a quantitative hydrogenation. Singha et. al. has studied the catalytic hydrogenation of NR using hydrogen gas and $\text{RhCl}(\text{PPh}_3)$ catalyst [12]. They used FTIR, ^1H - and ^{13}C -NMR to analyze the characteristic of hydrogenated NR. For FTIR, a very intense peak appears at 735 cm^{-1} , which is attributed to the $-(\text{CH}_2)_3-$ group formed through hydrogenation. They also studied the distribution of saturated units and found that the hydrogenated NR is a strictly alternating copolymer of ethylene and propylene when complete hydrogenation was achieved. Gan et. al. used ^1H -NMR spectroscopy to measure the hydrogenation of NR using catalytic hydrogenation [19]. The reaction led to the decrease of intensity signals of the isoprene unit of NR at 1.7, 2.2 and 5.2 ppm and the increase in the peaks at 0.89 and 1.1-1.3 ppm which belong to methyl and methylene protons of the propylene-ethylene block of hydrogenated product, respectively. Bhattacharjee et. al. [20] prepared the hydrogenation of NR and ENR by using hydrogen gas and palladium catalyst and found that the characteristic signals corresponding to the unsaturated units decreases with hydrogenation time and also new signals positioned at 1.4 and 0.9 ppm due to the methylene and methyl protons of saturated units as detect by ^1H -NMR. It was further evident from the ^1H -NMR spectra that no side reaction had taken place during the catalytic reduction.



(b) High-Resolution Solid-State NMR Spectroscopy

With the development of cross polarize (CP) and magic angle spinning (MAS), high resolution technique used in solution state NMR have become available in solid state sample. In general, solid state NMR has been applied for two general classes of polymer samples: (1) samples that are insoluble such as crosslinked or intractable system, and (2) samples for which solid state NMR spectroscopy provides information about the solid state nature such as chain conformation, crystallographic form, and the morphological character of the solid samples. Chain conformation is the most commonly studied by solid-state ^{13}C -NMR with cross polarization along with the magic angle spinning (CP/MAS) technique.

This technique becomes a powerful tool for characterising and studying the chemical structure and dynamic property of polymers. Moreover, both solid-state ^{13}C -NMR magic angle spinning and cross-polarization (MAS/CP) experiments have been widely used for the investigation of vulcanized NR [71-76]. The possibility of performing the experiment in solid form allows this spectroscopic technique been interested for analyzes of modified polymer such as hydrogenated polymer, which is normally obtained in solution form. No report has been published on using solid state NMR for characterization of chemical structure of hydrogenated natural rubber.

-High-Power Proton Dipolar Decoupling

The major contributions to the line widths in ^{13}C -NMR spectra of organic solids are the interactions arising from heteronuclear dipolar broadening by protons. The dipolar coupling is often strong, and the line widths are of the order of 30–50 kHz. A practical method for the removal of proton dipolar broadening is to employ a high-power proton decoupling field, i.e. *dipolar decoupling*. The way to remove the heteronuclear dipolar broadening is to irradiate protons with a strong radiofrequency field in the neighbourhood of their Larmor frequencies. This is analogous to the decoupling commonly used in solutions to remove the heteronuclear scalar couplings as well as the J couplings in the solid state, except that much larger power is required.

-Magic Angle Spinning “MAS”



-Magic Angle Spinning “MAS”

The NMR spectra of solids are fundamentally different from those in solution, primarily because the polymer matrix inhibits the molecular motion that averages the chemical shift anisotropy and dipolar interactions, which result in shape lines. Chemical shift anisotropy is a particularly severe problem when observing carbon nuclei because it has a large chemical shift range. Most polymer samples are not oriented relative to the field and the chemical shifts take a continuum of values and form the line shapes shown in Figure 3.13(a) and (b).

The chemical shift anisotropy arises from a nonspherical distribution of electrons that give rise to an orientation-dependent chemical shift in isotropic samples. In molecules of any degree of complexity there will be several such patterns that may strongly overlap, producing a broad, unresolved spectrum. Under these circumstances it usually becomes necessary to sacrifice the anisotropy information in order to observe a high-resolution spectrum.

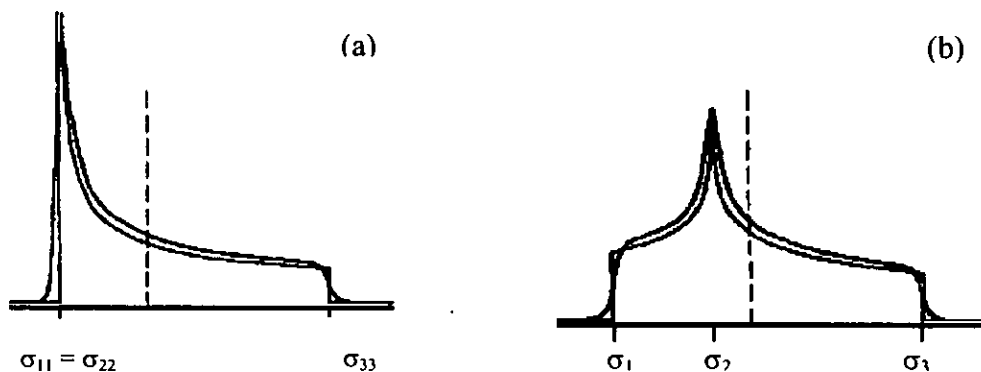


Figure 3.13 Chemical shift anisotropy patterns for (a) axially symmetric and (b) nonaxially symmetric atoms [68].

Under rapid sample rotation the orientations and chemical shifts become time dependent in the rotor period. Taking the time average under rapid rotation gives Equation 3.22:

$$\sigma = \sigma_{iso} + \frac{1}{2}(3 \cos^2 \beta - 1)(\sigma_{xx} \sin^2 \theta \cos^2 \phi + \sigma_{yy} \sin^2 \theta \sin^2 \phi + \sigma_{zz} \cos^2 \theta - \sigma_{iso})$$

(3.22)



where β is the angle between the rotation axis and the magnetic field direction equal to 54.7° (so called magic angle) as illustrated in Figure 3.14, σ_{xx} is one of the three tensor components, σ_{iso} is the isotropic value of the three tensor components.

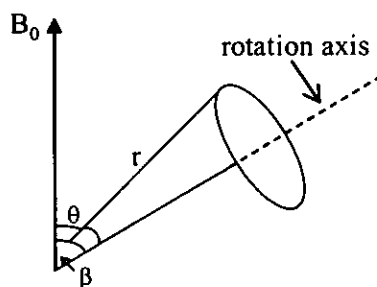


Figure 3.14 Macroscopic sample rotation at an angle to the applied magnetic field B_0 .

Thus, under magic angle rotation at several kilohertz, the chemical shift pattern collapses to the isotropic average, giving the high-resolution spectrum.

-Cross-Polarization "CP"

A further problem encountered in the NMR study of rare spins such as ^{13}C nuclei is the attainable sensitivity [22, 68, 69]. The resonance signal is proportional to the magnetization of the I spin system placed in an external field H_0 , which for a spin $\frac{1}{2}$ system, can be written as:

$$M_I = N_I \gamma_I^2 \hbar^2 H_0 / 4k T_L \quad (3.23)$$

where N_I is the number of I spin in the sample, γ_I is the gyromagnetic ratio of the I spins, and T_L is the absolute temperature of the lattice. Protons, which have high gyromagnetic ratio and 100 % natural abundance have of course a magnetization, M_H , much higher than that of the ^{13}C nuclei, M_C . A way of increasing M_C consists in transferring a small fraction of the proton magnetization to the carbon spin system. This can be achieved by spin-locking the protons with a radiofrequency field, H_{IH} , parallel to the proton rotating frame magnetization. The proton spins then pass suddenly from a high field (H_0) in the laboratory frame to a low field (H_{IH}) in the rotating frame. The M_H magnetization is maintained on passing from H_0 to H_{IH} and is written as follow:



$$M_H = N_H \gamma_H^2 \hbar^2 H_0 / 4k T_L = N_H \gamma_H^2 \hbar^2 H_{1H} / 4k T_0 \quad (3.24)$$

where T_0 is the proton spin-temperature in the spin-lock experiment: $T_0 = T_L H_{1H} / H_0$. The important result is that T_0 is much lower than T_L because H_{1H} is much weaker than H_0 . Then the proton magnetization follows a $T_{1\rho}^H$ decrease during the spin-lock sequence. During the proton spin-lock time, a second radiofrequency field is applied at the carbon resonance frequency under the Hartmann-Hahn condition: $\gamma_H H_{1H} = \gamma_C H_{1C}$.

Figure 3.15 shows the pulse sequence diagram the carbon-proton cross polarization experiment. The pulse sequence begins with a $90^\circ X$ pulse to the protons to tip them along the y-axis. The phase of the proton B_1 field is then shifted by 90° and the protons are spin-locking pulse, and are forced to precess about the y-axis of their rotating frame with a frequency $\omega_H = \gamma_H B_H$. Meanwhile, the carbons are put into contact with the protons by turning the carbon field B_C on during the spin-lock time. This causes the carbon magnetization to grow in the direction of the spin-lock field. The carbons are now precessing about their y-axis with a frequency $\omega_C = \gamma_C B_C$. The differences between the energy levels of the protons and the carbons are now equal in the doubly rotating frame. A fraction of the proton magnetization can thus be transferred to the carbon spin system by the flip-flop mechanism responsible for spin diffusion: the spin-temperature of the protons increases whereas the spin-temperature of the ^{13}C spins decreases. At equilibrium, the carbon magnetization can be written as:

$$M_H = N_C (\gamma_H / \gamma_C) (\gamma_C^2 \hbar^2 H_0 / 4k T_L) \quad (3.25)$$

Thus the carbon magnetization can be multiplied at most by a factor of $\gamma_H / \gamma_C = 4$. Moreover, before repeating the pulse sequence, one has only to wait for near-equilibrium recovery of the proton magnetization. This is characterized by a spin-lattice relaxation time $\tau_{1\rho}^H$, which is generally much shorter than $\tau_{1\rho}^C$.



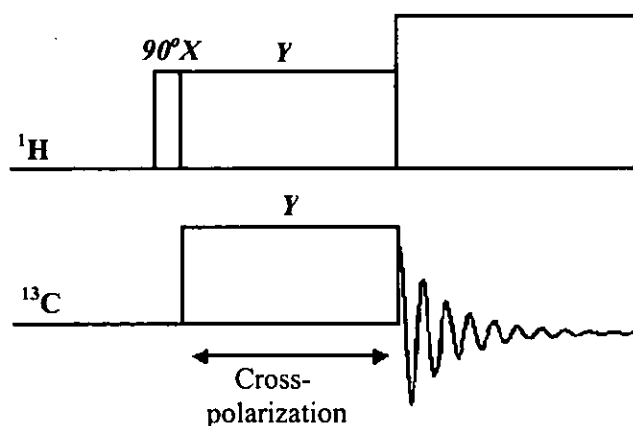


Figure 3.15 Pulse sequence diagram for cross-polarization.

As CP is based on heteronuclear dipolar interactions, it is sensitive to internuclear distances and the mobility of molecules or functional groups involved. This means that CP can also be used to establish the connectivity between coupled nuclei and to monitor molecular dynamics in solid.

In the case of insoluble sample, NMR in solid state is particularly useful. This technique is strongly developed to characterize the rubber and modified form in order to obtain the narrow line peak of resonance signal.

The use of solid-state ^{13}C -NMR to observe the change of structure of NR and *cis*-PB after vulcanization had been reviewed by Patterson and coworkers [71]. At least four structurally different methyl groups had been detected in the cross-linking of NR by dicumyl peroxide and the *cis-trans* isomerization occurred in NR by the rearrangement of the allylic free radical. In the case of PB, only methine and methylene carbons were present in the cross-linked network of PB. The line width of the elastomers increased with the increase of crosslink density.

Mori and Koenig [72, 73] had reported the solid state NMR studies of vulcanized natural rubber with and without carbon black. The solid-state ^{13}C -NMR spectra present the new characteristic peak associated with monosulfide and polysulfide as cross-linking of the rubber chains. They found the evidence of the occurrence of *cis-trans* isomerization from the carbon resonances of methylene



the increase in carbon black content as well as with the extent of cure. Klei and Koenig [74] also employed this technique to study the competitive vulcanization of blends of natural rubber and high *cis*-polybutadiene. The results suggested that competitive vulcanization altered the distribution of vulcanizate products such as *cis* polysulfide linkage at 57.4 ppm was favored over *trans* polysulfide at 64.3 ppm. Small additions of BR also hindered the *cis-trans* isomerization of NR. Gronski *et al* [75] used the solid-state ^{13}C -NMR with MAS to distinguish between monosulfidic crosslinks and polysulfidic structures and to quantify the chemical crosslink of vulcanized NR. The analysis of the chemical structure of NR and vulcanized NR by solid-state ^{13}C -NMR with HD/MAS technique had been studied by Buzare *et. al.* [76]. They indicated that *cis-trans* isomerization and different sulfide structures were detected and identified through the chemical shift values of the extra NMR lines, which were observed in various vulcanizates.

- Kinetic of Cross-Polarization

The variable contact time measurement is necessary in order to optimize the CP experiment, to obtain more information about the complete structural molecule on the samples [77, 78]. During the thermal contact, the ^{13}C magnetization increases rapidly in an exponential growth characterized by the cross-polarization time T_{CH} , which is governed by the strength of the ^1H - ^{13}C dipolar coupling. Simultaneously, the proton magnetization decreases according to a proton spin-lattice relaxation time in the rotating frame, $T_{1\rho}^H$, decay. The dependence of the ^{13}C magnetization as a function of the contact time, t , is written as:

$$M(t) = M_o (1 - T_{CH} / T_{1\rho}^H)^{-1} [\exp(-t / T_{1\rho}^H) - \exp(-t / T_{CH})] \quad (3.26)$$

where M_o is the absolute intensity of magnetization,

t is an any given cross-polarization contact time,

T_{CH} is a CP time constant, and its reciprocal, $1/T_{CH}$, is known as the CP rate constant,

$T_{1\rho}^H$ is the carbon rotating frame spin-lattice relaxation time constant.



$T_{1\rho}^H$ is the carbon rotating frame spin-lattice relaxation time constant.

Thus two opposing relaxation mechanisms operate during the contact time. For short contact times, the T_{CH} process dominates, and the carbon magnetization increases exponentially. At longer contact times, the process is dominated by the $T_{1\rho}^H$ process, and the magnetization decreases exponentially because of the proton spin-lattice relaxation in the rotating frame.

Kameda and Asakura [78] had performed the solid-state ^{13}C -NMR experiments under uniaxial deformation of NR to investigate the changes in the structural and dynamical behavior of the amorphous region induced by elongation. The change in the CP ^{13}C peak intensity as a function of contact time was also observed and was used to monitor the change of the dynamical behavior with time and temperature. The ^{13}C -magnetization decays behavior observed in variable H spin-locking times followed by $^1\text{H} \rightarrow ^{13}\text{C}$ cross polarization experiment. They found that the decay curves of ^{13}C -magnetization grew steep with decreasing temperature. This result showed that the $T_{1\rho}^H$ relaxation is sensitive to mobile part, and monotonically decreases when the flexibility of the chains is decreased. In addition, the strain-induced crystallization occurred at around 200% strain, the ^{13}C line shapes showed no significant change in the orientation of the amorphous chains. In contrast, the molecular dynamics of the amorphous chains was greatly affected even under low extension about at 30% strain.

In this study, high-resolution solid-state ^1H and ^{13}C -NMR are used to investigate the chemical structure of unsaturated rubber and the modified products. High-resolution solid-state ^{13}C -NMR can provide spectra of polymeric system by combining the techniques of magic angle spinning "MAS" and cross polarization "CP". This technique can be used to study the dipolar interaction between ^{13}C and ^1H that is operative in the rigid part of rubber upon hydrogenation. The CP experiment can be applied to study the molecular behavior of the rubber chains after modification in the case of the hydrogenated NR and hydrogenated ENR.



study of the shapes and widths of the peaks and of how they depend on the way in which the polymer was prepared could in principle give a great deal of information about the microstructure of the polymer. The width of the peaks can be regarded as a nuisance because it generally leads to the overlapping of peaks due to different modes of vibration and makes the interpretation of the spectra more difficult, especially in the case of polymers where the number of lines is important. A simple method of dealing with the problem of overlapping peaks when determining absorbance is to use the pseudo-baseline method. Another method of processing spectra is simply to scale one spectrum and subtract it from another. This subtraction method may be used, for instance, in finding the spectrum of one component of a two component mixture by subtracting the known spectrum of the other component from the spectrum of the mixture. In addition, this method does not help in separating the overlapping peaks due to a single component and other methods have therefore been devised for separating peaks. The curve-fitting is usually used to resolve the infrared and Raman spectra. According to the samples and the apparatus, the shape of the line is generally assumed Gaussian, Lorentzian, or a combination of Gaussian and Lorentzian function (named pseudo-voigt) [62]. The Lorentzian function is given by:

$$L(\bar{\nu}) = \frac{a_o}{1 + \left(\frac{\bar{\nu} - \bar{\nu}_o}{w} \right)^2} \quad (3.27)$$

where a_o is the amplitude of the peak, $\bar{\nu}_o$ is the wavenumber at the line centre, w is the width of the full width at half maximum (FWHM) intensity, $L(\bar{\nu})$ represents the infrared absorbance or the intensity of Raman scattering at wavenumber $\bar{\nu}$. If a complex region of overlapping peaks is assumed to be composed of a known number of Lorentzian peaks with unknown centres, half-widths and heights of the region can be computer fitted to find the values of these quantities. Such fits can also be made for other assumed line shapes, for example, the Gaussian function (in Equation 3.27) or combinations of Gaussian and Lorentzian functions (called Pseudo-voigt functions). The Gaussian function is given by:



The Gaussian function is given by:

$$L(\bar{\nu}) = a_o \exp \left[-0.5 \left(\frac{\bar{\nu} - \bar{\nu}_o}{w} \right)^2 \right] \quad (3.28)$$

The solid state NMR spectra are fitted by combinations of Gaussian and Lorentzian functions to obtain many parameters such as peak position, line intensity through peak area, and line-width. These parameters can be applied to investigate the %hydrogenation and molecular dynamic of the modified samples.

3.5 Thermal Analysis

Thermal analysis methods are used to determine glass transition, thermal expansion, thermal decomposition, and other thermal events in polymer materials. Polymers typically display broad melting endotherms and glass transitions as major analytic features associated with their properties. Characterization of polymers requires a detailed analysis of these characteristic thermal transitions using both differential scanning calorimetry (DSC) and thermal gravimetric analysis (TGA) which provides useful information involving the thermal behavior and stability of polymers before and after modification.

3.5.1 Differential Scanning Calorimetry (DSC)

A number of important physical changes in a polymer may be measured by DSC. These include the glass transition temperature (T_g), the crystallization temperature (T_c) etc.

Calorimetry involves the measurement of relative changes in temperature and heat or energy either under isothermal and adiabatic conditions. An adiabatic measurement is carried out on a closed system where determination of the heat, Q , associated with a change in temperature, dT , yields the heat capacity of the material,



Considering only the assumption of no difference in the heating rates for the sample and the reference and that the DSC curve turns to the original baseline after the transition, hence, the enthalpy can be described in the following:

$$\Delta H = \int_{T_i}^{T_f} C_p dT \quad (3.29)$$

where the T_i and T_f refer to the initial and final temperatures of the transition. DSC is a thermal analysis technique which is used to measure the temperatures and heat flows associated with transitions in materials as a function of time and temperature. Such measurements provide qualitative and quantitative information about physical and chemical changes that involve endothermic and exothermic processes, or changes in heat capacity. The typical DSC thermogram is schematically illustrated in Figure 3.16.

From a thermodynamic point of view, the glass transition, T_g , is one of the most important parameters for characterizing a polymer system. A polymer may be amorphous, crystalline, or a combination of both. Many polymers actually have both crystalline and amorphous regions, i.e., a semicrystalline polymer. The DSC measures the transition onset and ending temperatures as well as, the temperature at maximum transition so called glass transition temperature " T_g ". The T_g is a transition related to the motion in the amorphous regions of the polymers. Below the T_g an amorphous polymer can be said to have the characteristics of a glass, while it becomes more rubbery above T_g . On the molecular level, the T_g is the temperature of the onset of motion of short chain segments. The DSC is an important technique to measure the glass transition temperature which depends on the heating rate of the experiment and the thermal history of the samples. Also, any molecular parameter affecting chain mobility affects the T_g [79].



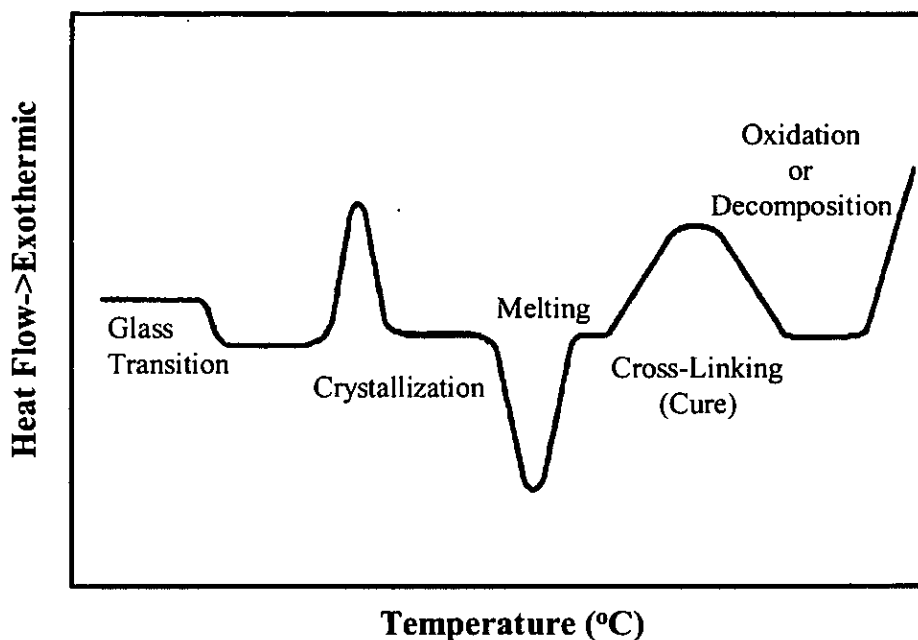


Figure 3.16 Typical DSC thermogram.

Generally, the DSC is useful to monitor polymer before and after modification to assess their similarities or differences on the thermal properties. The main feature of a glassy polymer is the transition from largely brittle glassy behavior at low temperature to a rubbery or viscoelastic state at high temperatures. This transition has many of the characteristics of a genuine second-order transition. DSC is a convenient method for determining the temperature change from glass to melt.

The thermal behaviors of the hydrogenated products studied by DSC had been reported in several literatures [11-13, 63, 80]. Mango and Lenz [11] reported the thermal behavior of hydrogenated butadiene rubber (HBR), hydrogenated polyisoprene (HPI) and hydrogenated styrene-butadiene rubber (HSBR) using DSC. Thermal analysis of the HBR indicated a polyethylene-like melting temperature at 118°C and two HSBR samples also exhibited endotherm at 70°C and 92°C, respectively, which can be assigned to melting transition of short-block polyethylene segments. Doi et. al. analyzed the glass transition temperature of the hydrogenated butadiene rubber with different microstructure [63]. It was found that T_g of the different microstructure of HBR increase in the order: T_g (syndiotactic) > T_g (atactic)

T_g (isotactic). The DSC analysis of SBR showed that the thermal stability of SBR increased upon hydrogenation level as mentioned by Saker De et. al. [80]. In addition, T_g of the HSBR samples (80-85% hydrogenation) is higher than that of the parent SBRs at all styrene level also found by Saker De and coworkers [56]. The glass transitions slightly increase on hydrogenation of NR, that is, the T_g increases 3°C at 100%hydrogenation as reported by Singha et. al. [12]. In addition, the heat capacity (C_p) giving an information the characteristic of the rigidity of the rubber chains was analyzed. This indicated that there is gradually increase in C_p with the increase in the hydrogenation level. DSC had been employed to investigate the thermal properties of SBR and HSBR obtained from diimide reduction in latex phase [80]. They suggested that the increase of T_g value might arise from the increase amount of crystalline segments in the HSBR samples. The thermal properties of different HPB samples had been studied by Rao et. al. [43]. In the range of $50\text{-}150^\circ\text{C}$, all the HBR go through an endothermic process corresponding to a melting temperature. Interestingly, the HBR samples showed melting peaks in between the above temperature indicating a structure equivalent to that of ethylene-butene copolymer.

3.5.2 Thermal Gravimetric Analysis (TGA)

Thermal gravimetric analysis (TGA) uses heat to drive reactions and physical changes in materials. TGA provides a quantitative measurement of any mass change in the polymer or material associated with a transition or thermal degradation under a controlled atmosphere. TGA can directly record the change in mass due to decomposition, or oxidation of a polymer with time and temperature while the material is subjected to a controlled temperature program. Because mass is a fundamental attribute of a material, any mass change is more likely to be associated with a chemical change, which may, in turn, reflect a compositional.

The sample is placed in a furnace while being suspended from one arm of a precise balance. The change in sample weight is recorded while the sample is either maintained isothermally at a temperature of interest or subjected to a programmed heating. The TGA curve may be plotted in either the weight loss of the sample or in differential form, (the change of sample weight with time) as a function of temperature.



and compositional analysis. The percent weight loss (%W) can be determined as follows:

$$\%W = 100(M_i - M_f) / M_i \quad (3.30)$$

where M_i and M_f refer to the initial and final weight, respectively.

The TGA analyzer records the temperature or time of the weight loss region and the temperature at maximum transition as represented in Figure 3.17. It provides an indication of a sample's thermal decomposition temperature, T_d and is used to estimate the relative amounts of volatiles, polymer, non-polymeric additives, and inorganic residues. It has become one of the most important tools for the characterization of the degradation of polymers. The importance of degradation studies of hydrogenated rubbers arises from the industrial service performance of manufactured items and commercial exploitation of the materials. Several publications are therefore interested to study the thermal stability of the hydrogenated rubbers by TGA.

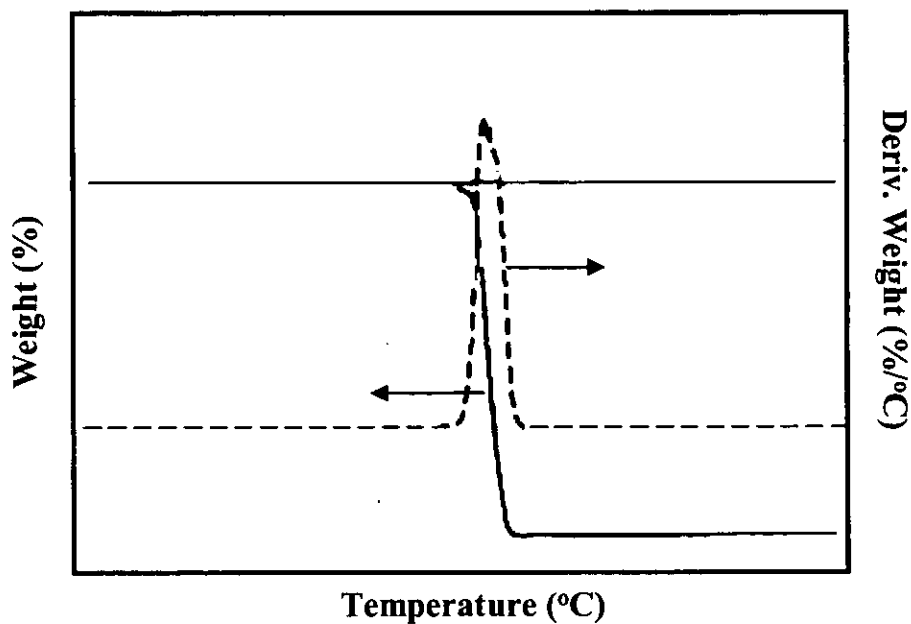


Figure 3.17 Typical TGA thermogram.

Thermal degradation of hydrogenated SBR having different unsaturation levels has been studied over a wide range of temperature under nitrogen and air conditions using TGA [80]. Thermal stability of HSBR in nitrogen atmosphere is higher than that

of SBR. But the stability against oxidative degradation is markedly higher for SBR samples mostly because of the formation of cross-linking.

The improvement of thermal behavior of hydrogenated NR (HNR) was studied by Singha et. al. [12]. By using TGA technique, they found that the initial decomposition temperature of HNR increased with increasing reduction of diene units in the samples compared to the NR. Roy et. al. [21] also studied the thermal properties of hydrogenated ENR. They found that the thermal stability and aging resistance were improved as compare to the ENR.

3.6 Rheology Behavior

Rheology is the science of the deformation and flow of materials when forces are applied to them. It is fundamentally drawn from mechanics, which mainly concerns with how materials differ from the ideal of classical mechanics. Rheology is concerned with the response of materials to mechanical forces, i.e. the relationship between stress, strain and time. There are three types of response to an applied stress: viscous flow, elastic deformation and rupture [81]. In viscous flow, a material continues to deform as long as the stress is applied and the energy of flow is dissipated as heat. Elastic deformation (reversible deformation) is the deformation spontaneously reverses to its original shape when the stress is removed and the applied work is largely recoverable. Rupture plays a crucial role in determining the maximum rate at which a deformation process can be carried out. However, rubber has both viscous and elastic responses to deformation. A viscous response is proportional to the rate of deformation while an elastic response is proportional to the amount of deformation. Therefore, measuring the elastic and viscous properties help characterize rubber behaviour in processing and final product performance [81].

3.6.1 Theoretical Analysis of Rheological Behavior

Oscillational dynamic rheometer is a convenient instrument to assess the viscoelastic properties of molten polymers. Complex viscosity is determined from the amplitudes of the stress and strain and the phase angle between them (δ). In oscillat



measurement, the melt is subjected to a sinusoidal varying shear strain (γ) and shear stress (σ) as follows [82, 83]:

$$\gamma = \gamma_0 \cos \omega t \quad (3.31)$$

$$\sigma = \sigma_0 \sin(\omega t + \delta) \quad (3.32)$$

The maximum values of the sinusoidal shear strain and shear stress are γ_0 and σ_0 , respectively. The shear stress and shear strain are commonly dealt with by using complex notation:

$$\gamma^* = \gamma_0 (\cos \omega t + i \sin \omega t) = \gamma_0 \exp(i\omega t) = \gamma' + i\gamma'' \quad (3.33)$$

$$\sigma^* = \sigma_0 [\cos(\omega t + \delta) + i \sin(\omega t + \delta)] = \sigma_0 \exp[i(\omega t + \delta)] \quad (3.34)$$

The complex shear modulus is defined as:

$$G^* = \frac{\sigma^*}{\gamma^*} = \frac{\sigma_0}{\gamma_0} \cos \delta + i \frac{\sigma_0}{\gamma_0} \sin \delta = G' + iG'' \quad (3.35)$$

where $G'(\omega)$ is the storage modulus associating with the stored energy and $G''(\omega)$ is the loss modulus associating with the dissipation of energy as heat.

The rheological properties of rubbers are of importance to industry involved in the processing and fabrication of materials in order to produce the useful products.

3.6.2 Measurement of Rheological Properties

A variety of instruments have been used to measure the viscosity and other rheological properties of polymers [81-84]. Most of these instruments are capable of measuring the rheological properties as a function of temperature, and shear rate. The rheological characterization of rubber and filled rubber compounds by means of rheometrical methods is not an easy task. An instrument apparently used to study rheological properties of rubber compounds before processing is a oscillating disc rheometer (ODR) or rubber process analyzer (RPA).

(a) Oscillating Disc Rheometers

The ODR technique gives the complete cure curves in a very short period of time. Recently, the Rubber Process Analyzer (RPA) is developed and designed to



classify and determine the processability of different grades of NR. The RPA strains the sample in shear by oscillating the lower die sinusoidally. Oscillation frequency can be set from 0.1 to 2000 cpm (cycles per minute). Viscoelastic properties of rubber vary with changes in applied strain, frequency and temperature. Samples are often tested over several frequencies, strains or temperatures in one test called a sweep. The magnitude of the lower die movement can be set by the angular oscillation of the lower die or by the required strain on a sample. The lower die can oscillate from $\pm 0.05^\circ$ of arc to $\pm 90^\circ$ of arc. This angular oscillation corresponds to strains of $\pm 0.7\%$ to $\pm 1256\%$. The test cavity is schematically described in Figure 3.18.

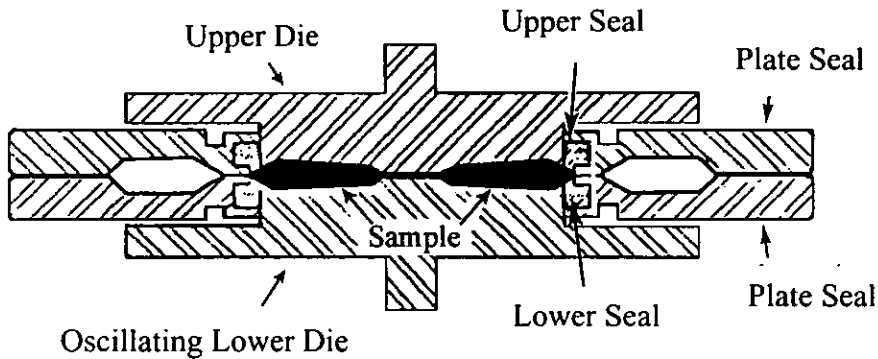


Figure 3.18 RPA dynamic torsional rheometer and testing principle [84].

It is designed to measure both elastic and viscous properties of elastomers and compounds. The upper die is attached to a torque transducer to eliminate noise from the lower die drive system and to measure the torque transmitted through the sample. This torque is called the complex torque or S^* and it is reduced by RPA computer into an elastic (S') component (in-phase with strain) and a viscous (S'') component (90° out-of-phase with strain) by applying a Fourier transform analysis to the S^* signal. The Fourier transform analysis can improve in accuracy resulting from the use of a microprocessor to collect multiple torque values at incremental strains. RPA complex torque (S^*), elastic torque (S') and viscous torque (S'') response from a sinusoidal strain as demonstrated in Figure 3.19. $\tan \delta$ is calculated from (S''/S').



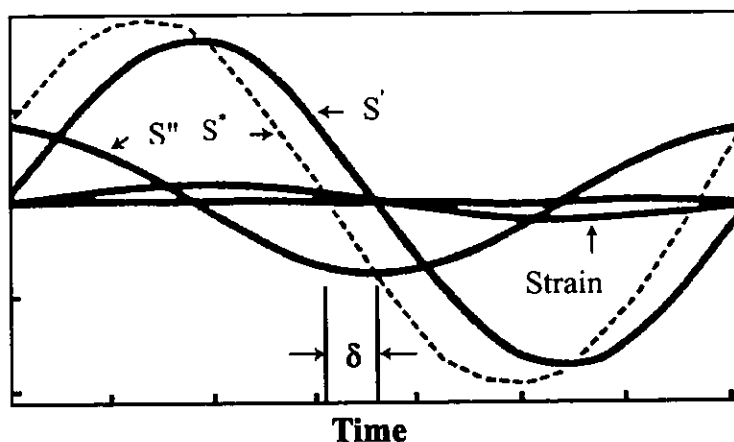


Figure 3.19 Complex torque (S^*), elastic torque (S') and viscous torque (S'') responses from a sinusoidal strain [85].

3.6.3 Basic Principle of Fourier Transform Rheology

Fourier transform rheometry is a new test technique that allows both linear and non linear viscoelastic domains of polymer materials behaviour to be accurately investigated. No commercial equipment is readily available, but any instrument can be easily modified in order to capture the full strain and torque signals generated when submitting samples to harmonic deformations at fixed frequency and temperature. Fourier transform calculation techniques are applied to captured signals in order to resolve them in their main component and other harmonics, if any. Contrary to standard dynamic testing methods whose validity in extracting the elastic and viscous components from the (measured) complex torque is limited to the linear viscoelastic range, Fourier transform rheometry provides valid results, whatever is the response of the tested material, even in the far non linear range [84, 86].

The basic principle of Fourier transform rheology is described as follows. Assuming no slip at die walls (in fact prevented by die grooves and the pressurization of the cavity), the applied shear strain in the rheometer cavity is $\gamma(t) = \gamma_0 \sin(\omega t)$, which implies obviously that the shear rate is given by $\dot{\gamma}(t) = \gamma_0 \omega \cos(\omega t)$, where γ_0 is the maximum strain amplitude, ω is the frequency and t is the time.

viscoelastic material, theoretical considerations show that the shear stress response can be expected to be given by a series of odd harmonics, i.e.:

$$\sigma(t) = \sum_{\substack{j=1 \\ \text{odd}}}^{\infty} \sigma_j \sin(j\omega t + \delta_j) \quad (3.36)$$

The viscosity function of the material can be approximated by a polynomial series with respect to the shear rate:

$$\eta(\dot{\gamma}) = \eta_0 + a|\dot{\gamma}| + b|\dot{\gamma}|^2 + C|\dot{\gamma}|^3 + \dots \quad (3.37)$$

If the applied strain is a harmonic oscillation, the absolute value of the shear rate is $|\dot{\gamma}| = |\dot{\gamma}_0 \omega \cos(\omega t)|$. Through Fourier expansion of $|\dot{\gamma}_0 \omega \cos(\omega t)|$ and substitution into Equation 3.37, an expression is obtained that can be rearranged and sorted in such a manner that the stress appears to be proportional to a polynomial series where only odd multiples of the frequency appears, i.e.:

$$\sigma(t) \propto A \cos(\omega t) + B \cos(3\omega t) + C \cos(5\omega t) + \dots \quad (3.38)$$

Consequently, a Fast Fourier Transform (FFT) of the measured stress signal can be expected to lead to distinct signals in the Fourier transform spectrum (FTS) at $\omega, 3\omega, 5\omega, \dots$. Clearly, if the tested material exhibits a pure linear viscoelastic response, Equation 3.38 reduces to the first term of the series, as considered in most standard dynamic test methods.

3.6.4 Factors Affecting the Rheological Properties

There are numerous factors which affect the rheological properties of rubber. Such factors are discussed below:

(a) Effect of Temperature

The effect of temperature on the flow properties of polymer may be expressed by the *Arrhenius* equation:

$$\eta = Ke^{E_a/RT} \quad (3.39)$$



where K is a constant, E_a is the activation energy, R is the ideal perfect gas constant and T is the absolute temperature. From this equation and a knowledge of these variables, the viscosity, η , of the polymer melts at any temperature can be calculated. The plots of $\log \eta$ against $1/T$ show only a restricted linear relationship and fairly good straight lines can only be drawn over the range of 50-60°C. Equation 3.39, thus, indicates that an increase in the temperature results in a decrease in viscosity [81].

(b) Effect of Pressure

The greater the free volume, the easier the flow can be taken place. The free volume increases with temperature (due to thermal expansion) and is much influenced by the pressure. An increase in the hydrostatic pressure decreases free volume and increases the viscosity of liquid. One approach is the modified Andrade equation:

$$\eta = K \exp\left(\frac{E_a}{RT} + \frac{CV_o}{V_f}\right) \quad (3.40)$$

where V_o is the close packed volume, V_f is the free volume defined as $V - V_o$ where V is the observed volume and C is a constant generally being 0.5-1.0.

(c) Effect of Molecular Characteristic

Molecular theories explaining the viscoelastic behaviour of high molecular weight polymers in the plateau and terminal relaxation zones those most relevant to processing behaviour are extensively reviewed by Sanders et. al. [87]. The molecular characteristic affecting the relaxation processes and the viscoelastic properties of an amorphous polymer are molecular weight, degree of branching along the chain, the length of the branches and molecular weight distribution (MWD).

Pearson et. al. had studied the stress relaxation behaviour of three narrow distributions of polyisoprene [88]. The results showed that the rate of relaxation was increased markedly towards the terminal relaxation time. This characteristic was found to be strongly dependent upon \overline{M}_w . The polymers having the greater molecular weight distribution exhibit the higher viscosity than the one having the narrower molecular weight distribution.



(d) Effect of Fillers, Plasticizers and Lubricants

Addition of filler tends to increase the viscosity of the rubbers. Several relationships have been proposed to describe this effect and a useful relationship is known as the *Maron-Pierce* relationship:

$$\eta_c / \eta_0 = [1 - (c/c_0)]^2 \quad (3.41)$$

where η_c is the viscosity at a volume concentration c , η_0 is the viscosity of the resin and c_0 is the volume concentration for close packing. The advantage of this relationship is that it allows a physical appreciation of the reduction in fluidity (inverse viscosity) as the volume of unconstrained liquid is reduced.

Plasticizers act by spacing out the molecules. The most obvious effect is to reduce viscosity, but they also tend to reduce the elastic modulus of the melt, so increasing the elastic response at a given stress. The effectiveness of a plasticizer depends on concentration, compatibility and its viscosity. For example, poly(vinyl chloride), whose T_g is 354 K, usually contains 30 to 40 wt% of plasticizers, such as dioctyl or dinonyl phthalate, to increase its toughness and flexibility at ambient temperatures [89].

3.6.5 Rheological Properties of Hydrogenated Rubbers

On hydrogenation there are changes in the rheological properties of diene elastomers. Bhattacharjee et. al. [90] studied the rheological behaviour of nitrile rubber (NBR) and hydrogenated NBR (HNBR) of different hydrogenation levels by using capillary rheometer. The results showed that HNBR has higher shear viscosity than NBR. It is interesting to note that HNBR (with 50% hydrogenation) has higher shear viscosity than HNBR with 80% hydrogenation. But in all cases shear viscosity decreases with an increase with shear rate. The die swell of NBR and HNBRs were also determined and found that the die swell decreases when degree of hydrogenation was increased. Raju et. al. [91] had investigated the melt rheology of linear and star-branched hydrogenated butadiene rubber (HBR). The storage modulus (G') and loss modulus (G'') of HBR melts were measured by using rheometric mechanical spectrometer. The loss modulus (G'') and storage modulus (G') for a typical



compared with that of PB found that at lower frequencies (10^{-3} sec^{-1}), G'' of HBR exists whereas G'' of PB starts at relatively higher frequencies (10^{-2} sec^{-1}). Loss modulus (G'') of HBR, at high frequency, falls more rapidly with increasing frequency. This phenomenon involves the relaxation of short chain segments, wherein the effect of local chain structure is very important. A comparison of loss and storage modulus of star hydrogenated PB (SHBR) and linear HBR showed that at low frequencies loss modulus (G'') for both polymers coincide, whereas at higher frequencies, G'' of HBR reaches maximum and then drops steadily. The storage moduli at low frequencies of HBR are somewhat higher than SHBR but at higher frequency, G' of HBR has much greater than that of HBR. Gotra and Graessley [92] studied the rheological property of polyisoprene (PI) and hydrogenated PI (HPI) by using rheometrics mechanical spectrometer. They reported that there is no change in the reduced master curves for PI and HPI. Whereas the plateau modulus (G') decreases and steady-state recoverable compliance increases on hydrogenation of PI.



CHAPTER 4

MATERIALS AND METHODS

This chapter listed the materials and instruments used in this research. The experimental procedures for the diimide hydrogenation of natural rubber and its epoxidized forms are also demonstrated as well as various techniques used to analyze the chemical and physical characteristics of the resulting products.

4.1 Materials

The materials used in this present thesis are given as follows:

1. High ammonia natural rubber (NR) latex was procured from Thai Rubber Latex Corporation (Thailand) Public Company Limited. Its specification was presented in Appendix A.

2. Deproteinized natural rubber (DPNR) latex was prepared by enzymatic treatment using proteolytic enzyme named proteinase B KP 3939 [33].

3. Four types of epoxidized natural rubbers (ENR) were used i.e. ENR-10, ENR-22, ENR-30 and ENR-40 which contained 10, 22, 30 and 40 % epoxide content, respectively. The preparation method was the use of *in situ* performic acid in latex phase at 50°C [93].

4. 4-Methyl-4-octene (MO) used as a model molecule of polyisoprene was kindly supported by Laboratoire de Chimie Organique Macromoléculaire (LCOM), Chimie (UMR CNRS UCO2M n° 6011), Université du Maine, Le Mans, France.

5. Synthetic polyisoprene latex was supported by Laboratoire de Chimie Organique Macromoléculaire (LCOM). Its dry rubber content is 60% and average molecular weight is about 29,000.

6. *p*-Toluenesulfonylhydrazide (TSH) is a practical grade product from Fluka Co. Ltd. The decomposition temperature is 140°C and its density is 0.903 g/cm³.



7. Xylene is a product from Carlo Co. Ltd. The boiling point temperature is 135°C.

8. Hydrazine monohydrate ($\text{H}_2\text{N}_4 \cdot \text{H}_2\text{O}$) was purchased from Carlo Co. Ltd. The assay is 98% and its density is 1.03 g/cm³.

9. Hydrogen peroxide was obtained from Fluka Co. Ltd. The assay is 30% and its density is 1.00 g/cm³.

10. Silicone antifoaming agent was supplied from Carlo Co. Ltd. and its density is 1.01-1.05 g/cm³.

4.2 Instruments

All instruments used in this research are listed in Table 4.1.

Table 4.1 Instruments used in the experiment for characterization

Instruments	Model	Manufacturer
Fourier transform infrared spectroscopy (FT-IR)	System 2000	Perkin Elmer
Raman spectroscopy	T64000	Jobin-Yvon
¹ H-NMR	DPX-300	Bruker
¹³ C-NMR for liquid analysis	DPX-300	Bruker
¹³ C-NMR for solid analysis	Avance 300	Bruker
High performance liquid chromatography (HPLC)	510	Water
RPA	RPA 2000	Alpha Technologies
Viscometer	PVS 5	Lauda
Gel Permeation Chromatography	150-CV	Water
Differential Scanning Calorimeter	DSC 7	Perkin Elmer
Thermogravimetric Analyzer	TA-SDT 2960	Thermal Analysis



4.3 Experiment Flow Chart

In this research, the study of hydrogenation reaction was carried out with NR and ENRs using diimide non-catalytic hydrogenation process. The reagents provided diimide molecule were *p*-toluenesulfonylhydrazide (TSH) and hydrazine in conjunction with hydrogen peroxide (N_2H_4/H_2O_2). The use of TSH was carried out in organic phase with NR, DPNR and ENRs, while the second type of reagent was processed in latex form with NR and DPNR latex. The overall of the study is summarized in a flow chart presented (see Figure 4.1).

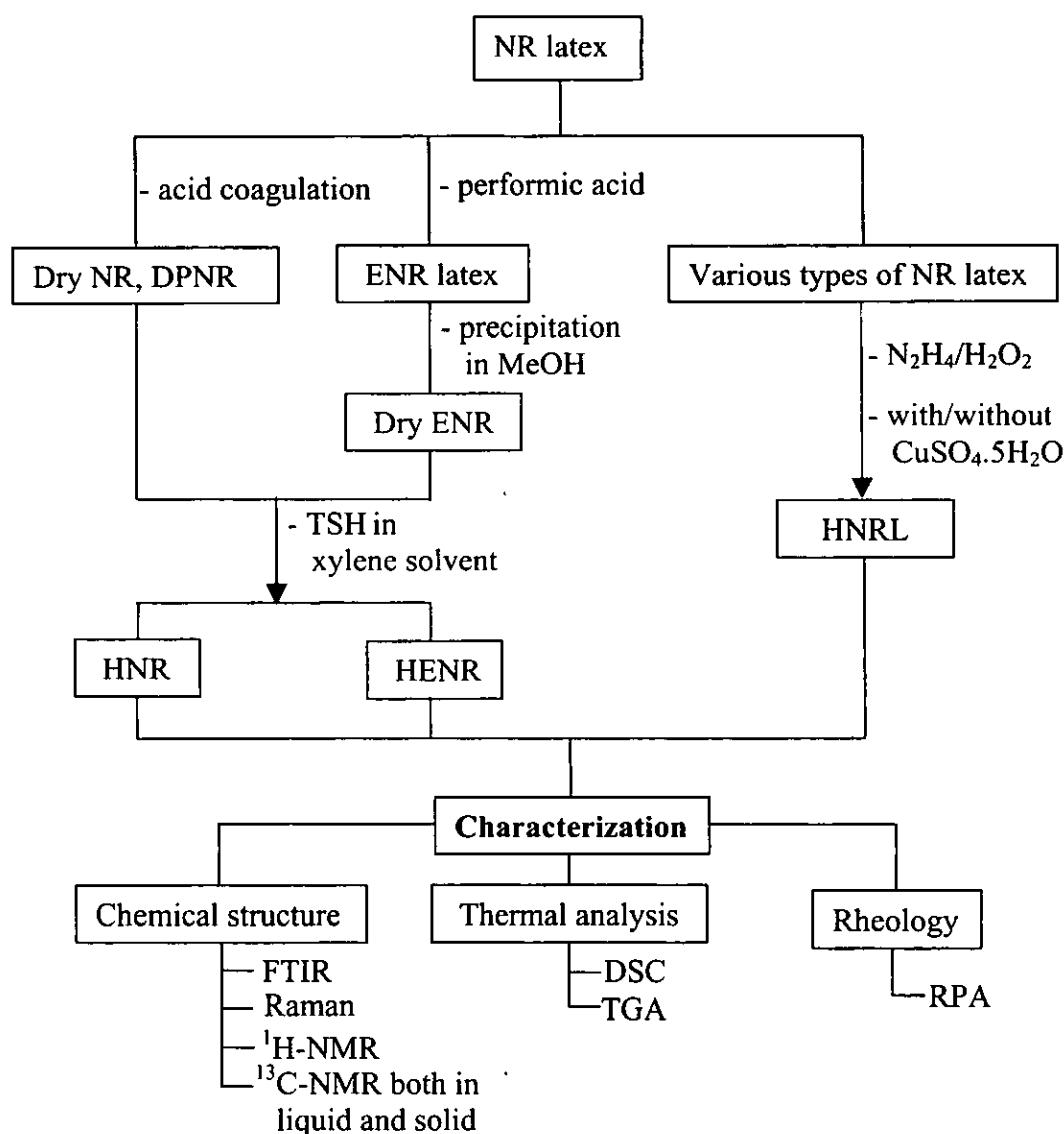


Figure 4.1 Flow chart of hydrogenation of NR and ENRs in this research.



4.4 Hydrogenation of Unsaturated Units by *p*-Toluenesulfonyl Hydrazide

4.4.1 Hydrogenation of Model Molecule

p-Toluenesulfonylhydrazide (TSH) was added to a three-necked round-bottomed flask fitted with a magnetic stirrer, a condenser and nitrogen inlet tube. Then 0.3052 g of 4-methyl-4-octene (MO) and 0.1651 g of mesitylene as an internal standard in 10 ml of xylene were introduced to the system. A mixture was heated at 135°C under nitrogen gas. The modified sample was sampling at various reaction times and was further monitored by HPLC. The crude mixture obtained at 24 h of reaction time was filtered to eliminate solid by-product. Finally, the xylene solvent was evaporated from the mixture by rotary evaporator before investigation by ¹H-NMR and ¹³C-NMR spectroscopies.

4.4.2 Hydrogenation of NR and ENRs

Hydrogenation of unsaturated rubber (NR and ENRs) was carried out in a 250 ml three-necked round-bottomed flask, equipped with a reflux condenser, and a nitrogen inlet tube. The solution of 2% (w/v) rubber in xylene introduced into the reaction flask, then with a molar ratio of TSH to unsaturated unit ($[TSH]/[C=C]$) equal to 2 was added. The hydrogenation reaction was taken place at 135°C under nitrogen atmosphere. The sample solution was drawn from the reaction at a selected time. At the end of the reaction, the mixture was concentrated by evaporation of the solvent under reduced pressure at 60°C before precipitation in distilled methanol. The hydrogenated product was purified by dissolving in distilled hexane and re-precipitated in methanol. Finally, the resulting product was dried in vacuum at room temperature.

The reaction conditions of hydrogenation of MO, NR and ENRs are listed in Table 4.2.



Table 4.2 Reaction conditions used for the preparation of hydrogenated rubbers in organic media

Sample code	Unsaturated types	Molar ratio of	
		[C=C]	[TSH]
HMO	4-Methyl-4-octene	1	2
HNR	NR	1	2
HDPNR	DPNR	1	2
HENR-10	ENR-10	1	2
HENR-22	ENR-22	1	2
HENR-30	ENR-30	1	2
HENR-40	ENR-40	1	2

4.5 Hydrogenation of Unsaturated Units by Hydrazine and Hydrogen Peroxide

4.5.1 Hydrogenation of Synthetic Polyisoprene (PI) latex

5.00 g of synthetic polyisoprene latex (10% DRC) was diluted with 25 g of water. After stirring for 0.5 h, aqueous solution of copper sulfate pentahydrate ($\text{CuSO}_4 \cdot 5\text{H}_2\text{O}$) was added to the reaction and stirred for 0.5 h. Then, hydrazine monohydrate was dropped by dropping funnel during 30 min. A specific volume of 98% aqueous hydrazine was added to the stirred solution by dropping funnel at 45°C. At a particular temperature, 35% hydrogen peroxide was then introduced dropwise over the specific period of time (6h) with dropping funnel. The recipes used in the hydrogenation study are shown in Table 4.3.



Table 4.3 Recipe used for the hydrogenation of PI latex

Components	Content
Sythetic PI (10% DRC)	3 g
Mole of DB	0.044 mol
CuSO ₄ ·5H ₂ O	8.02 x 10 ⁻⁴ mmol
Hydrazine hydrate (98%)	0.044 mol
Hydrogen peroxide (35%)	0.044 mol

4.5.2 Hydrogenation of Natural Rubber (NR) Latex

30 g of rubber latex (20%DRC) was added to a three-necked round bottom flask equipped with a condenser and a dropping funnel. After stirring for 0.5 h, a specific volume of hydrazine monohydrate (98%) was dropped for at least 0.5 h and then 35% hydrogen peroxide was slowly introduced by dropping funnel over a specific period of time. Antifoam agent was added periodically when the gas bubble was taken place during addition of hydrogen peroxide. Hydrogenated latex was sampling at certain period of reaction time. The resulting hydrogenated latex sample was coagulated in distilled methanol. The obtained white rubber solid was washed several times with water before drying in vacuum oven at room temperature.

Various conditions of hydrogenation in aqueous media were studied as given in Table 4.4-4.7.



Table 4.4 Various conditions used for the hydrogenation of NR in latex (20% DRC) at 60°C, using CuSO₄.5H₂O as a catalyst

Sample code	Molar ratio of			Surfactant	Amount of CuSO ₄ .5H ₂ O (mmol)
	[C=C]	[N ₂ H ₄]	[H ₂ O ₂]		
NRL1	1	1	1	-	-
NRL2	1	1	1	SDS	-
NRL3	1	1	1	-	4.00 x 10 ⁻³
NRL4	1	1	1	SDS	4.00 x 10 ⁻³
NRL5	1	1	1	SDS	2.40 x 10 ⁻³

Table 4.5 Various reaction temperatures and dry rubber contents used for the hydrogenation of NR latex

Sample code	%DRC	Molar ratio of			Temperature (°C)
		[C=C]	[N ₂ H ₄]	[H ₂ O ₂]	
NRL6	20	1	1	1	30
NRL7	20	1	1	1	45
NRL8	20	1	1	1	60
NRL9	20	1	1	1	70
NRL10	20	1	1	1	80
NRL11	10	1	1	1	60
NRL12	20	1	1	1	60
NRL13	30	1	1	1	60



Table 4.6 Various amount of reagents used for the hydrogenation of NR latex (20%DRC) at 60°C

Sample code	Molar ratio of		
	[C=C]	[N ₂ H ₄]	[H ₂ O ₂]
NRL14	1	0.5	1
NRL15	1	1	1
NRL16	1	1.5	1
NRL17	1	2.0	1
NRL18	1	1	0.5
NRL19	1	1	1
NRL20	1	1	1.5
NRL21	1	1	2.0
NRL22	1	0.5	0.5
NRL23	1	1	1
NRL24	1	1.5	1.5
NRL25	1	2.0	2.0

Table 4.7 Various types of NR latex used in the hydrogenation reaction at 60°C

Sample code	Types of latex	Molar ratio of		
		[C=C]	[N ₂ H ₄]	[H ₂ O ₂]
NRL8	High ammonia NR latex	1	1	1
DPNR(TER)	Deproteinized NR latex (stabilized by terric)	1	1	1
DPNR(SDS)	Deproteinized NR latex (stabilized by SDS)	1	1	1
SFNR	Skim fresh NR latex	1	1	1
CFNR	Cream fresh NR latex	1	1	1
UNR	Upper layer NR latex	1	1	1
LNR	Lower layer NR latex	1	1	1



4.6 Chemical Structure Characterization

The chemical structure of model molecule, NR, ENR and the hydrogenated products was investigated using IR, Raman, $^1\text{H-NMR}$ and $^{13}\text{C-NMR}$ spectroscopies.

4.6.1 FT-IR Spectroscopy

FT-IR spectra of all samples were recorded on FTIR spectrometer (Perkin Elmer PE 2000). Each sample was dissolved in chloroform and casted onto a NaCl cell. After evaporation of the chloroform, the rubber film was formed and it was then scanned for 16 times in the spectra range of $600\text{-}4000\text{ cm}^{-1}$ with 4 cm^{-1} resolution in order to obtain a good signal to noise ratio.

4.6.2 Raman Spectroscopy

Raman spectra of all samples were recorded on a T64000 Jobin-Yvon multichannel spectrometer adjusted in a simple spectrograph configuration with a 600 lines/mm grating. The picture of Raman spectrometer is shown in Figure 4.2. In this spectrometer the systematic single spectrograph is attached to an Olympus microscope which is equipped with a computer controlled stepping microscope stage. The system utilizes so called, back scattering configuration in which the scattered light is collected using the same objective as is used to focus the laser onto the sample. Sample was illuminated with a Coherent Argon-Krypton Ion Laser using the 647.1 nm red line in order to minimize luminescence and fluorescence bands compared to shorter possible wavelengths. To improve the signal/noise ratio, each spectrum was accumulated 20 times during 30 seconds. Calibration of the spectrometer was precisely checked on the 520.2 cm^{-1} silicon band and the resolution of each spectrum can be estimated to be smaller than 2 cm^{-1} . Background is estimated for each spectrum with a standard fitting procedure from Labspec software. The wavenumber range selected was $500\text{-}3200\text{ cm}^{-1}$ in the case of the collected Raman spectra to determine the percentage of hydrogenation.



For precisely assignment of peak positions of NR, the Raman spectrum was collected using a record configuration of triple spectrograph with a 1800 lines/mm grating in the Raman shift range of 1650-1680 cm^{-1} and 200-3500 cm^{-1} .

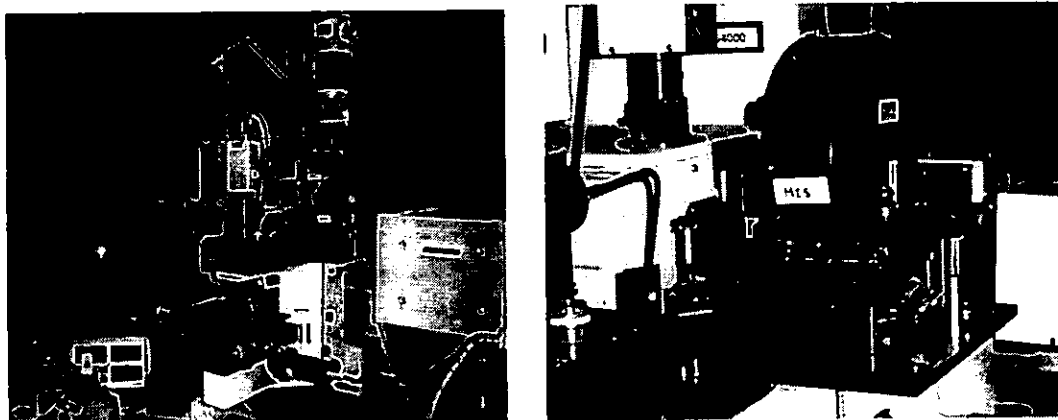


Figure 4.2 Picture of Raman spectrometer.

Raman Mapping

Raman Mapping process was also performed using this spectrometer by attaching the single spectrograph to an Olympus microscope which was equipped with a computer controlled stepping microscope stage. The instrument was used in the normal mode with a x 50 long distance objective work for Raman, and in confocal mode for depth profiling. The microscope was focused on a particular area of the surface sample as shown in Figure 4.3. By detecting the Raman spectra at several positions at regular intervals on the rubber surface, the distribution of components in the x-y direction was assessed. This mapping arrangement was utilized to investigate the heterogeneity in the rubber samples, at a microscopic scale.

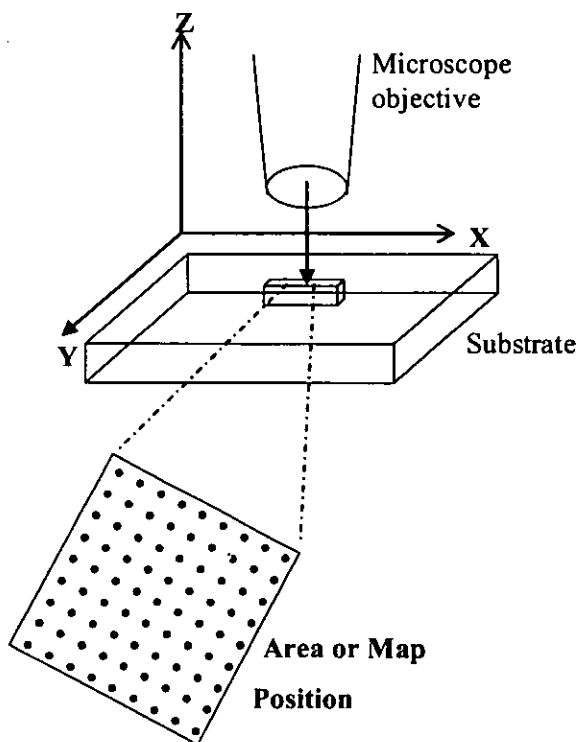


Figure 4.3 Schematic diagram of arrangements made to perform Raman mapping.

4.6.3 NMR Spectroscopy in Solution

^1H -NMR and ^{13}C -NMR spectra of the samples in solution state were recorded on Bruker DPX-300 MHz. Tetramethylsiloxane (TMS) was used as an internal reference. For ^1H -NMR analysis, about 10 mg of sample was dissolved in deuterated chloroform (CDCl_3) while for ^{13}C -NMR about 30 mg of sample was employed. Each sample was left overnight then filtered into NMR tube before analysis. The measurements were performed with 90° pulses and an acquisition time of 1 s.

4.6.4 NMR Spectroscopy in Solid State

Sample was packed in a zirconium oxide rotor with diameter of 3 mm and length of 2 cm. ^{13}C high resolution solid state NMR experiments were conducted at room temperature on a Bruker Avance 300 spectrometer operating at 75.47 MHz with a 4 mm cross-polarization (CP) magic angle spinning (MAS) probe. The instrument

shown in Figure 4.4 is equipped with a high-power amplifier for proton decoupling. Single pulse experiments combining MAS and ^1H decoupling were carried out using a pulse width of 90° ($4\ \mu\text{s}$) with a repetition time of 4 s. A spectral width of 25 kHz and 16 K data points was used for data collection. The MAS technique was applied at 10 kHz. The decoupling radio frequency was 60 kHz. The CP/MAS technique applied at 5 kHz for spin speed of rotor was employed to observe the molecular structure of the rubber chain before and after hydrogenation. In order to investigate the molecular behavior of the rubber chains of the hydrogenated samples, the CP/MAS with variable contact time (0.02-20 ms) was applied for characterizing these samples. The spectra were calibrated with respect to the methylene carbon signal of polyisoprene unit which was fixed at 32.5 ppm.



Figure 4.4 Picture of Solid state NMR spectrometer.

4.7 Evaluation of the Microstructure

4.7.1 Determination of Percentage of *Cis* and *Trans* Microstructures

(a) By High Performance Liquid Chromatography

High Performance Liquid Chromatography (HPLC) was employed to determine the amount of *cis* and *trans* units of 4-methyl-4-octene (MO) and hydrogenated MO sample. The HPLC (Water 510) was equipped with a specific column (C₁₈)



Kromasil C18) and refractive index detector (RD 410). The mobile phase is the solvent mixture of CH₃CN/H₂O = 87/13. The flow rate of 1 ml/min was used.

The HPLC chromatograph (see in Appendix B2) was used to determine the percentage of *cis* and *trans* isomers of MO before and after hydrogenation. The HPLC reveals the peak area of the signals of *cis* and *trans* microstructures compared to the signal of mesitylene used as an internal standard. The % *cis* and *trans* isomers were evaluated according to Equation 4.1 and 4.2.

$$\%cis = \frac{(A_{7.84} / A_{3.90})}{(A_{7.84} / A_{3.90}) + (A_{8.25} / A_{3.90})} \times 100 \quad (4.1)$$

$$\%trans = \frac{(A_{8.25} / A_{3.90})}{(A_{7.84} / A_{3.90}) + (A_{8.25} / A_{3.90})} \times 100 \quad (4.2)$$

where $A_{7.84}$, $A_{8.25}$ and $A_{3.90}$ are the integrated areas of peaks belonging to the *cis* and *trans* isomers and mesitylene, respectively.

(b) By ¹H-NMR Spectroscopy in Solution

The percentage of *cis* and *trans* configurations of polyisoprenic structure was calculated from the integrated areas of ¹H-NMR before and after hydrogenation as shown in Equation 4.3 and 4.4.

$$\%cis = \frac{A_{1.67}}{A_{1.67} + A_{1.60}} \times 100 \quad (4.3)$$

$$\%trans = \frac{A_{1.60}}{A_{1.67} + A_{1.60}} \times 100 \quad (4.4)$$

Here, $A_{1.67}$ and $A_{1.60}$ are the integrated areas of the proton signals of methyl groups corresponding to *cis* and *trans* configurations, respectively.

(c) By ¹³C-NMR Spectroscopy in Solid State

The microstructures of the hydrogenated products were also analyzed by ¹³C-NMR in solid state. The integrated area of peak position were determined using a curve fitting program in a DM 2002 software [94] utilizing a linear baseline function with pseudo voigt line shape as demonstrated in Figure 4.5. The percentage of *cis*



trans units, determined from the integrated areas of peak compared with total area of carbon signals of methyl groups in all units formed after hydrogenation.

$$\%cis = \frac{A_{23}}{A_{23} + A_{16}} \times 100 \quad (4.5)$$

$$\%trans = \frac{A_{16}}{A_{23} + A_{16}} \times 100 \quad (4.6)$$

Where A_{23} and A_{16} are the integrated areas of carbon signals of methyl group, belonging to *cis* and *trans* isomers, respectively.

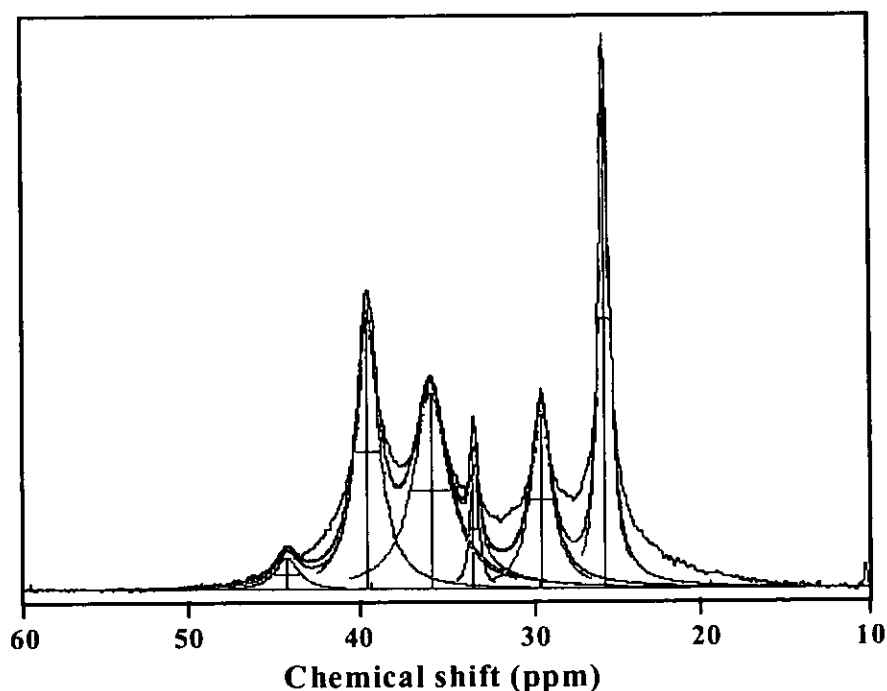


Figure 4.5 Typical curve fitting of solid state ^{13}C -NMR spectrum of hydrogenated NR (pseudo voigt line shape).

4.7.2 Determination of Epoxidation Level

^1H -NMR spectroscopy in solution was employed to determine the percent epoxide group of the epoxidized NR (ENR) as written in Equation 4.7.

$$\%Epoxidation = \frac{A_{2.70}}{A_{2.70} + A_{5.12}} \times 100 \quad (4.7)$$



where $A_{2.70}$ and $A_{5.12}$ represent the integrated areas of proton signal attached to oxirane ring and signal of proton adjacent to double bond, respectively.

4.7.3 Determination of Percentage of Hydrogenation

The percentage of hydrogenation of 4-methyl-4-octene, NR and ENR was determined by HPLC, ^1H , ^{13}C -NMR (both liquid and solid state) and Raman spectroscopies.

(a) By HPLC Chromatography

By comparing the chromatograms at time = 0 and at time = 24 h, it is possible to determine the percentage of residual model as follows:

$$\% MO_{t=24} = \frac{[(A_{7.84} + A_{8.25}) / A_{3.90}]_{t=24}}{[(A_{7.84} + A_{8.25}) / A_{3.90}]_{t=0}} \times 100 \quad (4.8)$$

where $A_{7.84}$, $A_{8.25}$ and $A_{3.90}$ are the integrated areas of peaks at retention time 7.84, 8.25 and 3.90 min representing to the *cis* and *trans* isomers and mesitylene, respectively.

$$\% \text{Hydrogenated model} = \frac{[(A_{6.80}) / A_{3.90}]_{t=T}}{[(A_{6.80}) / A_{3.90}]_{t=24}} \times (100 - \% MO)_{t=24} \quad (4.9)$$

where $A_{6.80}$ and $A_{3.90}$ are the integrated areas of peaks at retention time 6.80 and 3.90 min corresponding to the mesitylene and hydrogenated MO (HMO), respectively.

(b) By ^1H -NMR Spectroscopy in Liquid State

The characteristic peak assignments of ^1H -NMR spectra of the hydrogenated natural rubber were used to analyze the percentage of hydrogenation as shown in Equation 4.10.

$$\begin{aligned} \% \text{Hydrogenation} &= \frac{A_{0.84/3}}{(A_{0.84/3}) + A_{5.12}} \times 100 \\ &= \frac{A_{0.84}}{A_{0.84} + 3A_{5.12}} \times 100 \end{aligned} \quad (4.10)$$

where $A_{0.84}$ and $A_{5.12}$ are the integrated areas of signals of methyl protons of the hydrogenated sample and proton signal adjacent to carbon-carbon double bond units respectively.



In the case of synthetic polyisoprene, the percent hydrogenation can be calculated from the comparison of the integrated peak areas at 0.84 ppm belong to signals of methyl protons of the hydrogenated sample and at 5.1 and 4.75 correspond to proton signals adjacent to C=C bond of *cis* or *trans*-1,4 PI and 3,4-PI, respectively.

$$\% \text{Hydrogenation} = \frac{A_{0.84} / 3}{(A_{0.84} / 3) + A_{5.1} + A_{3.75}} \times 100 \quad (4.11)$$

(c) By ^{13}C -NMR Spectroscopy in Solid State

The integrated area of peak position corresponding to *cis*, *trans* and saturated units were determined using a curve fitting program in the DM2002 software

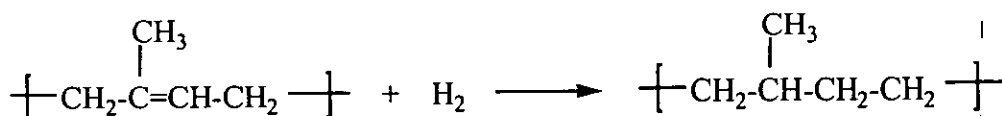
The percentage of saturated units formed was determined according to the ratio of integrated areas of methyl group of saturated unit and the total integrated areas of methyl group of all units in rubber chains.

$$\% \text{Hydrogenation} = \frac{A_{20}}{A_{20} + A_{16} + A_{23}} \times 100 \quad (4.12)$$

Where A_{20} , A_{23} and A_{16} are the integrated areas of carbon signals of methyl groups representing to saturation unit, *cis* and *trans* units of polyisoprene, respectively.

(d) By Raman Spectroscopy

Raman spectra of hydrogenated rubber in the region 500-3200 cm^{-1} were employed to estimate the achieved percent hydrogenation of the samples. The percent hydrogenation of each samples can be estimated from the ratio of band area arising from the stretching mode of the C=C bond at 1664 cm^{-1} and the bending mode of CH_2 , since each reduction of the C=C gives rise to one new CH_2 unit as shown in the following reaction.



The repeating unit of polyisoprene already presents 2 CH_2 groups, which the CH_2 bending mode appears to be moderately active at 1432 cm^{-1} as illustrated in Figure 4.5.

In Raman spectroscopy, the band intensity can be considered as



proportional to the concentration of each species as shown in Equation 4.13 and 4.14.

$$A(C=C) = a[C=C] \quad (4.13)$$

$$A(CH_2) = b[CH_2] \quad (4.14)$$

where $A(C=C)$ is the integrated intensity of the band located between 1660 and 1667 cm^{-1} assigned to the vibration of C=C bonds, $A(CH_2)$ is the integrated intensity area of the CH_2 bending band between 1452 and 1435 cm^{-1} , a and b are proportional constants of the C=C and CH_2 bending vibrational modes.

In the case of natural rubber, if the starting sample is composed of 100 repeating units, so 100 C=C and 200 CH_2 units are present, hence

$$\frac{a}{b} = \frac{2A_o(C=C)}{A_o(CH_2)} \quad (4.15)$$

where $A_o(C=C)$ and $A_o(CH_2)$ are the integrated peak areas of the C=C bond stretching and CH_2 bending modes, respectively. For spectra of NR and the hydrogenated samples, it was observed that the CH_2 bending band was overlapped by the CH_3 bending one at 1452 cm^{-1} . The standard "peakfit" software (Jandel) was then used to resolve area of the CH_2 bending band required for the calculation as shown, for instance, in Figure 4.6. A Lorentzian shape was assumed to simulate the Raman bands, and the integrated intensities were determined by subtraction of a near constant background.

If " X " units of the C=C units disappear during hydrogenation, " X " units of CH_2 units are created. For a partially hydrogenated product, X or the percentage of hydrogenation can be determined from the following.

$$A(C=C) = (100 - X)a \quad (4.16)$$

$$A(CH_2) = (200 + X)b \quad (4.17)$$

Equation 4.16 divided by Equation 4.17:

$$\frac{A(C=C)}{A(CH_2)} = \frac{(100 - X)a}{(200 + X)b} \quad (4.18)$$

If α is defined as the ratio of integrated area of bands corresponding to the C=C stretching and the CH_2 deformation vibration modes of hydrogenated rubber, then



$$\alpha = \frac{A(C=C)}{A(CH_2)} \tag{4.19}$$

Therefore
$$\alpha = \frac{(100 - X)a}{(200 + X)b}$$

Thus, simplified version of the percent hydrogenation quantification can be transformed into Equation 4.20 as follows:

$$200ab + \alpha Xb = 100a - Xa$$

$$\alpha Xb + Xa = 100a - 200\alpha b$$

$$X(ab + a) = 100(a - 2\alpha b)$$

$$X\left(\alpha + \frac{a}{b}\right) = 100\left(\frac{a}{b} - 2\alpha\right)$$

$$X = 100\left[\frac{K - 2\alpha}{K + \alpha}\right] \tag{4.20}$$

where K is equal to $\frac{a}{b}$ and both a and b are proportional constants as determined from the integrated area of the C=C and CH₂ bending vibrational modes of starting NR.

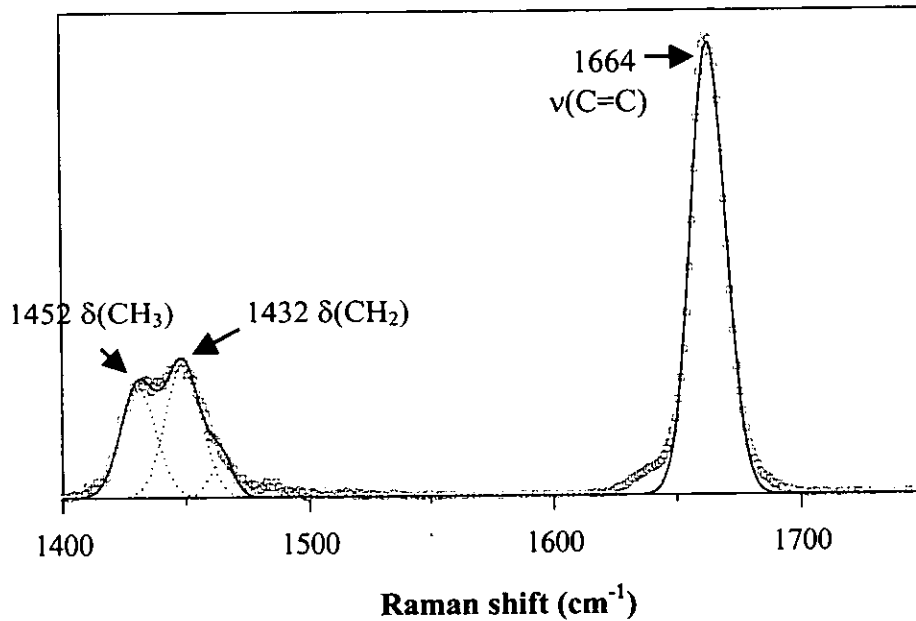


Figure 4.6 Typical curve fitting of Raman spectrum of natural rubber (Lorentzian shape).



Estimation of errors

The error on the area ratio of (C=C) to (C-H) of CH₂ was determined from the curve fitting (Lorentzian function) simulating the band areas of the C=C bond and the C-H bending of methylene bands repeatedly and the difference in the investigation of this area constituted the standard deviation obtained in the measurement of the band area (expressed as %) was about 1.5.

4.8 Average Molar Mass and Particle Size Measurement

4.8.1 Dilute Solution Viscosity Measurement

The viscosity average molecular weight (M_v) of the hydrogenated NR samples could not be determined because the values of constants, K, and a, in Mark-Houwink equation are not available for the hydrogenated NR. Only the intrinsic viscosity of the solution of the hydrogenated products was determined as comparing to that of the starting rubber at 30°C.

Intrinsic viscosity of the NR and hydrogenated NR samples was determined by measuring flow times of toluene and 4 different concentrations of the hydrogenated NR solutions in toluene using an Ubbelodhe viscometer immersed in a water bath at $30 \pm 0.1^\circ\text{C}$. Sample filtration through a coarse, sintered-glass filter provided a means of detecting insoluble gel. The relative viscosity, η_r and specific viscosity, η_{sp} can be measured and determined by Equation below.

$$\eta_r = \left(\frac{t}{t_o} \right) \quad (4.21)$$

$$\eta_{sp} = \left(\frac{t - t_o}{t_o} \right) \quad (4.22)$$

Where t_o is efflux time of a pure solvent and t is efflux time of polymer solution at a given concentration.

In a dilute solution, $\frac{\eta_{sp}}{C}$ is linear in concentration, C , and the intrinsic viscosity, $[\eta]$ may be obtained by extrapolating a plot of $\frac{\eta_{sp}}{C}$ versus C to $C = 0$ which has been described by a purely empirical Equation 4.23 by Huggins.



$$\frac{\eta_{sp}}{C} = [\eta] + k' [\eta]^2 C \quad (4.23)$$

where k' is the Huggins constant.

Another commonly also used empirical equation is called Kraemer Equation in 4.24

$$\frac{\ln \eta_r}{C} = [\eta] + k'' [\eta]^2 C \quad (4.24)$$

where k'' is the Kraemer constant.

4.8.2 Particle Size Analysis

The particle size analysis was done using a Horiba LA-910 Mastersizer. One drop of latex was dispersed in distilled water and stirred with speed of 2,000 rpm. The obtained results of particle size were analyzed from the distribution curve; particle size, volume weighted means, uniform and specific surface area.

4.9 Thermal Analysis

Thermal behaviors of starting material and hydrogenated products, were investigated with Raman Spectroscopy, a Perkin Elmer DSC 7 and thermogravimetric analyzer. The results were analyzed

4.9.1 Raman Spectroscopy

To observe the change of molecular behavior at varied temperature, Raman spectra of the samples were recorded using a T64000 Jobin-Yvon under temperature range -160 -150°C and primary vacuum atmosphere. Typically, the spectra were accumulated at 20 times for Raman shift in the range 500 to 3200 cm^{-1} as manipulated in the Section 4.6.2, but a slightly higher laser power of 100 mw was employed.



4.9.2 Differential Scanning Calorimetry (DSC)

The effect of the percentage hydrogenation on the glass transition temperature behaviour was studied using Perkin Elmer DSC7. Approximately 10 mg of sample was cut into a small piece before putting in the aluminium pan. The temperature range was set from -100 to 150°C. The sample was rapidly heated from -100 to 150°C with the heating rate of 50°C/min and then was cooled with the scanning rate of 20°C/min, the sample was then reheated with the scanning rate of 20°C/min. To determine the real glass transition of NR and its hydrogenated rubber, the heating scanning rates used were varied at 5, 10, 15 and 20°C/min, respectively.

The results are the following parameters:

-The enthalpy of transition, ΔH , provides the thermal history of the sample under the assumption of no difference in the heating rates for the sample and the reference and that the DSC curve then returns to the original baseline after the transition, then the enthalpy can be described in the following way:

$$\Delta H = \int_{T_i}^{T_f} C_p dT \quad (4.25)$$

where the ΔT is calculated from T_i and T_f which refer to the initial and final temperatures of the transition.

- Glass transition (T_g) is the temperature of the onset of motion of short chain segments.

4.9.3 Thermogravimetric Analysis (TGA)

Thermal stability of all resulting products was investigated by using TGA (Thermal analysis TA-SDT 2960) both in air and nitrogen atmosphere. The sample weight used was 10-15 mg. The thermogram of each sample was recorded by using heating rate of 20°C/min and the temperature range of 30-600°C. The onset and peak degradation temperatures were analyzed from the obtained thermogram using TA Universal Analysis software.



4.10 Rheological Measurement

The rheological behavior of the hydrogenated sample was investigated using RPA instrument. The 2 cm-thick circular cross-section slices of about 3.4 ± 0.2 g sample were cut from bale and test samples using a 18 mm diameter die. Test samples were packed by hand and put on RPA lower die. A series of strain sweep tests at 1 Hz were performed at 100°C on hydrogenated samples. For each test condition, 10,240 points were acquired and the last 8192th was used to extract the Fourier transform spectra of the harmonic motion of the lower die. Strain signals were recorded and analyzed through Fourier transform. The test condition was shown in Table 4.8.

Table 4.8 RPA test conditions and protocols

RPA test conditions	Temperature (°C): 20030 s; Frequency = 1 Hz; angle = 0.2 deg
Preheat 1:	3 min
Preheat 2:	2 min
Run 1:	Run 2
Strain (deg)	Strain (deg)
0.5	0.6
1.0	1.5
2.5	3.5
5.0	6.7
8.5	10.0
12.0	14.5
17.0	20.0
22.5	25.0
27.5	30.0
31.5	33.0



CHAPTER 5

RESULTS AND DISCUSSION

The study of hydrogenation of natural rubber (NR) and its modified form of epoxidized natural rubber (ENR), carried out in the present work is the use of diimide (N_2H_2) as hydrogen donor, considered as a non-catalytic hydrogenation process. *p*-toluenesulfonylhydrazide (TSH) and hydrazine were two types of molecule employed in the hydrogenation reaction. The TSH is decomposed at high temperature while the hydrazine needs an oxidizing agent such as hydrogen peroxide for the generation of diimide. Two systems of non-catalytic process were applied i.e. in organic solvent and in aqueous systems.

The contents of this study are classified into three parts. First, the hydrogenation was carried out using TSH in organic media. For this, 4-methyl-4-octene (MO), natural rubber (NR) and 4 types of partially epoxidized natural rubber (ENR) were investigated. Secondly, the reduction of unsaturated units of natural rubber in latex phase was carried out. The natural rubber latex (NRL), fresh natural rubber latex (FNRL) and deproteinized natural rubber latex (DPNRL) were treated with hydrazine (N_2H_4) in the presence of an oxidizing agent i.e. hydrogen peroxide (H_2O_2). The study of the molecular characteristic of the hydrogenated rubbers were then performed either to predict or to explain the behavior of the macromolecular chain, and physical properties of the materials. The investigation of the correlation of the molecular characteristic with physical properties of the samples, and the heterogeneities of the hydrogenated products were also included.



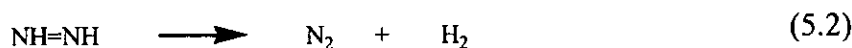
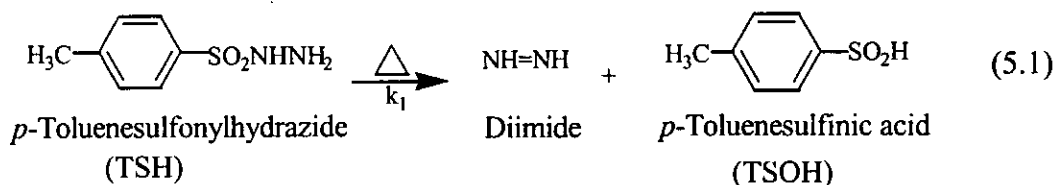


Figure 5.1 The decomposition of *p*-toluenesulfonylhydrazide (TSH) by thermal treatment at 135°C and disproportionation of diimide intermediate [11].

Part I: Hydrogenation by *p*-Toluenesulfonylhydrazide (TSH)

In general, one mole of TSH produces one mole of diimide under proper condition as shown in Equation 5.1 (see Figure 5.1), which might be sufficient for hydrogenation of one mole of unsaturated unit resulting in saturated counter part. However, it was reported by several authors that 4-5 moles of hydrazide molecule per mole of unsaturated units are required for complete hydrogenation of homopolymer or copolymer containing polyisoprene or polybutadiene segments [11, 25, 48, 50, 51]. This is due to the fact that the diimide can undergo disproportionation reaction giving nitrogen and hydrazine as shown in Equation 5.2. In our work, partial hydrogenation of natural rubber was expected as the intention was to improve the heat and oxidation resistance of the rubber therefore the unsaturated unit in the rubber needed to be left. The mole ratio of TSH to C=C of the rubber equal to two has been chosen in this part with various types of unsaturated molecules including 4-methyl-4-octene as a model compound, NR and ENRs. Structural characterization and the evaluation of the microstructures of the hydrogenated products were investigated and discussed.

5.1 Hydrogenation of 4-Methyl-4-octene

4-Methyl-4-octene (MO) is a small alkene molecule having similar structure as the repeating unit of 1,4-polyisoprene, therefore it was used to study the hydro



reaction using TSH before passing to the high molecular weight polyisoprene or natural rubber.

The hydrogenation of MO was carried out using 2:1 mole ratio of TSH to double bond of MO at 135°C in xylene solvent. The progress of the hydrogenation of MO was monitored by sampling the reaction mixture at various reaction times for analyzing by HPLC technique. The microstructures of MO before and after hydrogenation were investigated by ^1H - and ^{13}C -NMR spectroscopies.

5.1.1 Structural Analysis

Figure 5.2 (a) and (b) shows ^1H - and ^{13}C -NMR spectra of the MO used before hydrogenation and the peak position assignments are given in Table 5.1. ^1H -NMR spectrum of the MO in Figure 5.2 (a) indicates two peaks at 1.67 and 1.57 ppm which can be attributed to the characteristic of methyl protons of *cis* and *trans* isomers of the MO, respectively. The proton signal of olefinic unit was found at 5.12 ppm. The peaks located between 1.28-1.46 ppm are assigned to the methylene protons of the MO. While the peak positioned at 0.84 ppm could be attributed to the methyl protons at the end molecule of MO. By the results from the intensity of the methyl proton adjacent to the C=C of *cis* and *trans* units, the quantity of *cis* and *trans* isomers can be calculated and it was found that the MO used has 60 and 40% of *cis* and *trans* isomers, respectively.

In ^{13}C -NMR spectrum, the carbon signals of methyl groups of *cis* and *trans* isomers are observed at 14.1, 14.2, 14.3 and 14.4 ppm, as illustrated in Figure 5.2 (b). The olefinic carbon signals of the *cis*-isomer are found at 124.9 and 135.4 ppm and other signals at 125.7 and 135.6 ppm can be attributed to the carbon signals of olefinic *trans* isomer.

^1H - and ^{13}C -NMR spectra of hydrogenated MO (HMO) are displayed in Figure 5.3. By comparing with the starting model compound, the observed new proton signals in the chemical shift range of 0.74-0.78 ppm was considered to be the methyl proton of HMO and the multiplet signals at around 1.12-1.19 ppm are assigned to the methylene unit on MO after hydrogenation. Meanwhile, the proton signal adjacent to



the double bond at 5.12 ppm disappears when the hydrogenation progress up to 24 h of reaction time. In addition, an extra resonance signal in the region of 3.18-3.32 ppm attributed to proton signal of the hydroxyl group is found in this hydrogenation process.

For ^{13}C -NMR, the new extra signals are observed at 19.8, 31.4 and 38.4 ppm corresponding to the methyl carbon, the methylene and methine groups of the modified MO, respectively.



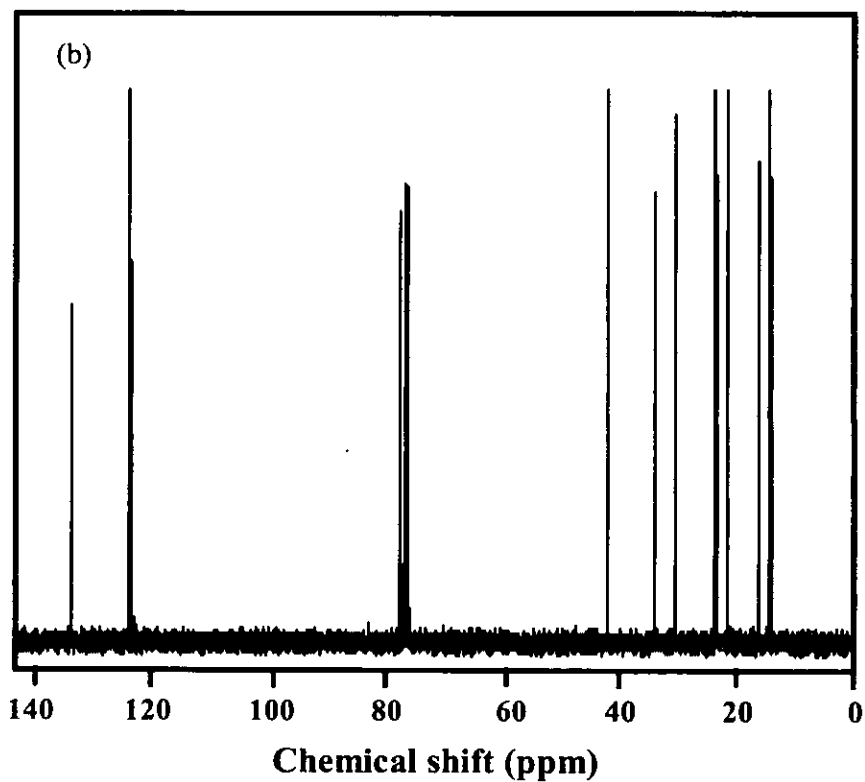
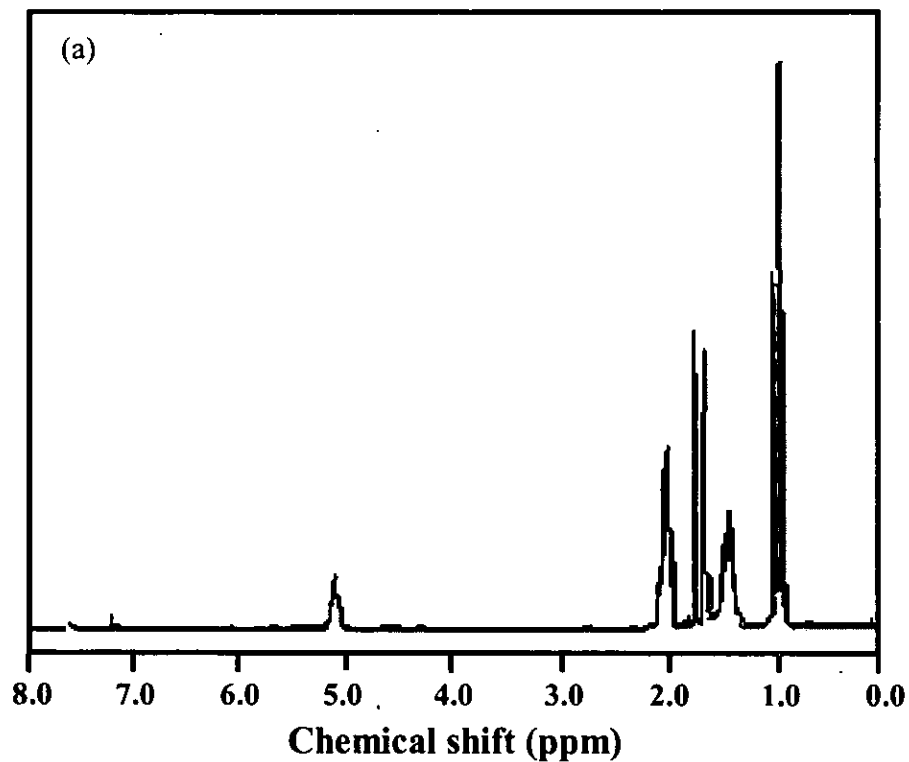


Figure 5.2 ^1H -NMR (a) and ^{13}C -NMR (b) spectra of 4-methyl-4-octene (MO)



Table 5.1 The assignment of proton and carbon signals of 4-methyl-4-octene (MO)

¹ H-NMR Analysis		¹³ C-NMR Analysis	
Assignment [95]	Proton chemical shift (ppm)	Assignment [95]	Carbon chemical shift (ppm)
a	0.82	C-1	14.1
g	0.85	C-1'	14.2
a'	0.89	C-8	14.3
g'	0.92	C-8'	14.4
b, c, b' and c'	1.28-1.46	C-9'	16.1
h'	1.57	C-7'	21.4
h	1.67	C-7	21.6
b' and f'	1.91	C-2	23.4
b and f	1.95	C-2'	23.6
c' and e'	1.98	C-3	23.7
c and e	2.03	C-3'	30.3
d and d'	5.12	C-6	30.4
		C-6'	34.2
		C-5	124.9
		C-5'	125.7
		C-4	135.4
		C-4'	135.6

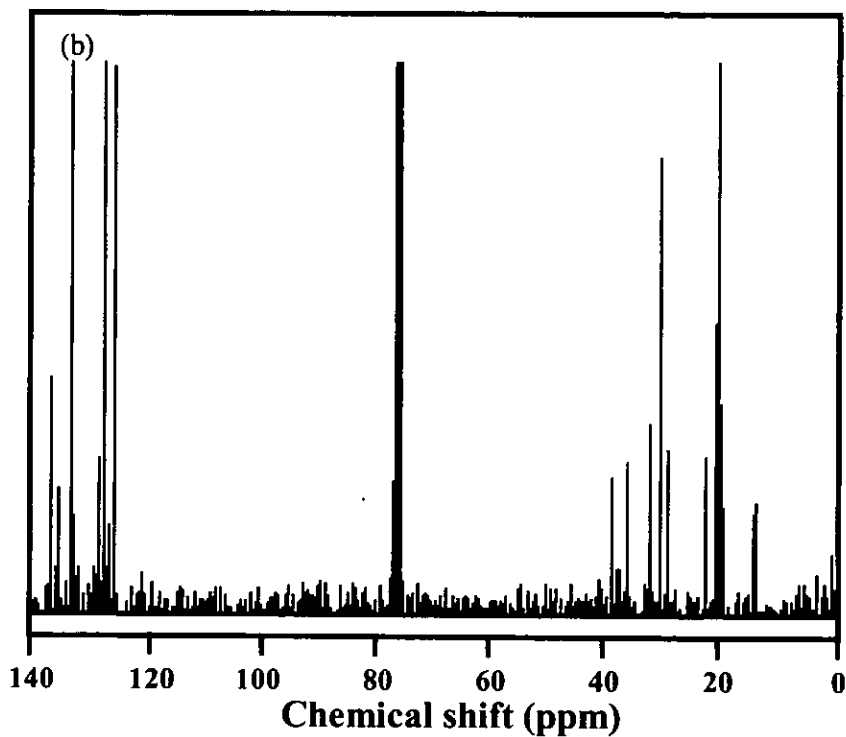
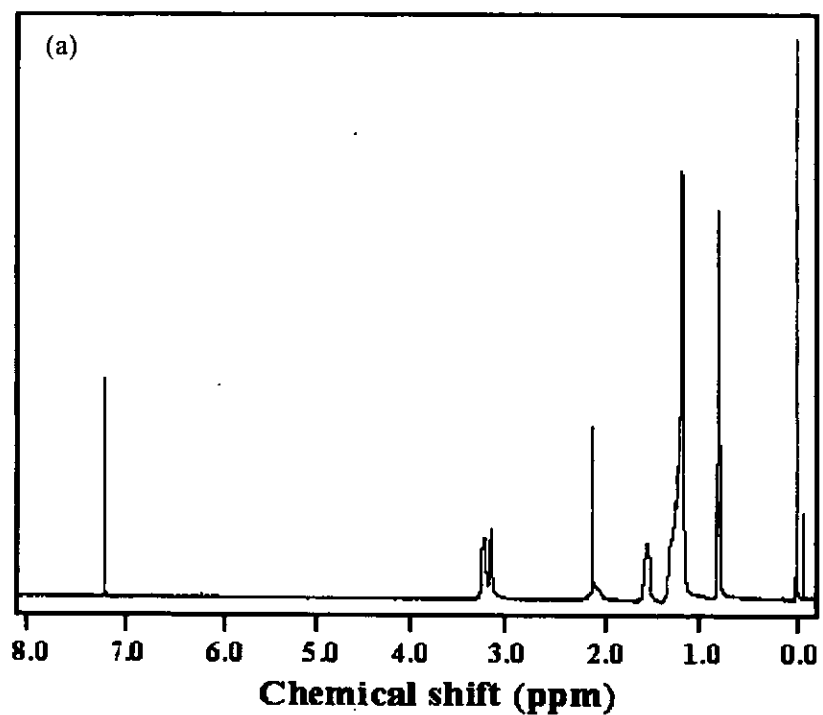


Figure 5.3 ^1H -NMR (a) and ^{13}C -NMR (b) spectra of the hydrogenated MO obtained at 24h of reaction time.



5.1.2 Evolution of Microstructures and Hydrogenation

The progress of the hydrogenation reaction of MO was examined by HPLC technique. The mesitylene was used as an internal standard to quantify the amount of each isomer at various reaction times. The HPLC chromatogram in Figure 5.4 shows the relative proportion of the *cis* and *trans* isomers as well as the HMO at 4h of reaction time, respectively. The percent microstructures are calculated using the integrated peak areas as described in section 4.7.1. In this study, a two-folded excess of TSH as compared to olefinic unit was used to hydrogenate the double bond of MO. The results in Table 5.2 and Figure 5.5 show the residual *cis* and *trans* isomers and the percent hydrogenation at various reaction times.

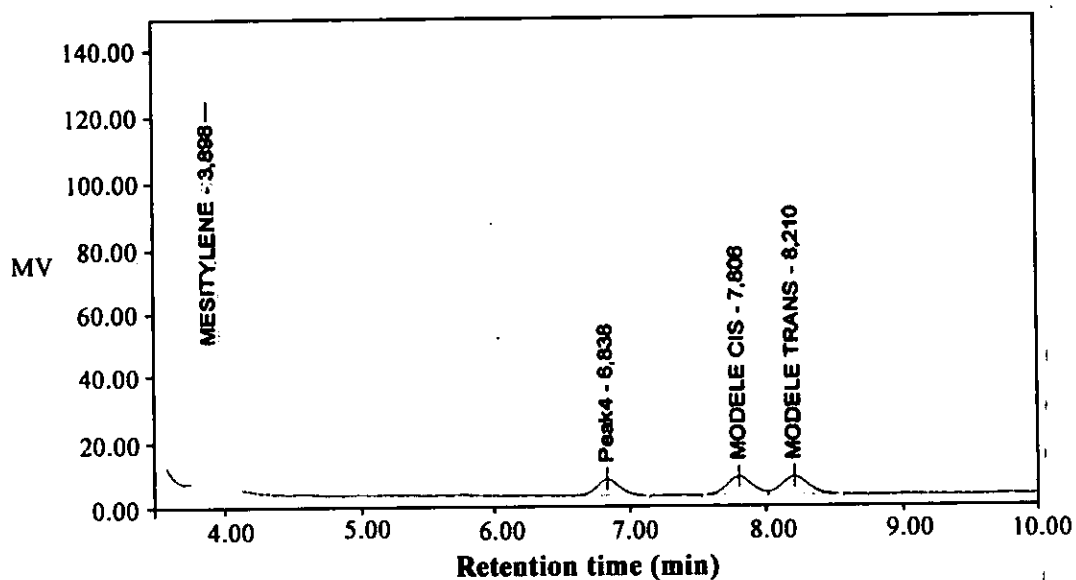


Figure 5.4 HPLC chromatogram of hydrogenated MO obtained at 4h of reaction time.

Table 5.2 Influence of the reaction time on the hydrogenation of MO

Reaction time (h)	<i>Cis</i> (%)	<i>Trans</i> (%)	Hydrogenation (%)
0	61.7	38.3	0
0.5	56.0	44.0	0
1	51.6	48.4	0
2	43.4	47.0	9.6
3	42	44.3	13.7
4	38.8	41.6	19.6
6	35.0	38.9	26.1
8	29.4	36.9	33.7
24	4.6	7.3	88.5

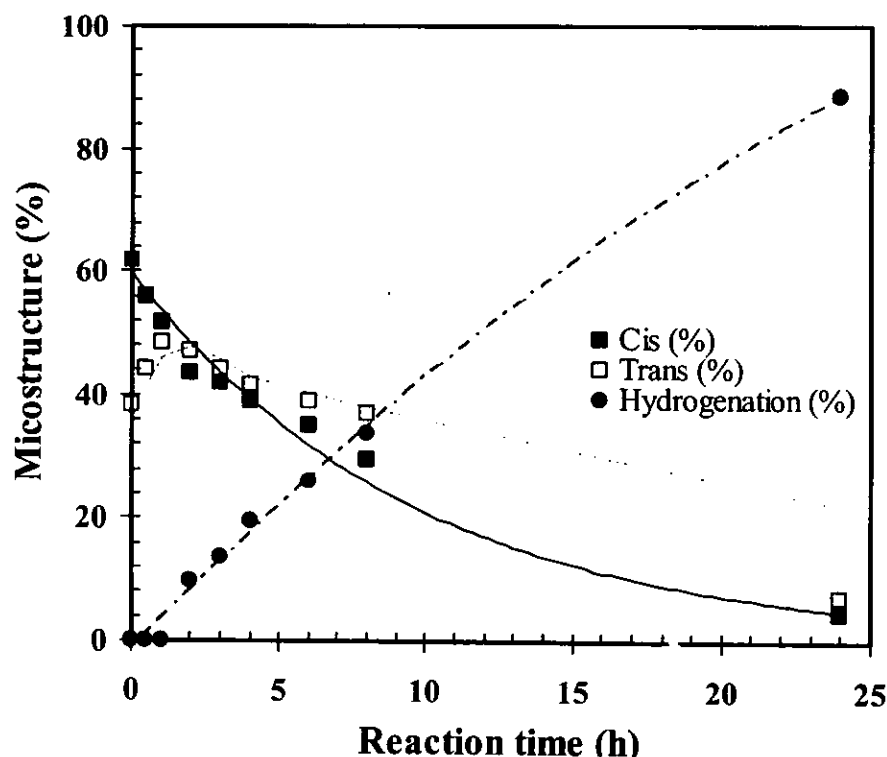


Figure 5.5 The percent microstructures of MO as function of reaction time; *cis* (■), *trans* (□) and hydrogenation (●).



Figure 5.5 reveals that the percent hydrogenation of MO increases with increasing the reaction time. The maximum percent hydrogenation of MO is found to be about 90 % at 24 h of reaction time. The complete hydrogenation does not achieve in this study as similar to the case of hydrogenation of synthetic PB or PI using TSH [11, 25, 50]. The depletion of *cis* isomer is obviously observed at the early stage of reaction (<2h) while *trans* isomer was increased. This may be supposed that the *cis-trans* isomerization of MO was occurred at the first stage of reaction. After reaction time 2h, it can be seen that the % hydrogenation was increased whereas the decrease of amount of *cis* isomer is faster than that of *trans* isomer which is similar to the results obtained for diimide hydrogenation of PB, SBR and SIR [25, 50]. This can be assumed that the rate of addition of hydrogen molecule to the olefinic sites in the *cis* configuration is faster than that of the *trans* unit. The possible explanation is that the steric hindrance plays a significant role in the reaction since the *cis* unit has two bulky CH_2 groups on one side, on the other, only hydrogen atom and the methyl are presented as demonstrated in Figure 5.6. Meanwhile, the *trans* unit possesses one CH_2 on both sides. Hence, it is easier for the *cis* configuration to form an intermediate species with the diimide molecule, resulting in a more rapid addition transfer of hydrogen molecule to the $\text{C}=\text{C}$. Therefore, it could be concluded that reactivity of *cis* isomer for hydrogenation reaction is higher than that of *trans* isomer. However, after 6 h of reaction, the ratio of the *cis* and *trans* units are almost equal even though the hydrogenation level was increasing.

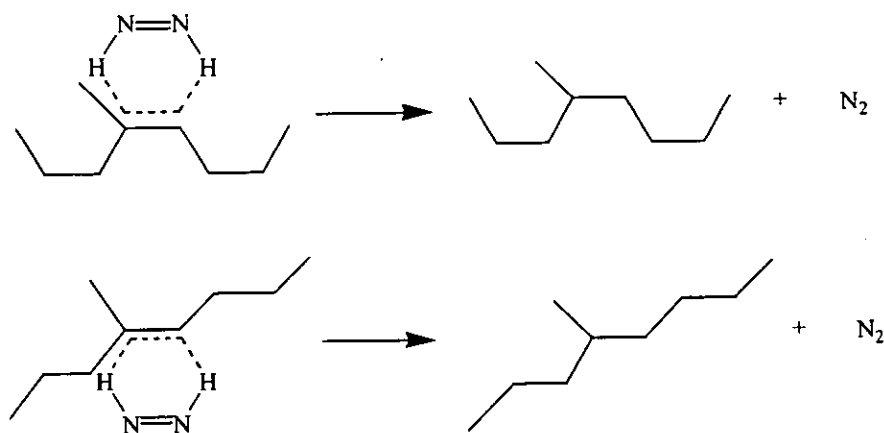


Figure 5.6 Hydrogenation of MO in *cis* (upper) and *trans* (lower) units.

5.1.3 Side Reaction

When the TSH was heated at 140°C; *p*-toluenesulfonic acid (TSOH) as a by-product was also generated. The TSOH might release a proton as it is considered as an acidic compound. ¹H-NMR spectrum of the modified form of MO at 24h shows a small extra proton signal at 3.18-3.32 ppm which can be assigned to the methine proton adjacent to the hydroxyl group. It may be proposed that the TSOH may react with the double bond of MO during hydrogenation progress and then followed by the hydrolysis reaction as schematized in Figure 5.7. Eventually, the attachment of the hydroxyl group on the MO was found on the molecule as detected by ¹H-NMR.

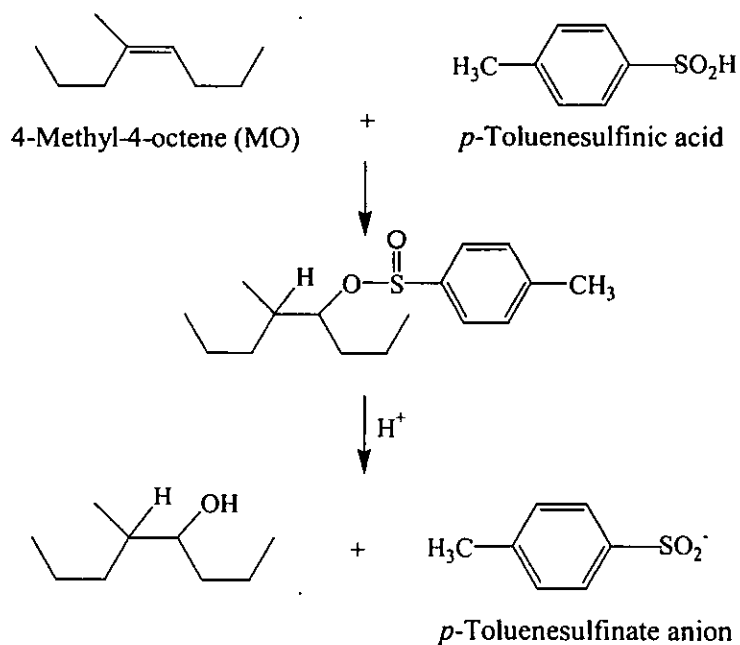


Figure 5.7 Schematic representation of the addition of *p*-toluenesulfonic acid, followed by hydrolysis.

5.2 Hydrogenation of NR

This section concerns the hydrogenation of NR and DPNR in xylene solvent using TSH. The mechanism of addition of hydrogen molecule from diimide onto the carbon-carbon double bond of polydienes has been well established [11, 50-52]. The reaction starts with the generation of diimide (N_2H_2) molecule performed *in situ* from the thermal decomposition of TSH as described in section 5.1. The diimide then releases a hydrogen molecule directly to the carbon-carbon double bonds of polyisoprene units as represented in Equation 5.3 in Figure 5.8.

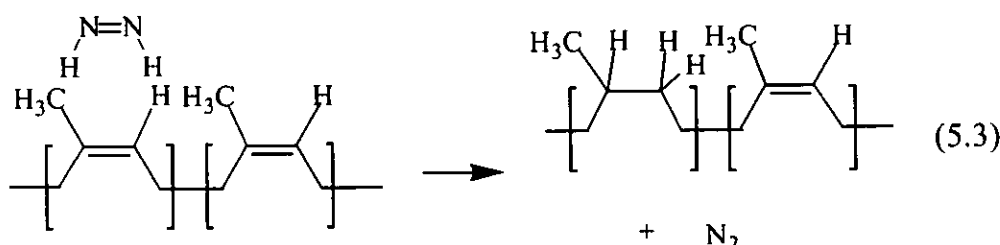


Figure 5.8 The addition of hydrogen molecule from diimide onto double bond of *cis*-1,4 polyisoprene units.

5.2.1 Microstructure Analysis of NR and Hydrogenated NR

In general, the IR technique has been used for qualitative analysis, whereas the determination of the degree of modification has mostly been studied using NMR technique in liquid state. The characterization of elastomers by Raman spectroscopy has long been used as the $C=C$ vibration frequency is sensitive to its environment in a similar way of IR mode but much clearer. This technique was successfully used for the microstructure study of elastomers and hydrogenated polybutadienes [22-25], only a few studies have been done to characterize the unsaturated units in NR after modification.

When the number of vibration modes of IR and Raman is known, the structural characteristic of NR obtained from vibration spectroscopic techniques is analyzed and identified in terms of peak position, and intensity. Consequently, the results obtained



from calculation of the number of vibration modes and experimental can be compared. The chemical structure of hydrogenated NR can then be also detected and identified by using nuclear magnetic resonance spectroscopy.

(a) Vibrational Analysis

Infrared and Raman spectroscopic techniques have substantially contributed to reveal the chemical structure of NR after modification [13, 22, 23]. But no report works have been done toward the analysis of fundamental vibration modes of the NR. In the present work, a vibrational spectroscopic study of natural rubber has been undertaken with the identification of the principal vibration features of polyisoprene unit on the macro-molecular chain. It will then be possible to observe the characteristic of hydrogenated product after diimide reduction.

Group theory has been employed for predicting the number of vibrational modes of molecule. It is well known that NR possesses a highly regular structure, entirely composed of linear sequences of *cis*-1,4 polyisoprene units. On the basis of the NR structure, the *cis*-1,4 polyisoprene unit possesses a low symmetry point group, probably identical with C_s symmetry of the single unit. This point group was then considered to analyze the number of vibration modes of the NR. It is assumed that the CH_3 group of the *cis*-1,4 polyisoprene units is spherical and lies in the same plane with the main chain atoms and hydrogen. According to a classical group theory analysis, a number of vibration modes " A_i " of symmetry species " i " can be determined by Equation 3.16 as described in section 3.4.1.1.

As previously mentioned, polyisoprene unit can be regarded as planar with a symmetry according to the point group C_s . The character table of the species " A' " and " A'' " corresponding to the two different symmetries associated with point group C_s is presented in Table 5.3.



Table 5.3 Character table of point group C_s

C_s	E	σ_h		
A'	1	1	x, y, R_z	x^2, y^2
A''	1	-1	z, R_x, R_y	yz, xz

Therefore, the number of vibration mode of each species is calculated as follows:

$$A' = \frac{1}{2}[(1 \times 1 \times 39) + (1 \times 1 \times 13)] = 26 \quad (5.4)$$

$$A'' = \frac{1}{2}[(1 \times 1 \times 39) + (1 \times (-1) \times 13)] = 13 \quad (5.5)$$

So we get $\Gamma_{vib} = 26A' + 13A'' \quad (5.6)$

As a result of predicting the number of vibration modes, it was found that there are 26 modes and 13 modes for species A' and A'' , respectively.

The determination of the number of vibration modes has been performed and the distribution of the normal modes among the irreducible representations for point group, C_s , is given by $\Gamma_{vib} = 26A' + 13A''$. Because of the low symmetry of the unit without any symmetry centre, all the vibrations are active in both Raman and infrared spectroscopies. A typical recorded Infrared and Raman spectra of NR are illustrated in Figure 5.9. The observed wavenumbers of *cis*-1,4 polyisoprene in infrared and Raman scattering along with their relative intensities and proposed assignments are summarized in Table 5.4. The suggested attribution was done on the basis of literature in iso-structural compounds exhibiting the same kinds of entities or molecular bonds. It can be noted that the number of vibration modes experimentally observed in Raman spectrum (31 modes) is lower than that one predicted by group theory (39 modes). The observed number of Raman line for this investigation is consistent with the literatures [24, 64, 95], while the roughly assignment of infrared spectrum obtained is 22 modes. It is noticed that the broad distribution absorption of each mode causes peaks overlapping. Hence, the vibrational absorption mode number observed from IR spectrum is less than that of prediction and this technique appears not as powerful as Raman spectroscopy to determine the percentage of hydrogenation.



The recorded IR spectrum of NR is depicted in Figure 5.9 (a). Considering, the assignments of CH_3 group wavenumber which make a significant contribution to FT-IR spectrum of NR. The peak seen at 2961 cm^{-1} can be assigned to the CH_3 asymmetric stretching mode. The $=\text{CH}$ stretching mode is normally located between 3000 and 3100 cm^{-1} . The $=\text{CH}$ stretching vibration in trisubstituted olefinic compound is usually weak. Thus, the weak peak appeared at 3036 cm^{-1} is assigned to the $=\text{CH}$ stretching mode. The CH_3 and CH_2 rocking vibration modes are found at 1038 and 760 cm^{-1} respectively. Moreover, the characteristic peaks in the region of 1500 - 1400 cm^{-1} are associated to the deformation mode of CH_3 and CH_2 group. The peaks appearing at 1452 and 1437 cm^{-1} are assigned to the C-H deformation of the methyl and methylene groups of *cis*-1,4 polyisoprenic unit. The significant peaks of IR spectrum at 1664 and 836 cm^{-1} are the C=C double bond stretching and the C-H out of plane deformation modes of the polyisoprene unit. The assignments of the $-\text{CH}_2-$ wagging and the CH_2 twisting occur over a frequency range about 1200 - 1100 cm^{-1} .

Figure 5.9 (b) represents the observed Raman shift of the NR. The $=\text{C-H}$ stretching vibration in tri-substituted olefinic compounds is usually of weak intensity and is generally observed in the range 3000 - 3100 cm^{-1} . Thus, the weak Raman band which appears at 3033 cm^{-1} is assigned to the $=\text{C-H}$ stretching mode. The $-\text{CH}_2-$ and $-\text{CH}_3$ stretching vibrations in both symmetric and asymmetric modes typically appear in the 2800 - 3000 cm^{-1} range. Note that the position of the C=C stretching vibration is particularly clear and sensitive to its environment. The strong emission band then observed at 1664 cm^{-1} assigned to the C=C stretching mode is in good agreement with the literatures as $\nu(\text{C}=\text{C})$ is particularly clear and sensitive to its environment. The deformation vibrations of methylene and methyl groups give rise to the medium bands in the region 1400 - 500 cm^{-1} . The bands at 1452 and 1432 cm^{-1} are attributed to the C-H deformation of the methyl and methylene groups, respectively. The band at 1357 cm^{-1} is considered to be the $-\text{CH}_2-$ deformation mode. The medium bands at 1327 and 1286 cm^{-1} can be attributed to the $=\text{C-H}$ deformation in plane and CH_2 bending mode, respectively. The bands observed at 1243 , 1147 and 1130 cm^{-1} are assigned to the $-\text{CH}_2-$ twisting, C-H out of plane of *cis*- $\text{C}(\text{CH}_3)=\text{CH}$ and $-\text{CH}_2-$ wagging modes, respectively. The bands appearing in the 900 - 1100 cm^{-1} range are associated to the C-C skeleton stretching modes. The medium bands found at 1000 and 983 cm^{-1}



ascribed to the C-CH₂- and the C-CH₃ stretching vibration modes, respectively. Moreover, the C-H wagging of CH₂, =C-C-C and -C-C-C-rocking modes are observed at low Raman shift in the range of 350-800 cm⁻¹[96]. Other Raman bands at 491 and 372 cm⁻¹ are found and assigned to the =C-C-C and -C-C-C- rocking, respectively.



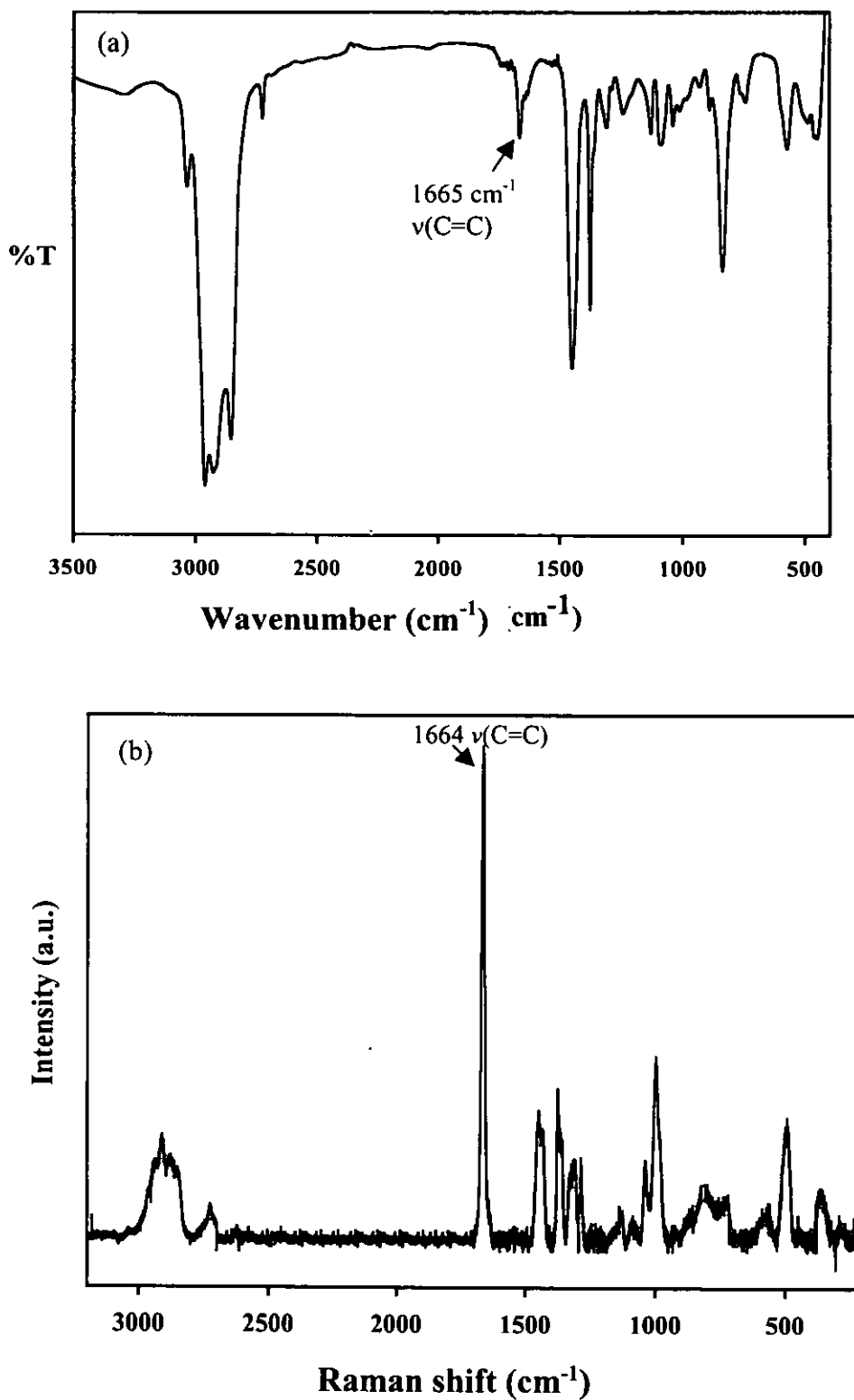


Figure 5.9 Infrared (a) and Raman (b) spectra of NR.



Table 5.4 Wavenumber (cm^{-1}) and assignment of bands observed in Infrared and Raman spectra of NR

Wavenumber (cm^{-1})			Description of assignments
Literatures [24, 64, 96, 97]	Experimental (IR)	Experimental (Raman)	
a	3286 (vw)	c	NH stretching
3032	3036 (vw)	3033 (vw)	=C-H stretching
2962	2962(vs)	2965 (m)	CH ₃ asymmetric stretching
2931	2928 (vs)	2940 (m)	CH ₂ asymmetric stretching
2912	b	2911 (s)	CH ₃ symmetric stretching
2885	b	2881 (m)	d
2854	2855 (vs)	2850 (m)	CH ₂ symmetric stretching
2727	2727(vw)	2725 (vw)	d
a	1740	c	d
1666	1665 (w)	1664 (vs)	C=C stretching
1452	1449 (s)	1452 (m)	CH ₃ asymmetric stretching
1440	b	1432 (m)	CH ₂ deformation
1375	1376 (s)	1371 (m)	d
1363	1361 (vw)	1357 (m)	CH ₂ deformation
1325	b	1327 (m)	=C-H deformation in plane
1311	1309 (w)	1314 (m)	CH ₂ twisting
1287	1288(vw)	1286 (m)	CH bending
1243	1242(w)	1243 (w)	CH ₂ twisting
1208	b	c	=C-H in plane bending
1143	b	1147 (vw)	C-H out of plane of cis- C(CH ₃)=CH wagging
1131	1128 (w)	1130 (w)	CH ₂ wagging
a	1091	c	d
1040	1038 (w)	1039 (m)	CH ₃ rocking
1000	989 (w)	1000 (m)	C-CH ₂ stretching
a	b	983 (m)	C-CH ₃ stretching
a	929	c	d
a	889	c	d
a	836 (m)	840 (w)	=CH out of plane bending



Table 5.4 (continued)

820	b	815 (m)	CH wagging
a	b	788	CH ₂ rocking
a	760(w)	759 (m)	CH ₂ rocking
a	742	c	d
724	b	729	d
a	b	596 (w)	C-C in plane bending
572	575 (w)	569 (w)	d
510	b	c	d
492	b	491 (s)	-CC ₂ rocking
a	b	223 (vw)	CH ₃ torsion

vw = very weak, w = weak, m = medium, s = strong, vs = very strong, a = no reported in literatures, b = not found in IR spectra, c = not found in Raman spectra and d = no proposed assignment.

If the diimide hydrogenation process occurs, the hydrogen molecule added to the unsaturated part in the rubber chain will be transformed into the saturated unit. Vibrational spectroscopy i.e. FT-IR and Raman spectroscopy were used to observe and to elucidate the change of chemical structure of the hydrogenated natural rubbers (HNR). Infrared and Raman spectra of HNR are illustrated in Figure 5.10. The assignments of the peaks are summarized in Table 5.5. Generally, if complete hydrogenation is attained, all signals attributed to double bond of isoprene unit should disappear. However, both infrared and Raman spectra of hydrogenated products still remain the characteristic peaks of polyisoprene unit at reaction time of 8 h. It is not surprising that the total disappearance of the characteristics of unsaturated units is not observed as it has been reported that the complete reduction of unsaturation of PB and PI can be obtained with a five-folded excess of TSH [11, 50, 52]. In our case, only two-mole excess of TSH comparing to the C=C unit was employed.

For IR analysis of the HNR, the decrease of two important characteristic peaks at 1665 and 836 cm⁻¹, attributing to the C=C stretching and the C-H out of plane deformation of the trisubstituted olefin of polyisoprene, respectively, were observed as shown in Figure 5.10 (a). The features observed at 1459, and 1375 cm⁻¹ are assigned to the C-H deformation of both CH₂ and CH₃, and the C-H deformation of only



respectively. Moreover, the appearance of peak positioned at 735 cm^{-1} is assigned in the literature as signal of sequences of three connective methylene units of the saturated fraction on the macromolecular chain [97]. These observations are similar to the hydrogenated synthetic PI and SIS copolymer [11, 51]. This evidence can therefore be used to confirm that the hydrogenation of NR is in a manner similar to several reports of the form of saturated part. Otherwise, unexpected absorption peaks at 810, 1079, and 1141 cm^{-1} were noted and assigned to the signals of SO_2 belonging to TSOH as demonstrated by Mango and Lenz [11].

As previously mentioned, it is noted that the C=C stretching vibration mode at 1664 cm^{-1} is strongly active in Raman spectroscopy. Therefore, the decrease of absorption band at 1664 cm^{-1} can be clearly detected with increasing of the vibrational intensity of the band at 1432 cm^{-1} , attributed to the $-\text{CH}_2-$ deformation vibration with hydrogenation reaction proceeds as can be seen in Figure 5.10 (b). On the other hand, no alteration of the Raman band at 1452 cm^{-1} which belongs to an asymmetric vibration of $-\text{CH}_3$ group was noted after hydrogenation. An extra band at 2925 cm^{-1} corresponding to the C-H stretching vibration of $-\text{CH}_2-$ group of the saturated units was also detected. In addition, Raman spectrum of the HNR exhibit the new characteristic absorption bands at 1299 and 939 cm^{-1} , assigned to the $-(\text{CH}_2)_n-$ in plane twisting and symmetrical stretching of $-\text{C}-\text{C}-\text{C}-$ modes in the rubber chains [97]. Edward et al. found the signal at 1593, 1148 and 795 cm^{-1} , assigned to the signal of the C=C stretching mode of aromatic ring, N-N and C-S stretching modes of TSOH [53]. In our case, after several precipitations in non solvent, no such peaks were detected.

Poshyachinda and Kanitthanon had found the evidence of the *cis-trans* isomerization of polybutadiene during hydrogenation using diimide by Raman technique [25]. Unfortunately, the unsaturated units of synthetic *cis*-1,4 polyisoprene and *trans*-1,4 polyisoprene are very difficult to differentiate by vibrational spectroscopy because the *cis* and *trans* structures of trisubstituted olefin contribute to very close frequencies [22, 62]. Similarly, in our case, no significant peak of *trans* structure of NR was detected. Then in order to confirm the occurrence of *cis-trans* isomerization in the HNR samples, $^1\text{H-NMR}$ and $^{13}\text{C-NMR}$ in solution and $^{13}\text{C-NMR}$ in solid state were used.



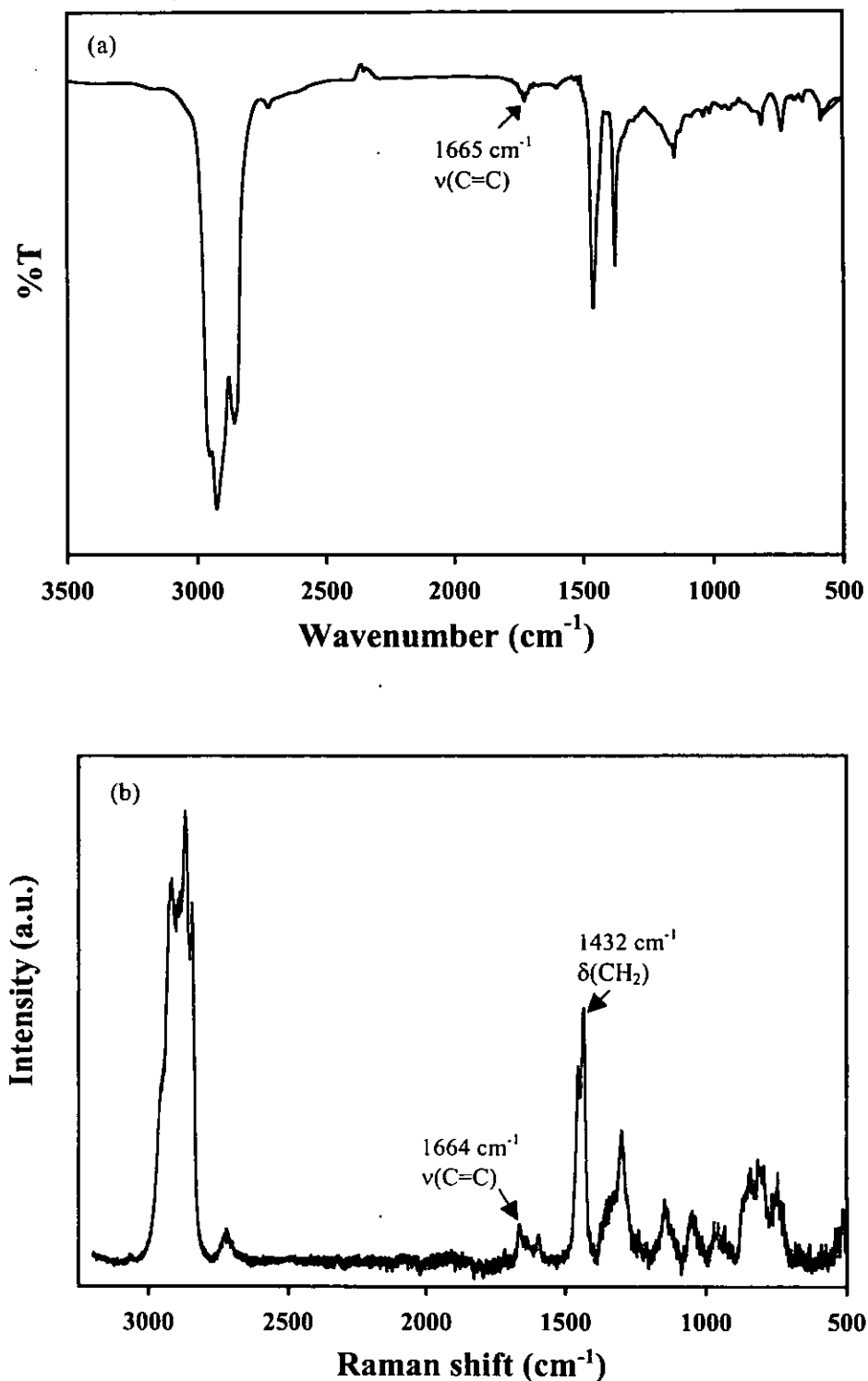


Figure 5.10 Infrared (a) and Raman (b) spectra of hydrogenated rubber obtained at 8h of reaction time.



Table 5.5 Wavenumber (cm^{-1}) and assignment of bands observed in Infrared and Raman spectra of hydrogenated NR

Wavenumber (cm^{-1})			Description of assignments
Literatures [11, 19, 96,97]	Experimental (IR)	Experimental (Raman)	
3032	b	c	=C-H stretching in (C(CH ₃)=CH)
a	b	2992	CH ₃ asymmetric stretching
2962	2963	2955	CH ₂ asymmetric stretching
2931	2923	2924	CH asymmetric stretching
2912	b	c	CH ₃ symmetric stretching
a	b	2896	d
2885	b	2867	CH ₃ symmetric stretching
2854	2856	2844	CH ₂ symmetric stretching
2727	2724	2723	d
a	1731	c	d
1666	1665	1664	C=C stretching
1452	1454	1457	CH ₃ asymmetric vibration
1440	b	1432	CH ₂ asymmetric deformation
1375	1377	c	CH ₃ wagging
1363	b	c	CH ₂ wagging
a	b	1344	d
1325	b	c	=CH deformation in plane
1311	b	c	CH ₂ torsion
a	b	1299	-(CH ₂) _n - twisting in plane
1287	1285	c	CH bending deformation
1243	b	c	CH ₂ torsion
1143	1145	1142	CH ₂ -CH ₂ stretch, C-H out of plane of <i>cis</i> -C(CH ₃)=CH
1131	b	c	(C-C) <i>cis</i> stretching
1040	b	1047	CH ₂ C(CH ₃)=CH rocking
1000	b	c	C-C stretch(C-CH ₂ , C-CH ₃)
a	b	966	d



Table 5.5 (continued)

a	b	939	-C-C-C- symmetrical stretching
a	b	870	-C-C-C- symmetrical stretching
a	b	845	d
820	b	c	CH wagging
a	809	806	d
a	b	770	d
a	735	745	sequence of $-(CH_2)_3-$
a	584	c	d
492	b	c	$=CC_2$ rocking, $=CC_2$ sissoring
428	b	c	C-C ₂ rocking

a = no reported in literatures b =not found in IR spectra c = not found in Raman spectra

d = no proposed assignment.

As a reference, the Raman spectrum of TSH was also examined by Raman spectroscopy as presented in Figure 5.11, and the assignment proposed is given in Table 5.6. It was found that the peak positions at 3082, 3063, 3050, 3039, 3025, and 2921 cm^{-1} correspond to the C-H stretching mode of aromatic ring and the bands at 2978, 2949, 2896, and 2868 cm^{-1} belong to the C-H stretching mode of aliphatic CH_3 . Prominent bands attributable to the aromatic ring stretching vibrations are also observed at 1593, 1582, and 1492 cm^{-1} . The C-H deformations are observed at 1302, and 1089 cm^{-1} , whilst the symmetric C- CH_3 deformation appears at 1383 cm^{-1} . The bands at 642 and 557 cm^{-1} can be assigned to SO_2 deformation and SO_2 rocking modes, respectively.



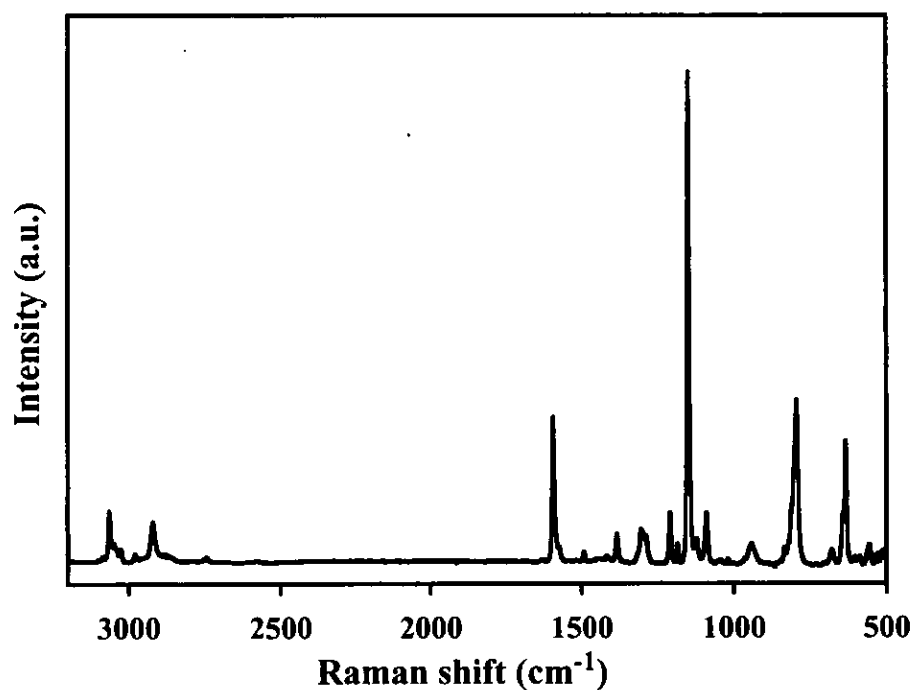


Figure 5.11 Raman spectrum of *p*-toluenesulfonylhydrazide (TSH).

Table 5.6 The assignment of Raman spectrum of TSH

Wavenumber (cm ⁻¹)		Approximate description of vibrational modes
Literature [53, 97]	Experimental	
3067	3063	CH of aromatic symmetric stretching
3046	3050	CH of aromatic asymmetric stretching
a	3035	CH of aromatic asymmetric stretching
a	2978	CH of aliphatic symmetric stretching
a	2949	CH aliphatic stretching
2924	2921v	CH symmetric stretching
a	2896	CH aliphatic stretching
a	2868	CH aliphatic asymmetric stretching
2750	2747	CH aliphatic
1598	1594	NH ₂ deformation; aromatic ring stretching
a	1582	NH deformation; aromatic ring stretching
a	1492	aromatic ring deformation

Table 5.6 (continued)

a	1383	CH ₃ deformation, C-CH ₃
1307	1315	SO ₂ asymmetric stretching
a	1302	C-H deformation
1292	1287	C-H deformation
1212	1209	C-C of aromatic ring stretching
1188	1184	C-SO ₂ -N stretching; C-C of aromatic ring stretching
1152	1148	N-N stretching
1130	1125	C-SO ₂ -N stretching
1092	1089	C-H deformation in-plane
945	942	CH ₃ rocking
a	812	Ring deformation para-disubstituted aromatic ring
797	795	C-S stretching
680	678	CH rocking
641	642	SO ₂ deformation
635	633	S-N stretching
557	557	SO ₂ rocking

a = no reported in literatures

(b) Nuclear Magnetic Resonance Analysis

The characteristics of the NR and the HNR were also investigated by ¹H-NMR and ¹³C-NMR spectroscopy both in liquid and solid state.

By ¹H-NMR and ¹³C-NMR spectroscopy in liquid state

Figure 5.12 shows the ¹H-NMR and ¹³C-NMR spectra of NR. The proton and carbon position of NR structure as *cis*-1,4 polyisoprene unit, were assigned in detail as tabulated in Table 5.7. ¹H-NMR analysis of NR in Figure 5.12 (a) indicates three main characteristic signals of proton adjacent to the C=C, methylene and methyl protons of the unsaturated unit at 5.12, 2.05 and 1.67 ppm, respectively.



In the case of ^{13}C -NMR analysis (see Figure 5.12 (b)) in solution, the carbon signals of $\text{C}=\text{C}$ of the *cis* structure are positioned at 135.2 and 125.5 ppm. Three signal characteristics of the methyl and two methylene carbons of the unsaturated unit are found at 23.4, 26.4 and 32.2 ppm, respectively [12, 97].

The microstructure of HNR was investigated by ^1H - and ^{13}C -NMR and the spectra after 8h of hydrogenation were shown in Figure 5.13. The detail of the assignments of the HNR is given in Table 5.8. For ^1H -NMR analysis, it can be seen that the signal of proton adjacent to the unsaturated unit of the hydrogenated NR at 5.12 ppm decreases upon diimide reduction as the hydrogenation proceeded, as well as the decrease of signal at 1.67 ppm characteristic of the methyl proton of *cis*-1,4 structure. The appearance of the signals at 0.84 and 1.1-1.3 ppm, which represent the methyl and methylene proton of the saturated unit, confirms the hydrogenation reaction process [11, 12, 19]. The ^1H -NMR spectrum of the HNR also exhibits another extra signal at 1.60 ppm, which can be assigned to the methyl proton of *trans*-1,4 polyisoprene unit.

^{13}C -NMR spectra of the NR and HNR were shown in Figure 5.12 (b) and Figure 5.13 (b), respectively. The extra peaks at 19.5, 32.8 and 37.1 ppm are found in the HNR samples. These signals correspond to the carbon of the methyl, methylene, and methine of the saturated unit. The observed chemical shifts are in good agreement with those reported in the literatures [12, 99]. The ^{13}C -NMR spectrum of the partially hydrogenated product reveals the evidence of *cis-trans* isomerization of the polyisoprene units in the macro-molecular chains. The carbon signals of *cis*-structure are positioned at 135.2 and 125.5 ppm, while the signals at 134.9 and 124.7 ppm, corresponding to olefinic carbons of the *trans*-PI structure are also detected.



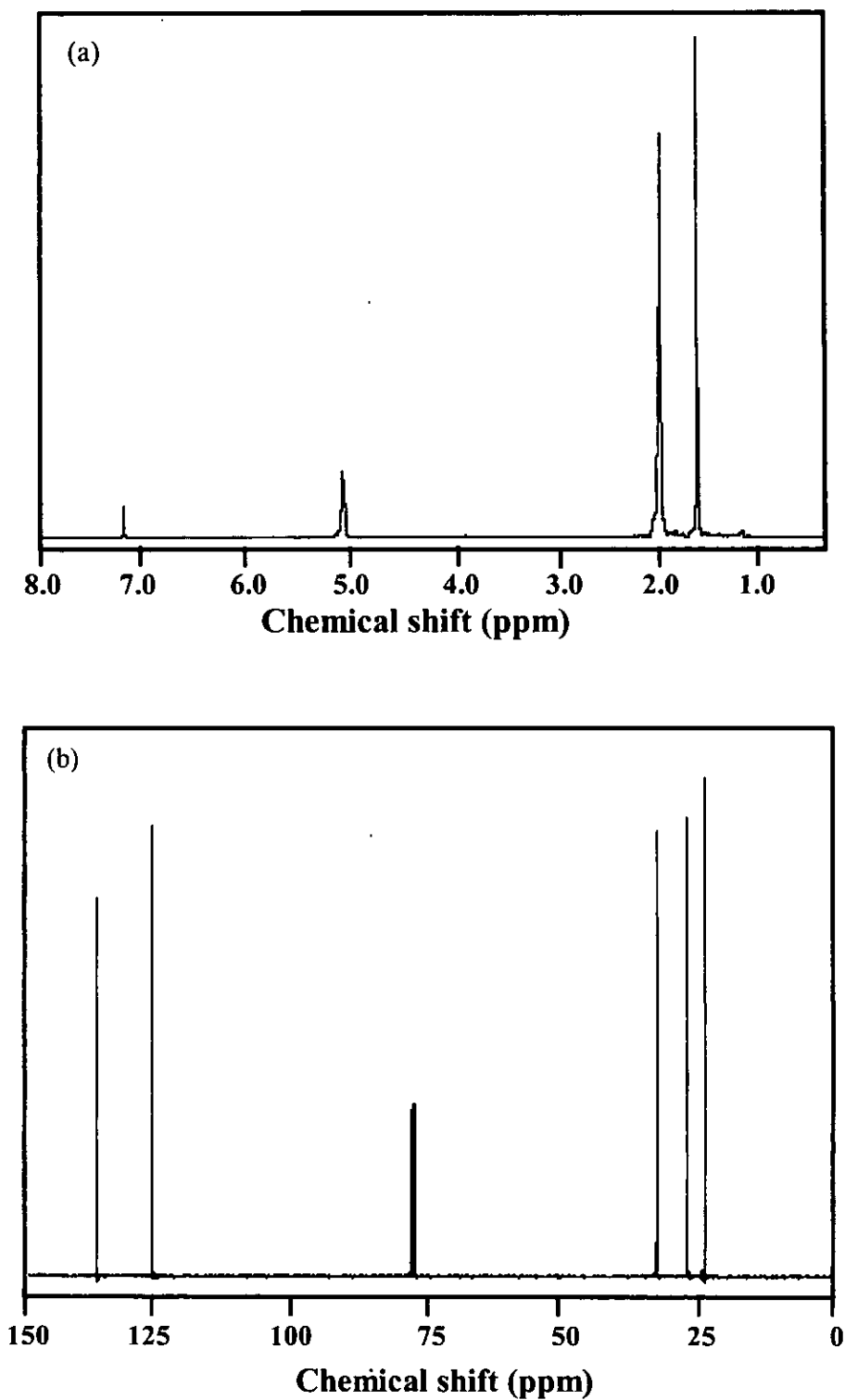


Figure 5.12 ¹H-NMR (a) and ¹³C-NMR (b) spectra of NR in liquid state.



Table 5.7 The assignment of ^1H - and ^{13}C -NMR resonances of NR spectra in liquid state

Chemical structure	^1H -NMR analysis		^{13}C -NMR analysis	
	Literatures [12, 21, 98]	Experimental	Literatures [12, 98]	Experimental
	a = 1.69 (1,4- <i>c</i>) b = 2.03 (1,4- <i>c</i>) c = 5.12	a = 1.67 b = 2.05 c = 5.12	C-1 = 32.3 (1,4- <i>c</i>) C-2 = 134.8 (1,4- <i>c</i>) C-3 = 125.3 (1,4- <i>c</i>) C-4 = 26.5 (1,4- <i>c</i>) C-5 = 23.4 (1,4- <i>c</i>)	C-1 = 32.2 C-2 = 135.2 C-3 = 125.5 C-4 = 26.4 C-5 = 23.4

c = *cis*-configuration

Table 5.8 The assignment of ^1H - and ^{13}C -NMR resonances of the hydrogenated NR in liquid state

Chemical structures	^1H -NMR analysis		^{13}C -NMR analysis	
	Literature [12, 19, 99]	Experimental	Literature [12, 99]	Experimental
	a = 1.68 (1,4- <i>c</i>) b = 2.03 (1,4- <i>t, c</i>) c = 5.12 d = 0.77, 0.98 e = 1.25 (m) f = 1.60 (1,4- <i>t</i>)	a = 1.67 b = 2.05 c = 5.12 d = 0.80-0.89 e = 1.18 f = 1.60	C-1 = 32.3 C-2 = 134.8 C-3 = 125.3 C-4 = 26.5 C-5 = 23.4 C-6 = 37.1 C-7 = 33.3 C-8 = 37.9 C-9 = 24.9 C-10 = 19.7 C-11 = 39.7 C-12 = 134.4 C-13 = 124.8 C-14 = 26.8 C-15 = 16	C-1 = 32.4 C-2 = 135.2 C-3 = 125.5 C-4 = 26.4 C-5 = 23.4 C-6 = 37.4 C-7 = 32.8 C-8 = 37.5 C-9 = 24.5 C-10 = 19.7 C-11 = 40.0 C-12 = 134.9 C-13 = 124.7 C-14 = 25.5 C-15' = 15.8

c = *cis*-configuration, *t* = *trans*-configuration, and *m* = multiplet



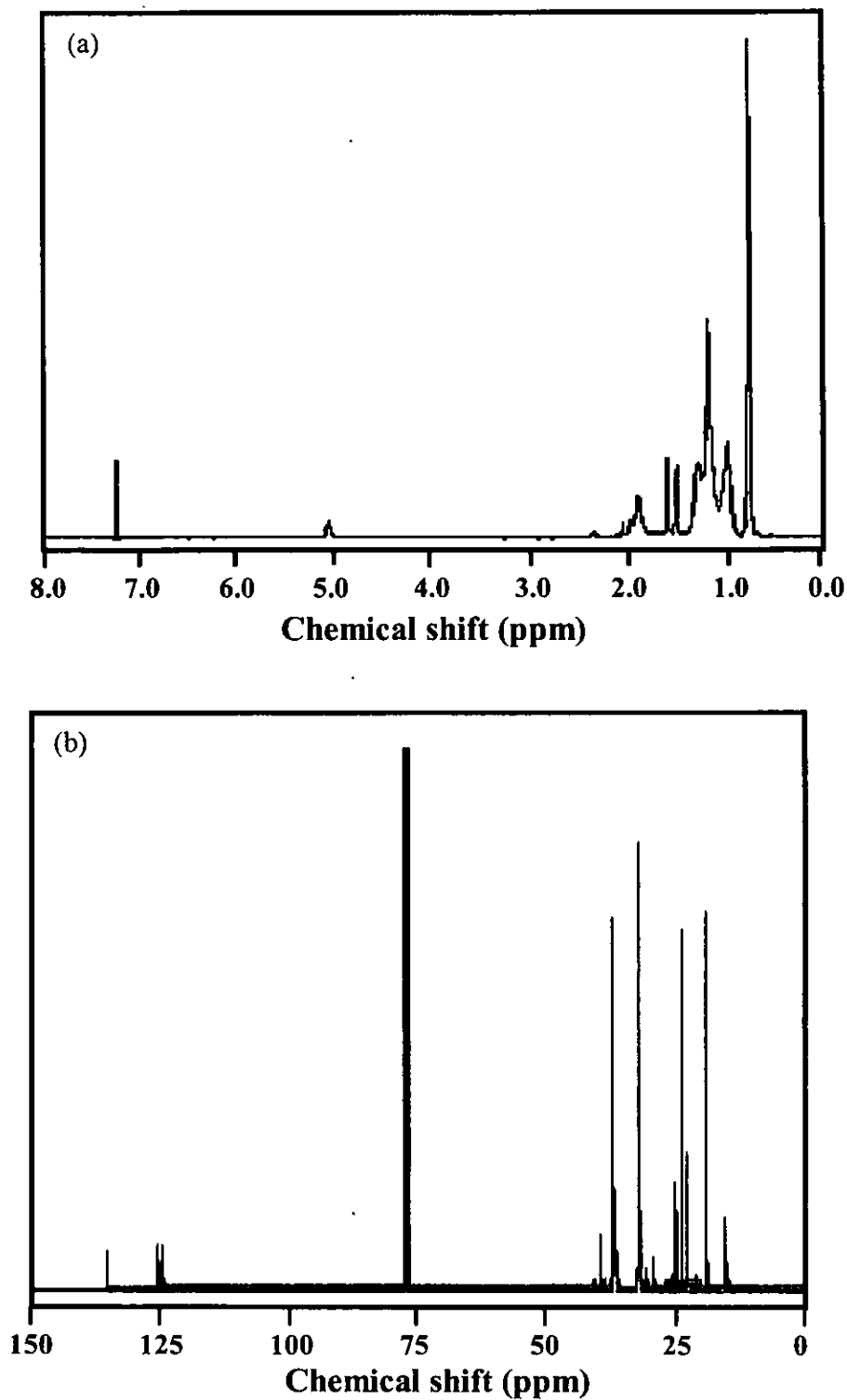


Figure 5.13 ^1H -NMR (a) and ^{13}C -NMR (b) spectra of the hydrogenated NR in liquid state at 8h of reaction time.



In order to confirm the carbon assignments of HNR, the ^{13}C -NMR spectrum of 2,6,10,15,19,23-hexamethyltetracosane ($\text{C}_{30}\text{H}_{62}$) was simulated by NMR software package (WINNMR) as shown in Figure 5.14 and the assignment is given in Table 5.9. It was found that the four signals at about 37.5 ppm can be contributed to the carbon signals of the methylene group (C-5, C-7, C-9 and C-11 ppm) in zig-zag conformation, while the chemical shift at 27.5 ppm was represented to the carbon of ethylene unit in the close packing of molecular chain. In comparison with the ^{13}C -NMR spectrum of HNR, the characteristic peaks at around 37.5 ppm are usually detected as the methylene and methine groups presented in the saturated part of the HNR sample which is in agreement with the NMR spectrum of simulated $\text{C}_{30}\text{H}_{62}$. On the basis of ACD simulation, the peak at 24.9 ppm (C-8 and C-17) and 27.5 ppm (C-12 and C-13) are assigned to the methylene carbons and another peak assigned at 19.8 is the signal of methyl (C-26 and C-29) groups.

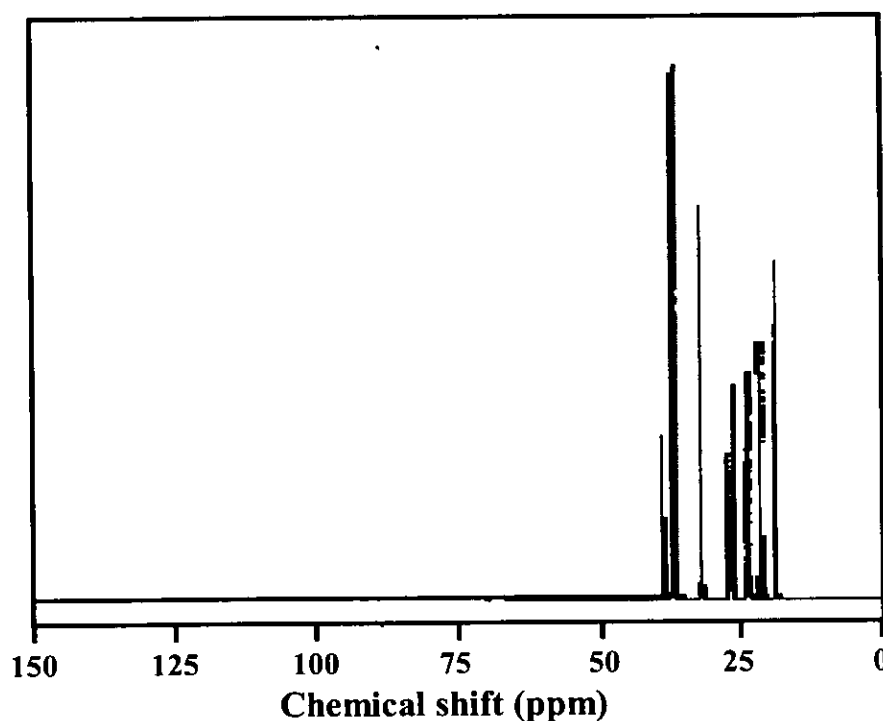
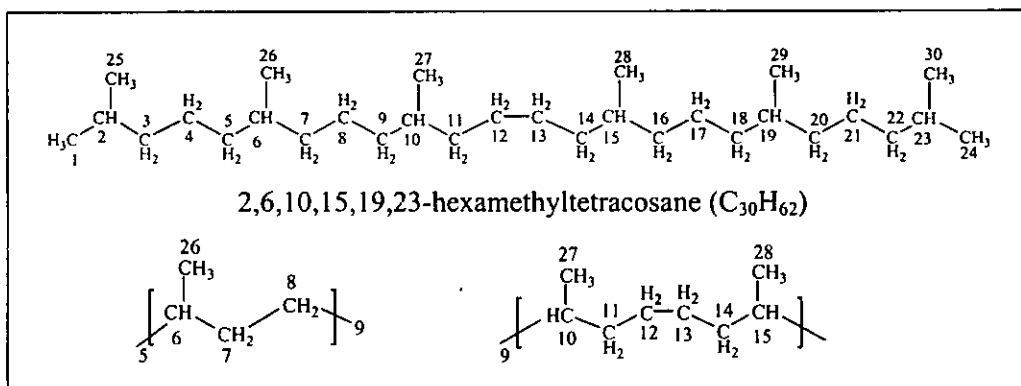


Figure 5.14 ^{13}C -NMR spectrum of 2,6,10,15,19,23-hexamethyltetracosane ($\text{C}_{30}\text{H}_{62}$).

Table 5.9 The assignment of carbon positions of 2,6,10,15,19,23-hexamethyltetra-
cosane obtained from NMR software

Assignment	Chemical shift (ppm)	
	2,6,10,15,19,23-hexamethyltetra- cosane	HNR
C-1, C-24, C-25, C-30	22.7	-
C-2, C-23	28.1	-
C-3, C-22	39.5	-
C-4, C-21	24.6	-
C-5, C-20	37.5	37.4
C-6, C-19	32.9	32.8
C-26, C-29	19.8	19.7
C-7, C-18	37.5	37.5
C-8, C-17	24.9	24.5
C-9, C-16	37.5	37.5
C-10, C-15	32.9	32.7
C-27, C-28	19.8	19.6
C-11, C-14	37.5	37.2
C-12, C-13	27.5	-



By ^{13}C -NMR Spectroscopy in Solid State

High resolution ^{13}C -NMR in solid state is more widely used than ^1H -NMR because the ^{13}C -NMR spectra may be simplified by proton decoupling, which makes all carbon resonances appear as a singlet. The HNR sample is composed of ethylene and propylene units in the macromolecular chains. It is rather difficult to dissolve it in organic solvent. Then in this study solid state NMR can be used to investigate the microstructure characteristic and to study the molecular mobility of the solid hydrogenated NR samples. In this section, the sample was characterized by solid state NMR spectroscopy, using the HD/MAS technique as described in section 4.6. The ^{13}C -NMR study in solid state of the NR and HNR was carried out at room temperature, which is the temperature far above their glass transition temperatures (T_g). Under this condition, the dipolar interactions and chemical shift anisotropy that leads to line broadening are partially averaged by chain motion, and sharp lines are observed with high power decoupling and magic angle spinning. The motional averaging is such that high resolution signals of NR and HNR can be observed with spinning. Then, peak assignments can be established using the data published from traditional ^{13}C -NMR in liquid method.

^{13}C -NMR solid state spectra of NR and HNR are compared in Figure 5.15. The observed dominant peaks of NR spectrum at 23.6, 26.7, 32.5, 134.8 and 125.3 ppm were related to the five carbon atoms of the *cis*-1,4 polyisoprene units as given in Table 5.10, similar to the assignments using ^{13}C -NMR in solution (see Table 5.7). These characteristic peaks were found decreasing when the amount of unsaturated fraction of polyisoprene units were reduced as the hydrogenation reaction proceeded. Then, the significant resonance peaks at 33.1, 37.8, and 20.1 ppm appeared in Figure 5.15 (b) and listed in Table 5.11. Based on literatures [12, 19, 99] and by making comparisons with the NMR spectrum in liquid state, these peaks are assigned to the carbon signals of the methine, methylene and methyl groups, respectively. Moreover, the peak width of ^{13}C -NMR spectrum is broader than that of NR (see Figure 5.15). It can be suggested that there is more stiffness fraction in the molecular structure after modification. The signals located at 40.3, 27.1 and 16.1 ppm are found as presented in Figure 5.15 (b) and assigned to the methine, methylene and methyl groups of *trans*-1,4 polyisoprene structure, respectively. This is the confirmation of



isomerization that occurred simultaneously with diimide hydrogenation by TSH. When the solid state NMR with HD/MAS technique was applied, small peaks at 34.6, 43.7 ppm, which can be assigned to the methine carbon ($-\text{CH}-$ cyclic) and quaternary carbon of cyclic units, respectively were detected. The weak peak at 129.7 ppm observed at the high-field resonance is due to the cyclized trisubstituted end group. These characteristics of cyclized units are in agreement with the investigation of the cyclized structure of NR by Patterson et.al. [36]. They reported the utilization of solid state NMR technique to detect the chemical structure of NR after treatment with toluenesulfonic acid, forming cyclized product.



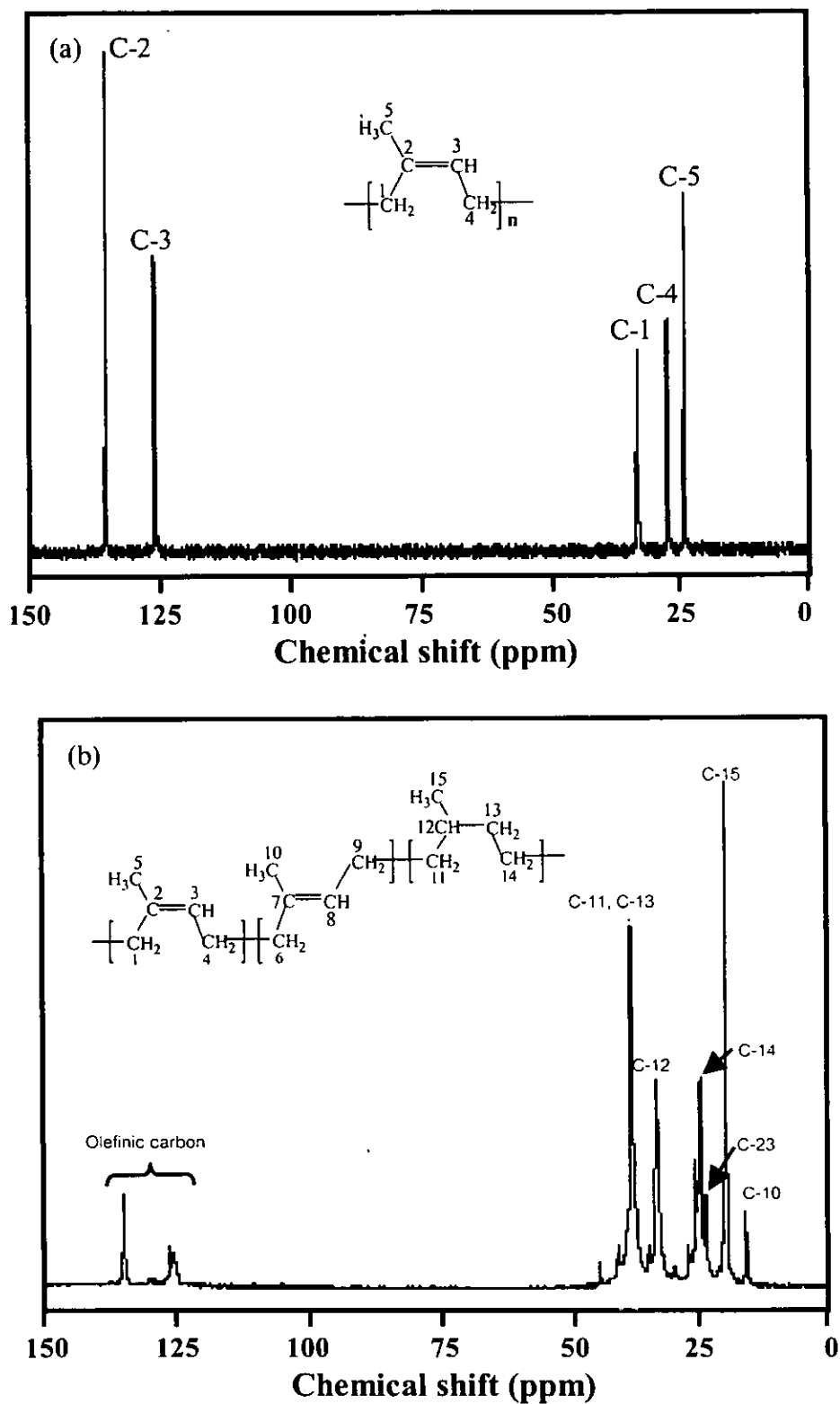


Figure 5.15 ¹³C-NMR solid state spectra of NR (a) and the hydrogenated NR after 8 h of the hydrogenation (b).



Table 5.10 The results of chemical shift and peak widths obtained from resolving ¹³C-NMR spectrum of NR in solid state

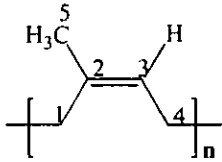
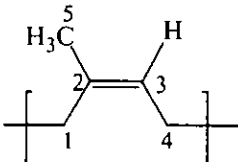
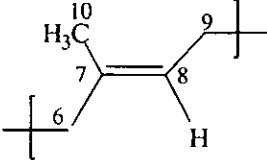
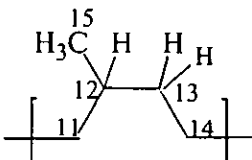
Chemical structure	Position (ppm)	Peak width (ppm)	Assignment [72-76,98]
	134.8	0.11	C-2
	125.3	0.15	C-3
	32.5	0.22	C-1
	26.7	0.19	C-4
	23.6	0.14	C-5

Table 5.11 The results of chemical shift and peak widths obtained from resolving ¹³C-NMR spectrum of HNR in solid state

Chemical structure	Position (ppm)	Peak width (ppm)	Assignment [12, 21,99]
	16.1	0.26	C-10
	20.1	0.28	C-15
	23.8	0.24	C-5
	24.8	0.39	C-14
	25.7	0.46	C-4
	27.1	0.26	C-9
	32.7	0.47	C-1
	33.1	0.51	C-12
	37.8	0.54	C-11, C-13
	40.3	0.42	C-6
	124.5	0.51	C-2
	125.8	0.4	C-7
	134.2	0.23	C-8
	134.8	0.23	C-3



5.2.2 Evaluation of Percent Hydrogenation of NR

The percent hydrogenation of NR and DPNR can be determined by Raman, ^1H -NMR in liquid and ^{13}C -NMR in solid state spectroscopy, which is associated to the decrease of unsaturated units and the increase of saturated part in the macromolecular chain.

(a) By Raman Spectroscopy

As formerly described for the microstructure analysis of the HNR by FT-IR and Raman techniques, it can be seen that the vibrational absorption modes obtained from IR spectrum is not as powerful as Raman mode. The intensity of the C=C absorption peaks at 1665 and 836 cm^{-1} are not strong for quantitative analysis of the percent hydrogenation in FT-IR spectra of the HNR samples.

A comparison between the Raman spectra of the starting NR and hydrogenated NR samples taken at various hydrogenation times is given in Figure 5.16. As hydrogenation reaction proceeds, the decrease of the intensity of the C=C stretching modes is obviously evidenced, together with the increase of the vibrational intensity of the band at 1432 cm^{-1} , attributed to the $-\text{CH}_2-$ deformation vibration. The bands ratio at 1664 and 1432 cm^{-1} was used for calculation of the percent hydrogenation at various reaction times (see section 4.7.3). The results shown in Table 5.12 reveal that at higher reaction time, higher percent hydrogenation was achieved.



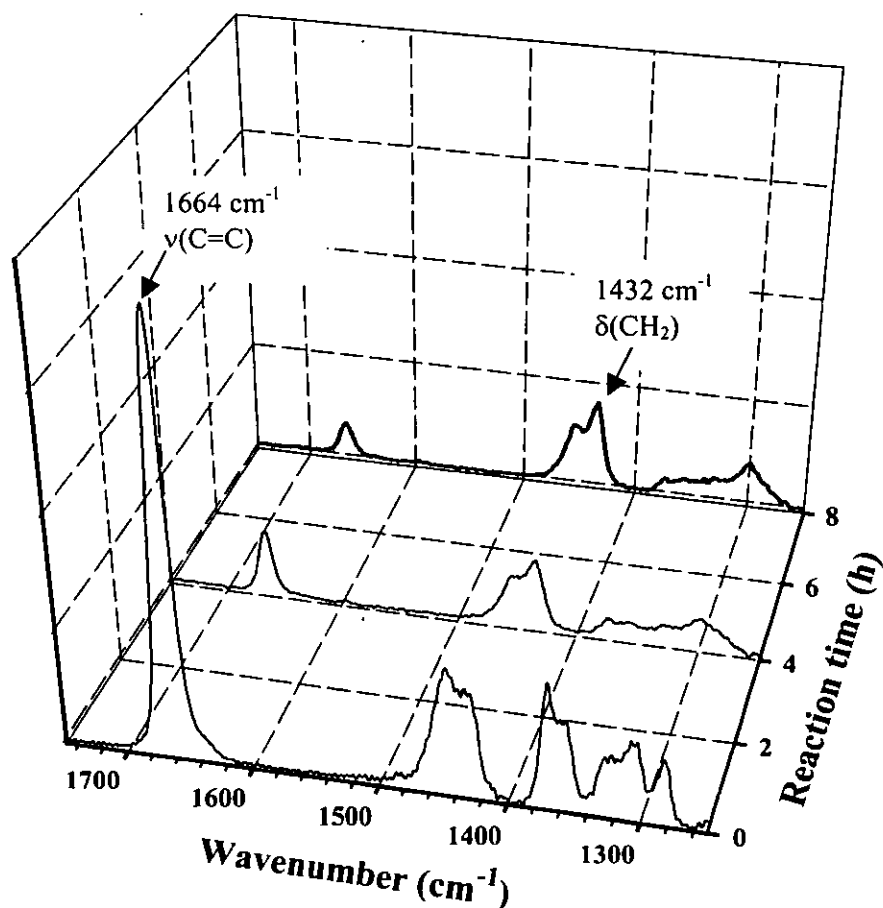


Figure 5.16 Comparison between the Raman spectra of NR and hydrogenated NR samples taken at reaction time 4 and 8h.

(b) By $^1\text{H-NMR}$ Spectroscopy in Liquid

A comparison between the $^1\text{H-NMR}$ spectra of the NR and hydrogenated NR samples taken at 4 and 8h is shown in Figure 5.17. The intensity of the proton signal adjacent to the $\text{C}=\text{C}$ bonds at 5.12 ppm decreases with the increase of reaction time, as well as the decrease of signal at 1.67 ppm characteristic of the methyl proton of *cis*-1,4 PI units of the NR. The intensity of the methyl and methylene proton signals at 0.84 and 1.10-1.30 ppm indicated a strong increment due to the transformation of double bonds into saturation moieties. From $^1\text{H-NMR}$ spectroscopy, the integrated areas of the signals at 5.12 and 0.84 ppm, corresponding to the proton adjacent to the olefinic

unit and the methyl proton of the saturated unit, respectively, were used for the determination of percentage of hydrogenation and the results at various reaction times were given in Table 5.12.

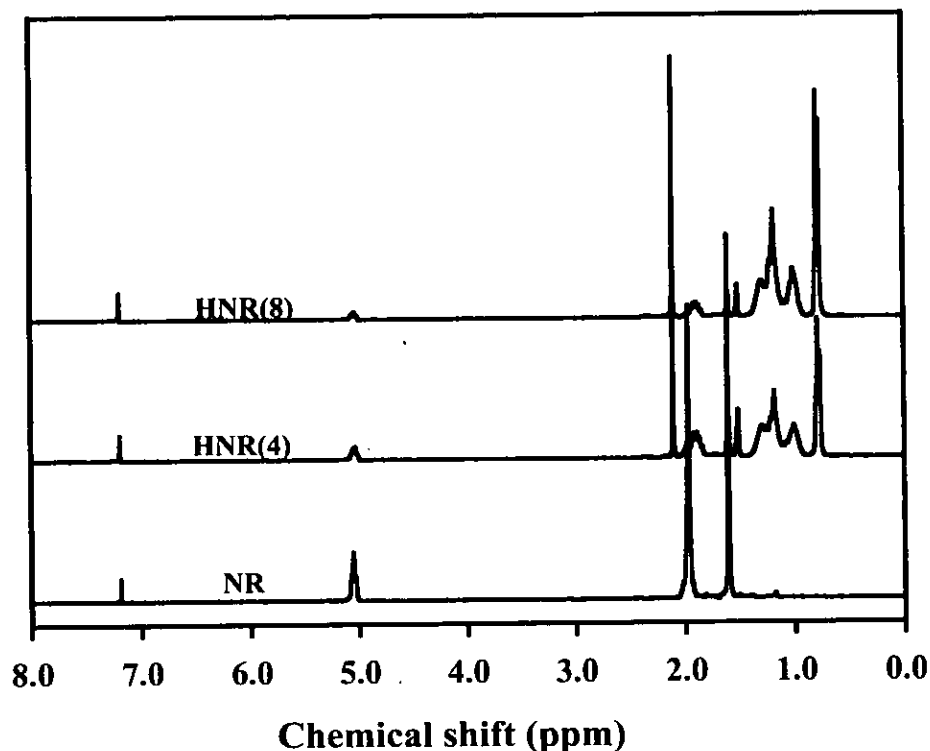


Figure 5.17 ^1H -NMR spectra of NR and hydrogenated NR samples taken at 4 and 8h analyzed in liquid state.

(c) By ^{13}C -NMR Spectroscopy in Solid State

Although, there have been reports of the utilization of spectroscopic methods to monitor the hydrogenation reaction of NR, a search of the literature revealed that there are no previous reports describing the determination of the percent hydrogenation by solid state ^{13}C -NMR technique.

The ^{13}C solid state HD/MAS NMR spectra of NR and hydrogenated NR are shown in Figure 5.18. The progress of hydrogenation by solid state ^{13}C -NMR was obtained by using the integrated areas of the signals of saturated methyl carbon at 20.1

ppm comparing with the methyl carbon of both *cis* and *trans* unsaturated units at 23.8 and 16.1 ppm, respectively, as summarized in Table 5.12.

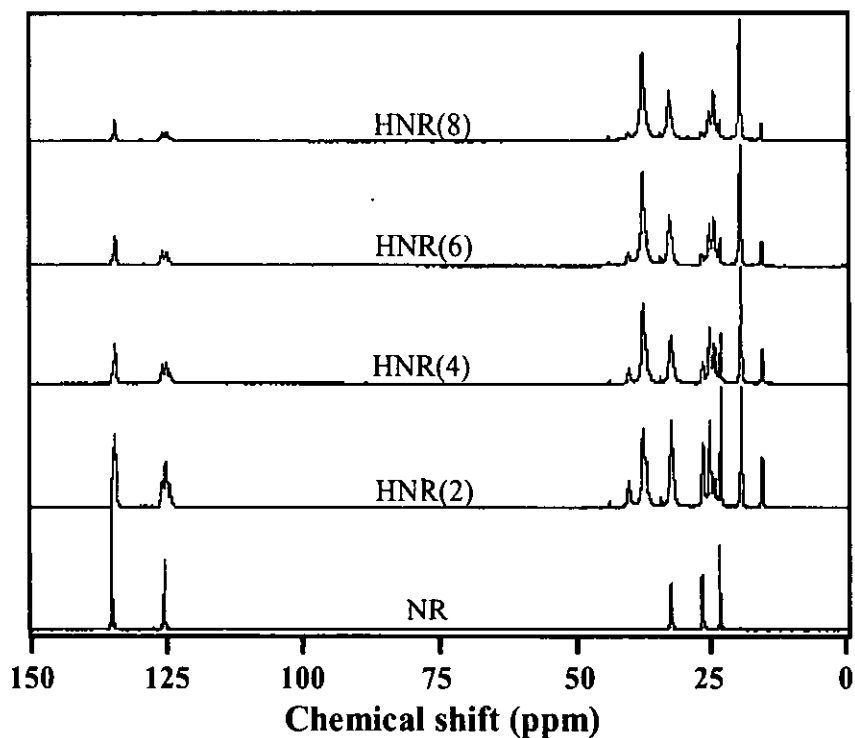


Figure 5.18 ^{13}C -NMR spectra of NR and hydrogenated NR samples taken at 2, 4, 6 and 8h analyzed in solid state.

The results of percentage of hydrogenation at various reaction times of NR determined by three techniques illustrated in Table 5.12 and Figure 5.19 revealed good agreement of quantitative results among these techniques. The percentage of hydrogenation increases with increasing of the reaction time. The maximum percentage of hydrogenation of NR is approximately 80-85 % when a two-folded mole excess of TSH was used.

Table 5.12 The percent hydrogenation of NR at various reaction times as determined by Raman, $^1\text{H-NMR}$ and $^{13}\text{C-NMR}$

Reaction time (h)	Hydrogenation (%)		
	Raman ^a	$^1\text{H-NMR}$ ^b	$^{13}\text{C-NMR}$ ^a
0	0	0	0
0.5	4.3	8.2	n
1	27.7	30.8	29.8
2	39.1	43.1	41
3	57.5	55.2	n
4	57.5	62.1	58.4
6	79.4	75.5	72
8	84.9	80	80

^a in solid sample and ^b in solution, n = not determine

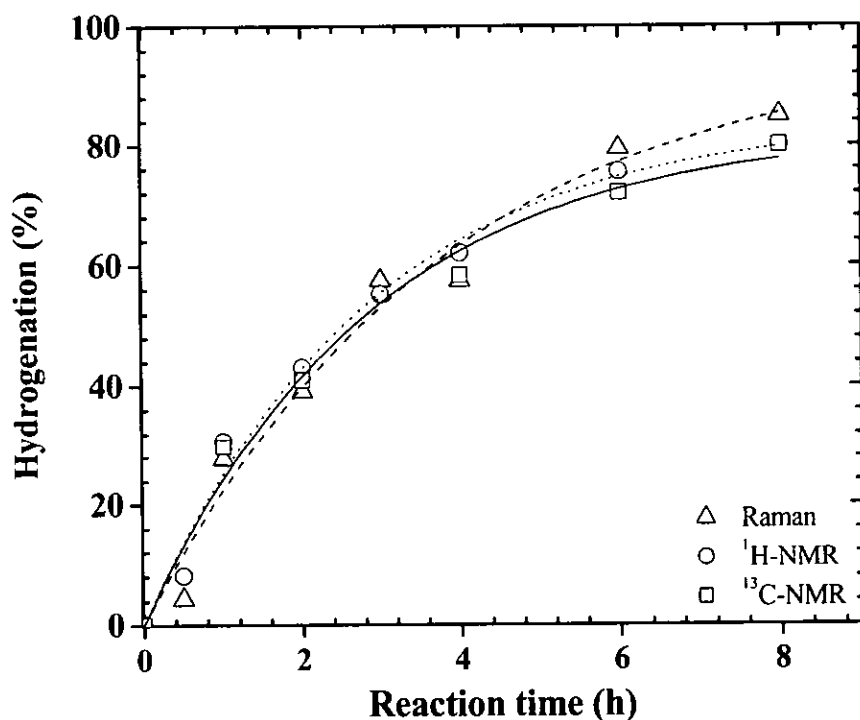


Figure 5.19 The percent hydrogenation at various reaction times of NR determined by $^1\text{H-NMR}$ in solution (\circ), Raman scattering (Δ) and $^{13}\text{C-NMR}$ in solid state (\square).

The hydrogenation by TSH was applied with DPNR and the hydrogenation results were determined by $^1\text{H-NMR}$ and compared with HNR shown in Table 5.13. It was found that the percentage of hydrogenation of DPNR significantly increases with the hydrogenation time, and the maximum hydrogenation is reached at approximately 97%. It was shown that the rate of hydrogenation of DPNR is faster than that of NR. Similar results were also reported by Gan et. al. that the NR was hydrogenated at a lower rate than the DPNR using catalytic hydrogenation [19]. It can be proposed that the DPNR has less impurity or non-rubber constituents than NR as it was subjected to several centrifugations or lower molecular weight of DPNR than NR that facilitated the hydrogenation reaction [33, 100].

Table 5.13 The percent hydrogenation of NR and DPNR at various reaction times as determined by $^1\text{H-NMR}$

Reaction time (h)	Hydrogenation (%)	
	NR	DPNR
0	0	0
2	43.1	76.0
4	62.1	91.1
6	75.5	95.7
8	80.0	97.3



5.2.3 Side Reactions

The side reaction of diimide hydrogenation by employing TSH can be occurred since the *p*-toluenesulfonic acid (TSH) by-product obtained from the decomposition of TSH acts as an accelerator for other reactions such as *cis-trans* isomerization, degradation and cyclization.

(a) *Cis-Trans* Isomerization

Cis-trans isomerization of unsaturated rubbers occurs in several ways such as photo-induced, radiation-induced, thermal and catalytic isomerizations [4, 6]. It was reported that the use of TSH as a diimide releasing agent for hydrogenation of *cis*-polybutadiene resulted in the *cis-trans* isomerization [25, 51]. Unfortunately, the *cis-trans* isomerization of polyisoprene units of NR during hydrogenation cannot be detected by infrared and Raman spectroscopy as the vibrational frequency of the *cis* and *trans* structures of trisubstituted olefinic unit in vibration modes are very close. While the ¹H-NMR spectra of the hydrogenated rubber exhibit the signal of methyl proton of the *cis*- and *trans*-1,4 polyisoprenic units at 1.67 and 1.60 ppm, respectively. The percentage of the remaining double bonds in *cis* and *trans* configurations of the hydrogenated samples at various reaction times was then calculated and the results are shown in Table 5.14 and Figure 5.20 (a). The ¹³C-NMR spectrum in solution of the partially hydrogenated product reveals the evidence of the *cis-trans* isomerization. The carbon signals of *cis*-1,4-polyisoprene structure of NR were located at 135.2 and 125.5 ppm while the signals at 134.9 and 124.7 ppm, corresponding to olefinic carbons of 1,4-*trans* polyisoprene units, were also detected after hydrogenation. For solid state ¹³C-NMR spectra, the signal of the methyl carbons of *cis*- and *trans*- structures can be clearly seen at 23.6 and 16.1 ppm, respectively. The results of the percentage of *cis* and *trans* isomers at various reaction times are illustrated in Figure 5.20 (b). It was found that the amount of *trans* isomer of polyisoprene units increased up to 4 h of hydrogenation time. After that the amount of *cis* and *trans* isomers are comparable. This may be proposed that the *cis-trans* isomerization is a reversible process. The evidence of *cis-trans* isomerization is similar to that of PB and isoprene-styrene diblock copolymer [25, 51]. It was reported that catalytic *cis-trans* isomerization of synthetic 1,4-polyisoprene could be carried out with thiol acids, sulfur dioxide, and



other related materials that function as catalysts. It can be taken place through the rotation of the weakened double bond via the formation of an unstable complex as demonstrated in Figure 5.21. In our case, TSH was used at reaction temperature rather high (135°C). The isomerization of the highly *cis*-structure of NR into the *trans*-isomer could be inevitably occurred via similar manner.

Table 5.14 The percent of hydrogenation, *cis* and *trans* isomers of HNR as determined by $^1\text{H-NMR}$ in liquid state and $^{13}\text{C-NMR}$ in solid state

Reaction time (h)	$^1\text{H-NMR}$ in liquid state			$^{13}\text{C-NMR}$ in solid state		
	Hydrogenation (%)	<i>Cis</i> (%)	<i>Trans</i> (%)	Hydrogenation (%)	<i>Cis</i> (%)	<i>Trans</i> (%)
0	0	100	0	0	100	0
0.5	8.2	88.8	3.03	n	n	n
1	30.8	54.4	14.8	29.8	53.4	16.8
2	43.1	38.6	18.3	41	38.4	20.6
3	55.2	23.2	21.6	n	n	n
4	62.1	19.6	18.3	58.4	22.3	19.3
6	75.5	11.2	13.3	72.0	12.2	15.8
8	80.0	10	10	80.0	9.3	10.7

n = not determine



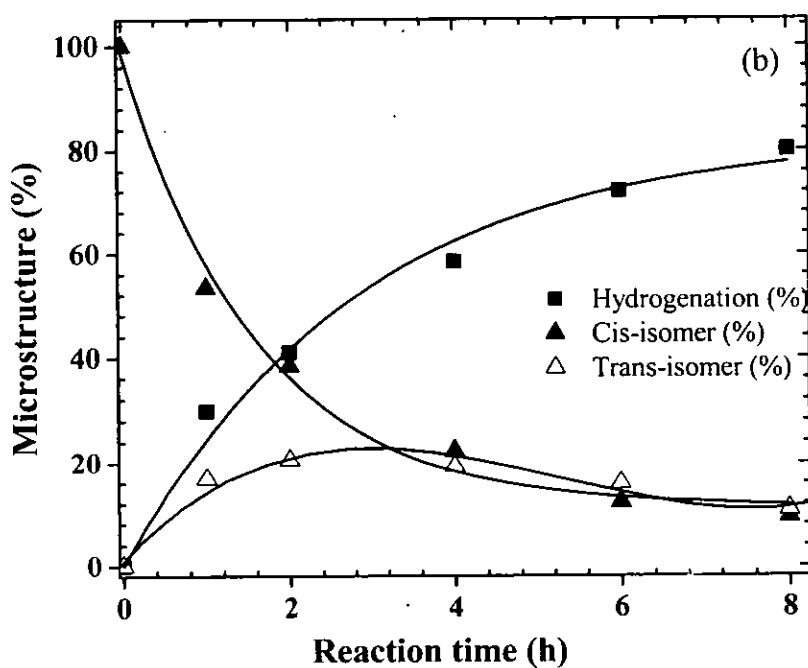
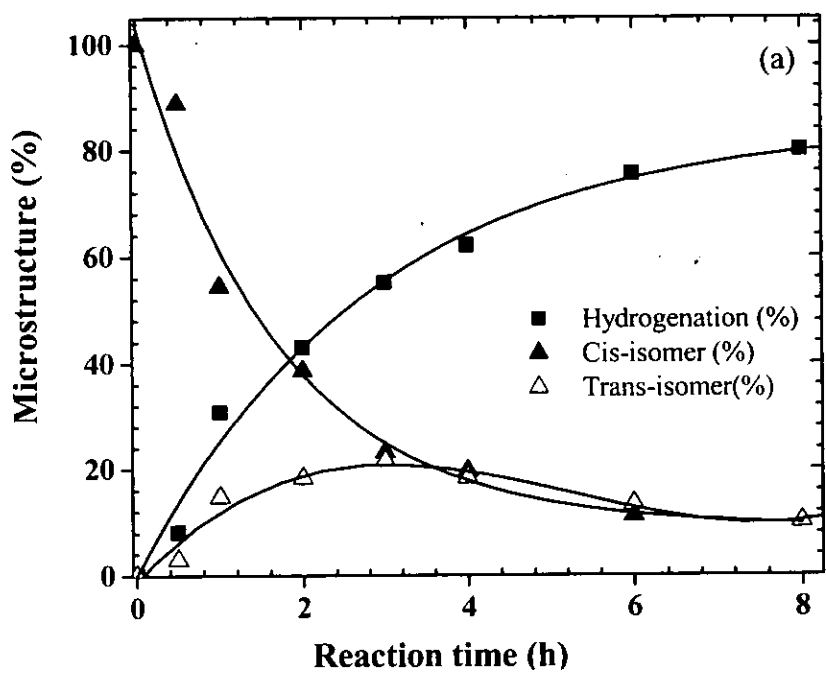


Figure 5.20 Progress of *cis-trans* isomerization rate during hydrogenation of NR determined by $^1\text{H-NMR}$ in solution (a) and $^{13}\text{C-NMR}$ in solid state (b) as symbolized of the %*cis* (■) and %*trans* (□).

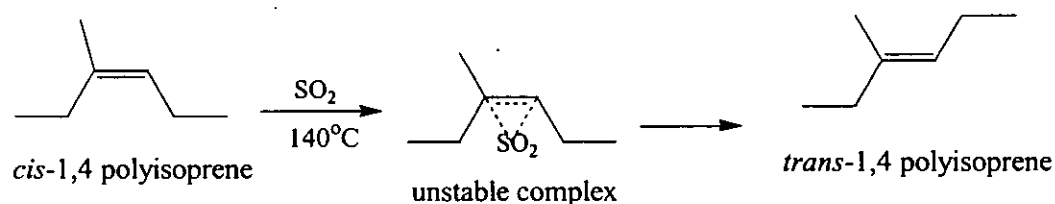


Figure 5.21 *Cis-trans* isomerization of *cis*-1,4 polyisoprene [51].

(b) Degradation Reaction

In order to investigate the presence of side reactions, such as degradation and crosslinking during the chemical modification processes, the modified products were examined by dilute solution viscometry technique. This technique has been employed to follow the change of the physical properties of polymer by monitoring the shifts of average viscosity molecular weight that are created by such side reactions. The method has the drawback of an ambiguous relationship of viscosity (η) to molecular weight, especially for copolymers with composition or structure diversity. Nevertheless, the space occupied by a macromolecule in solution is related to its molecular weight, type of solvent and evident in the solution viscosity. Therefore, the intrinsic viscosity of the NR and modified forms provides a simple and effective means of examining the side reaction. The intrinsic viscosities of NR and the hydrogenated NR are presented in Table 5.15. It was found that the intrinsic viscosity of hydrogenated rubbers was lower than that of NR. The decrease of intrinsic viscosity suggests the occurrence of degradation during the non-catalytic hydrogenation by TSH at 135°C . Beside the *cis-trans* isomerization of the double bond in the case of NR, the hydrogenation of NR with TSH at 135°C mainly causes the chain cleavage of NR. This result is in accordance with several works [11, 50, 101] showing the degradation reaction of polybutadiene and styrene-isoprene copolymer could occur during hydrogenation using TSH.

Table 5.15 Intrinsic viscosity data at different hydrogenation levels

Hydrogenation (%)	Intrinsic viscosity $[\eta]$
0	3.62
43.1	2.06
62.1	2.13
75.5	1.78
80.0	1.06

(c) Cyclization Reaction

As formerly mentioned in the characterization of hydrogenated samples by solid state NMR, the small signal peaks corresponding to the cyclized units were observed. It might be proposed that the TSOH produced from TSH caused the cyclization of *cis*-1,4 PI. TSOH by product is an acid, protonation of polyisoprene units could be possibly occurred to form carbonium ion at tertiary carbon which underwent cyclization [36, 37] as shown in Figure 3.3 in section 3.2.1.



5.3 Hydrogenation of ENR

Epoxidized natural rubber (ENR) is one of the chemically modified forms of NR. It has better oil resistance and property of gas impermeance than the NR upon epoxidation. The primary drawback of ENR like NR is its poor aging property. The hydrogenation of the ENR is expected to give a product with improved thermal behavior, due to the reduction of double bond content in molecular chain. In this present work, the non-catalytic hydrogenation of ENR was also carried out with diimide molecule generated from thermal decomposition of TSH. Similar to hydrogenated NR, in this case of hydrogenation of ENR two-folded mole excess of TSH comparing to the C=C unit was utilized. Hydrogenation was performed on four ENRs containing 10 (ENR-10), 22 (ENR-22), 30 (ENR-30) and 40 mol% (ENR-40) of epoxidized units, respectively.

5.3.1 Structural Analysis of ENR and Hydrogenated ENR

The chemical structure of epoxidized natural rubber (ENR) and hydrogenated ENR (HENR) was analyzed by infrared, Raman, and NMR spectroscopies. By using NMR analysis of ENR, Bradbury et al. [101] reported that the repeating units containing epoxide and isoprene units are randomly arranged in the molecular chains. Therefore, the number of vibration modes can not be determined by group theory, only the chemical structure of the ENR could be analyzed.

(a) Vibration Analysis

Typical vibrational spectra of ENR and hydrogenated products are depicted in Figures 5.22 and 5.23, respectively. The assignment of peak positions and relative intensities are tabulated in Table 5.16.

FT-IR spectra of ENR and HENR were recorded in the wavenumber range of 500-3500 cm^{-1} , as shown in Figure 5.22. For ENR, the aliphatic C-H stretching vibration is located between 3010 and 2850 cm^{-1} , and the $-\text{CH}_2-$ deformation vibration is observed at 1452 cm^{-1} . A sharp peak appears at 1377 cm^{-1} due to the deformation vibration mode of the $-\text{CH}_3$ group. Two distinct peaks for the C-O-C of epoxy group



are found at 870 cm^{-1} (epoxide asymmetric stretching) and 1250 cm^{-1} (epoxide symmetric stretching) [21, 38, 93, 97] of ENR, while the out of plane deformation of *cis*-1,4-polyisoprene is positioned at 836 cm^{-1} . Figure 5.22 (b) illustrates the IR spectrum of the hydrogenated ENR. Similar changes as in the case of hydrogenation of NR can be observed for the HENR. The IR spectrum of HENR reveals the decrease of signals at 1665 and 836 cm^{-1} , contributing to the C=C bond and the characteristic of *cis*-polyisoprene in the backbone. The characteristics of the oxirane ring also disappear after hydrogenation, as a result of ring opening during hydrogenation. The strong absorption band at 3450 cm^{-1} is observed and assigned to the O-H stretching of the hydroxy group. The FT-IR spectrum of HENR also contains the characteristic signals contributing to SO₂ asymmetric and symmetric stretching at 1334 and 1145 cm^{-1} , respectively [11, 53]. These signals were not disappeared after several precipitations in non solvent. This evidence supported that the fixation of TSOH might fix on the ENR backbone. Additionally, two absorption peaks at 811 and 1035 cm^{-1} are observed which correspond to the *p*-tolyl aromatic ring as reported in the literatures [11, 52, 53].

The characterization of microstructures of ENR and HENR was also carried out by Raman spectroscopy and the spectra of ENR-22 containing 22 mol% epoxy group (ENR-22) and the HENR obtained after 8h of hydrogenation time were illustrated in Figure 5.23. The peak assignments were demonstrated in Table 5.17. As can be seen in Figure 5.23 (b), similar to hydrogenation of NR, the peak at 1664 cm^{-1} corresponding to C=C bond of ENR decreases significantly with the progress of the hydrogenation. The intensity band of the -CH₂- deformation at 1432 cm^{-1} increases with an increase of the reaction time. Moreover, the intensities of Raman bands between 3010 and 2850 cm^{-1} contributing to the aliphatic C-H and -CH₂- stretching modes increase as compared with the starting material.

The Raman band assigned to the C-O-C ring vibration of epoxide groups at 1248 cm^{-1} associated with a weak band at 836 cm^{-1} of ENR were disappeared during hydrogenation process. The bands at 1330 and 1152 cm^{-1} depicted as asymmetric and symmetric -C-SO₂-C- vibration modes, respectively, were detected after hydrogenation. The appearance of Raman band at 1592 cm^{-1} , attributing to the C=C stretching mode of aromatic ring, may confirm that the TSOH attaches the rubber backbone of ENR.



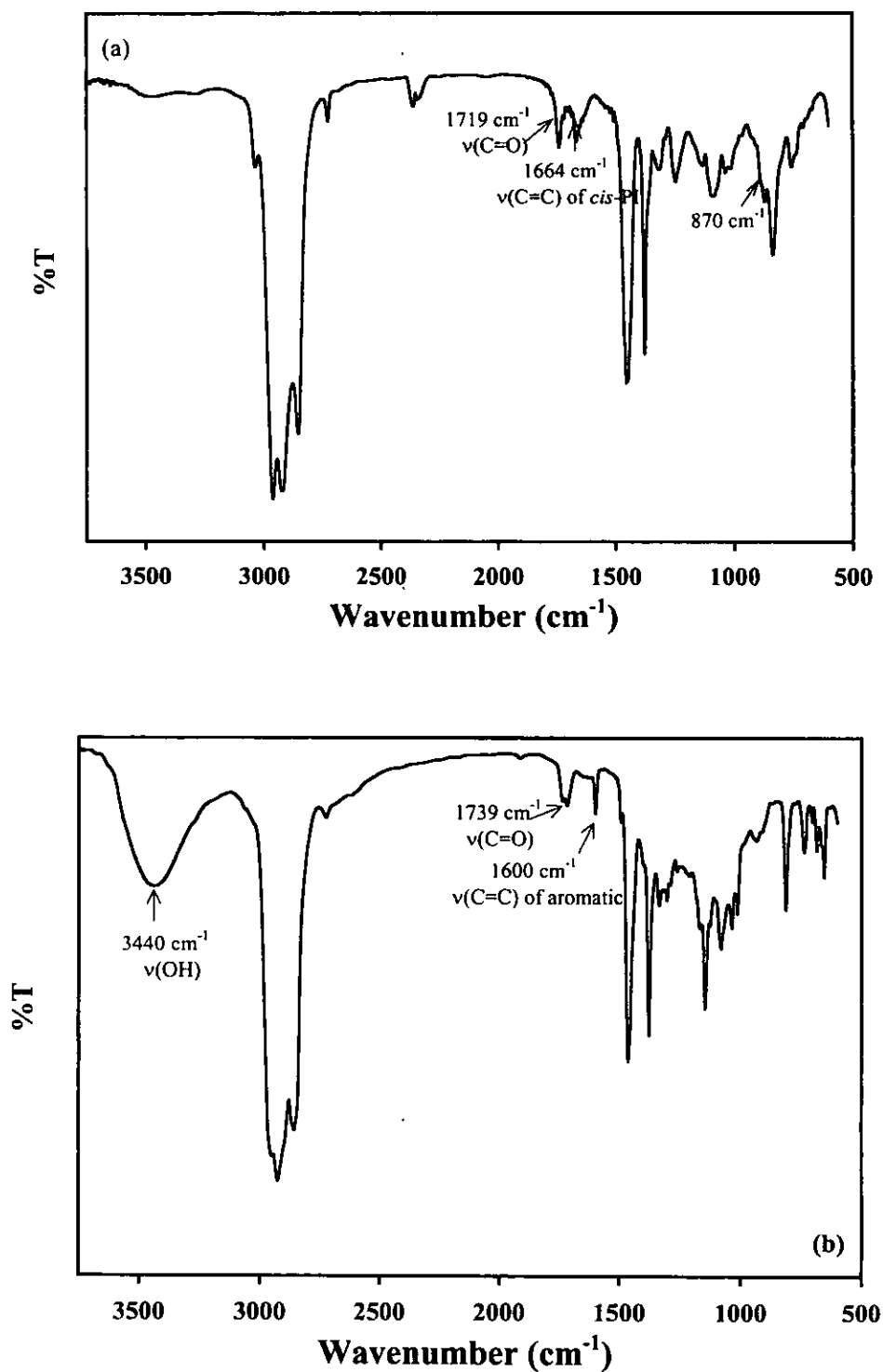


Figure 5.22 Infrared spectra of ENR-22 containing 22 mol% epoxy group (ENR-22) (a) and the hydrogenated ENR-22 after 8h (HENR-22(8)) reaction time (b).

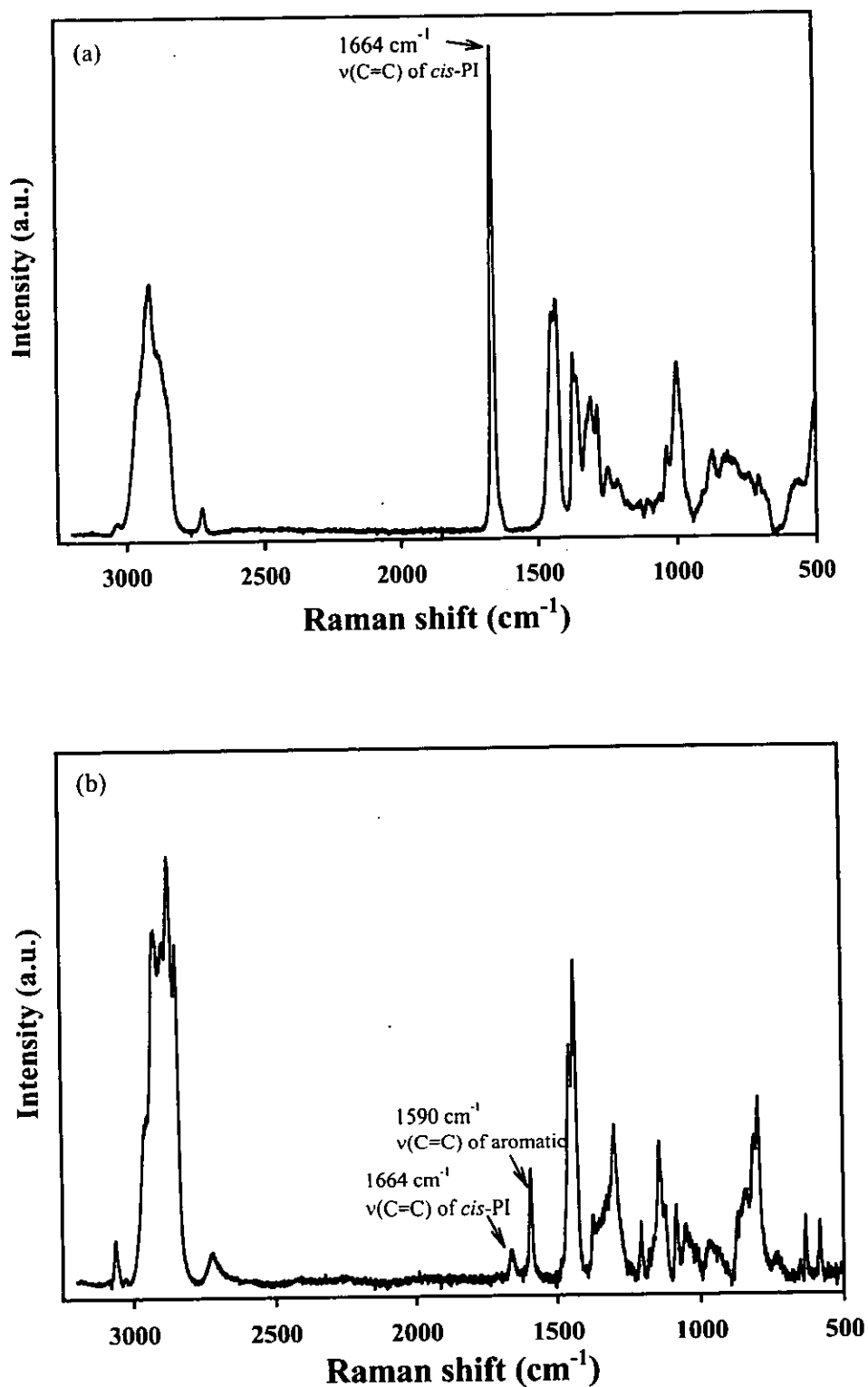


Figure 5.23 Raman spectra of ENR-22 containing 22 mol% epoxy group (ENR-22) (a) and the hydrogenated ENR-22 after 8h (HENR-22(8)) reaction time (b).

Table 5.16 The assignment of vibration modes of Infrared and Raman spectra of ENR and the hydrogenated ENR

Wavenumber (cm ⁻¹)					Description of assignments
Literatures [20, 38, 93,97]	Experimental (IR)		Experimental (Raman)		
	ENR	HENR	ENR	HENR	
a	b	3450	d	e	O-H stretching
a	3036(w)	3036(w)	3032(w)	3062(w)	-CH ₂ asymmetric stretching
a	b	c	2980(m)	e	CH ₃ symmetric and -CH ₂ stretching
2962	2963(vs)	2962(vs)	2961(vs)	2958(vs)	CH ₃ asymmetric stretching
2931	2927(vs)	2927(vs)	2938(vs)	e	f
2912	b	c	2911(vs)	2919(vs)	CH ₃ symmetric stretching
2885	b	c	2877(s)	2888(s)	CH ₃ symmetric stretching
2854	2857(s)	2858(s)	2842(s)	2843(s)	CH ₂ symmetric stretching
2727	2728(vw)	2726(vw)	2724(vw)	2721(vw)	CH aliphatic
a	b	1716(vw)	d	e	C=O symmetric stretching
1666	1665(w)	1665(vw)	1664(vs)	1664(w)	C=C stretching
a	b	1597(vw)	d	1590(m)	NH ₂ deformation; C=C stretching of aromatic ring
a	b	1492	d	e	-CH deformation of aromatic ring
1452	1451(s)	1462(s)	1452(m)	1454(m)	-CH ₂ deformation for IR -CH ₃ deformation for Raman
1440	b	c	1431(m)	1432(m)	CH ₃ deformation for IR -CH ₂ deformation for Raman
1375	1378(m)	1377(m)	1371(w)	1371(w)	-CH ₃ wagging
1363	b	c	1354(w)	e	-CH ₂ - wagging
1325	1323	1334	d	e	=CH deformation in plane
1311	b	c	1316(w)	e	-CH ₂ - twisting
a	b	1304	d	e	-SO ₂ -N stretching
1287	b	c	1288	e	-CH bending
a	b	1261	d	e	C-C stretching of aromatic
1243	1249	c	1248	e	Ring symmetric stretching

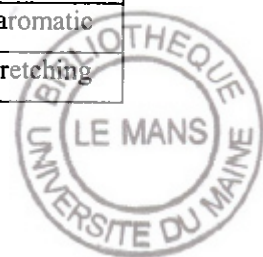


Table 5.16 (continued)

1208	b	c	1207	e	f
a	b	1145	d	e	N-N stretching
1040	b	c	1032	1050	CH ₂ rocking C(CH ₃)=CH
1000	b	c	996(m)	e	C-H out of plane of cis-
a	b	c	872(w)	e	CH bending of oxirane units
a	b	c	836(m)	e	=CH out of plane deformation of polyisoprene
820	b	812	811	e	CH ring wagging
a	b	c	785	e	Ring symmetric deformation
a	b	736(w)	d	e	Sequence of -(CH ₂) ₃ -

vw = very weak, w = weak, m = medium, s = strong, vs = very strong

a = no reported in literatures, b = no peaks of ENR in IR spectra, c = no peaks of HENR in IR spectra, d = no peaks of ENR in Raman spectra, e = no peaks of HENR in Raman spectra, and f = no proposed assignment

(b) Nuclear Magnetic Resonance Analysis

By ¹H and ¹³C-NMR Spectroscopy in Liquid State

¹H- and ¹³C-NMR spectra of ENR are illustrated in Figure 5.24, along with the assignment of resonance signals summarized in Table 5.17.

¹H-NMR spectrum of the ENR in Figure 5.24 (a) showed signals at 5.12 ppm (olefinic methine proton), 2.70 ppm (oxirane methine proton), 1.67 ppm (olefinic methyl proton), 1.30 ppm (oxirane methyl proton) and 2.05 ppm (methylene proton of isoprene unit) similar to those of NR. In all ENR samples obtained, no observation of signals at 3.40, 3.90 and 8.00 ppm, which might belong to secondary reactions of formation of diol and furan, as previously mentioned in the literature [8, 93]. The epoxidation level is generally calculated by comparing the signal of proton adjacent to C=C at 5.12 ppm and the signal of proton adjacent to oxirane ring at 2.70 ppm (as described in section 4.7.2).

The ¹³C-NMR spectrum of the ENR-22 (Figure 5.24 (b)) gives the characteristic of the methine carbon and quaternary carbon of oxirane ring at 64.5 and 60.5 ppm, respectively. The peaks at 126 and 135 ppm are the olefinic double bond carbons in the unmodified polyisoprene units.



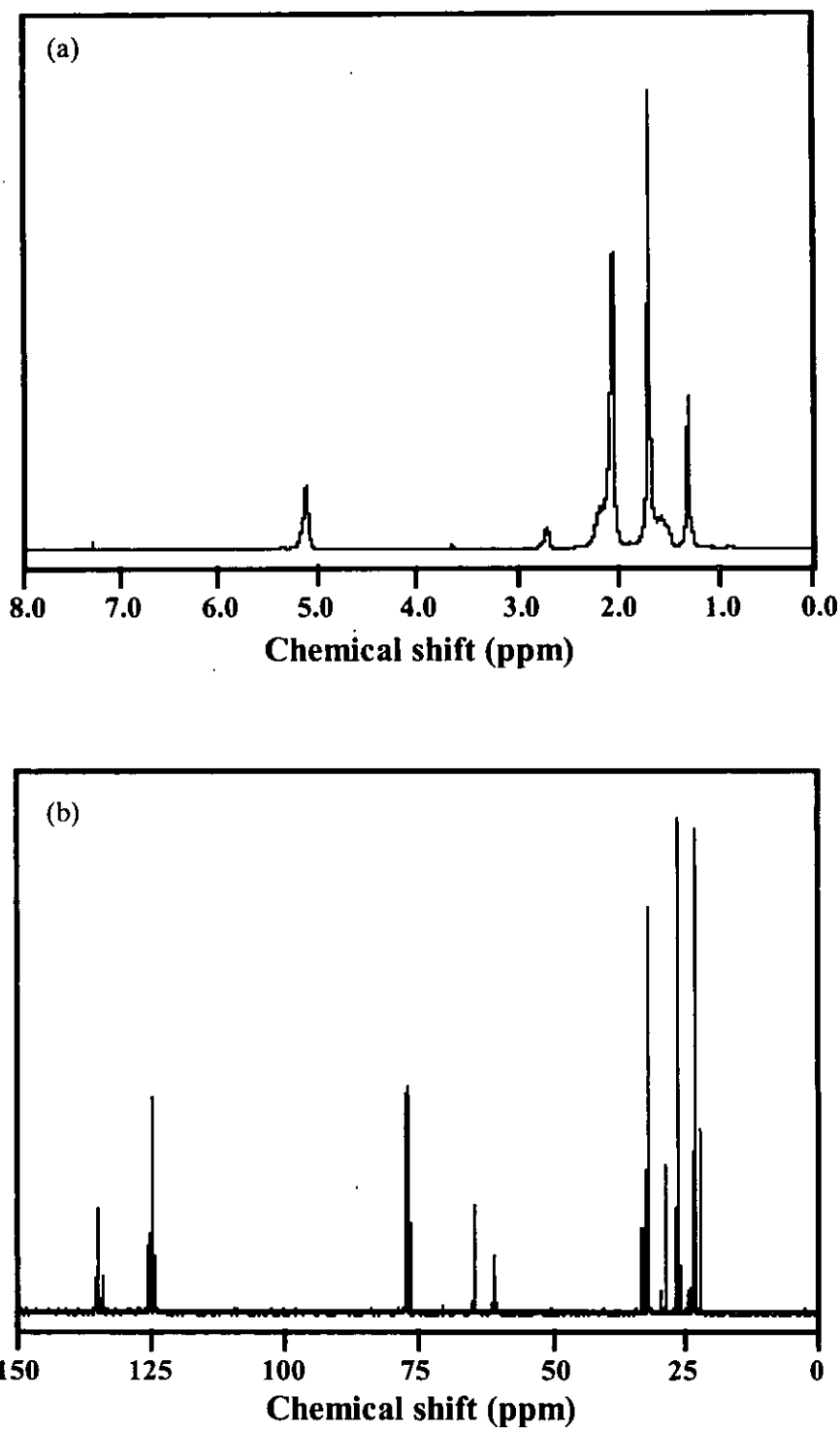


Figure 5.24 ^1H -NMR (a) and ^{13}C -NMR (b) of ENR-22 containing 22 mol% epoxy group.



Table 5.17 The assignment of ^1H - and ^{13}C -NMR resonances of the partially epoxidized NR

^1H -NMR analysis		^{13}C -NMR analysis	
Literatures [8, 93, 102]	Experimental	Literatures [8, 38, 93, 101]	Experimental
a = 1.68 (1,4-c)	a = 1.67	C-1 = 32.3 (1,4-c)	C-1 = 32.2
b = 2.05 (1,4-c)	b = 2.05	C-2 = 134.8 (1,4-c)	C-2 = 135.2
c = 5.12	c = 5.12	C-3 = 125.3 (1,4-c)	C-3 = 124.9
d = 1.35	d = 1.30	C-4 = 26.5 (1,4-c)	C-4 = 26.4
e = 2.68	e = 2.70	C-5 = 23.4 (1,4-c)	C-5 = 23.4
		C-6 = 60.8	C-6 = 60.5
		C-7 = 64.5	C-7 = 64.5
		C-8 = 33.3	C-8 = 33.4
		C-9 = 28.6	C-9 = 28.8
		C-10 = 22.2	C-10 = 22.3
		C-11 = 24.8	C-11 = 24.7
		C-12 = 125.7	C-12 = 125.6
		C-13 = 134.4	C-13 = 134.3
		C-14 = 27.1	C-14 = 27.0
		C-15 = 135.6	C-15 = 135.6
		C-16 = 124.4	C-16 = 124.4
		C-17 = 125.2	C-17 = 125.1
		C-18 = 134.4	C-18 = 134.6
		C-19 = 22.3	C-19 = 22.1
		C-20 = 29.7	C-20 = 29.6

The ^1H -NMR and ^{13}C -NMR spectra of HENR are displayed in Figure 5.25, and the peak assignments are given in Table 5.18. Figure 5.25 (a), shows the new signals at 0.84 ppm, which can be assigned to the methyl proton of the saturated unit and the signal at 1.1-1.3 ppm attributed to the methine and methylene protons of the saturated units. These signals tend to increase with reaction time. With the progress of hydrogenation, the integrated area of olefinic peak of HENR at 5.12 ppm decreases considerably compared with the starting rubber. Concurrently, proton signal peaks which can be assigned to methyl and methylene protons of saturated portion were found as similar in the case of HNR samples.

On the other hand, the signal at 2.70 ppm due to the methine proton of the epoxy unit disappears in all HENRs. The ^1H -NMR spectrum of the HENR revealed the presence of sulfur containing substitute in the HENR samples. The peak of *p*-tolyl in the polymer chains can be clearly seen at 2.35 and 7.70 ppm, corresponding to the proton signals of *p*-methyl and the aromatic ring of *p*-toluenesulfonic group [11, 48]. These characteristic peaks could not be eliminated by reprecipitating the HENR samples with non solvent. These signals are not observed in the case of NR. Hence, it is due to the fixation of *p*-tolyl onto the backbone chains of the HENR. In addition, it is also noted in Figure 5.25 (a) that the observation of extra signals in ^1H -NMR at 1.83, 3.40, and 3.87 ppm can be assigned to signals of a methylene proton of a large membered ring, a proton at the α -position of the hydroxyl group, and a methine proton, respectively [102].

Similar to HNR, the ^{13}C -NMR spectrum of HENR in Figure 5.25 (b) exhibited the signals at 37.8, 32.8, and 19.7 ppm. These results are assigned to the methine carbon of methyl and methylene respectively.



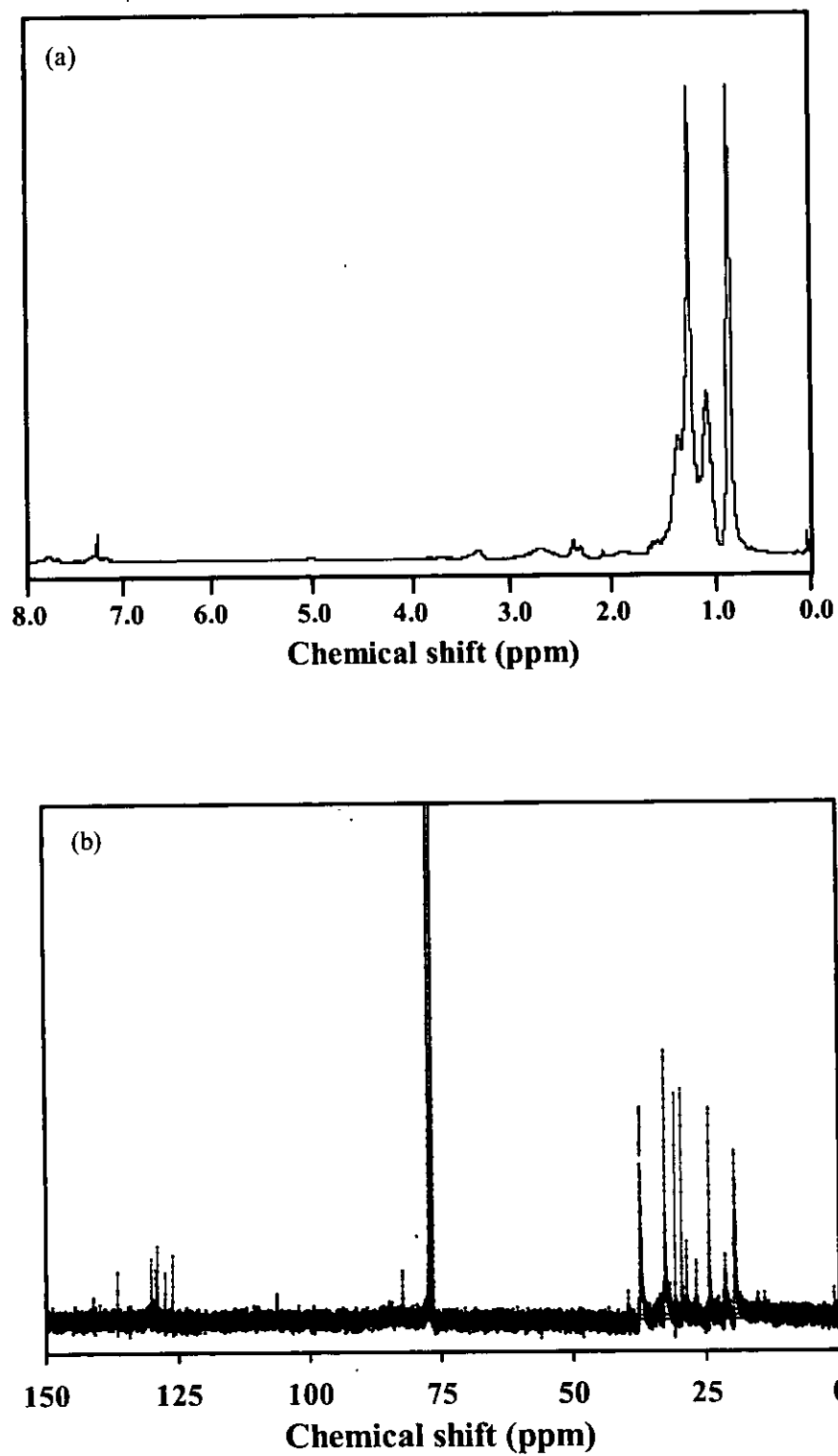


Figure 5.25 $^1\text{H-NMR}$ (a) and $^{13}\text{C-NMR}$ (b) spectra of the hydrogenated ENR-22 after 8h (HENR-22(8)) reaction time as analyzed in liquid state.

Table 5.18 The assignment of ¹H-NMR and ¹³C-NMR resonance of the hydrogenated ENR in liquid state

partially epoxidized NR

⇓ TSH

¹ H –NMR analysis		¹³ C-NMR analysis	
Literatures	Experimental	Literatures	Experimental
[19, 21, 99, 102]		[19, 99, 102]	
a = 0.77, 0.98	a = 0.84	C-1' = 37.1	C-1' = 37.5
b = 1.25 (m)	b, c, d = 1.25	C-2' = 33.3	C-2' = 32.8
	m = 1.18	C-3' = 37.9	C-3' = 37.5
	i, j = 1.83	C-4' = 24.9	C-4' = 24.5
	h = 2.35	C-5' = 19.7	C-5' = 19.7
	l = 3.40	-	C-6' = 29.7
	e = 3.78	C-7' = 97.5	C-7' = 97.6
	k = 3.91	-	C-8 = 106.3
	g = 7.15	C-12 = 84.5	C-9, C-12 = 82.3
	f = 7.65	C-10 = 26.9	C-10 = 26.9
		C-11 = 30.7	C-11 = 30.9
		C-13 = 72.4	-
		C-14 = 139.8	C-14 = 141.0
		C-15 = 129.7	C-15 = 129.3
		C-16 = 131.7	C-16 = 130.2
		C-17 = 149.2	-
		C-18 = 21.8	C-18 = 21.4



By ^{13}C -NMR Spectroscopy in Solid State

The confirmation of the change of microstructure characteristics of ENR after diimide hydrogenation was investigated by solid state ^{13}C -NMR with HD/MAS technique. This technique is a powerful method to characterize ENR and HENR samples as illustrated in Figure 5.26. The curve fitting by DM2002 was used to simulate the peak positions of ENR-22 spectrum as shown in Table 5.19. The ^{13}C -NMR spectrum also exhibits the peaks at 60 and 64 ppm, corresponding to the methine and quaternary carbons in the epoxide unit, respectively. The peaks at 126 and 135 ppm are the olefinic double bond carbons in the unmodified polyisoprene units. The results obtained from solid state NMR are consistent with liquid state NMR spectroscopy for the peak assignments.

In Figure 5.26 (b), the HD/MAS spectrum of the HENR-22 indicated the characteristic peaks at 38, 33, 25 and 20 ppm corresponding to the saturated units of the hydrogenated ENR. Moreover, the small peaks appearing in the region 75 and 84 ppm are assigned to the carbon resonance of methyl and two methylene carbons of furan ring, ether linkage carbons and carbons attached to hydroxy group. The solid state ^{13}C -NMR spectrum of the HENR-40 containing 40 mol% epoxy group also evidences the appearance of furan units after hydrogenation. These characteristic peaks are strong intense depending on the epoxidation level. In Figure 5.27, the comparison between the solid state NMR spectra of HENR-22 and HENR-40 obtained from 8 h of hydrogenation time was obviously found that the more intense peaks in the region 75 and 84 ppm assigned to carbon signals of furan ring and the carbon of aromatic ring appeared at 120-150 ppm can be detected in the case of high epoxide content.



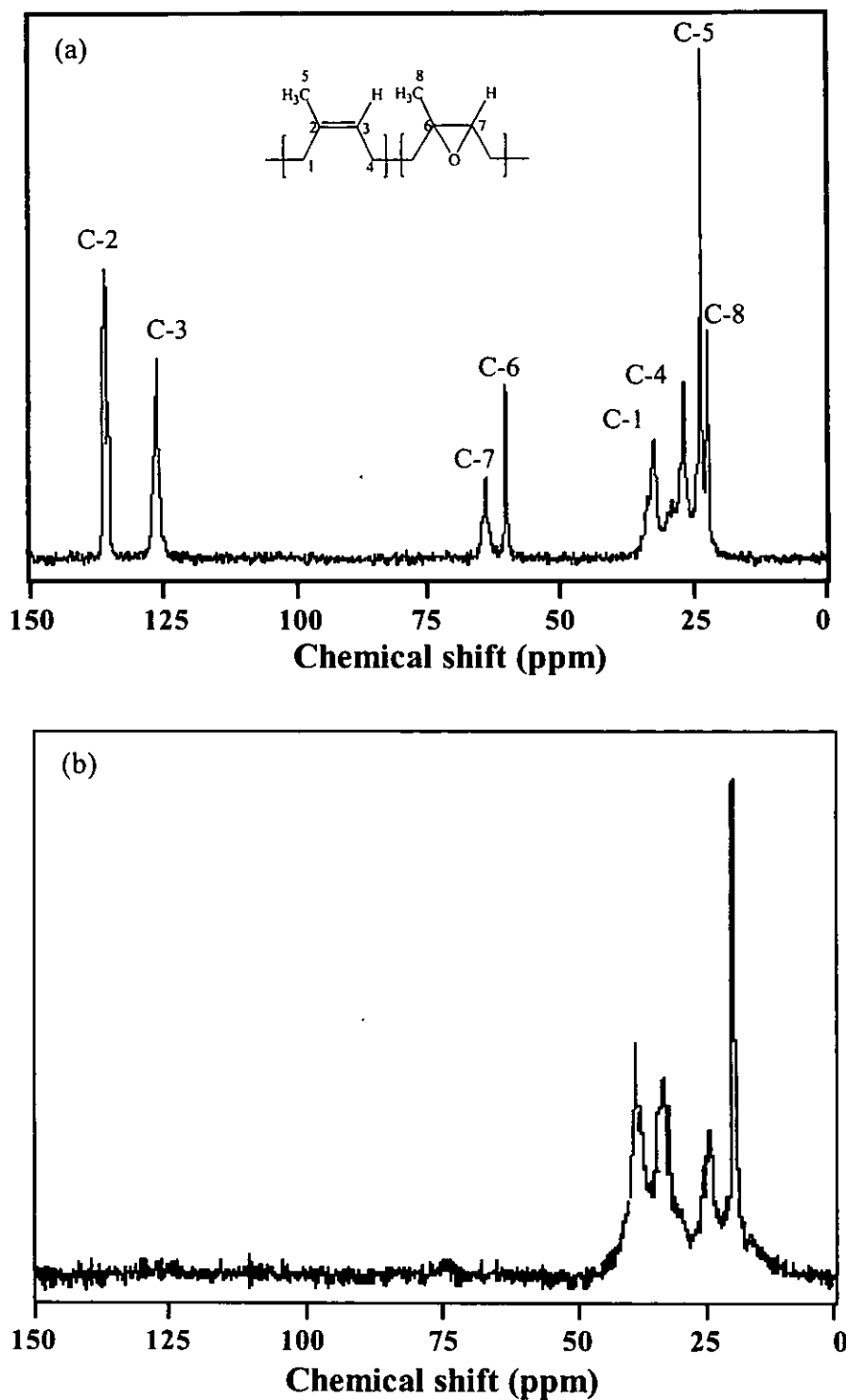


Figure 5.26 HD/MAS ¹³C-NMR spectra of ENR-22 containing 22 mol% epoxy content (a) and HENR-22(8) taken at 8h.



Table 5.19 The assignment of chemical shift of ENR and HENR spectra of HD/MAS technique in solid state

partially epoxidized NR

↓ TSH

X' = SO_2 -14 -18 CH₃

¹³ C-NMR analysis of ENR-22		¹³ C-NMR analysis of HENR-22	
Chemical shift (ppm)	Assignment	Chemical shift (ppm)	Assignment
32.8	C-1	20	C-5'
134.7	C-2	25	C-4'
125.7	C-3	33	C-2'
27	C-4	38	C-1',C-3'
24	C-5	75	C-13
60.3	C-6	84	C-12
64	C-7	130	C-15, C-16
23	C-8	150	C-14, C-17

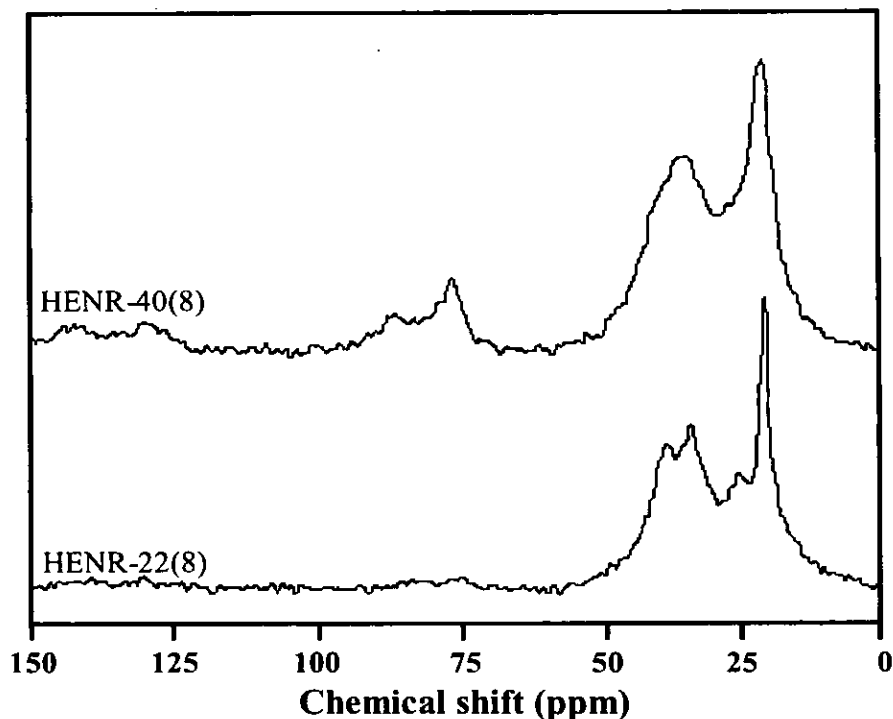


Figure 5.27 Stack plots of HD/MAS/CP ¹³C-NMR spectra of HENR-22(8) and HENR-40(8) containing 22 and 40 mol% epoxy content.

5.3.2 Evaluation of Percent Hydrogenation of ENR

The change in the chemical structure of ENRs after hydrogenation reaction can be quantified using Raman and ¹H-NMR spectroscopies.

The Raman spectra of the hydrogenated ENR-22 containing 22mol% epoxy group at various reaction times are illustrated in Figure 5.28. A progress of the hydrogenation in ENR can be determined from the decrease in the area of C=C band at 1664 cm⁻¹ as compared to that of an original material. As can be seen in Figure 5.28, a significant decrease of double bond content is observed with increasing the reaction time. The percent hydrogenation can be determined by comparing between the Raman band of the C=C double bond and the methylene band as described in section 4.7.3.

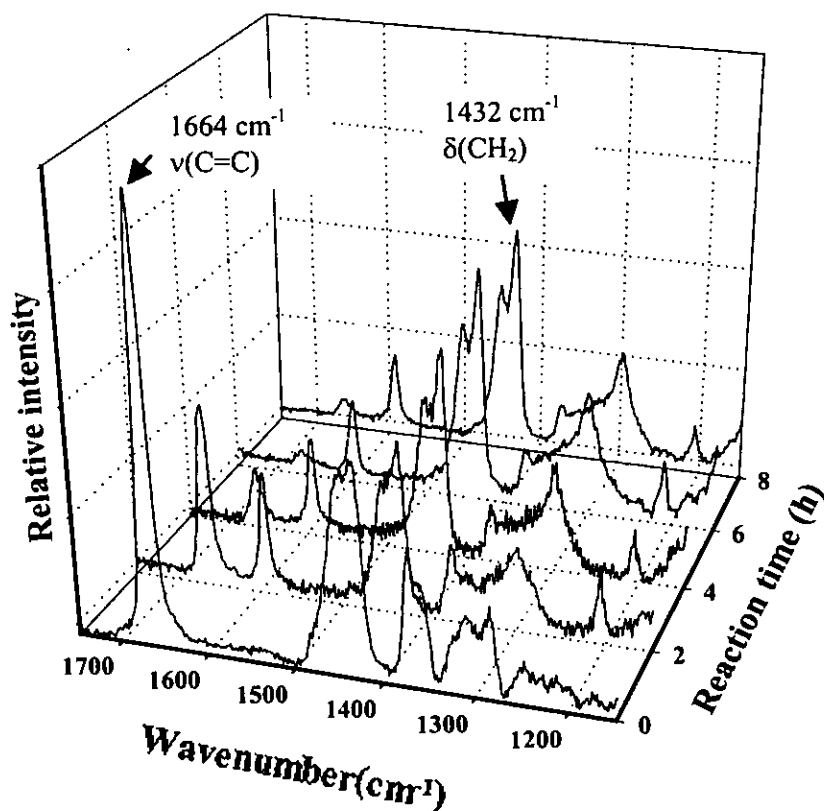


Figure 5.28 Comparison between the Raman spectra of ENR-22 containing 22% epoxide content and the hydrogenated ENR samples taken at various reaction times.

The obtained ¹H-NMR spectra of hydrogenation of ENR-22 at various reaction times are also shown in Figure 5.29. It should be emphasized that as longer reaction time employed, the peak intensity of the olefinic proton at 5.12 is significantly decreased as compared with that of starting material. This result is in agreement with all of our experiments observed in a higher amount of epoxide content of ENRs.

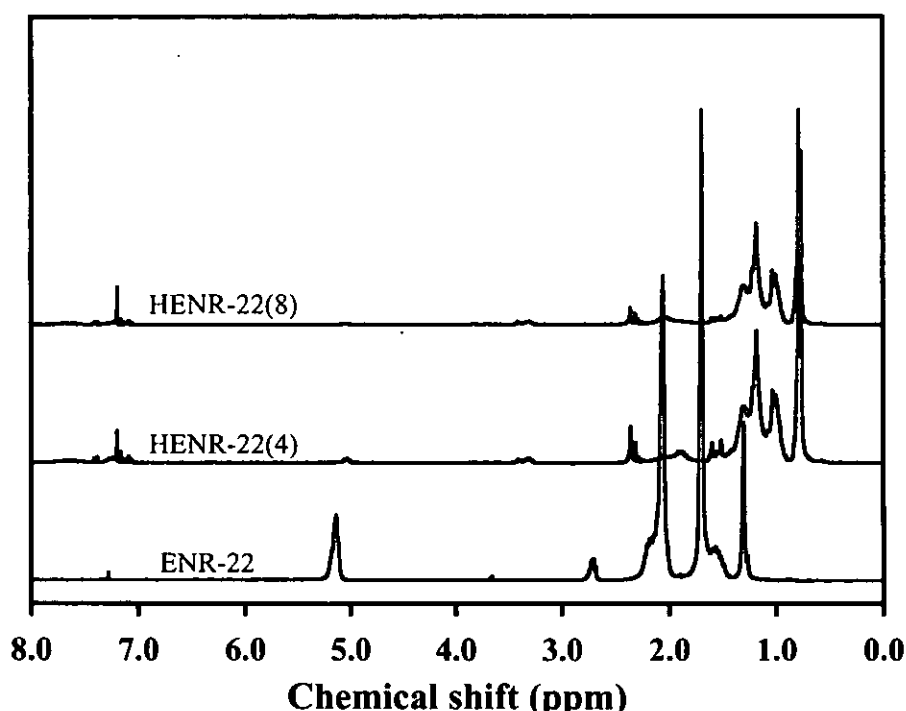


Figure 5.29 ^1H -NMR spectra of epoxidized NR containing 22% epoxide content (ENR-22) and hydrogenated ENR samples taken at 4h (HENR-22(4)) and 8h (HENR-22(8)).

The results of hydrogenation of the four types of ENR at various reaction times are shown in Table 5.20 and Figure 5.30. It was found that the percentage of hydrogenation increases with the increasing of reaction time. The maximum percent hydrogenation of ENR-10, ENR-22, ENR-30 and ENR-40 as determined by Raman technique is found to be about 93-96%, while by ^1H -NMR technique, the %hydrogenation is around 96-100. As can be seen in Figure 5.30, it can be observed that the hydrogenation of ENR is very fast at the early stage of the reaction. It seems likely that the rate of hydrogenation increases with increasing epoxide levels and much faster than that of NR. These results are in contrast to the work reported by Bhattacharjee et. al. [20] using a homogeneous palladium acetate catalyst for hydrogenation of ENR. In their case, they explained that the presence of the epoxide group might coordinate with the metal center, which competes with the coordination of the metalhydride complex with the carbon-carbon double bond of the rubbers.

hence decreasing the rate of hydrogenation when the amount of the epoxide group increased. But in our case, the diimide generated from the decomposition of TSH can react directly with the double bond of the polyisoprenic unit, which is preferably at the *cis* structure. In the case of NR, there was *cis-trans* isomerization, which might be due to the formation of an unstable complex between the double bond and *p*-toluenesulfonic acid by-product. But in the case of ENR, the formation of the epoxide ring-opened product and the addition of *p*-toluenesulfonic acid on the rubber chain were found, which is discussed former in this section. Therefore, by increasing the epoxide content, the possibility that the *p*-toluenesulfonic acid encounters the epoxide unit increases, resulting in a decrease in the interference at the double bond of the rubber chains, therefore the hydrogenation reaction of ENR is much faster than that of NR. It was found that the signal of the proton at 5.12 ppm almost disappears at 6h reaction time in all cases of ENR. It may be postulated that the degree of hydrogenation is about 100% at this duration.

Table 5.20 The percent hydrogenation of ENRs at various reaction times as determined by Raman and ¹H-NMR techniques

Reaction time (h)	Hydrogenation (%)							
	ENR-10		ENR-22		ENR-30		ENR-40	
	Raman	¹ H-NMR	Raman	¹ H-NMR	Raman	¹ H-NMR	Raman	¹ H-NMR
0	0	0	0	0	0	0	0	0
0.5	35.0	41.0	n	n	34.6	39.3	n	n
1	n	n	n	n	41.0	65.0	n	n
2	70.0	75.2	43.0	71.3	67.0	78.5	84.9	89.0
4	84.6	93.0	86.5	92.9	82.0	96.0	94.5	95.9
6	92.0	95.0	95.9	96.2	96.0	98.5	94.2	98.3
8	93.0	96.0	93.9	97.7	95.0	99.7	95.8	99.3

n = not determine



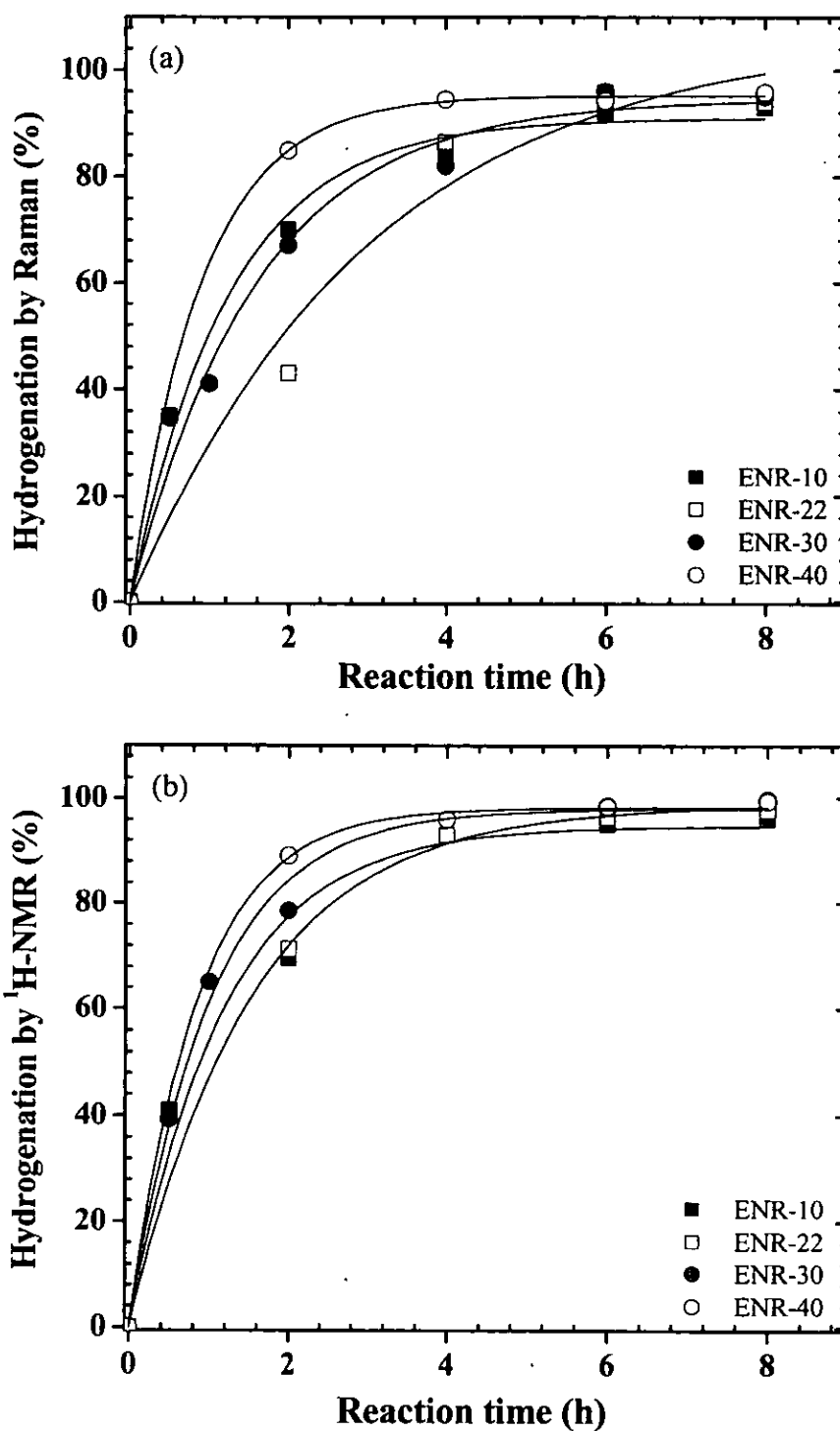


Figure 5.30 %Hydrogenation of epoxidized natural rubber containing 10, 22, 30 and 40 % epoxy content at various reaction times as determined by Raman (a) and ¹H-NMR (b).



5.3.3 Side Reactions

The diimide hydrogenation of ENR in solution system was performed using TSH at 135°C. This condition may cause the presence of side reaction during reaction as follows.

(a) *Cis-trans* Isomerization

As mentioned before in section 5.2.3, the *cis-trans* isomerization occurred during hydrogenation of NR by TSH at 135°C. In the case of HENR, the evidence of a small signal of *trans* configuration was found at 1.60 ppm as detected by ¹H-NMR in liquid state. This result indicated that the transformation of *cis* to *trans* units was also occurred but a very small extent. This may be due to the TSOH acid by-product could not play a perfect role for *cis-trans* isomerization as it reacts with the epoxide group of the ENR as detected and mentioned earlier.

(b) Degradation Reaction

Similar to the result of chain degradation in the case of hydrogenation of NR by TSH are obtained. It was found that the hydrogenated ENR products obtained from diimide hydrogenation were brown solid. According to the results in our experiments that increasing the reaction times, the increase of carbonyl and hydroxyl signals was observed. In addition, at prolonged reaction time, the degradation seemed to be slow down while the intensity of the carbonyl signal of the modified rubber did not increase. It could be therefore postulated that the TSOH had oxidized the double bond of the ENR then partially cleaved, resulting in chain degradation forming aldehyde and carboxylic functional ends which was evidenced by the appearance of hydroxyl and carbonyl signals in IR spectrum.

(c) Addition of TSOH and Furanization Reaction

The incorporation of TSOH by product on the HENR was observed by both the vibrational and resonance spectroscopies. In a Raman spectrum of the HENR, the bands at 1331 and 1152 cm⁻¹ were detected and assigned to asymmetric and symmetric -C-SO₂-C vibrations, respectively. In a ¹H-NMR spectrum, a resonance of ¹H-NMR due to the *p*-toluene substituent is clearly present at 2.4 ppm for the paramethyl and at



7.70 ppm from the aryl ring protons [11, 48, 53]. In addition, the signals of the HENR observed both in the NMR spectroscopy as mentioned in section 5.3.2 showed the evidence of a large membered ring and the methine group adjacent to hydroxyl group. It may be noted that the side reaction occurs during hydrogenation process of ENR. The literature mentioned [7] that the major problems encountered in chemical modification of ENR are the cyclization of polyisoprene, furanization of epoxy unit and degradation caused the ring opening of epoxy groups. In this case, the epoxide ring-opened product may occur by the influence of *p*-toluenesulfonic acid by-product, followed by the furanization process as schematized in Figure 5.31. The epoxide ring is protonated, followed by the formation of the ring-opened product containing carbocationic intermediate. The epoxide ring at the adjacent unit then reacts with the carbocationic site, forming a furan unit. Propagation of furanization then proceeds with the other epoxide groups. A termination reaction can then occur by the fixation of the *p*-toluenesulfinate anionic group, resulting in the fixation of *p*-toluenesulfonic acid by-product onto the rubber chain. The formation of secondary epoxide ring-opened product so called furanization also occurred on the preparation of epoxidized natural rubber when high concentrations of peroxyacid and elevated temperature were employed [103].



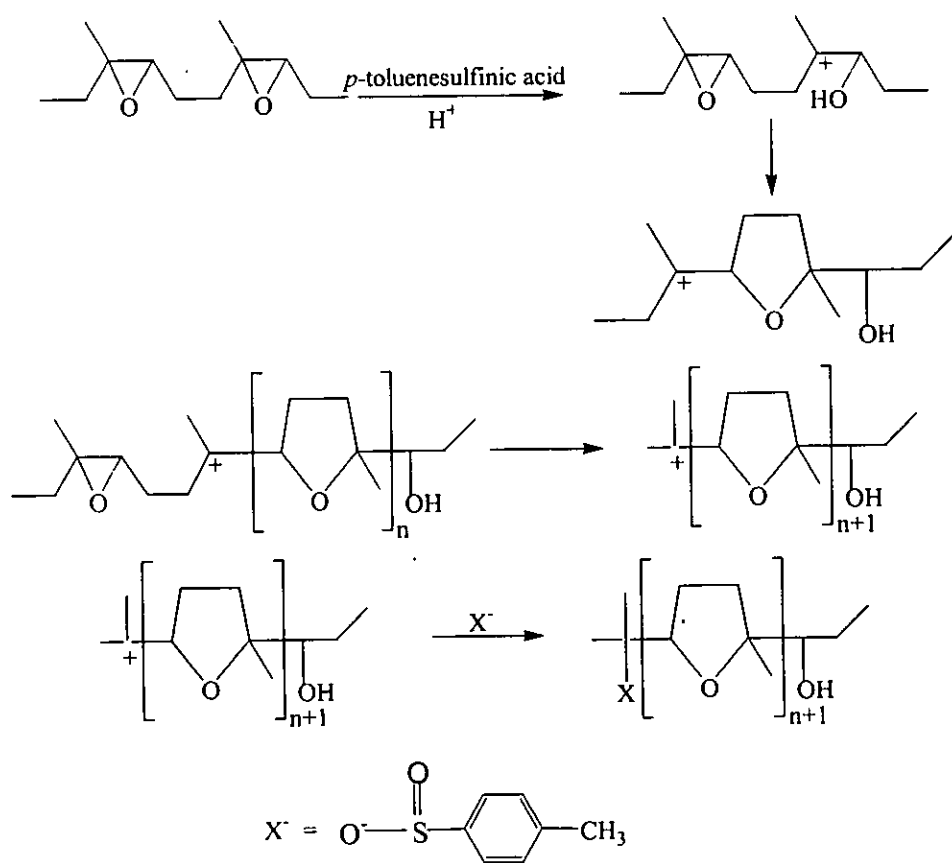


Figure 5.31 Schematic of furanization reaction of partial epoxidized polyisoprene after hydrogenation by TSH [103].

Part II: Hydrogenation by Hydrazine and Hydrogen Peroxide

It has been shown in part I that TSH is an effective reagent for hydrogenation of NR and ENRs, resulting in desired amount of hydrogenated units on the molecular chain. However, this method needs to be carried out in organic solvent and the TSH is rather expensive. Hydrogenation of natural rubber in the original latex form is of interest as the resulting product may be applied directly in this form. Diimide molecule that can be generated in aqueous media has to be considered. It has been reported that oxidation of hydrazine results in formation of diimide that has been successfully used to hydrogenate polydiene such as nitrile rubber latex and styrene-butadiene latex [54-59]. Generally, various oxidizing agents could be employed for the oxidation reaction of hydrazine such as HNO_3 , KMnO_4 , and H_2O_2 . In the case of hydrogenation of rubber latex, H_2O_2 was an important oxidant which can oxidize the hydrazine into diimide molecule in aqueous medium.

In this part, hydrogenation of NR latex with diimide molecule generated *in situ* from the oxidation of hydrazine (N_2H_4) by hydrogen peroxide (H_2O_2) has been investigated. First, the hydrogenation of synthetic polyisoprene (PI) latex was studied, and then diimide reduction of NR latex was followed, including the investigation of parameters affecting the degree of hydrogenation. The characterizations of the resulting products were carried out by spectroscopic methods i.e. ^1H - and ^{13}C -NMR spectroscopy.

5.4 Hydrogenation of Synthetic Polyisoprene Latex

In this present section, the diimide reduction process of synthetic polyisoprene (PI) in latex stage has been attempted to prepare the hydrogenated PI by using $\text{N}_2\text{H}_4/\text{H}_2\text{O}_2$ redox system in aqueous medium. It has been reported in the literature that hydrogenation of styrene-butadiene rubber latex was occurred by using $\text{N}_2\text{H}_4/\text{H}_2\text{O}_2$ in the presence of $\text{CuSO}_4 \cdot 5\text{H}_2\text{O}$. Therefore, the hydrogenation of PI latex was attempted by using 1:1:1 mole ratio of $[\text{C}=\text{C}]:[\text{N}_2\text{H}_4]:[\text{H}_2\text{O}_2]$ in the presence of $\text{CuSO}_4 \cdot 5\text{H}_2\text{O}$ at 45°C . FT-IR and ^1H -NMR analysis were used to analyze the resulting product at various reaction times.



5.4.1 Evidence of Diimide Hydrogenation of Polyisoprene

(a) FT-IR Analysis

Figure 5.32 shows the FT-IR spectra of synthetic PI and hydrogenated PI latex carried out at 24h. The spectrum of synthetic PI exhibited two main characteristic absorption peaks at 1665 and 1644 cm^{-1} corresponding to the C=C stretching mode of 1,4- and 3,4- polyisoprene, respectively. The deformation modes of methyl and methylene groups of PI were observed at 1448 and 1376 cm^{-1} , respectively. The absorption peaks at 1329 and 1312 cm^{-1} are the characteristics of =C-H deformation of *trans*-1,4 and *cis*-1,4 PI structures. Other vibrational frequencies of the synthetic PI found at 888 and 837 cm^{-1} belong to the =C-H deformation of 3,4-PI and 1,4-PI, respectively.

In Figure 5.32 (b), the intensity of $\nu(\text{C}=\text{C})$ modes of synthetic-PI at 1665 and 1644 cm^{-1} slightly decreased after hydrogenation. The intensity absorption peak of $\nu(\text{C}=\text{C})$ mode at 1644 cm^{-1} belonging to 3,4 PI was also found decreasing. The small intensity of extra peak located at 723 cm^{-1} might be due to the characteristic of $-(\text{CH}_2)-$ group. An unexpected small absorption peak was appeared at 3440 cm^{-1} , which can be assigned to the hydroxyl characteristic.



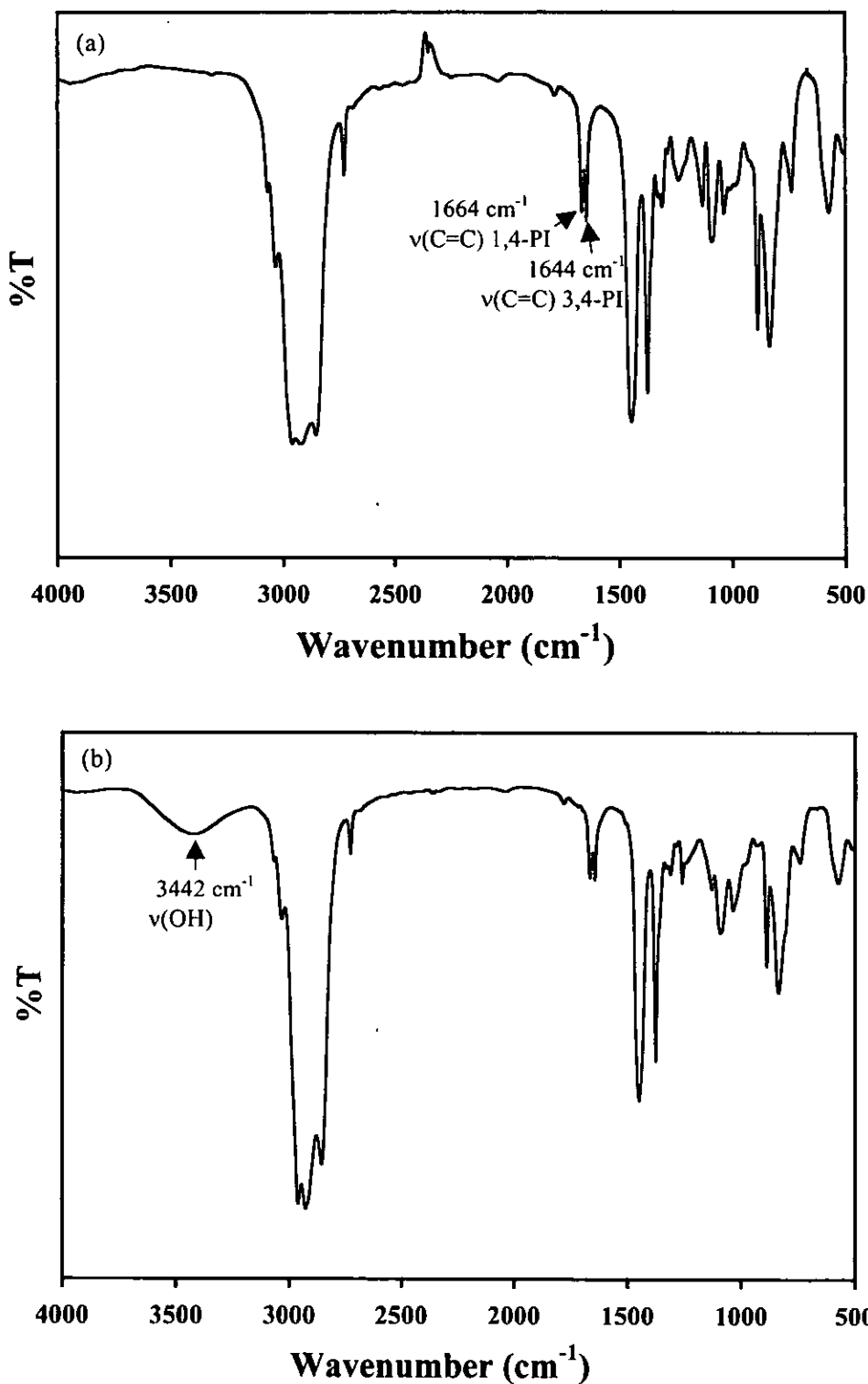


Figure 5.32 FT-IR spectra of synthetic polyisoprene (PI) (a) and hydrogenated PI (b) prepared by using 10% dry rubber content, molar ratio of $[\text{C}=\text{C}]=[\text{N}_2\text{H}_4]=[\text{H}_2\text{O}_2] = 1$ at 45°C for 24h.



(b) $^1\text{H-NMR}$ analysis

The characteristic peaks found in $^1\text{H-NMR}$ spectrum (Figure 5.33) of synthetic PI can be assigned that the signals at 5.1 ppm and 4.75 ppm are of the protons at double bonds of 1,4-PI and 3,4-PI, respectively. The amount of 1,4-PI and 3,4-PI presented in PI structure can usually be calculated from the integrated peak area ratio of these two signals by Equations 5.7 and 5.8 below.

$$\%1,4\text{-PI} = \left(\frac{2A_{5.1}}{2A_{5.1} + A_{4.75}} \right) \times 100 \quad (5.7)$$

$$\%3,4\text{-PI} = \left(\frac{A_{4.75}}{2A_{5.1} + A_{4.75}} \right) \times 100 \quad (5.8)$$

Where $A_{5.1}$ and $A_{4.75}$ are the integrated peak areas of proton signals attached to the C=C of 1,4-PI at $\delta = 5.1$ ppm and of 3,4-PI at $\delta = 4.75$ ppm, respectively. The characteristics of methyl protons of *cis*-1,4 and *trans*-1,4 PI are different from that of 3,4-PI by $^1\text{H-NMR}$ analysis. The signals of methyl proton adjacent to C=C of *cis*-1,4 PI and *trans*-1,4 PI are found located at 1.68 and 1.60 ppm, respectively. While the signal in $^1\text{H-NMR}$ found at 1.64 ppm can be assigned to the methyl proton adjacent to the C=C of 3,4-PI.

After hydrogenation, the proton signals at 5.10 and 4.75 ppm of starting PI were decreased as shown in Figure 5.33. It was also found a new characteristic proton signal at 0.84 ppm, assigned to the methyl proton of saturated units of hydrogenated PI (HPI). Moreover, a small proton signal at 3.42-3.81 ppm corresponding to the characteristic proton of carbon attached to hydroxyl group was found after hydrogenation. It can be noted that the C=C of 3,4-PI was not totally hydrogenated in the condition used.



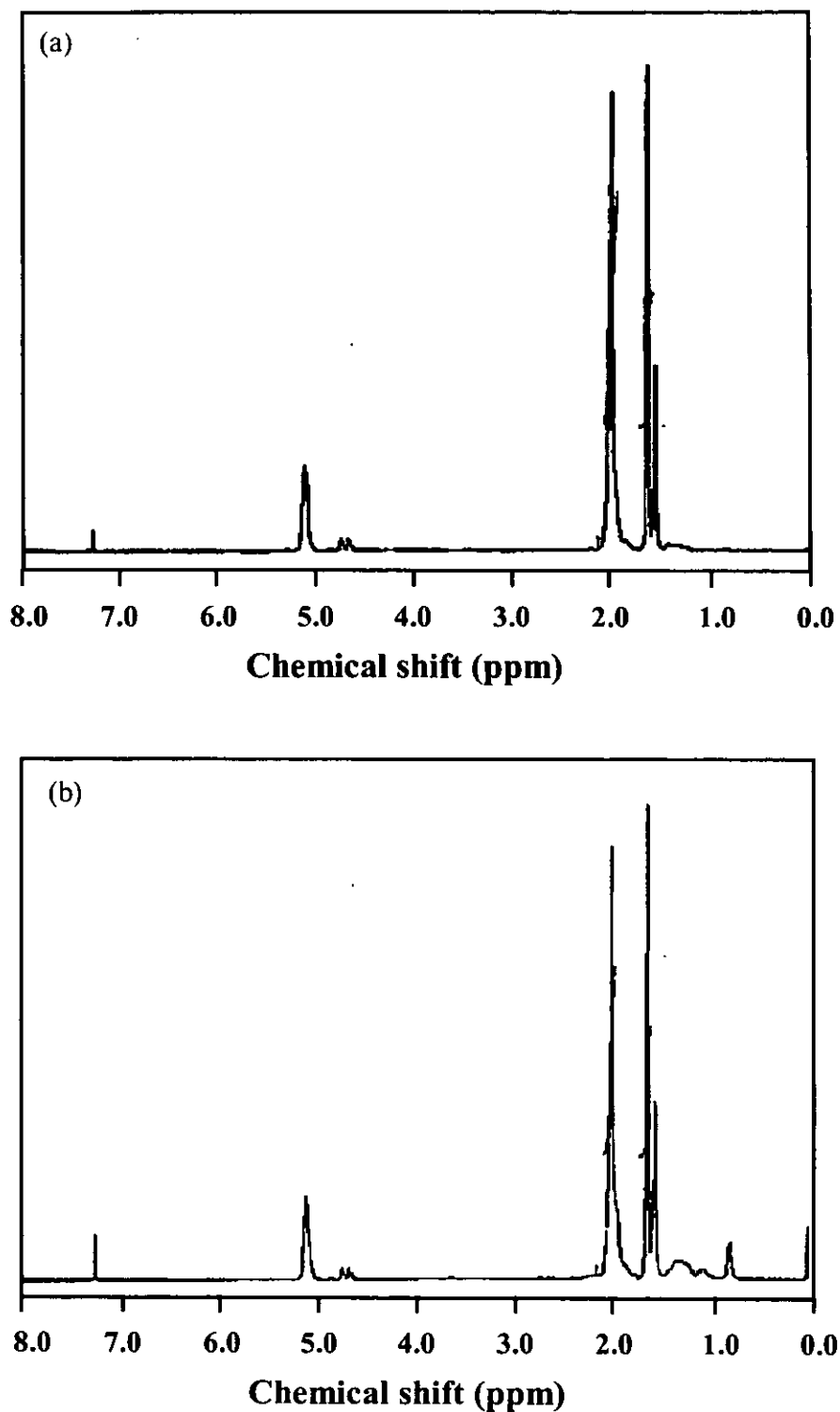


Figure 5.33 ^1H -NMR spectra of synthetic polyisoprene (PI) (a) and hydrogenated PI (b) prepared by using 10% dry rubber content, molar ratio of $[\text{C}=\text{C}]:[\text{N}_2\text{H}_4]:[\text{H}_2\text{O}_2] = 1:1:1$ at 45°C for 24h.



5.4.2 Percentage of Hydrogenation and Microstructures

The percent hydrogenation and microstructures (1,4-PI and 3,4-PI) of partially hydrogenated products were analyzed using $^1\text{H-NMR}$ spectroscopy. The results are shown in Table 5.21 and Figure 5.34. The % hydrogenation can be calculated from $^1\text{H-NMR}$ by comparing the integrated signal areas of methyl proton of saturated part of HPI at 0.84 ppm with the integrated area of proton adjacent to the $\text{C}=\text{C}$ of polyisoprene units at 5.12 and 4.75 ppm before and after hydrogenation using Equation 4.11 described in section 4.7. It is shown in Table 5.21 that the percentage of hydrogenation was gradually increased when the reaction time was increased. It was found that after 10h of reaction, the percent hydrogenation reached 23% and no further increase of hydrogenation degree was obtained even though longer reaction time was carried out upto 24h. The maximum percentage of hydrogenation approximately 23% was obtained when 1 molar ratio of $[\text{N}_2\text{H}_4]/[\text{isoprene units}]$ was used in the presence of 1mole of $[\text{H}_2\text{O}_2]$. It can be noted in Figure 5.34 that the $\text{C}=\text{C}$ of 3,4 PI was hydrogenated faster than 1,4-PI at early stage of reaction time (2h), then become slightly increasing. It was reported that the diimide generated from N_2H_4 and H_2O_2 exhibited two isomers of diimide i.e. *syn* and *anti* forms [55]. Only the *syn* form can react with the $\text{C}=\text{C}$ bonds of PI. It can be assumed that quantitative hydrogenation could not be achieved because of the loss of the active diimide. The 1,4-PI has more steric effect than the 3,4-PI so slower rate of hydrogenation of 1,4-PI than 3,4-PI was obtained. The diimide hydrogenation at side chain double bond of PI is easier than at the position of 1,4-PI [50, 51]. In addition, the diimide may undergo disproportionation reaction, giving nitrogen molecule and hydrazine so it is not possible to achieve 100% hydrogenation by using equal amount of hydrazine to concentration of unsaturated unit. However, it was reported in several publications that maximum hydrogenation of approximately 85-90% was obtained when varying from 1.0-2.0 molar ratio of $[\text{N}_2\text{H}_4]:[\text{butadiene units}]$ [54-56]. Therefore several parameters might affect on the hydrogenation of PI, which have to be investigated such as the rubber particle size, amount of reagents, reaction time and temperature.



Table 5.21 The amount of hydrogenation content, residual 1,4-PI and 3,4-PI determined by ¹H-NMR

Reaction time (h)	Microstructures		
	Hydrogenation (%)	1,4-PI (%)	3,4-PI (%)
0	0	82.1	17.9
2	11.8	78.3	9.9
10	22.6	68.9	8.5
14	22.6	69.2	8.2
24	22.9	69.1	8.0

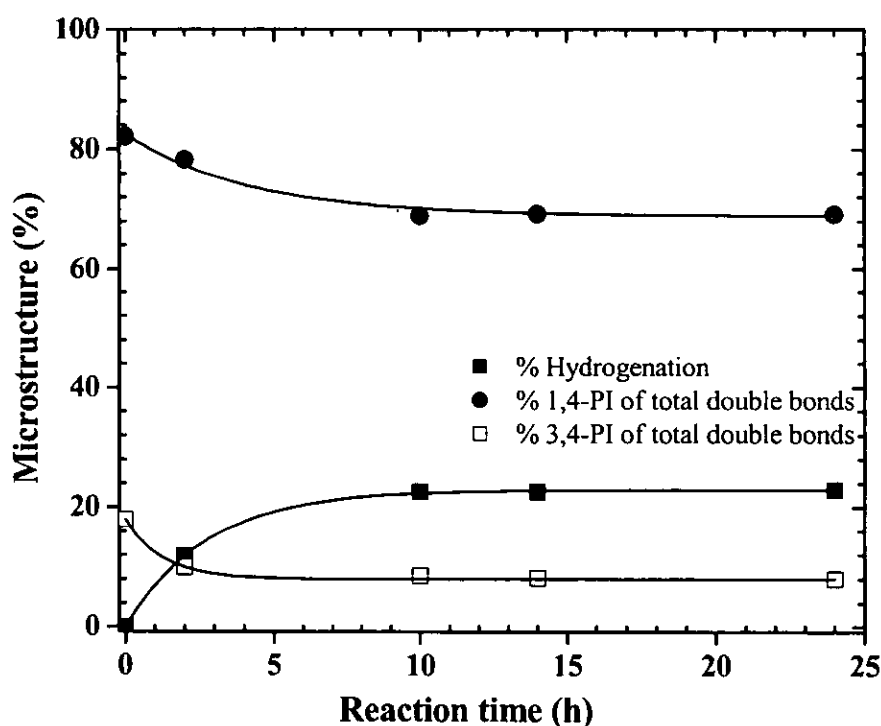


Figure 5.34 Percent hydrogenation of synthetic PI and microstructures versus reaction times prepared by using 10% dry rubber content with the molar ratio of $[C=C]:[N_2H_4]:[H_2O_2] = 1:1:1$ at 45°C.



5.4.3 Proposed Reaction Mechanism

The mechanism of diimide hydrogenation of the double bonds of synthetic rubber latex has been established [54-58]. The diimide hydrogenation reaction is realized by two steps: (1) the reaction between hydrazine and hydrogen peroxide to produce diimide and (2) the reaction between diimide and carbon-carbon double bonds to form the hydrogenated product, as shown in Figures 5.35 and 5.36 for 1,4-PI and 3,4-PI, respectively.

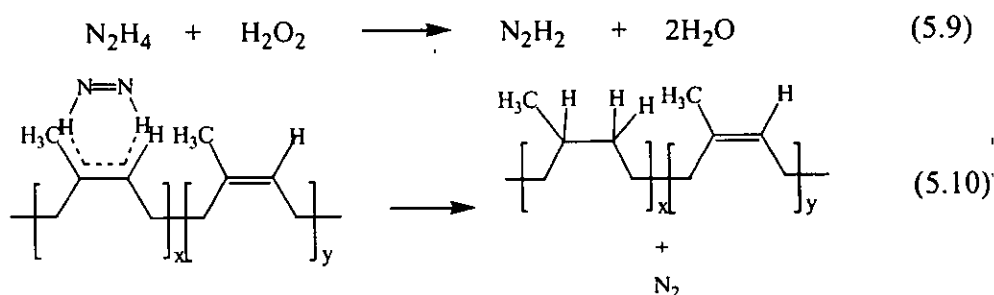


Figure 5.35 Proposed mechanism of diimide reduction of NR in latex phase using $\text{N}_2\text{H}_2/\text{H}_2\text{O}_2$.

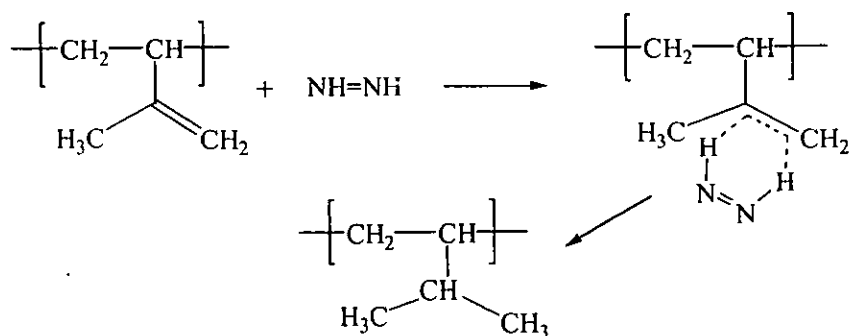
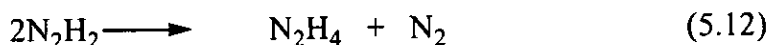
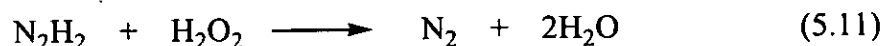


Figure 5.36 Diimide reduction of 3,4-PI units of synthetic PI.

However, 100% hydrogenation could not be achieved according to the reactivity of diimide itself. The diimide formed can react with hydrogen peroxide in the system, giving nitrogen and water. Another reaction is the interaction between two diimide molecules to form one hydrazine molecule and one nitrogen molecule.



5.4.4 Side Reaction

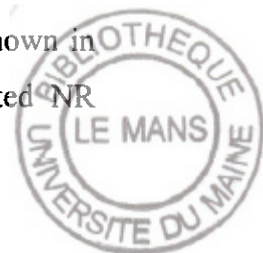
It was reported in the case of SBR that two possible side reactions can be occurred in diimide reduction i.e., crosslinking and cyclization reactions [54-57]. In our case, it was found that the results of spectroscopic method exhibited the signal of hydroxyl group, which might be caused by the chain scission of polyisoprene units forming aldehyde or carboxylic group. It may be postulated that the presence of H_2O_2 and $\text{CuSO}_4 \cdot 5\text{H}_2\text{O}$ caused the degradation reaction. Similar results were obtained when NR was depolymerized in the redox system, which present H_2O_2 and transition metal oxide as studied by Nor Mohd and Ebdon [104].

5.5 Hydrogenation of NR in Latex Form

Although, diimide reduction process of synthetic rubber latex had been progressively reported in the literatures [54-59], no attempt has been done to reduce the carbon-carbon double bonds of NR in latex. In this study, the diimide reduction of NR latex was investigated by using the oxidation reaction of hydrazine (N_2H_4) with hydrogen peroxide (H_2O_2) with and without copper sulfate pentahydrate ($\text{CuSO}_4 \cdot 5\text{H}_2\text{O}$). Various parameters affecting the degree of hydrogenation were also investigated such as reaction time and temperature, amount of reagents etc.

5.5.1 Evidence of Hydrogenation of NR

First, hydrogenation of NR latex was carried out by using 1:1:1 mole ratio of $[\text{C}=\text{C}]:[\text{N}_2\text{H}_4]:[\text{H}_2\text{O}_2]$ was applied in the presence of $\text{CuSO}_4 \cdot 5\text{H}_2\text{O}$ at 60°C . The hydrogenated NR (HNR) had been characterized by FT-IR, $^1\text{H-NMR}$ and $^{13}\text{C-NMR}$. Typical FT-IR spectra of the NR and the hydrogenated product at 24h are shown in Figure 5.37. It was found that the characteristic peaks of the hydrogenated NR



spectrum obtained in latex are similar to that of the hydrogenated NR in organic media. As the hydrogenation progress, the intensity of the characteristic peak at 1665 and 836 cm^{-1} assigning to the C=C stretching of PI units and C-H out of plane deformation of tri-substituted of PI, respectively gradually decrease.

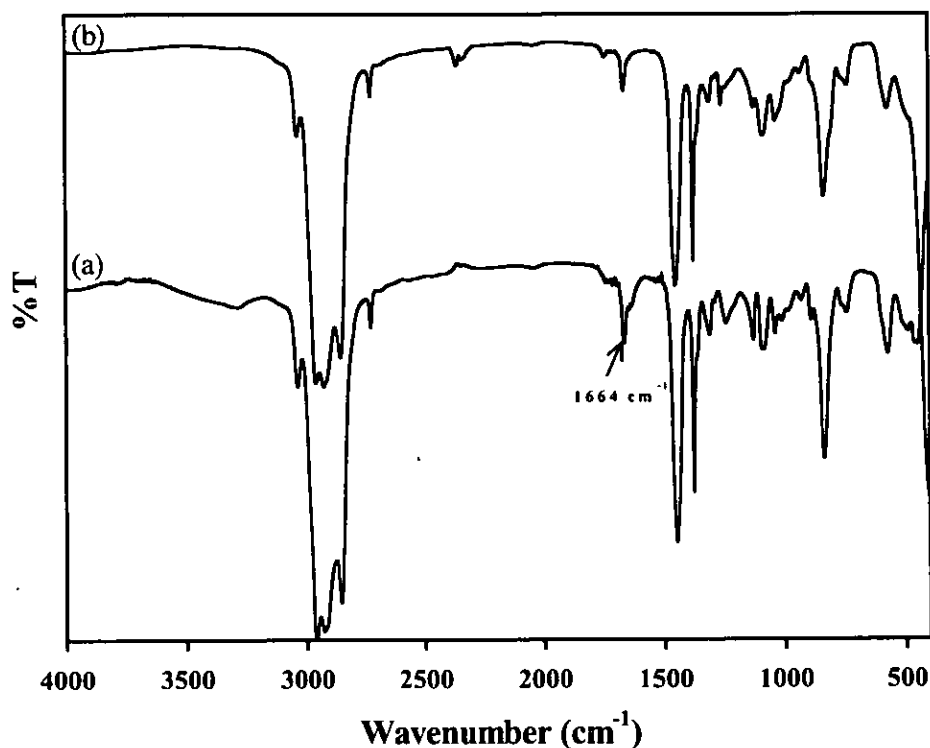


Figure 5.37 FT-IR spectra of NR (a) and hydrogenated NR (b) prepared by using 20% dry rubber content, molar ratio of $[\text{C}=\text{C}]:[\text{N}_2\text{H}_4]:[\text{H}_2\text{O}_2] = 1:1:1:1$ at 60 °C for 24h.

The microstructure of the HNR was further analyzed based on ^1H - and ^{13}C -NMR data as shown in Figure 5.38. For NR, the characteristic of olefinic unit, methylene and methyl groups of *cis*-1,4 polyisoprene units were detected at the chemical shifts discussed in the previous section. After hydrogenation, the appearance of new signals was observed at 0.84 and 1.20-1.35 ppm, which can be assigned to the signals of methyl and methylene protons of saturated part, respectively. This observation is in accordance with the work reported in section 5.2. It is believed that partially hydrogenated product was obtained i.e. the HNR obtained is composed of C=C of the

polyisoprene and saturated units. The level of hydrogenation was calculated by using integrated area of the proton signals obtained from $^1\text{H-NMR}$ spectrum as indicated in Equation 4.10 (section 4.7.3). It was found in this case that 21% hydrogenation was obtained when 1:1:1 mole ratio of $[\text{C}=\text{C}]:[\text{N}_2\text{H}_4]:[\text{H}_2\text{O}_2]$ was used.

According to $^{13}\text{C-NMR}$ analysis, the presence of the ethylene-propylene segment on the rubber chain was evidenced by carbon resonance signals at 19.5 ppm (methyl carbon), 24.5 and 37.4 ppm (methylene carbon) and 32.8 ppm (methine carbon). Signals in Figure 5.38 (b) confirmed the existence of the residual polyisoprene units positioned at 23.4, 26.5, 32.3 ppm corresponding to the methyl and methylene carbon and at 125.5 and 135.2 ppm belong to olefinic carbon of double bond, therefore, partially hydrogenated NR was obtained.



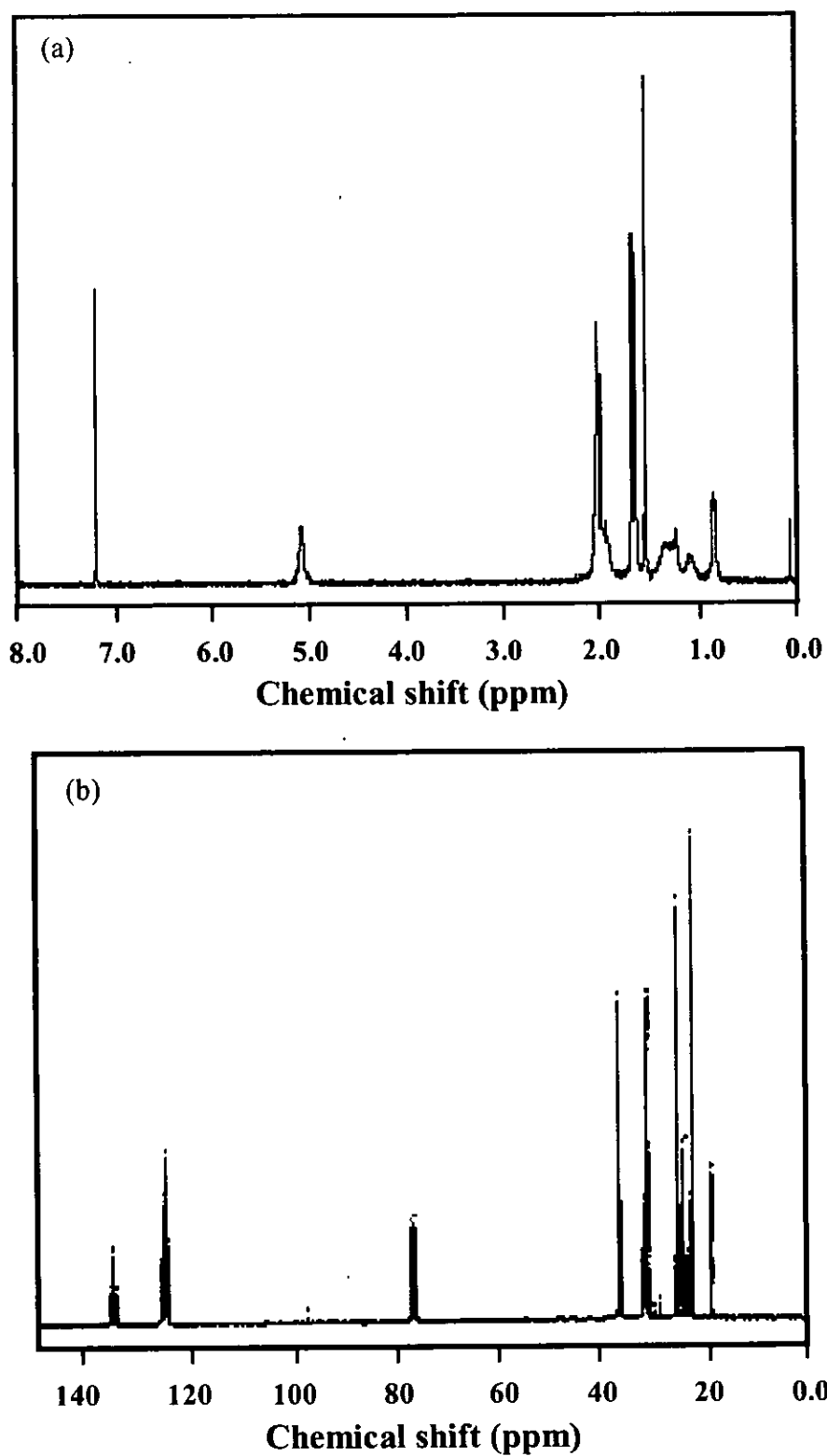


Figure 5.38 ^1H -NMR (a) and ^{13}C -NMR (b) spectra of HNR prepared by using 20% dry rubber content, molar ratio of $[\text{C}=\text{C}]:[\text{N}_2\text{H}_4]:[\text{H}_2\text{O}_2] = 1:1:1$ at 60°C for 24h.

5.5.2 Parameters Affecting on Hydrogenation Reaction

It has been reported that various parameters affected on the hydrogenation of SBR and NBR in latex stage using diimide reduction derived from N_2H_4/H_2O_2 [54-59], i.e., the amount of reactants, type and amount of metal catalyst. In all cases, the increasing of the amount of reactants was affected in increasing the degree of hydrogenation. It was found that $CuSO_4$ is an affective catalyst for hydrogenation in their systems and the maximum hydrogenation level was achieved approximately 80% when 0.0064 mmol $CuSO_4.5H_2O$ was used. Additionally, the effect of pH range on hydrogenation reaction of SBR latex was studied by Sarker De et. al. [56]. They found that the best condition of pH to give the optimum hydrogenation is approximately 9.36 when the molar ratio of reagents per double bond was fixed at 1. NR latex used in this study was high ammonia natural rubber latex. The pH of NR latex is about 9.8 which was a suitable condition for hydrogenation process.

In this section, hydrogenation of NR latex was investigated by using diimide generated for the oxidation of hydrazine by hydrogen peroxide. The NR latex has an average particle size of 720 nm, which is bigger than the synthetic rubber latex such as SBR latex. The hydrogenation reaction may not be occurred in the same manner as in the case of synthetic rubber latex. Therefore, various parameters that might affect on the diimide reduction of NR latex will be investigated such as the presence of $CuSO_4.5H_2O$, reaction time and temperature, amount of reactants and swelling agent. The progress of hydrogenation at selected reaction times was monitored by 1H -NMR.

(a) Influence of $CuSO_4.5H_2O$

First, hydrogenation of NR latex was carried out by using 1:1 mole ratio of C=C of NR to hydrazine concentration and $[N_2H_4]:[H_2O_2]$ equal to 1 mole ratio was applied in the presence of $CuSO_4.5H_2O$ at 60°C. He et al. had studied the effect of catalyst such as $CuSO_4.5H_2O$ on the hydrogenation process of SBR in latex stage [59]. They demonstrated that the hydrogenation involves a copper ion (II) catalyzed procedure in which diimide hydrogenation agent is generated in situ at the surfaces of latex particles. The surface density of the copper ion at the rubber particle surfaces was found to be a crucially important parameter in controlling the hydrogenation level as



the copper helps in accelerating the formation of diimide from the N_2H_4/H_2O_2 redox system in the case of synthetic SBR hydrogenation.

In present work, four diimide reduction conditions were investigated as given in Table 4.3 in section 4.5 to study the effect of the addition of $CuSO_4.5H_2O$ on the diimide reduction process of NR latex. The investigation of the addition of the sodium dodecyl sulfate in the reaction media was also carried out. The white latex product was obtained after diimide reduction process and precipitated in distilled methanol and washed with water several times. After drying in vacuum oven, the obtained product was sticky brown liquid in the case of the addition of $CuSO_4.5H_2O$ (symbolized as NRL3 and NRL5), while the colorless solid sample was obtained in the reaction condition without $CuSO_4.5H_2O$ (symbolized as NRL1 and NRL2).

The spectroscopic investigation of the chemical structure was also analyzed by FT-IR and NMR techniques. Figure 5.39 illustrated the FT-IR spectra of NR and partial hydrogenated rubbers obtained from the hydrogenation of NR. It can be seen that the band intensity of 1665 cm^{-1} , attributing to the $C=C$ gradually decreases after hydrogenation. In the case of the addition of $CuSO_4.5H_2O$, another absorption peak of carbonyl group is detected at around 1720 cm^{-1} and the signal found at 3440 cm^{-1} belonging to the hydroxyl group. It seems that after hydrogenation, there is hydroxyl and carboxylic functional groups occurred on the rubber chain. This is possible that the resulting hydrogenated rubber is a colored viscous liquid. It can be concluded in this stage that color liquid rubber was occurred from degradation of NR because of the presence of Cu_2O as a by product and H_2O_2 .



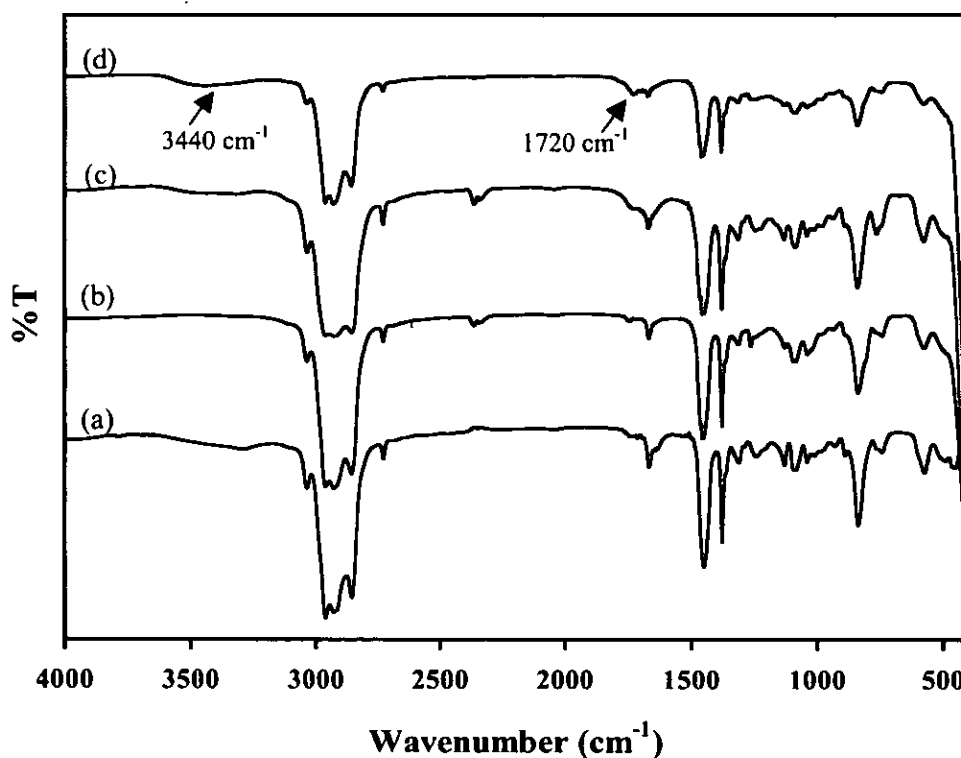


Figure 5.39 FT-IR spectra of NR (a) and hydrogenated NR obtained from: (b) without sodium dodecyl sulfate (SDS), (c) with 4.00×10^{-3} mmol of $\text{CuSO}_4 \cdot 5\text{H}_2\text{O}$ and (d) with SDS and 4.00×10^{-3} mmol of $\text{CuSO}_4 \cdot 5\text{H}_2\text{O}$ using molar ratio of $[\text{C}=\text{C}]:[\text{N}_2\text{H}_4]:[\text{H}_2\text{O}_2] = 1:1:1$ at 60°C .

¹H-NMR spectra of hydrogenated rubber obtained from diimide reduction process with the use of $\text{CuSO}_4 \cdot 5\text{H}_2\text{O}$ and $\text{CuSO}_4 \cdot 5\text{H}_2\text{O}/\text{SDS}$ are shown in Figure 5.40. The characteristic of the partial hydrogenated rubber obtained in this condition is similar to that obtained from diimide hydrogenation with TSH. No extra signal was detected at 1.60 ppm. This indicated that there is no *cis-trans* isomerization of *cis*-1,4 polyisoprenic structure in this diimide hydrogenation process.

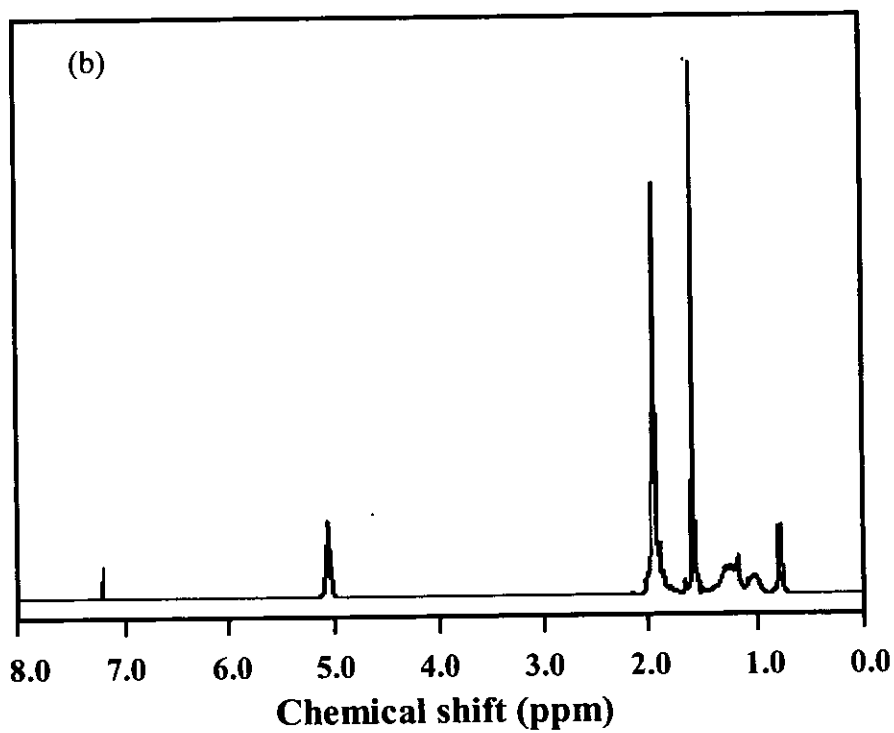
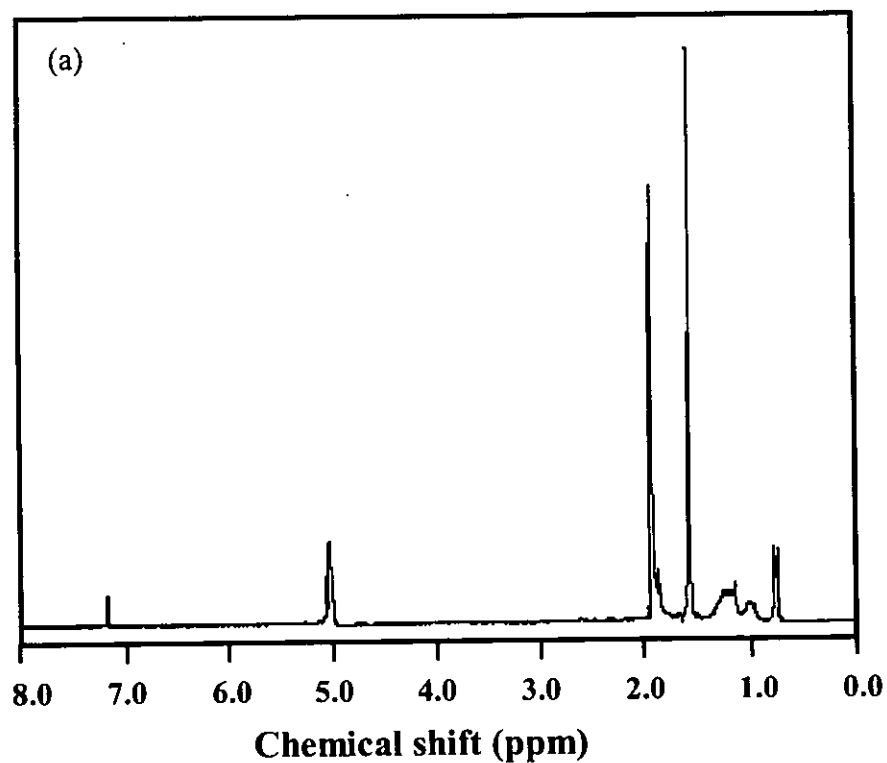


Figure 5.40 ^1H -NMR spectrum of hydrogenated rubber obtained from the presence of $\text{CuSO}_4 \cdot 5\text{H}_2\text{O}$ (a) and $\text{CuSO}_4 \cdot 5\text{H}_2\text{O}$ and SDS as a surfactant (b) using molar ratio of $[\text{C}=\text{C}]:[\text{N}_2\text{H}_4]:[\text{H}_2\text{O}_2] = 1:1:1$ at 60°C .

The results of using $\text{CuSO}_4 \cdot 5\text{H}_2\text{O}$ affecting on the percent hydrogenation as determined by $^1\text{H-NMR}$ are presented in Table 5.22. A comparison of the rate of hydrogenation between using $\text{CuSO}_4 \cdot 5\text{H}_2\text{O}$ and without $\text{CuSO}_4 \cdot 5\text{H}_2\text{O}$ systems is plotted in Figure 5.41. It can be seen that the hydrogenation rates of the reaction using $\text{CuSO}_4 \cdot 5\text{H}_2\text{O}$ are slower than those of without $\text{CuSO}_4 \cdot 5\text{H}_2\text{O}$. The maximum hydrogenation degree is about 19.5% with the addition of the $\text{CuSO}_4 \cdot 5\text{H}_2\text{O}$ while without the $\text{CuSO}_4 \cdot 5\text{H}_2\text{O}$, the percent hydrogenation reached around 27.4% (NRL2). It was demonstrated that the addition of $\text{CuSO}_4 \cdot 5\text{H}_2\text{O}$ did not improve the degree of hydrogenation. This result is different from the hydrogenation of SBR latex studied by He et al. in which $\text{CuSO}_4 \cdot 5\text{H}_2\text{O}$ was used as a catalyst [59]. They found that about 90% hydrogenation of SBR was obtained which was higher than that found in our system. It may be due to the large difference in the average particle size of these two systems i.e. NR particle size is about 700 nm while the rubber particle size of SBR latex was found to be 50 nm. Another reason might be due to the nature of NR latex which its particle surface is surrounded by several types of proteins, fatty acids, phospholipid and other non-rubber constituents as detailed in section 3.1. It is, therefore, difficult for diimide molecule to diffuse into the rubber particle of NR. A comparison between the diimide reduction without and with surfactant (symbolized as NRL1 and NRL2) was investigated. It seems likely that the initial hydrogenation rates are comparable, but at longer reaction time (>6h) the hydrogenation rate of NRL2 is faster than that of NRL1 (see Figure 5.42). In general, the main role of surfactant is to keep the rubber particles dispersed in colloidal form.



Table 5.22 Hydrogenation level taken place without and with $\text{CuSO}_4 \cdot 5\text{H}_2\text{O}$ and surfactant

Reaction time (h)	Hydrogenation (%)			
	NRL1 ^a	NRL2 ^b	NRL3 ^c	NRL4 ^d
0	0	0	0	0
2	9.4	7.9	6.2	7.2
6	17.5	21.7	8.5	15.1
12	22.6	25.3	14.1	15.6
24	21.3	27.4	18.4	19.5

a = without sodium dodecyl sulfate (SDS)

b = with sodium dodecyl sulfate (SDS)

c = with 4.00×10^{-3} mmol of $\text{CuSO}_4 \cdot 5\text{H}_2\text{O}$

d = with SDS and 4.00×10^{-3} mmol of $\text{CuSO}_4 \cdot 5\text{H}_2\text{O}$

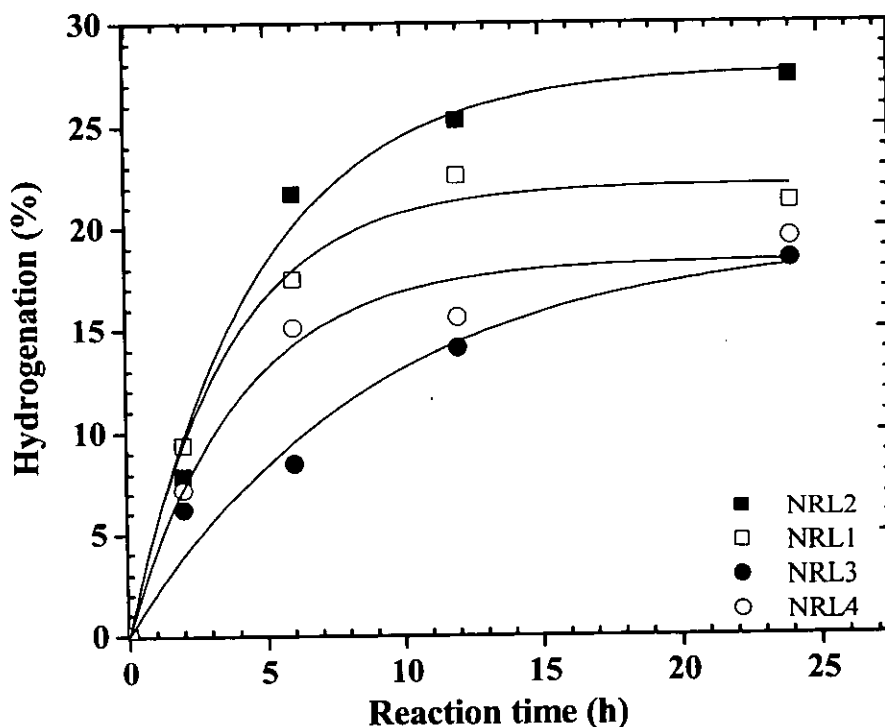


Figure 5.41 Effect of $\text{CuSO}_4 \cdot 5\text{H}_2\text{O}$ and surfactant on the hydrogenation rate: (□) without SDS, (■) with SDS, (●) with 4.00×10^{-3} mmol of $\text{CuSO}_4 \cdot 5\text{H}_2\text{O}$ and (○) with 4.00×10^{-3} mmol of $\text{CuSO}_4 \cdot 5\text{H}_2\text{O}$ and SDS using molar ratio of $[\text{C}=\text{C}]:[\text{N}_2\text{H}_4]:[\text{H}_2\text{O}_2] = 1:1:1$ at 60°C .

Two different amounts of $\text{CuSO}_4 \cdot 5\text{H}_2\text{O}$ were investigated on the effect of the % hydrogenation. NRL4 was the experiment using 2.4×10^{-3} mmol $\text{CuSO}_4 \cdot 5\text{H}_2\text{O}$ and NRL5 was that of 4.0×10^{-3} mmol $\text{CuSO}_4 \cdot 5\text{H}_2\text{O}$. The analysis of the percent hydrogenation by $^1\text{H-NMR}$ is shown in Table 5.23 and the plots between the percent hydrogenation and reaction time with different amount of $\text{CuSO}_4 \cdot 5\text{H}_2\text{O}$ are displayed and compared with the reaction using only surfactant in Figure 5.42. It was found that the percent hydrogenation of NRL4 is higher than that of NRL5. It was reported that during the reduction process, the copper ion is able to greatly accelerate the formation of diimide from the $\text{N}_2\text{H}_4/\text{H}_2\text{O}_2$ redox system [55, 56, 58]. Copper ion, when added to the reaction can be present in three locations: (a) in water medium; (b) at the rubber particle surface; (c) inside the rubber particle. The concentration of copper ion at the particle surface is an important factor to reach a high degree of hydrogenation so the copper ions should reside only at the surface of the latex particle as mentioned by Sarkar De et al. [55, 56]. But in this research work the NR particle size (average particle size 720 nm) is larger than that of synthetic SBR as studied by He et al. [59], hence, the copper ion might prefer to reside in water phase which it does not perfectly accelerate the reaction of hydrazine and hydrogen peroxide to form diimide molecule. When the concentration of the catalyst is too high, it might be possible that the catalyst stays in water phase and the Cu(II) was reduced to cuprous oxide by the mild reducing agent, hydrazine, and thus the catalytic activity of Cu(II) decreases, resulting in lower degree of hydrogenation [55]. Therefore, NRL4 has higher degree of hydrogenation than NRL5 as the former has lower amount of copper catalyst. It can be concluded that the addition of $\text{CuSO}_4 \cdot 5\text{H}_2\text{O}$ to the diimide reduction process in NR latex shows no beneficial effects upon improving hydrogenation reaction for this study.



Table 5.23 Effect of amount of $\text{CuSO}_4 \cdot 5\text{H}_2\text{O}$ on the percent hydrogenation of NR

Reaction time (h)	Hydrogenation (%)		
	NRL2 ^a	NRL5 ^c	NRL4 ^d
0	0	0	0
2	7.9	7.6	7.2
6	21.7	15.5	15.1
12	25.3	15.7	15.6
24	27.4	24.2	19.5

a = with sodium dodecyl sulfate (SDS)

e = with SDS and 2.40×10^{-3} mmol of $\text{CuSO}_4 \cdot 5\text{H}_2\text{O}$

d = with SDS and 4.00×10^{-3} mmol of $\text{CuSO}_4 \cdot 5\text{H}_2\text{O}$

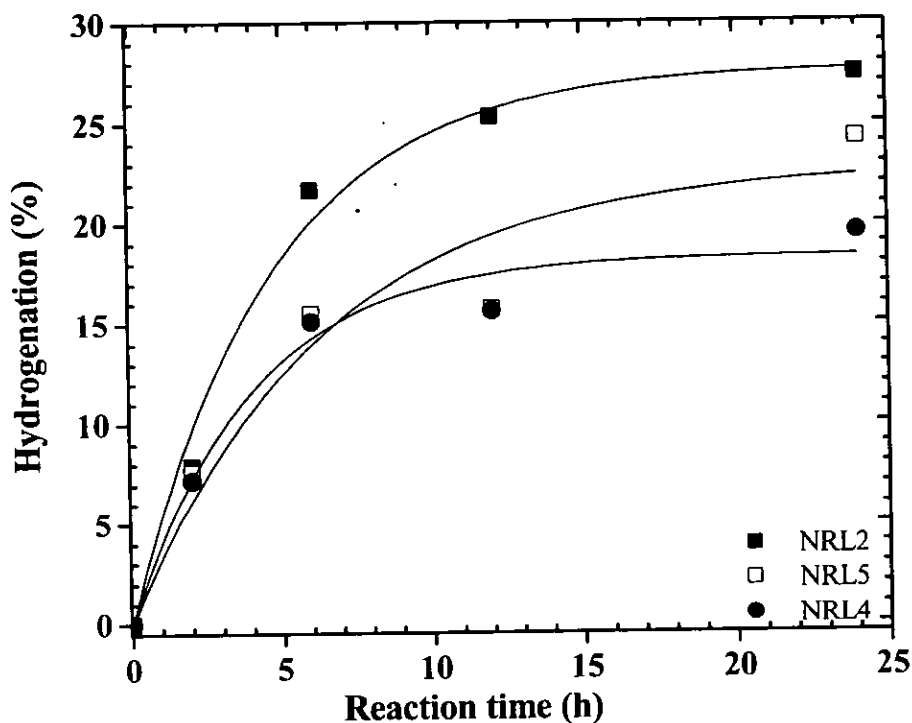


Figure 5.42 The percent hydrogenation of NR in latex form with the presence SDS as a surfactant (■), SDS and 2.40×10^{-3} mmol of $\text{CuSO}_4 \cdot 5\text{H}_2\text{O}$ (□), and SDS and 4.00×10^{-3} mmol of $\text{CuSO}_4 \cdot 5\text{H}_2\text{O}$ (●) using molar ratio of $[\text{C}=\text{C}]:[\text{H}_2\text{N}_4]:[\text{H}_2\text{O}_2] = 1:1:1$ at 60°C .

(b) Influence of Reaction Time and Temperature

It was found in former section that hydrogenation time affected on hydrogenation level. At longer reaction time, higher percentage of hydrogenation was obtained. The diimide molecule generated from the oxidation of hydrazine by hydrogen peroxide may be affected by the reaction temperature. Therefore, various reaction temperatures i.e. 30, 45, 60, 70 and 80°C for hydrogenation of NR latex as well as reaction time were investigated under the condition of equal mole ratio of carbon-carbon double bond, hydrazine and hydrogen peroxide. In all cases, the colorless solid form of hydrogenated NR was obtained. The chemical structure of hydrogenated product was investigated by using FT-IR and NMR techniques.

Figure 5.43 shows the IR spectra of hydrogenated products obtained from hydrogenation reaction carried out at various reaction temperatures during 24h reaction time. Similar characteristic peaks of hydrogenated NR were obtained as in the former case that the rubbers still possess the signals of C=C and =C-H deformation at 1664 and 836 cm^{-1} , respectively, which mean that only partial hydrogenation was occurred in each experiment.

The analysis by $^1\text{H-NMR}$ of the partially hydrogenated product (Figure 5.44) shows the presence of the characteristic signals of proton attached to C=C of polyisoprenic unit at 5.12 ppm and methyl proton of saturated unit at 0.84 ppm, respectively. The methyl proton adjacent to the C=C is positioned at 1.67 ppm. These results are in accordance with the previous report in part I. Additionally, there is other signal indicating the formation of *trans*-1,4 units resulting from secondary reaction that is *cis-trans* isomerization at 1.60 ppm (methyl proton adjacent to the C=C of *trans*-1,4 polyisoprene unit). The amount of *cis* and *trans* isomers can be calculated from the integration area of the signal of methyl proton adjacent to the C=C of *trans*-1,4 PI unit and the methyl proton adjacent to the C=C of *cis*-1,4 PI unit and the results are shown in Table 5.24.



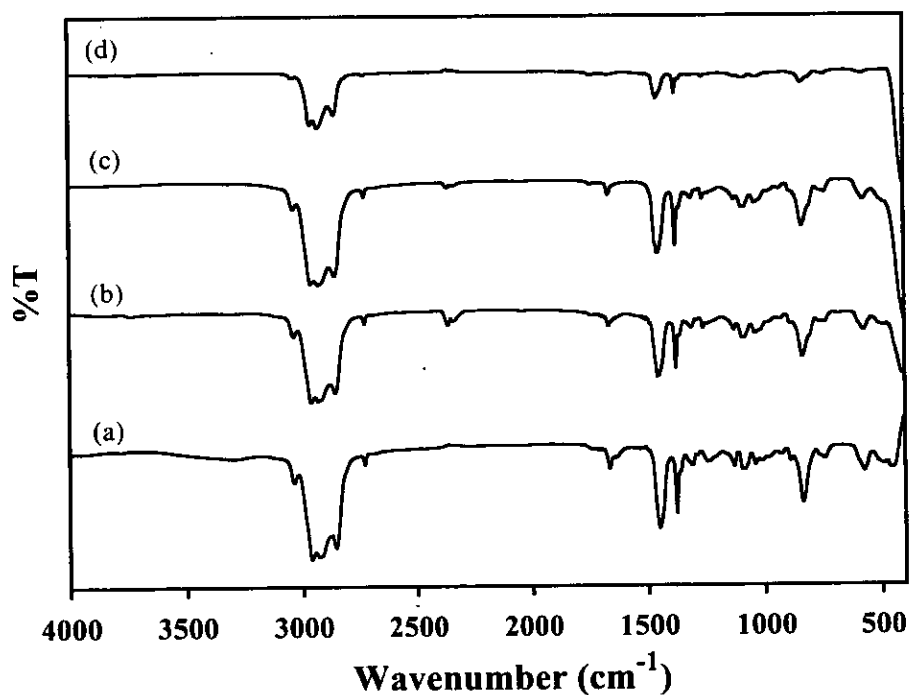


Figure 5.43 FT-IR spectra of NR (a) and HNR obtained from various reaction temperatures: 30 (b), 60 (c), and 80°C (d) using molar ratio of $[C=C]=[N_2H_4]=[H_2O_2]=1$.

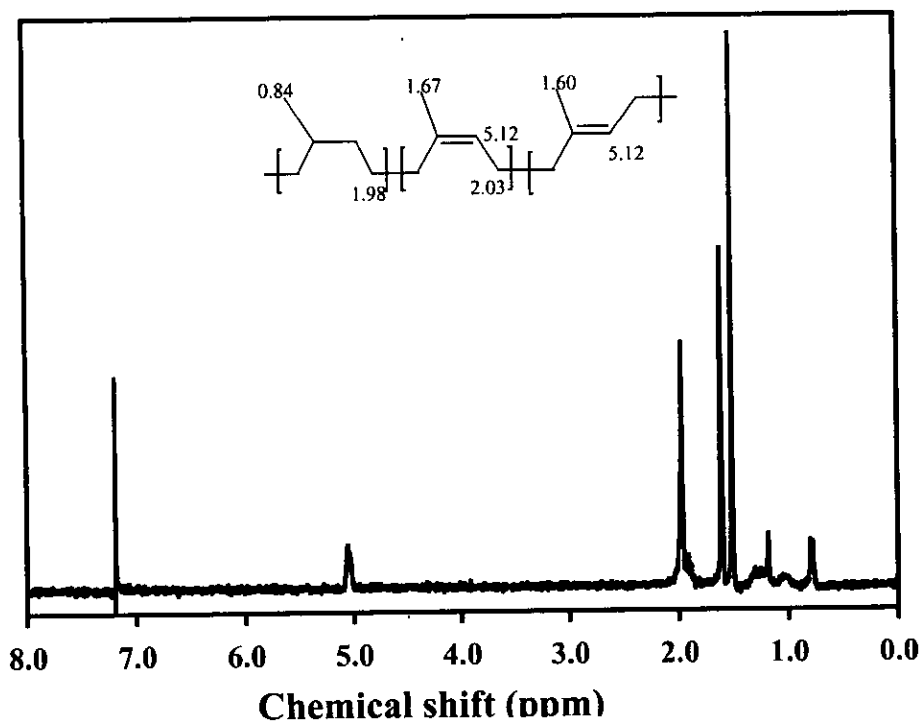


Figure 5.44 1H -NMR spectrum of the hydrogenated NR obtained from 60°C using molar ratio of $[C=C]:[N_2H_4]:[H_2O_2]=1:1:1$ at 24h.

The results of the percent hydrogenation obtained at different temperatures and times were determined and shown in Table 5.24. They were also presented in Figure 5.45. It can be seen that the percentage of hydrogenation increased at longer reaction times. The maximum level of hydrogenation was achieved after 12h of reaction time and, then relatively constant. By comparing with diimide hydrogenation of SBR latex, longer reaction time for hydrogenation of NR latex was needed [54-56, 58]. It was found that the maximum hydrogenation reaches 27 % after 12h, whereas the hydrogenation of SBR latex is 80% after 1h [59]. This result can be described by two possible factors which involve the average particle size of rubber and the nature of rubber particle. The major factor concerns with the average rubber particle size of NR (720 nm) that is larger than that of synthetic SBR latex (50 nm) as mentioned in section 3.3.2. By this reason, the distance for diffusion of the diimide molecules from the surface to react with the double bonds residing at the inner side of the latex particle is greater than that of synthetic latex. Another reason is the nature of rubber particle that has a membrane of proteins covered its rubber surface. Hence, diimide molecules in *syn* form are not easily to penetrate into the double bonds of the macro-chain of the rubber.

It is noted that the extent of hydrogenation increased gradually with reaction temperature. Only 30 % hydrogenation was obtained at 80°C in this case study. It might come from the disproportionation of diimide molecule as described in section 3.3.2.2. In addition, small amount of rubber particle coagulation observed at longer reaction time and higher temperature is due to less stability of rubber latex.

The effect of temperature on the diimide reduction reaction could be considered from Figure 5.45. It can be seen that the extent of reduction increased with increasing the reaction temperature in the studied range of 30-80°C. The maximum hydrogenation was obtained at the reaction temperature of 80°C. The hydrogenation rate of *cis*-1,4 PI unit of NR at 80°C is faster than that of the other temperature as shown in Figure 5.45. The degree of hydrogenation was progressively increased at the early state of the reaction (6h), then slight increase of hydrogenation was performed at longer reaction time. This result is obvious, as with an increase of the reaction temperature, the more energy is supplied to overcome the activation energy for the addition of hydrogen molecule onto the unsaturated units of the rubber chains.



Subsequently, the probability of collision between the diimide molecule and the C=C bond of NR molecules increased at higher temperature, resulting in increasing the hydrogenation level of the rubber particle in emulsion stage. However, the gel formation of the resulted product was observed after 24h of reaction time at 70 and 80°C. It might be postulated that an increasing temperature may increase the amount of hydroxyl radical formed from the decomposition of hydrogen peroxide at higher temperature, and then active radical sites increased the possibility of intermolecular reaction or cross-linking reaction. Therefore, the reaction temperature at 60°C was chosen, which necessitate the use of mild conditions to balance the reaction condition.

Table 5.24 The percent hydrogenation of NR latex at various reaction times and temperatures as determined by ¹H-NMR

Reaction time (h)	Hydrogenation (%)				
	NRL6 (30°C)	NRL7 (45°C)	NRL8 (60°C)	NRL9 (70°C)	NRL10 (80°C)
0	0	0	0	0	0
2	2	6.6	9.4	12.2	10.3
6	5.9	10.7	17.5	23.7	23.8
12	8.5	16.2	22.6	25	27.1
18	10.6	16.6	20.2	-	26.4
24	9.6	17.9	21.3	25.5	29.4
30	9.8	17.3	23.6	26.5	29.9



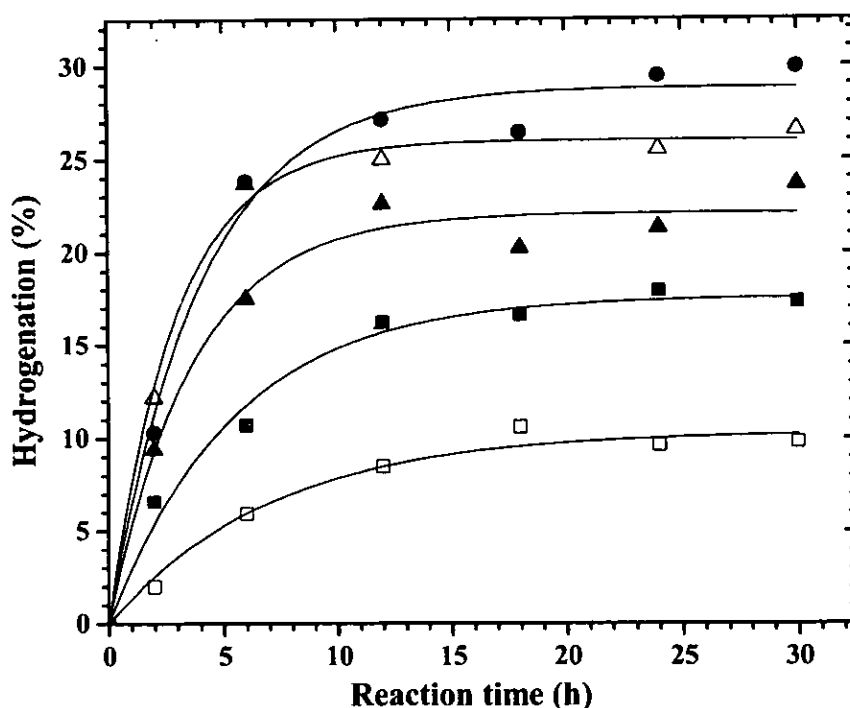


Figure 5.45 Effect of reaction time and temperature on hydrogenation of NR in latex phase varied at 30°C (□), 45°C (■), 60°C (▲), 70°C (△) and 80°C (●) by using 20% dry rubber content, molar ratio of $[C=C]:[N_2H_4]:H_2O_2 = 1:1:1$.

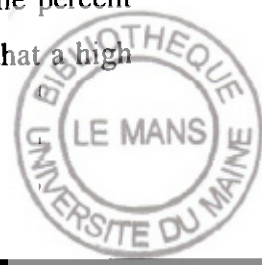
The effect of temperature on the secondary reactions of the hydrogenation was also examined. The summarized results on the effect of the reaction temperature on percentage of *cis* and *trans*-polyisoprene units are shown in Table 5.25. Using the molar ratio of $[C=C]=[N_2H_4]=[H_2O_2]$ equal to 1, the *trans* unit content were found occurring in a random manner for an example of the hydrogenation reaction at 24h the amount of *trans* units were found to be 16.7, 8.0, 52.3, 55.6 and 39.6% as the reaction temperature was 30, 45, 60, 70 and 80°C, respectively. It can be also seen that the formation of *trans* unit in HNR was not linearly dependent on the reaction time. It seems likely that the *cis-trans* isomerization was occurred at any time but roughly the transformation of *cis* to *trans* unit increased with the increase of reaction temperature. This may be due to the fact that when the temperature increased, the higher rate the formation of diimide intermediate as well as the molecular motion of the rubber chain were increased, which will increase the collision efficiency of the reagents and the rubber molecules.

Table 5.25 The percentage of *cis* and *trans*-polyisoprene units determined by ^1H -NMR obtained during hydrogenation reaction at various temperatures

Reaction time (h)	30 °C		45 °C		60 °C		70 °C		80 °C	
	%cis	%trans	%cis	%trans	%cis	%trans	%cis	%trans	%cis	%trans
0	100	0	100	0	100	0	100	0	100	0
2	89.8	10.2	89.8	10.2	88.5	11.5	67	33	89.8	10.2
6	93.5	6.5	99	1	98	2	74.2	25.4	87.1	12.9
9	97.4	2.6	98.3	1.7	98	2	63.9	36.1	53.6	46.4
12	98.3	1.7	98.3	1.7	79.1	20.9	67.3	32.7	78.6	17.8
24	83.3	16.7	92	8	47.7	52.3	44.4	55.6	60.4	39.6
30	86.5	13.5	88.5	11.5	62.9	37.1	98	2	52.9	47.1

(c) Influence of Rubber Content

The effect of dry rubber content (DRC) of NR latex on the percent hydrogenation of NR was studied at 60°C in the presence of stoichiometric molar ratio of hydrazine hydrate per double bond fixed (i.e., one mole of double bond per one mole of hydrazine). The results of hydrogenation level are listed in Table 5.26 and the plots between the %hydrogenation against the reaction time at different DRC are illustrated in Figure 5.46. It can be seen that the hydrogenation level increases with an increase in the DRC from 10 to 20%. When increasing the DRC to 30%, a decrease of hydrogenation degree was observed. It was also found some gel formation in the reaction medium. This suggested that very high dry rubber content allows the rubber particles to come closer; this may facilitate the intermolecular reaction between macroradical probably generated by side reaction of hydrogen peroxide, leading to gel formation. Therefore, our system the hydrogenation in aqueous medium is favored with low concentration of rubber i.e. 20% DRC. It can be seen in Figure 5.46 that 20% DRC gives the best percent hydrogenation of 23.6 at 30h reaction time. The percent hydrogenation tends to be increased with the reaction time. It is obvious that a high



rate of hydrogenation of 20% DRC was observed at the early stage of reaction (6h of reaction time). This suggests by the fact that at 20%DRC the more diimide molecule can diffuse into the rubber particles as a result of an increase of hydrogenation degree. The hydrogenation level of NR latex at 10%DRC give the lowest value. This is because less amount of the diimide can penetrate to the NR particle due to loss in the water medium. The N_2H_4 might be lost from the reaction with water.

The investigation of the secondary structures resulting from hydrogenation of NR latex with various DRCs was carried out. The signal of proton corresponding to the methyl of *trans*-1,4 polyisoprenic structure was found to be appeared at the position at 1.60 ppm. The *cis-trans* isomerization also found randomly during hydrogenation reaction.

Table 5.26 Influence dry rubber contents on the hydrogenation of NR in latex phase using molar ratio of $[C=C]:[N_2H_4]:[H_2O_2] = 1:1:1$ at $60^\circ C$

Reaction time (h)	Hydrogenation (%)		
	NRL11 (10%DRC)	NRL12 (20%DRC)	NRL13 (30%DRC)
0	0.0	0.0	0.0
2	3.34	9.4	5.6
6	9.24	17.5	13.1
12	13.6	22.6	n
18	n	20.2	17.0
24	15.3	21.3	17.9
30	16	23.6	n

n = not determine



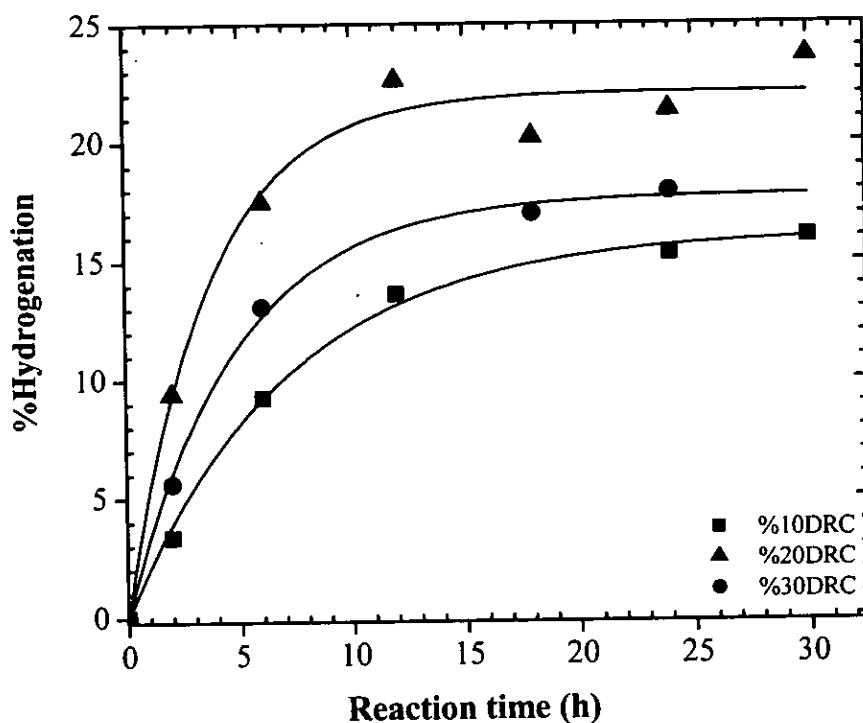
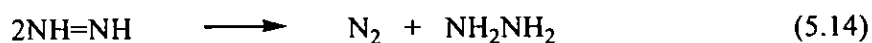
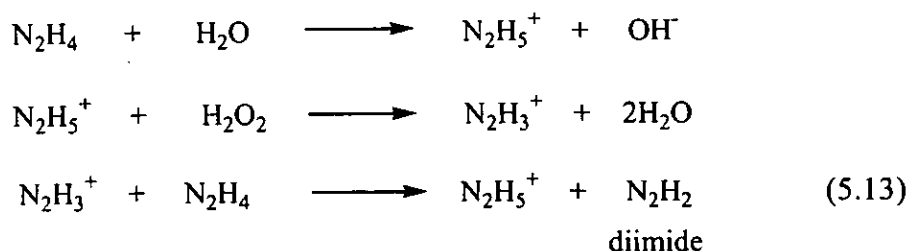


Figure 5.46 Influence of dry rubber contents on diimide reduction of NR in latex phase using molar ratio of $[C=C]:[N_2H_4]:[H_2O_2] = 1:1:1$; %10DRC (■), %20DRC (▲) and %30DRC (●).

(d) Influence of Hydrazine Hydrate

It was found in former sections that less than 100% hydrogenation was achieved by using equivalent in molar ratio of the unsaturation, hydrazine and hydrogen peroxide in various reaction times and temperatures. It can be estimated that not all the diimides formed can react with the C=C of the NR or it may be possible that there are some lost of the reactants during the formation of diimide. It has been mentioned in the literature that the generation of diimide molecule from the reaction of hydrazine and hydrogen peroxide is a redox system and can be schematized in Equation 5.13. The diimide can be formed through the reaction of hydrazine with water forming hydrazinium ion ($N_2H_5^+$) before reacting with H_2O_2 or the hydrazine can react directly with the H_2O_2 forming the diimide intermediate. The diimide formed may also react with each other and transform into N_2 and N_2H_4 again (see Equation 5.14). Therefore, it is necessary to study the different ratio of N_2H_4 and H_2O_2 .



In this section, the influence of hydrazine hydrate content (molar ratio of $[\text{N}_2\text{H}_4]/[\text{H}_2\text{O}_2] = 0.5, 1.0, 1.5$ and 2.0) was investigated by fixing the molar ratio of $[\text{C}=\text{C}]:[\text{H}_2\text{O}_2]$ equal to 1.0 at 60°C . Similar characteristic of the partially hydrogenated NR was obtained in this condition as compared with other diimide reduction systems. For $^1\text{H-NMR}$ investigation, the doublet peak at 0.84 ppm which can be assigned to the proton signal of methyl group was observed. The signals of methyl proton in $^1\text{H-NMR}$ were found at 1.67 and 1.60 , assigned to the methyl proton of *1,4-cis* and *1,4-trans* polyisoprenic structure. This indicated also that the *cis* isomer can be transformed to *trans* isomer during diimide reduction.

Table 5.27 and Figure 5.47 shows results of % hydrogenation found at various reaction times for diimide hydrogenation using various amount of N_2H_4 . It can be seen that the molar ratio of $[\text{N}_2\text{H}_4]:[\text{H}_2\text{O}_2]$ equal to 1 and 1.5 gave better results of hydrogenation than the molar ratio of $[\text{N}_2\text{H}_4]:[\text{H}_2\text{O}_2]$ equal to 0.5 . The maximum hydrogenation of about 23% was achieved after 24h when 1.0 and 1.5 mol of $[\text{N}_2\text{H}_4]:[\text{H}_2\text{O}_2]$ were used. This may be explained by the fact that, by increasing amount of N_2H_4 the concentration of the diimide molecule formed may be increased, leading to an increase of the possibility of the addition reaction of diimide onto the $\text{C}=\text{C}$ bond of the NR chain, which is similar to the results obtained from hydrogenation of polybutadiene units in the SBR latex [55, 56]. However, when the amount of N_2H_4 was less than H_2O_2 , less amount of diimide can be formed, resulting automatically less amount of $\text{C}=\text{C}$ was hydrogenated. In the case of using an excess amount of N_2H_4 (2.0 mol) a slight decrease of percent hydrogenation was found. Therefore, it is not interesting to add an excessive amount of N_2H_4 in the medium. By varying the amount of N_2H_4 , *cis-trans* isomerization was also detected.



Table 5.27 Influence of amount of hydrazine on the degree of hydrogenation in NR latex molar ratio of $[C=C]:[H_2O_2] = 1$ at $60^\circ C$

Reaction time (h)	Hydrogenation (%)			
	NRL14	NRL15	NRL16	NRL17
	$[N_2H_4]/[H_2O_2] = 0.5$	$[N_2H_4]/[H_2O_2] = 1$	$[N_2H_4]/[H_2O_2] = 1.5$	$[N_2H_4]/[H_2O_2] = 2.0$
0	0	0	0	0
2	7.8	9.4	4.8	7.4
6	14.9	17.5	13	16.2
9	15.4	n	17.8	17.8
12	15.7	21.3	19.6	18.4
24	n	22.6	21.1	20.5
30	16.5	23.6	23.7	20.8

n = not determine

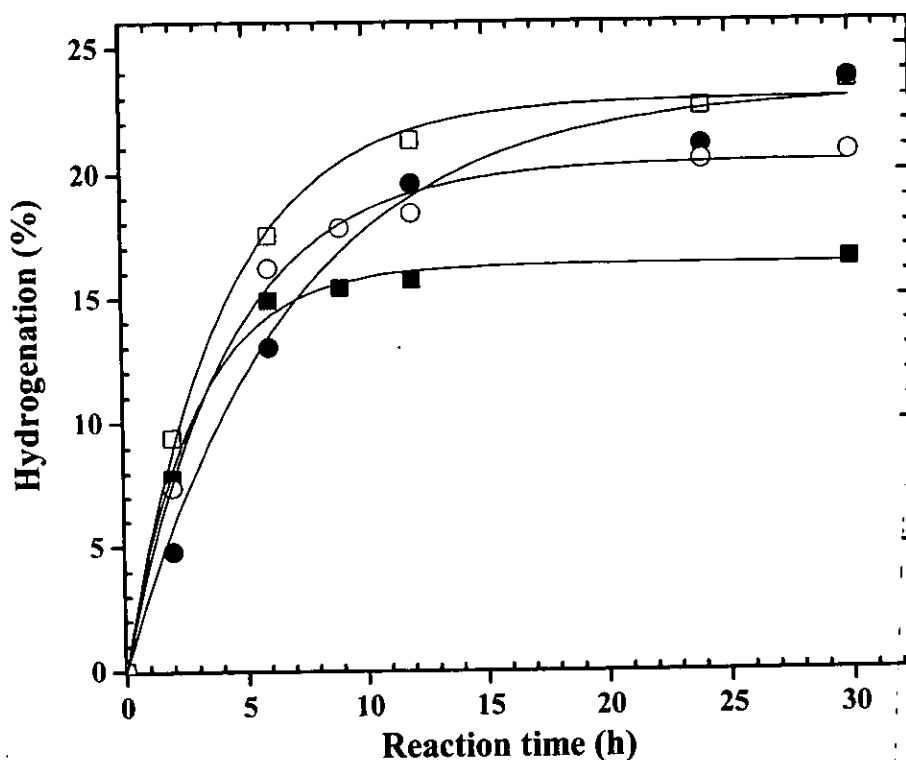
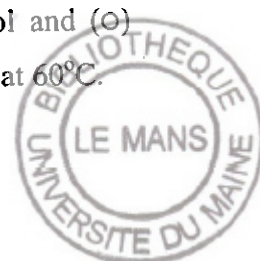


Figure 5.47 Influence of hydrazine concentration on the hydrogenation level of NR latex at various amount of N_2H_4 ; (■) 0.5mol, (□) 1.0mol, (●) 1.5mol and (○) 2.0mol carried out using 20 %DRC and the molar ratio of $[C=C]:[H_2O_2] = 1$ at $60^\circ C$.

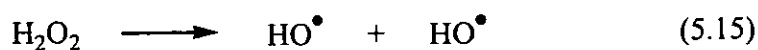


(e) Influence of Hydrogen Peroxide

As hydrogen peroxide (H_2O_2) is an oxidizing agent widely used for oxidation of hydrazine to generate the diimide molecule, the amount of H_2O_2 may effect on the amount of diimide molecule which probably influence on the efficiency of hydrogenation. It has already been found only about 23.5% hydrogenation was obtained when one to one mole ratio of hydrazine to H_2O_2 was applied. In this section, various amounts of H_2O_2 i.e. 0.5, 1.0, 1.5 and 2.0 mol compared to the amount of N_2H_4 were investigated for the hydrogenation reaction of NR latex in the presence of the molar ratio of $[\text{C}=\text{C}]:[\text{N}_2\text{H}_4]$ equal to 1 at 60°C .

The results of % hydrogenation of NR in latex at various amounts of H_2O_2 are given in Table 5.28. It can be seen that excess amount of H_2O_2 compared to the N_2H_4 i.e. $[\text{H}_2\text{O}_2]:[\text{N}_2\text{H}_4]$ equal to 1.5 and 2.0 gave better % hydrogenation than the ratio of $[\text{H}_2\text{O}_2]:[\text{N}_2\text{H}_4]$ equal to 0.5 and 1.0 and the use of excess of N_2H_4 i.e. $[\text{N}_2\text{H}_4]:[\text{H}_2\text{O}_2]$ is higher than 1. The maximum hydrogenation is achieved about 37% when the $[\text{H}_2\text{O}_2]:[\text{N}_2\text{H}_4]$ equal to 1.5 was used to reduce the double bond at 24 h. The plots of %hydrogenation against various reaction times at different amounts of H_2O_2 used are also shown in Figure 5.48. It reveals that the addition of hydrogen molecule on the rubber chain at a constant content of N_2H_4 increased with an increase in the amount of H_2O_2 from 0.5 to 1.5 mol. However, increasing the molar ratio of $[\text{H}_2\text{O}_2]:[\text{N}_2\text{H}_4]$ to 2 mol did not accelerate further the hydrogenation, the decrease of hydrogenation level was observed. The H_2O_2 is therefore a key reagent that controls the diimide formation because the H_2O_2 is consumed, while N_2H_4 can be regenerated (see Equation 5.14). Hence, higher amount of H_2O_2 results in the formation of higher amount of diimide molecule, then higher amount of hydrogenated fraction can be formed. However, when the amount of H_2O_2 was increased up to 2.0 moles, the % hydrogenation slightly decreased. This suggested that the excess of H_2O_2 content may lead to an increase in the dissociation reaction forming active radical sites as shown in Equation 5.15, thus the possibility of intermolecular reaction or crosslink reaction might be occurred. It was also found some gel formation when excess amount of H_2O_2 was used.





It was found that by varying the amount of H_2O_2 , *cis-trans* isomerization was occurred. Increasing the amount of H_2O_2 i.e. 0.5, 1.0 and 1.5mol at 24h resulted in the percentage of *trans*-polyisoprenic structure of 11.8, 52.3 and 20.7%, respectively.

Table 5.28 Influence of amount of hydrogen peroxide on the degree of hydrogenation in NR latex using molar ratio of $[\text{C}=\text{C}]:[\text{N}_2\text{H}_4] = 1$ at 60°C

Reaction time (h)	Hydrogenation (%)			
	NRL18	NRL19	NRL20	NRL21
	$[\text{H}_2\text{O}_2]/[\text{N}_2\text{H}_4]$ = 0.5	$[\text{H}_2\text{O}_2]/[\text{N}_2\text{H}_4]$ = 1.0	$[\text{H}_2\text{O}_2]/[\text{N}_2\text{H}_4]$ = 1.5	$[\text{H}_2\text{O}_2]/[\text{N}_2\text{H}_4]$ = 2.0
0	0	0	0	0
2		9.4	7.4	6.8
6	15.9	17.5	26	19.5
9	17.5	20.2	n	n
12	18.1	20.2	30.2	23.9
18	n	n	33.1	24.4
24	20.5	22.6	33.4	28.9
30	21.3	23.6	37	31.2

n = no determination



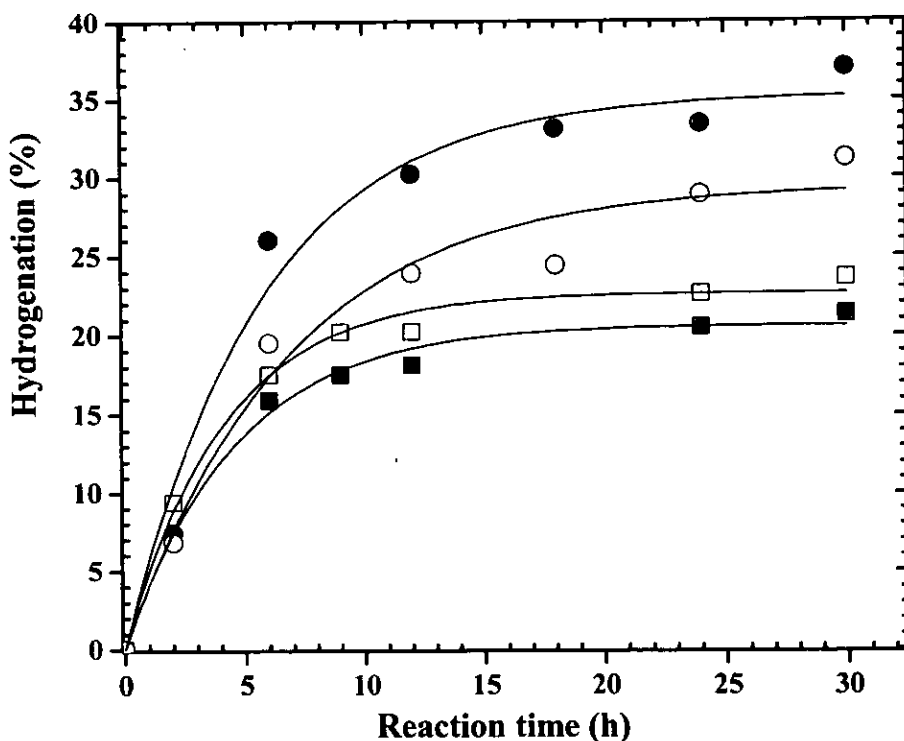


Figure 5.48 Influence of hydrogen peroxide concentration on the hydrogenation level of NR latex at various amount; (■) 0.5mol, (□) 1.0mol, (●) 1.5mol and (○) 2.0mol carried out using 20 %DRC and the molar ratio of $[C=C]:[N_2H_4] = 1$ at $60^\circ C$.

(f) Influence of Molar Ratio of Hydrazine to Carbon-Carbon Double Bond

The influence of molar ratio of hydrazine to C=C on the diimide hydrogenation reaction of NR latex was conducted by varying the molar ratio of hydrazine hydrate to double bonds from 0.5 to 2 (the molar ratio of hydrazine to hydrogen peroxide equal to 1) at $60^\circ C$. The results of hydrogenation level are presented in Table 5.29. It can be seen that the level of hydrogenation increased with the molar ratio of $[N_2H_4]:[C=C]$ increase from 0.5 up to 1.5 at 24 h of reaction time. This can be estimated that increasing the amount of N_2H_4 resulted in higher amount of diimide molecules hence more double bonds of the NR may be reduced into saturated units. The 1H -NMR analysis of the partially hydrogenated rubbers showed the presence of approximately 38% of hydrogenation content when the molar ratio of $[N_2H_4]:[C=C]$ is 1.5, whereas in the case of $[N_2H_4]:[C=C]$ equal to 2, the percent hydrogenation was dropped to 32.5



as shown in Figure 5.49. This may be due to the fact that increasing the amount of diimide may also increase the possibility of the reaction between the diimide generating nitrogen gas and hydrazine (see Equation 5.14). In addition, the oxidation of hydrazine with hydrogen peroxide is an exothermic reaction, too high amount of the reactants may result in excessive heat occurred in the reaction medium. Consequently, the NR latex loss its stability as some gel formation was found. The optimum hydrogenation condition of NR latex was obtained when the molar ratio of $[\text{N}_2\text{H}_4]:[\text{C}=\text{C}]$ equal to 1.5 was employed.

Table 5.29 Effect of the molar ratio of $[\text{N}_2\text{H}_4]:[\text{C}=\text{C}]$ on the percent hydrogenation at 60°C by keeping the equal molar ratio of $[\text{N}_2\text{H}_4]$ and $[\text{H}_2\text{O}_2]$

Molar ratio of $[\text{N}_2\text{H}_4]:[\text{C}=\text{C}]$	Hydrogenation (%)
0.5	17.3
1	21.3
1.5	38.0
2	32.5



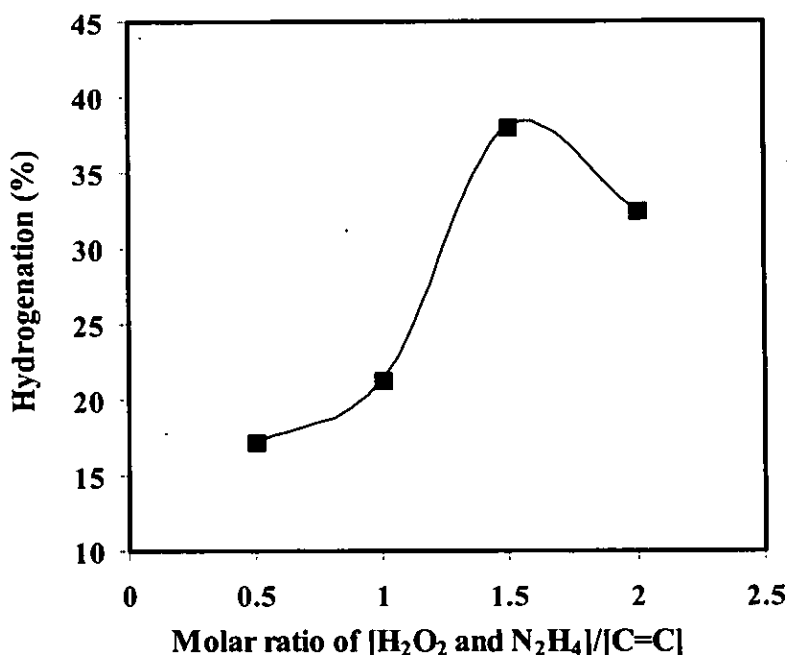


Figure 5.49 Influence of molar ratio of $[N_2H_4]:[C=C]$ on the percent hydrogenation at $60^\circ C$ by keeping the equal molar ratio of $[N_2H_4]$ and $[H_2O_2]$, using 20 %DRC at $60^\circ C$.

(g) Effect of Type of NR Latex

As it is well-known that NR latex has a larger particle size than the synthetic rubber latex such as NBR and SBR latex and the natural product contains some non-rubber constituents that may cover on the rubber particle. These characteristics may effect on the degree of hydrogenation. Therefore, it is important to study the hydrogenation of various NR latex types using diimide hydrogenation reduction. NRL was the NR latex obtained directly from tapping, normally stabilized by adsorbed long chain fatty acid and proteins, it was then centrifuged and stabilized with ammonia so called as high ammonia concentrated latx. Deproteinized NR or DPNL was obtained from treatment with the rubber latex with proteolytic enzyme, then stabilized by terric 161, named as DPNLT and sodium dodecyl sulfate (SDS), named DPNLS, skim fresh NR (SFNR), cream fresh NR (CFNRL), lower zone NR and upper zone NR were 7 types of rubber latex. The hydrogenation was carried out using the molar ratio of

$[C=C]=[N_2H_4]=[H_2O_2]$ equal to 1 at 60°C. The results of hydrogenation are shown in Table 5.30 and Figure 5.50.

It is expected that the indigenous proteins and phospholipids layer on the NR particle surface acted as a protector, resulting in retardation of diimide diffusion into the rubber particle. However, the DPNR latex was prepared to study this effect on hydrogenation because the removal of a large proportion of the proteins caused a broken membrane at the DPNR particle surface. The diimide molecule is therefore expected, to diffuse from the aqueous phase into the rubber phase within the DPNR particle through the small voids left on the membrane despite of the existence of SDS and terric 16A16. It was of interest to emphasize that the SDS added in DPNR latex did not affect on the hydrogenation. However, the presence of terric 16A16 found slightly effecting on the increase of hydrogenation level. It can be seen that the maximum of hydrogenation degree approximately 29% was found in the case of skim fresh NR latex. The explanation may involve the rubber particle size of SFNR is the smallest among the 7 different types of rubber latex.

Figure 5.51 shows a typical particle size distribution of NR latex at various types. The SFNR latex exhibits a bimodal particle size distribution range of 0.1 μm and 3.0 μm whereas other latex found a unimodal distribution, with the average particle size as given in Table 5.31. It can be seen that the average particle size of SFNR latex (0.473) is smallest as comparing with other types of latex, hence, the highest rubber surface area. This latex gave the maximum percent hydrogenation which is reached 29%.



Table 5.30 Results of percent hydrogenation of different types of NR latex obtained at various reaction times using molar ratio of $[C=C]:[N_2H_4]:[H_2O_2] = 1:1:1$ at $60^\circ C$

Reaction time (h)	Hydrogenation (%)						
	NR	DPNR (TER)	DPNR (SDS)	SFNR	CFNR	LNR	UNR
0	0	0.0	0.0	0.0	0.0	0.0	0.0
2	7.9	6.4	7.7	9.1	6.1	5.4	5.2
6	21.7	17.7	13.9	20.8	17.6	11.8	14.4
12	25.3	21.0	18.3	26.8	20.5	17.4	19.4
24	27.4	25.4	21.2	29.1	23.7	19.3	20.3

NR = NR latex stabilized by SDS, DPNR(TER) = deproteinized NR latex stabilized by terric, DPNR(SDS) = Deproteinized NR latex stabilized by SDS, SFNR = Skim fresh NR latex, CFNR = Cream fresh NR latex, LNR = Lower layer NR latex obtained from rubber zone 2, and UNL = Upper layer NR latex obtained from rubber zone 2.

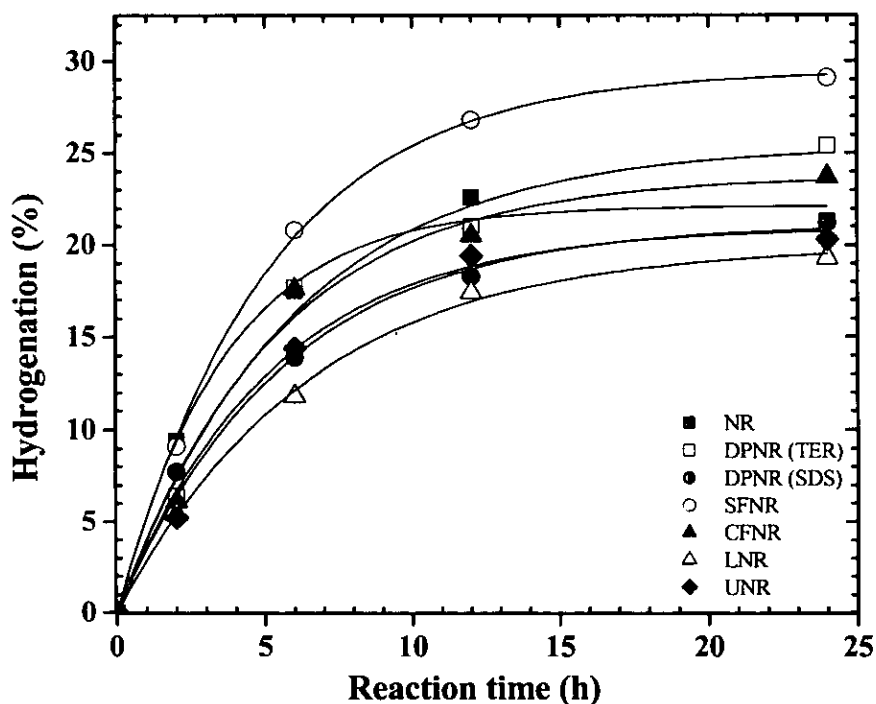


Figure 5.50 The percent hydrogenation of different types of NR latex obtained at various reaction times using 20% DRC with molar ratio of $[C=C]:[N_2H_4]:[H_2O_2] = 1:1:1$ at $60^\circ C$.



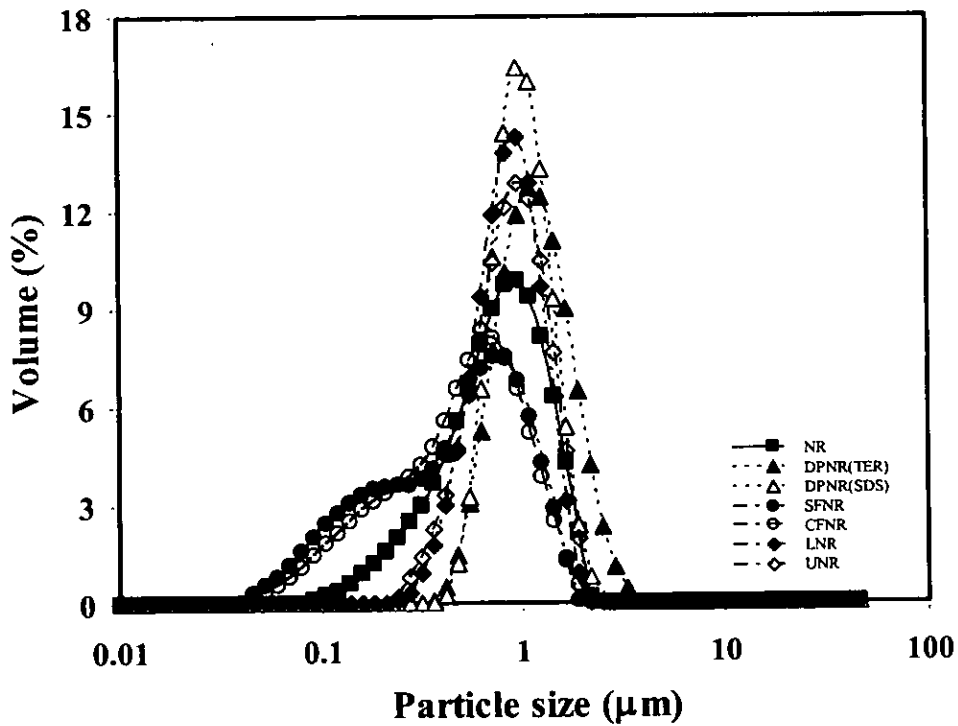


Figure 5.51 Particle size distribution of various types of rubber latex: (■) NR, (▲) DPNR(TER), (Δ) DPNR(SDS), (●) SFNR, (○) CFNR, (◆) LNR and (◇) UNR.

Table 5.31 Average particle size of NR latex at various types

Result analysis	NR	DPNR (TER)	DPNR (SDS)	SFNR	CFNR	LNR	UNR
D(0.1)	0.281	0.626	0.617	0.111	0.132	0.471	0.444
D(0.5)	0.724	1.063	0.984	0.473	0.489	0.811	0.832
D(0.9)	1.336	1.819	1.410	1.053	1.045	1.267	1.350
Specific surface area (m ² /g)	11.1	6.11	6.76	22.9	20.3	8.2	8.25
Uniformity	0.446	0.352	0.265	0.633	0.585	0.302	0.333



5.5.3 Side Reactions

(a) *Cis-Trans* Isomerization

As mentioned in former section, the detection of *trans*-1,4 polyisoprene isomer was observed by $^1\text{H-NMR}$ technique during hydrogenation of NR latex using oxidation of hydrazine by hydrogen peroxide. This evidence is similar to the hydrogenation of NR in organic solution using TSH.

The release of hydrogen molecule from diimide has been proposed to be occurred by the complex formation of the diimide and the C=C of the rubber. Hence, it can be proposed that the complex is an unstable intermediate for the isomerization to be taken place through the rotation of the weakened double bond as proposed by [25]. The mechanism of the *cis-trans* isomerization in this case is proposed here as demonstrated in Figure 5.52. It was found in several conditions the *cis-trans* isomerisation depending on the amount of reactants, the reaction time and temperature. This reaction could not be controlled as it was occurred randomly and the diimide complex formation may be probably taken place both with the *cis* and *trans* form of the polyisoprenic structure. It can be only concluded that *cis-trans* isomerization could occur during diimide reduction in latex system.

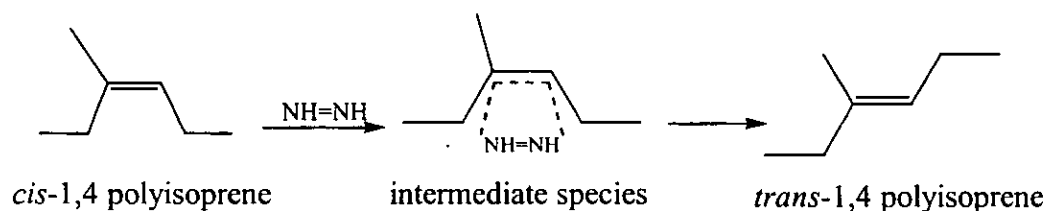


Figure 5.52 Formation mechanism of *cis-trans* isomerization occurred in diimide reduction in latex form.

(b) Crosslinking Reaction

In some conditions of hydrogenation of NR latex, the coagulation was detected Parker and co-workers [53] revealed that the conversion of nitrile butadiene rubber (NBR) latex to hydrogenated NBR latex is prone to a crosslinking side reaction that



was occurred concurrently with the desired reduction double bonds. The amount of gel content at different reaction temperatures was therefore investigated after recovery of the hydrogenated products in order to confirm the crosslinking reaction. Dried hydrogenated rubber 0.5 g (W_1) was put into 50 ml distilled toluene and kept for 24 h. The hydrogenated rubber solution was filtrated and dried at 60°C. After weighed hydrogenated rubber (W_2), gel content can be determined from the following formula:

$$\text{Gel content} = (W_2/W_1) \times 100$$

Table 5.32 The percent gel content of the hydrogenated products obtained from various reaction temperatures

Temperature (°C)	Gel content (%)
0	25.7
45	38.8
60	45.3
70	52.5
80	59.1

This was not surprising as the hydrogenation of NR in latex phase involved the presence of H_2O_2 which is prone to be dissociated to hydroxyl radicals. At a suitable condition, these radicals may subtract an allylic proton of the *cis*-1,4 polyisoprenic unit on the rubber chains, forming the rubber macroradicals. The rubber macroradical can interact with each other forming a crosslinked product as shown in Figure 5.53, depending probably on the concentration of the radical species and the concentration of the reaction medium as well as the reaction time and temperature. It was found in our studies that, after the hydrogenated rubber obtained was dried and kept in solid form for a few days, incompleted redissolution was observed. It can be assumed that hydroxyl radical induce the intermolecular reaction between the rubber chains as shown in Figure 5.53.



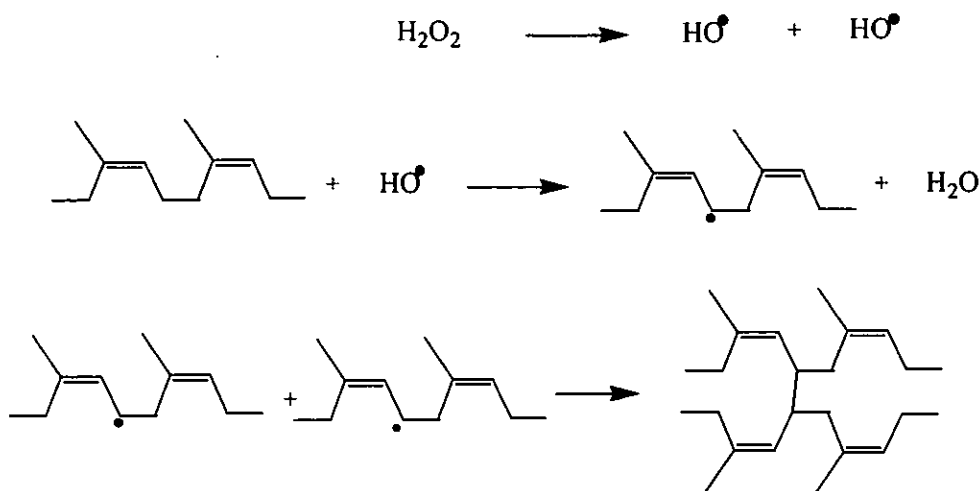


Figure 5.53 Proposed crosslinking reaction during diimide hydrogenation of NR in the presence of hydrogen peroxide.

5.5.4 Kinetic Study of Diimide Hydrogenation of NR Latex

The kinetic study of the addition of hydrogen molecule onto *cis*-1,4 polyisoprenic units of NR was considered by using the data collected from ¹H-NMR analysis at different temperatures. Considering the plots of the degree of hydrogenation with reaction time at various temperatures (section 5.5.2), it was found that the diimide reduction reaction followed apparently the first-order at the early stage of reaction time in an olefin substrate. The first-order dependence was also reported by Sarker De et. al. [55, 56] for hydrogenation of SBR copolymer.

To determine the activation energy of the hydrogenation, the kinetics of hydrogenation of NR latex at 30, 45, 60, 70 and 80°C performed with the molar ratio of [C=C]=[N₂H₄]=[H₂O₂]=1 were investigated. By assuming that the reaction is first-order, the differential rate law of hydrogenation of NR can be written in Equation 5.16.

$$\begin{aligned}
 -\frac{d[\text{C}=\text{C}]}{dt} &= k[\text{C}=\text{C}] \\
 &= k[1-x_a]
 \end{aligned}
 \tag{5.16}$$



where x_a is the fraction of double bond hydrogenated, k is the first-order rate constant and t is the reaction time. The determination of k was explored on the basis of integral method. ^1H NMR was used to monitor the number of the residual carbon-carbon double bonds of the rubber chains.

$$\frac{d[1-x_a]}{[1-x_a]} = -kdt$$

$$\ln[1-x_a]_t = -kt + \ln[1-x_a]_0 \quad (5.17)$$

The first order rate coefficient was determined from the slope of the linear $-\ln[1-x_a]_t$ versus reaction time (t) plot in accordance with Equation 5.17 hence the reaction rate constant (k) can be determined as shown in Table 5.33.

Table 5.33 The rate constant (k) and $\ln k$ of hydrogenation reaction at different temperatures

T (°C)	T (K)	k (sec ⁻¹)	$\ln k$
30	303	2.43×10^{-4}	-8.32
45	318	3.05×10^{-4}	-8.09
60	333	5.54×10^{-4}	-7.50
70	343	6.68×10^{-4}	-7.31
80	353	6.82×10^{-4}	-7.29

The activation energy (E_a) for the addition of hydrogen molecule onto the carbon-carbon double bond of rubber molecule can be estimated from Arrhenius equation in Equation 5.18.

$$k = Ae^{-E_a/RT} \quad (5.18)$$

The plot of $\ln k$ versus reciprocal of temperatures (Figure 5.54) gave a straight line in which expressed as $\ln k = \frac{-2478}{T} - 0.175$. The calculated activation energy is found to be 32.0 kJmol^{-1} . This activation energy (E_a) obtained corresponds in magnitude to the activation energy of the addition of hydrogen molecule onto



unsaturated units of NR. The obtained E_a value is actually higher than the E_a (9.5 kJmol^{-1}) needed to hydrogenate the butadiene units of SBR carried out in a similar procedure. This can be used to explain the difficulty in approaching the diimide toward the double bond of NR latex.

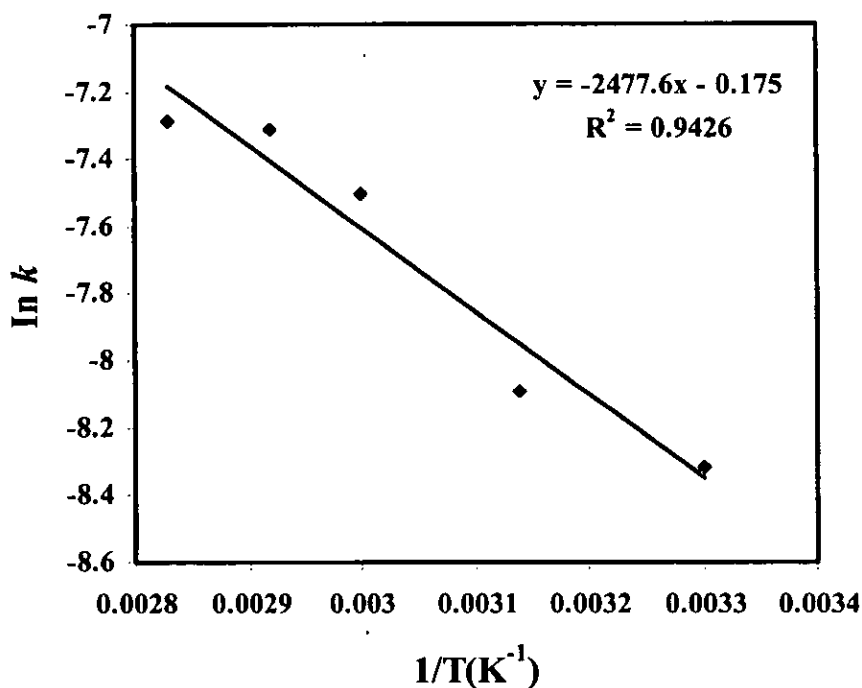


Figure 5.54 Plots of $\ln k$ and $1/T$ from diimide hydrogenation of NR latex.



Part III: Molecular Characteristic, Thermal and Rheological Properties of Hydrogenated Rubbers

This part concerned the investigation of the molecular characteristic of NR and the hydrogenated products using Raman and ^{13}C -NMR spectroscopies in solid state. The thermal behaviour of NR, ENRs and the hydrogenated samples obtained were analyzed by differential scanning calorimeter (DSC) and thermo-gravimetric analyser (TGA). In addition, the change of chemical structure of the samples at various temperatures investigated by using Raman spectroscopic technique i.e. Raman shift evidence is also presented. In rheological study, the flow properties of the samples at different hydrogenation levels are studied in the terms of storage (G') and loss moduli (G''). Finally, the correlation between molecular characteristic and physical properties will be discussed.

5.6 Molecular Dynamic Characteristic Analysis

Raman scattering and solid state ^{13}C -NMR techniques were used to study the molecular dynamic characteristic of the natural rubber modified by hydrogenation. These techniques can provide information on the molecular scale as they concern the mobility of the molecular chain such as vibration, and rotation of the chemical bond.

5.6.1 By Raman Spectroscopy

Raman spectroscopy has been successfully used to analyze the percentage of hydrogenation of NR and ENRs as described in section 5.2 and 5.3 as the signal of $\text{C}=\text{C}$ of the rubber is strongly Raman active. However, it has also been effectively used to investigate the molecular deformation of other polymers such as polyethylene and poly(ethylene terephthalate) [105,106]. The orientation of the sample can be related to the molecular polarizabilities therefore Raman scattering can be applied for molecular characteristic of polymers.



As the Raman spectra of NR and ENR showed a strong vibration band of C=C at 1664 cm⁻¹ and the evolution of this signal was obviously observed after hydrogenation. As a result, this peak can be used for the investigation of the molecular scale by observing the shift on the position of the C=C signal after hydrogenation i.e. at 1664 cm⁻¹. Generally, the vibrational wavenumber in the stretching mode of a diatomic molecule relates with the force constant or the stiffness of the bond. Therefore it can be estimated that if the vibrational wavenumber is increased the force constant of the two carbon atoms is increased.

The model of a chemical bond in vibration spectroscopy is one of point masses connected by a harmonic spring. The relationship of the vibrational wavenumber of the stretching mode of a diatomic molecule can be determined using Equation 5.19 (see also section 3.4).

$$\nu(cm^{-1}) = \frac{1}{2\pi c} \sqrt{k_f \frac{[M_A + M_B]}{M_A M_B}} \tag{5.19}$$

where k_f is the force constant, or stiffness of the bond, and M_A and M_B are the masses of two atoms.

The correlation between force constant, k_f and square of wavenumber, $(\bar{\nu})^2$ is shown in the following:

$$E = h\nu = \frac{hc}{\lambda} = hc\bar{\nu} \tag{5.20}$$

$$\bar{\nu} = \frac{1}{2\pi} \sqrt{k_f \frac{[M_A + M_B]}{M_A M_B}} \tag{5.21}$$

$$\bar{\nu} = \frac{1}{2\pi} \sqrt{k_f \mu}$$

$$(\bar{\nu})^2 \propto k_f \mu \tag{5.22}$$

where $\bar{\nu}$ is the wavenumber, and μ is the reduced mass of the carbon-carbon double bond, respectively.

By this assumption, the force constant between two carbon atoms of the carbon-carbon double bond is one dimension along with the molecular rubber chains. The estimated force constant of C=C bond can be estimated according to Equation 5.22.



The relative variation force constant (Δk_f) of modified form can be also determined by using the estimated force constant of C=C bond in modified rubber $(k_f)_1$ comparing with unmodified rubber $(k_f)_0$ as follows:

$$\Delta k_f = \frac{(k_f)_1 - (k_f)_0}{(k_f)_0} \quad (5.23)$$

where Δk_f is relative variation force constant, $(k_f)_0$ is the estimated force constant of unmodified rubber and $(k_f)_1$ is the estimated force constant of modified rubber.

In this work, the Raman scattering spectra of the hydrogenated samples were collected using a triple spectrograph configuration with a 1800 lines/mm grating in the Raman range of 1640-1750 cm^{-1} as described in section 4.6. The background was to be subtracted from all spectra obtained for each sample before analysis as the artifact from the background scattering might be occurred from the air in the beam path, and from the sample stage. The precise peak position of C=C bond of NR is resolved by fitting with Lorentzian function.

(a) Raman Shift of C=C Bond of HNR

The relationship between Raman shift of the characteristic line at 1664 cm^{-1} attributing to the C=C stretching mode of NR and HNR at various hydrogenation levels (30-85%) was investigated. Figure 5.55 shows the Raman spectra of the NR and various HNRs in the Raman shift range of 1664-1700 cm^{-1} . It can be seen that the signal position of C=C has increasingly shifted to higher wavenumber with the evolution of hydrogenation level. The Raman shift evolution of the C=C bond position was found from 1665.66 cm^{-1} of NR to 1668.05 cm^{-1} of 85% hydrogenation. The results of the Raman position of the C=C bond was used to estimate the force constant and relative variation force constant using Equation 5.22 and 5.23 and the results are shown in Table 5.34.

The plot between the relative variation force constant and hydrogenation level is shown in Figure 5.56. It was found that the relative variation force constant of the hydrogenated sample is linearly increased when the hydrogenation level is increased. This might be estimated that after hydrogenation the molecular chain of the rubber is more rigid or less flexible as the force constant is increased, the molecular bonds in



rubber chain needs more energy for the vibration. The explanation can be due to the transformation of the *cis*-1,4 polyisoprenic structure into partially hydrogenated form which possess the close packing structure of ethylene-alt-propylene moiety in the molecular structure. In addition, it was also found that the *cis*-structure was transformed into *trans*-structure of the 1,4-polyisoprene and the later structure is more rigid than the former one [34]. These results are in accordance with the macroscopic behavior of the hydrogenated product that the less elastic rubber is resulted after hydrogenation.

It can be concluded that the study of the signal in Raman shift might be reliable to the level of hydrogenation of the resulting product as well as its physical properties. This method appears to be an alternative to follow the degree and rate of hydrogenation of the rubber.

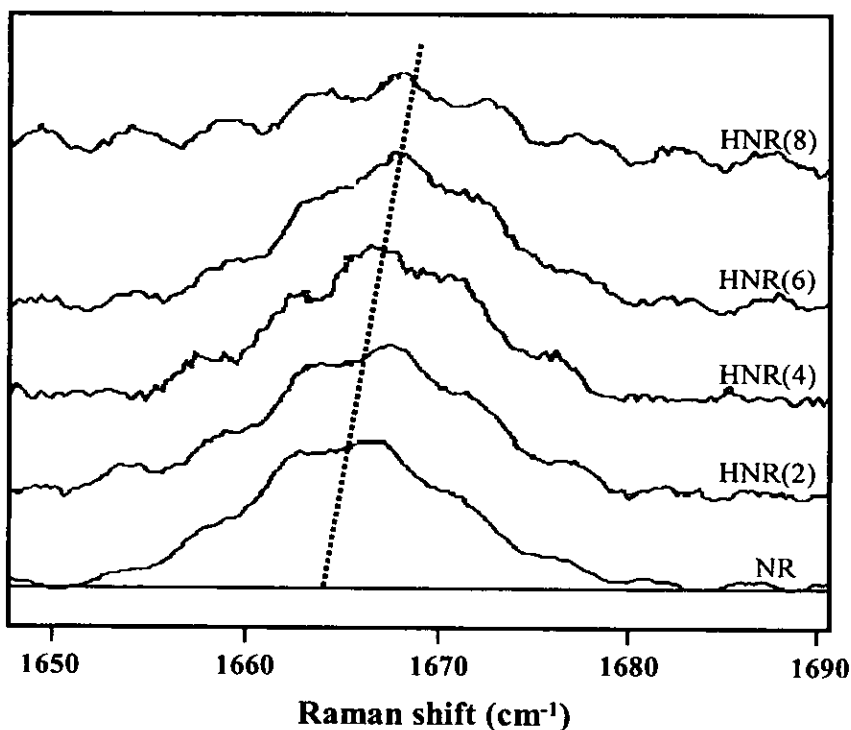


Figure 5.55 Characteristic of Raman shift of C=C bond at 1664 cm⁻¹ of NR and HNR samples.

Table 5.34 Raman shift, square of wavenumber ($\bar{\nu}^2$), estimated force constant ($\approx k_f$) and relative variation force constant (Δk_f) of the characteristic peak of C=C stretching mode of the HNRs at various hydrogenation levels

Sample code	Hydrogenation (%)	Raman shift (cm^{-1})	Square of Raman shift ($\bar{\nu}^2$)	Estimated force constant ($\approx k_f$)	Relative variation force constant (Δk_f)
NR	0	1665.66	2774436	16613391	0.000
HNR(1)	5.7	1665.70	2774548	16647287	0.004
HNR(2)	27.7	1666.40	2776875	16661248	0.088
HNR(3)	39.1	1666.61	2777589	16665533	0.114
HNR(4)	57.5	1667.21	2779584	16677505	0.186
HNR(6)	79.4	1667.63	2780975	16685853	0.236
HNR(8)	84.9	1667.56	2780772	16684634	0.228

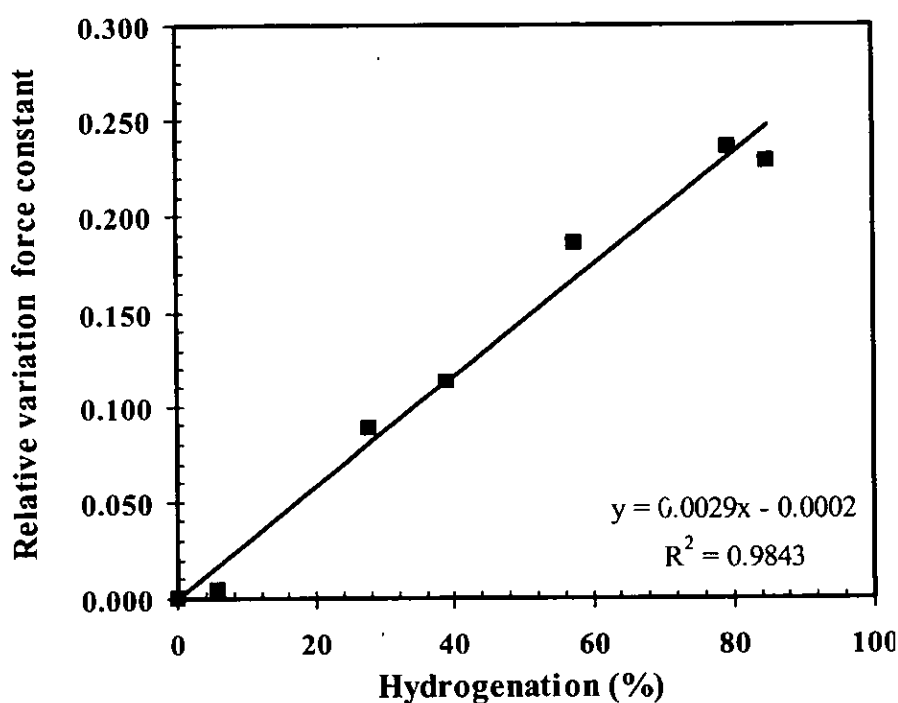


Figure 5.56 The plot of the relative variation force constant versus the hydrogenation level of the HNR samples.

(b) Raman Shift of C=C Bond of HENR Molecular Chain

The study of the Raman shift was then applied to the hydrogenated ENR. Figure 5.57 presents the Raman scattering spectra in the region of 1650-1700 cm^{-1} of the ENR-10 containing 10 mol% epoxide content and the hydrogenated ENRs at various reaction times. As can be seen in Figure 5.57, there are slightly shift of the wavenumber of C=C bond in the hydrogenated ENR similar to in the case of hydrogenated NR. It seems likely that increasing the hydrogenation level, the higher force constant is increased. This should give the information that the transformation of the unsaturated rubber into partially saturated one would result in increasing the rigidity of the molecular chain or increasing the fraction of the stiffness part in the samples.

The Raman shift, estimated force constant ($\approx k_f$) and relative variation force constant at different hydrogenation degrees are summarized in Table 5.35. The plot of the relative variation force constant and the percent hydrogenation of the ENR-10 shown in Figure 5.58 did not show a linear relationship between the two variables which is different from in the case of hydrogenated NR. It was found that the force constant is slowly increased when the percent hydrogenation was less than 50% but far above that point the high increase of the force constant was found significantly. This may be due to the fact that at low degree of hydrogenation, there is not much difference in molecular characteristic between the ENR-10 and the hydrogenated sample as the ENR is considered more rigid than the NR. But when the hydrogenation was occurred there was also epoxide ring opening and the fixation of the TSOH by-product on the molecular chain, then the difference in the molecular characteristic is progressively observed. This is confirmed by the fact then when hydrogenation was increased upto more than 50%, the chain stiffness was revealed significantly. This result confirmed that the fixation of the TSOH and the epoxide ring opening or the formation of oxirane ring in the molecular chain leads to the more rigid structure in the rubber chains after modification.



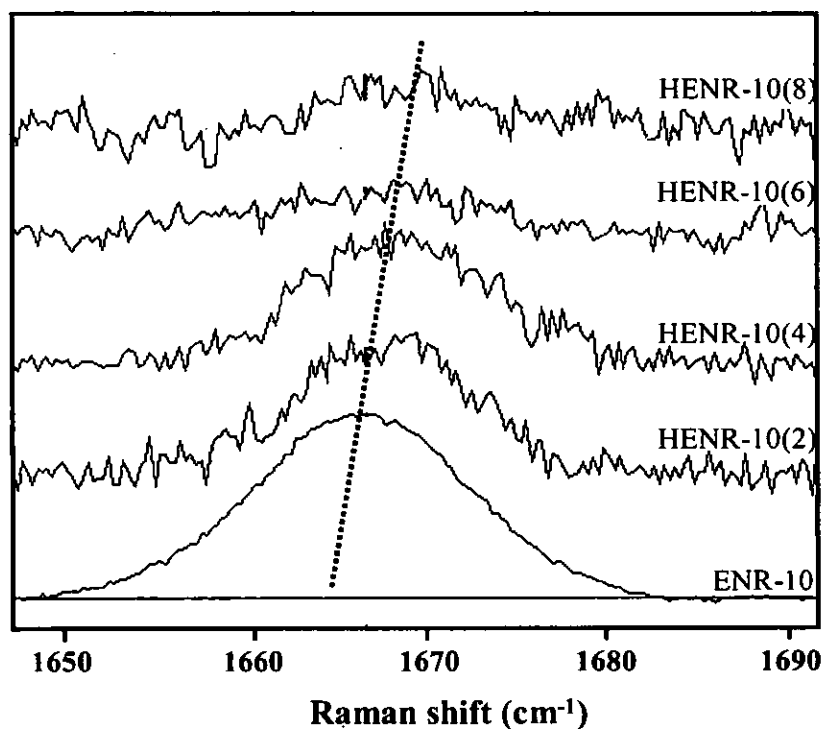
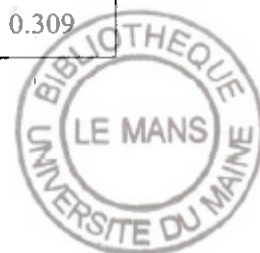


Figure 5.57 Characteristics of Raman shift of the C=C bond at 1664 cm^{-1} of HENR-10 samples.

Table 5.35 Raman shift, square of wavenumber (ν^{-2}), estimated force constant ($\approx k_f$) and relative variation force constant (Δk_f) of the characteristic peak of C=C stretching mode of the HENR-10

Sample code	Hydrogenation (%)	Raman shift (cm^{-1})	Square of Raman shift (ν^{-2})	Estimated force constant ($\approx k_f$)	Relative variation force constant (Δk_f)
ENR-10	0.0	1666.33	2776656	16659934	0.000
HENR-10(0.5)	35.0	1666.69	2777856	16667133	0.043
HENR-10(2)	70.0	1667.65	2781057	16686339	0.158
HENR-10(4)	84.6	1668.41	2783592	16701552	0.250
HENR-10(6)	92.0	1668.72	2784626	16707759	0.287
HENR-10(8)	93.0	1668.90	2785227	16711363	0.309



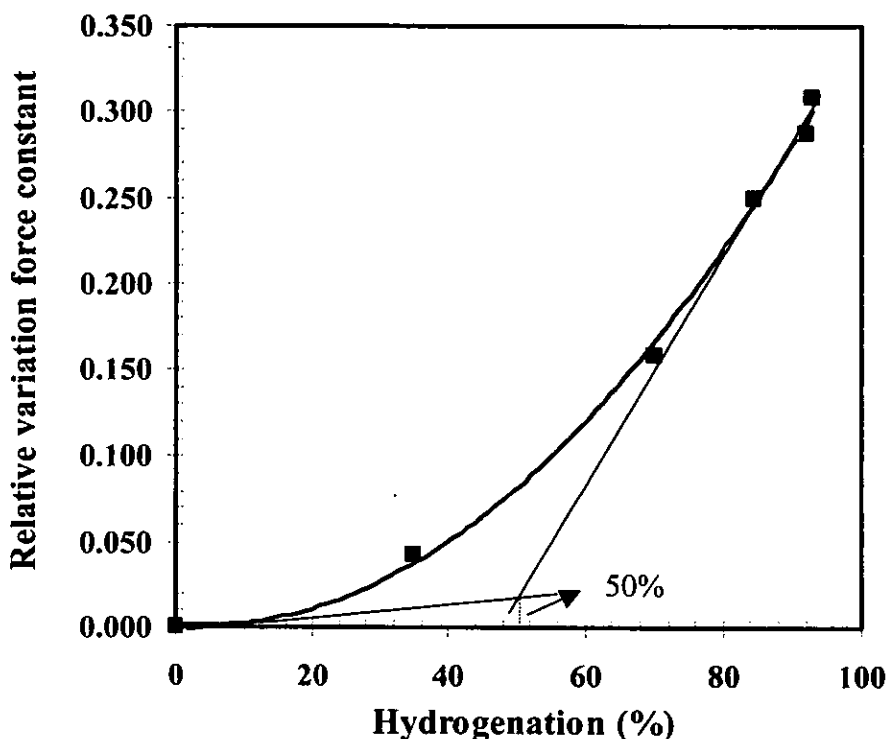


Figure 5.58 The plot of the relative variation force constant versus the hydrogenation level of the HENR-10.

5.6.2 By Solid State NMR Spectroscopy

In this section, the molecular characteristic of NR, ENR and hydrogenated rubbers are investigated by solid state ^{13}C NMR spectroscopy with HD/MAS and HD/MAS/CP techniques in term of peak width of carbon signal of the molecular chain. The dynamic of cross polarization experiment is also applied to study the molecular dynamic of the rubber chain after modification.

(a) Molecular Characteristic of NR and HNR

A stack plot of the solid state NMR spectra of NR and HNRs at different hydrogenation times is shown in Figure 5.59. The ^{13}C -NMR spectra of the HNRs consist of two well separated aliphatic and olefinic regions as previously assigned in section 5.2. It can be seen that the NMR line widths of carbon signals of HNRs are broader than those of the NR before hydrogenation. The ^{13}C -NMR line widths can be

then estimated from curve fitting by DM 2002 software of the spectra of NR and HNRs. The values of line width of various carbons i.e. methyl (C-5 of *cis*-1,4 polyisoprene unit and C-10 of saturated unit), methylene (C-1 and C-4 of *cis*-1,4 polyisoprene unit and C-6, C-8 and C-9 of the hydrogenated unit), and the methine carbon (C-7 of the hydrogenated unit), are presented in Table 5.36. The line widths and hydrogenation level are plotted in Figure 5.60. It was obviously observed that the line widths of carbon signals on the molecular chains increase with increasing the hydrogenation level. Usually, the line widths of solid state NMR spectra with HD/MAS technique in the single radio frequency pulse mode are mainly determined by the magnitude of carbon-proton dipolar interaction, which depends on the relative position of the randomly oscillating nuclei. In the hydrogenated samples, the more line broadening was observed, with the higher hydrogenation level. The explanation is concerned with anisotropy in the segmental motion of the rubber chains which should be due to the presence of several conformations (the formation of molecular packing of saturated units and probably the *trans*-structure of *cis*-1,4 polyisoprene unit) and the stiffness fractions. In addition, it was observed that the line width of methyl carbon has narrower than that of methylene and methine carbons on the molecular rubber chains. This is due to rate of methyl group motion enough to average hetero-nuclear interaction.



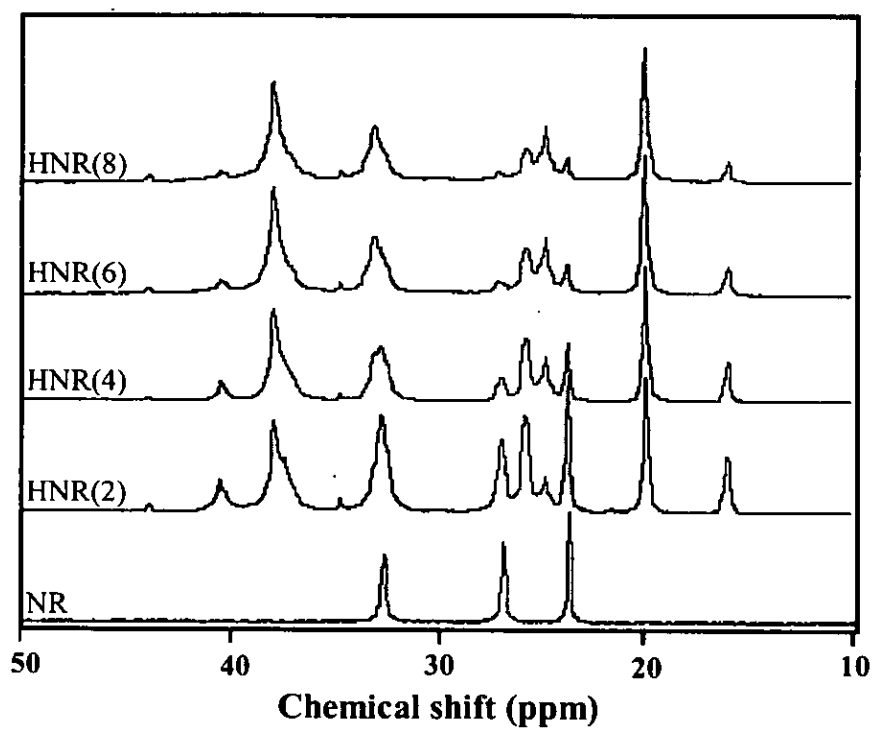


Figure 5.59 A stack plot of solid state HD/MAS ^{13}C -NMR spectra of NR and the HNR samples obtained at 2, 4, 6 and 8h.

Table 5.36 The line widths of NMR peaks of hydrogenated rubber at various hydrogenation levels

Hydrogenation (%)	NMR Line width (Hz)						
	C-1	C-4	C-5	C-7	C-6,C-8	C-9	C-10
41	25.66	26.42	15.10	26.42	33.96	20.38	16.60
58.4	26.42	27.93	15.85	32.46	36.23	26.42	18.11
72	30.95	31.70	17.36	34.72	39.25	30.95	19.62
80	35.47	34.72	18.11	38.49	40.76	29.44	21.13

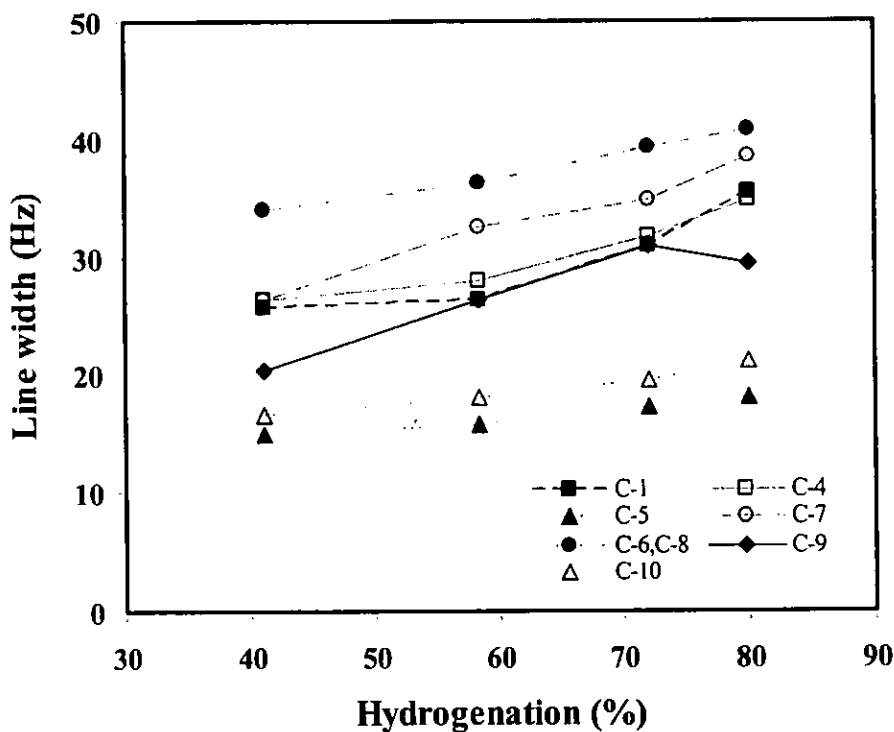


Figure 5.60 The plot of line widths of solid state HD/MAS ¹³C-NMR spectra of the HNRs obtained at various hydrogenation levels: (■) C-1, (●) C-5, (▲) C-6 and C-8, (□) C-4, (○) C-7, (△) C-9 and (◇) C-10.



-Dynamic of the Cross-Polarization (CP)

In this study, the CP experiment was carried out and monitored in order to optimize the condition for further achievement of the molecular structure.

The solid state NMR spectra of HNR at various contact times were investigated and illustrated in Figure 5.61. It was found that at very small contact time (0.08 ms), the resonances assigned to signals of methine and methylene groups (33 and 38 ppm) of hydrogenated fraction are clearly present. This result reflects the largest dipolar ^1H - ^{13}C interaction. The intensity of the carbon resonance of methyl group at 20ppm progressively increased at longer contact times.

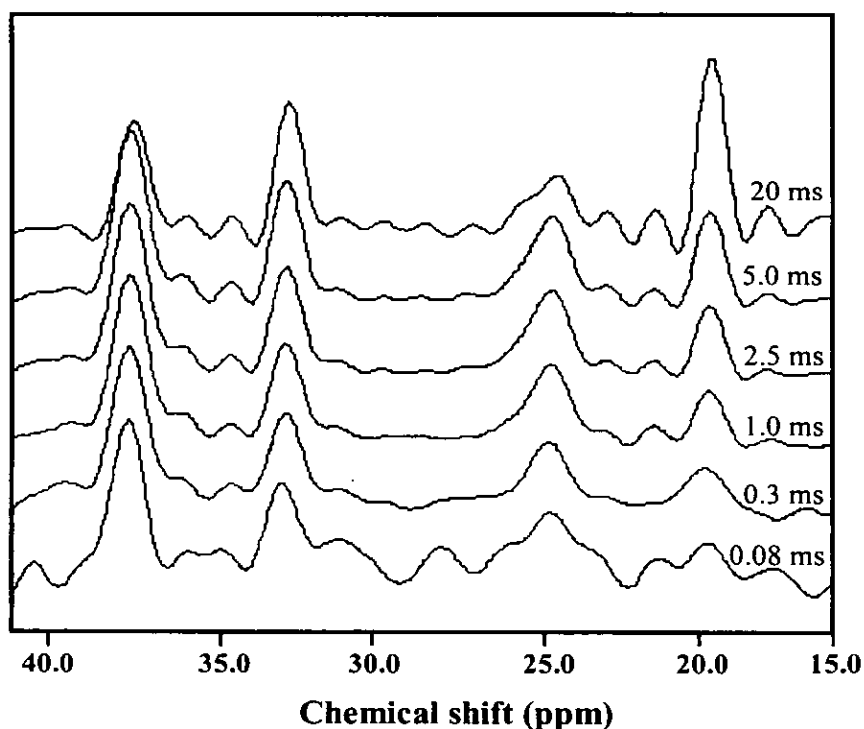


Figure 5.61 A Stack plot of solid state ^{13}C -NMR spectra of the hydrogenated NR (85%) at various contact times in the chemical shift range of 15- 40 ppm.

The kinetic of cross polarization was estimated to optimize the CP experiment, to obtain chemical structural information on the sample and to study the molecular dynamic of the rubber chains. In the variable contact-time experiments, the peaks of

carbon signal were fitted by using DM2002 software to simulate the carbon position, line width and intensity of solid state NMR spectra.

Figure 5.62 shows the plots of the normalized peak intensity as function of the contact time (t) of the ^{13}C signal of the aliphatic carbons as a function of contact time. The normalized peak intensity of carbon signal of methyl group (20 ppm) clearly increases with contact time after that it remains constant as shown in Figure 5.62(a). This means that methyl group of saturated units on the molecular chains has the highest mobility corresponding to lower relaxation rates. Other CP experimental curves show the changes in the ^{13}C signal intensities of the aliphatic carbons as a function of contact time. At the beginning of the curve, the intensities of peak progressively increase and reach the maximum prior to decreasing with increasing contact time. The increase in the ^{13}C intensities at short contact times is dominated by the CP rate ($1/T_{CH}$), whereas the decrease in the intensities for the longer contact times by the ^1H spin-lattice relaxation rate ($1/T_{1\rho}^H$).

By basing on Equation 3.26, it can be described the double exponential behavior of CP intensity $M(t)$ versus contact time t . The dependence of the peak shape on contact time (see Figure 5.61) would mean that the peak under consideration consists of several components which have different line widths and cross polarization at different rates. Hence, in this study, the line width and line sharp of each carbon resonance peaks were kept constant value during the simulation process.

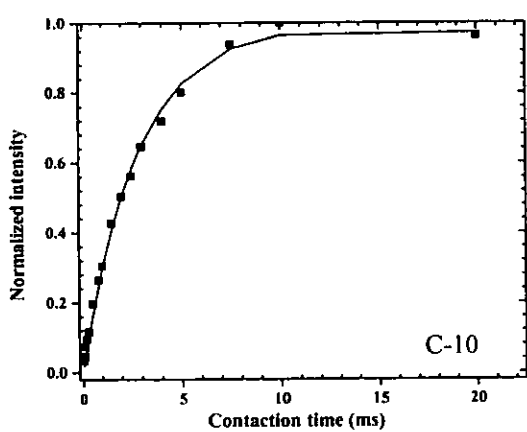
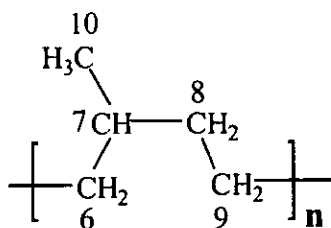
The mathematic function was used to simulate the kinetic curve (see in Figure 5.62), of which parameters are the most important about the physical meaning. Then, the physical parameters can be analyzed and given in Table 5.37. It was found that $T_{1\rho}^H$ relaxation of methyl group (> 100 ms) has a remarkably high value with respect to the $T_{1\rho}^H$ relaxation of methylene (16.3 ms) and methine (31.7 ms) groups because of the highest mobility of methyl group on the molecular chains. The $T_{1\rho}^H$ of methine (CH) carbon is larger than the $T_{1\rho}^H$ of methylene (CH_2) carbons. This indicated that the methylene carbon is less mobile than methine carbon on the saturated fractions of the rubber chains.



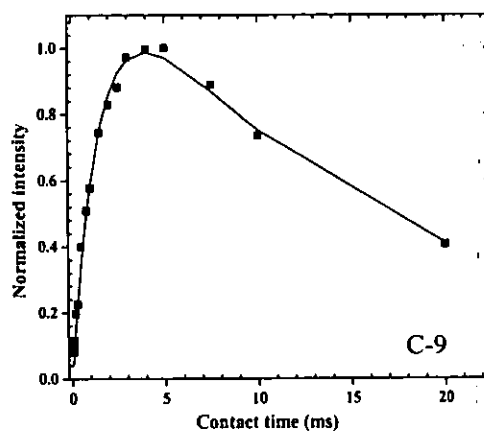
In addition, the contact times that provide the maximum peak intensities of methylene (4 ms) and methine (5 ms) carbon are different. This is due to the difference in contribution of the molecular motion to the CP efficiency.

Table 5.37 shows that the cross polarization time T_{CH} of methyl carbon (2.91) is also the highest value as comparing with other values i.e. for methylene and methine carbon are 1.51 and 1.81 ms, respectively. This means that the methylene groups of the molecular chains take shorter time to cross polarize, while the methyl group need longer time to be polarized. This is due to the methylene carbons of saturated units appearing on the molecular chains connected with other carbons along the rubber chains. The CP time constants T_{CH} are the characteristic of specific functional groups, since they are governed by dipolar interactions between the source spins H and the target spins C. The dipolar interaction has a $1/r^3$ dependence on the interaction distance r , so that in general T_{CH} depends on the number of the nuclei involved in CP and on their distance position. The CP rate constant $1/T_{CH}$ depends on the number of protons and the mobility of the modified group in the macro-molecular chain. The larger a number of protons in the modified part was found, the stronger the C-H dipolar interaction and the faster the cross-polarization were observed. This reason explains why the C-25 and C-38 of the CH_2 groups cross-polarizes faster than the CH group. On the other hand, the rate of methyl carbon cross-polarization is the slowest as compared to CH, and CH_2 group. The rapid rotation of methyl group reduces dipolar interactions between its component spins.

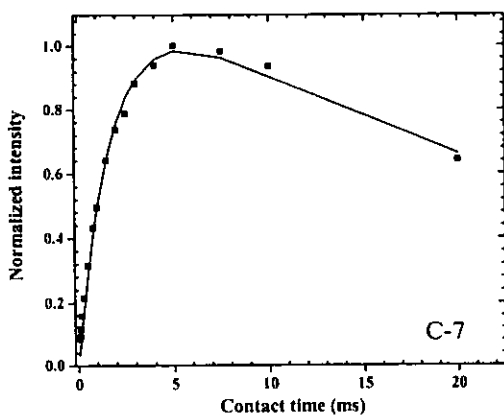




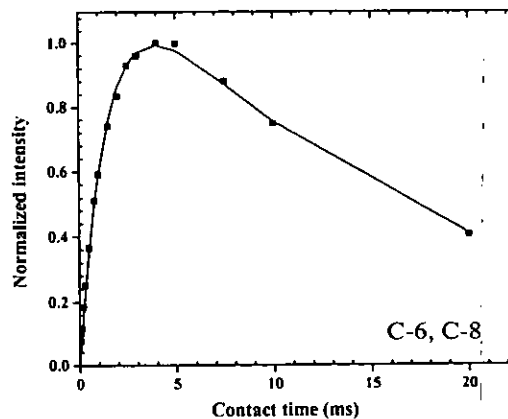
(a)



(b)



(c)



(d)

Figure 5.62 Variation of the magnetization with contact time in a CP experiment for HNR (85%) of carbon positions at C-10 (a), C-9 (b), C-7 (c) and C-6, C-8 (d).



Table 5.37 The spin-lattice relaxation time ($T_{1\rho}^H$) and cross-polarized time (T_{CH}) obtained from the fitting kinetic CP curve in all carbon resonances of HNR (85%)

Carbon position	Group	$T_{1\rho}^H$ (ms)	T_{CH} (ms)
C-20	CH ₃	>100	2.91±0.23
C-25	CH ₂	16.4±1.4	1.51±0.1
C-33	CH	31.7±4.6	1.81±0.14
C-38	CH ₂	16.3±1.0	1.51±0.07

(b) Molecular Characteristic of ENR and HENR

The MAS and HD/MAS ¹³C-NMR solid state spectra of ENR-22 having 22 mol % epoxidation levels are illustrated in Figure 5.63. A comparison between the MAS and HD/MAS spectra of ENR-22 was noticed that the broader line widths and extra signals appeared in the MAS spectrum as a result of ¹H-¹³C J coupling of the macromolecular chains. From the MAS spectrum of ENR-22, the extra peaks at 64 and 125 ppm provide information about the ¹H-¹³C J coupling of proton attached on the oxirane and olefinic units of partially epoxidized NR. The line broadening of carbon signals were also found in the range of 15-35 ppm due to the ¹H-¹³C coupling of proton from methylene and methyl groups. Therefore, the ¹H-¹³C dipolar interactions were removed using high power decoupling (HD) technique and the HD/MAS spectra of ENR-22 is present.



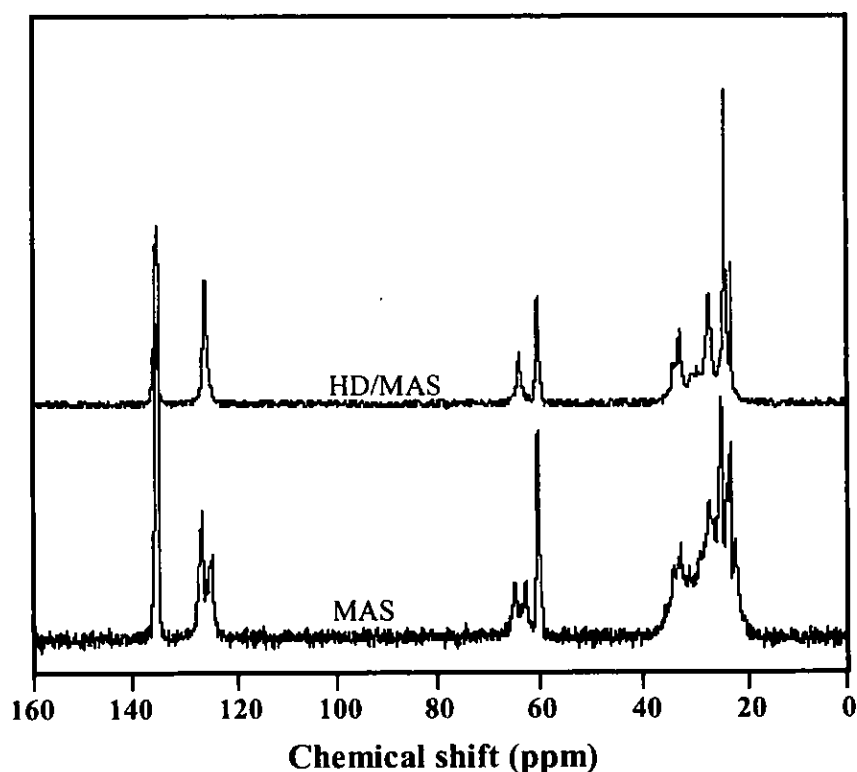


Figure 5.63 A stack plot of MAS and HD/MAS ^{13}C -NMR spectra of ENR-22 containing 22 mol% epoxy content.

Figure 5.64 shows the stack plots of HD/MAS spectra of ENR-10, ENR-15, ENR-22 and ENR-40 containing 10, 15, 22 and 40 % mol epoxide units, respectively. From the NMR spectra of ENR, the curve fitting (DM2002) was used to simulate the line width of each carbon signal. The line widths of HD/MAS spectra of ENR are broader than that of the NR one. It can be seen in Figure 5.64 that the line broadenings of carbon signals of ENR significantly increase with the extent of epoxidation. The result of line widths of the carbon signals at 64 and 60 ppm corresponding to the characteristic of oxirane units as a function of epoxidation ENR are shown in Table 5.38. Line broadenings of two carbon signals of epoxy units in ENR occur related to distributions of isotropic chemical shifts and to dipolar interactions which may not be completely averaged and arising from a variety of local conformations. In addition, the increment of the line width of oxirane units on the molecular chains was detected, which resulted in the increase of rigid segments of the

macromolecular chains after epoxidation. In Figure 5.65, the line width value of the signal at 64 ppm belong to methine carbon is broader than that of quaternary carbon signal at 60 ppm. It might be assumed that the higher amount of oxirane units is connected together along with the rubber chains presenting the broader line width.

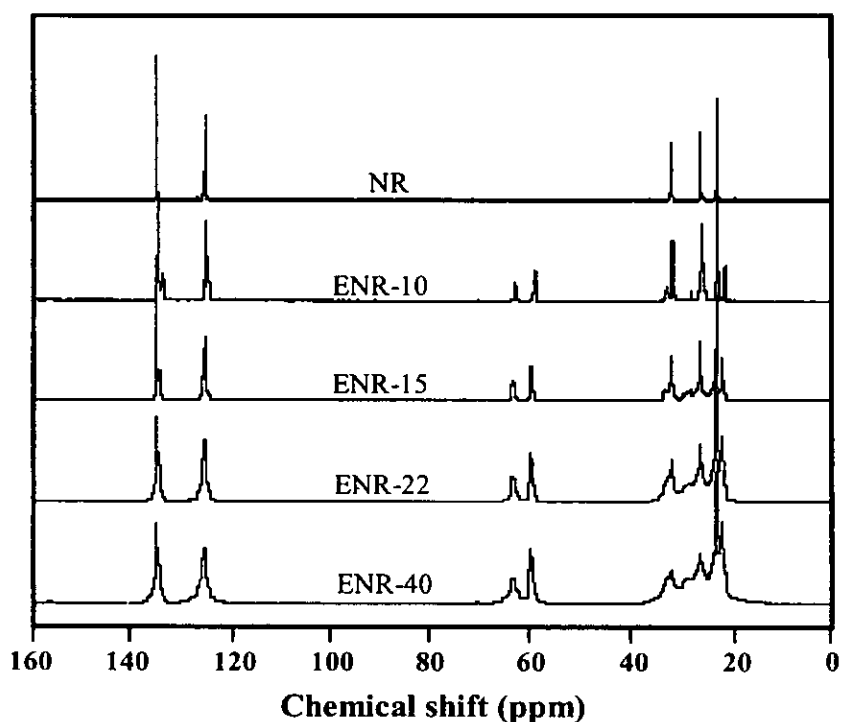
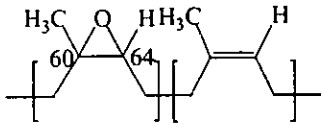


Figure 5.64 Stack plots of HD/MAS ^{13}C -NMR spectra of NR, ENR-10, ENR-15, ENR-22 and ENR-40 containing 10, 15, 22, and 40 mol% epoxy content, respectively.

Table 5.38 The line widths of the NMR lines at 60 and 64 ppm in ENR with various epoxidation levels

			
Sample code	Epoxidation (%)	line width of C-64 (Hz)	line width of C-60 (Hz)
ENR-10	10	20.38	13.59
ENR-15	15	42.27	20.38
ENR-22	22	55.85	30.19
ENR-40	40	111.71	43.02

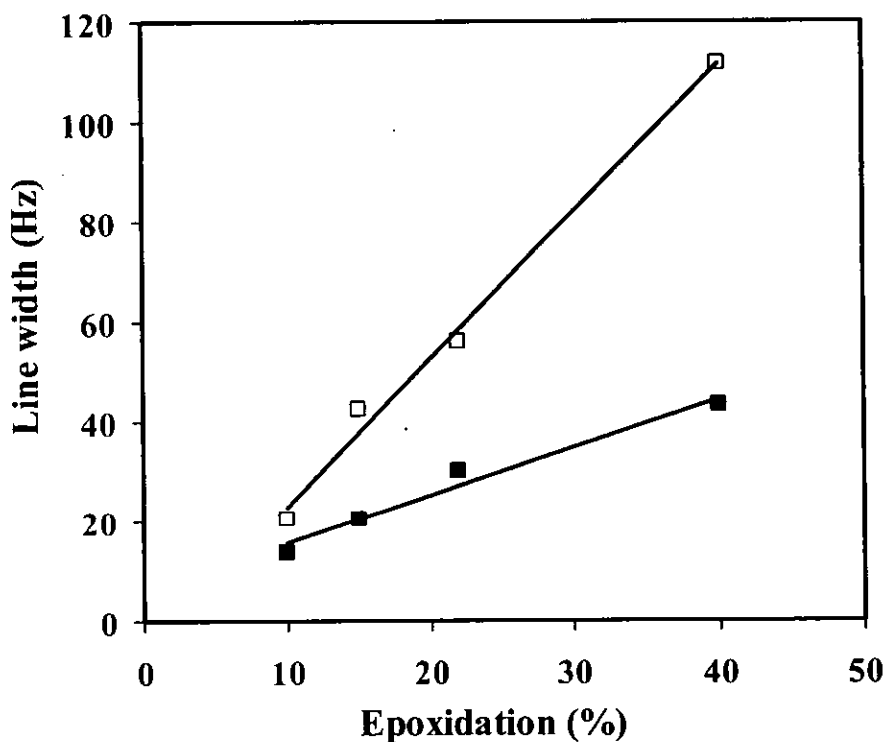


Figure 5.65 Line widths of the characteristic of oxirane units with extent of epoxidation: (□) quaternary carbon at 60 ppm and (■) methine carbon at 64 ppm.

A comparison stack plots between the HD/MAS spectra of ENR-10 and the HENR-10 obtained at 8h is illustrated in Figure 5.66. No characteristic resonances of oxirane units are observed in the spectrum of the hydrogenated sample as mentioned in section 5.3. The line broadenings (see Figure 5.66) clearly observed in the recorded solid state NMR spectra of the hydrogenated samples with respect to the non-hydrogenated one. The increment of line widths of carbon characteristic on molecular chains may be attributed to three factors: (i) strong isotropic dispersion, (ii) dipolar interaction and (iii) several conformations in the rubber chains.

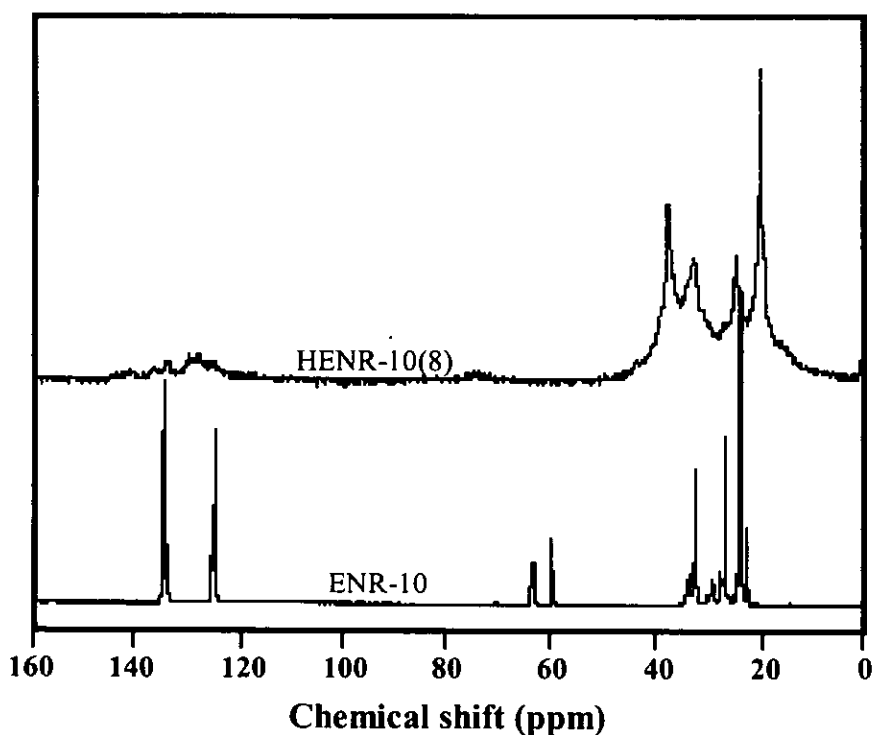


Figure 5.66 HD/MAS ^{13}C -NMR spectra of ENR containing 10 mol% epoxy content and hydrogenated ENR (HENR-10(8)) obtained at 8h.

HENR-10, HENR-15, HENR-22, HENR-30 and HENR-40 were also characterized by solid state NMR with HD/MAS and HD/MAS/CP techniques in order to observe the mobile and rigid segments on the molecular chains after modification. Figure 5.67 compares the experimental spectra of the hydrogenated ENRs by using HD/MAS technique which can be detected the signal of mobile component. It is clear

from the spectra that the sharp carbon resonance peak at 20 ppm related to the methyl carbon in the saturated fractions of the rubber chains was observed. In addition, the carbon signal at 38 ppm corresponding to methylene units can be detected, which provides information about the higher mobility of this CH₂ group than the another CH₂ one (25 ppm). Clearly, the carbon peaks of HENR-40 spectrum are broader than that of the HENR-10, HENR-15, HENR-22 and HENR-30. This is due to a more reduced mobility of components of HENR-40 arising from furan units and the addition of TSOH in the molecular chain as described in section 5.3.

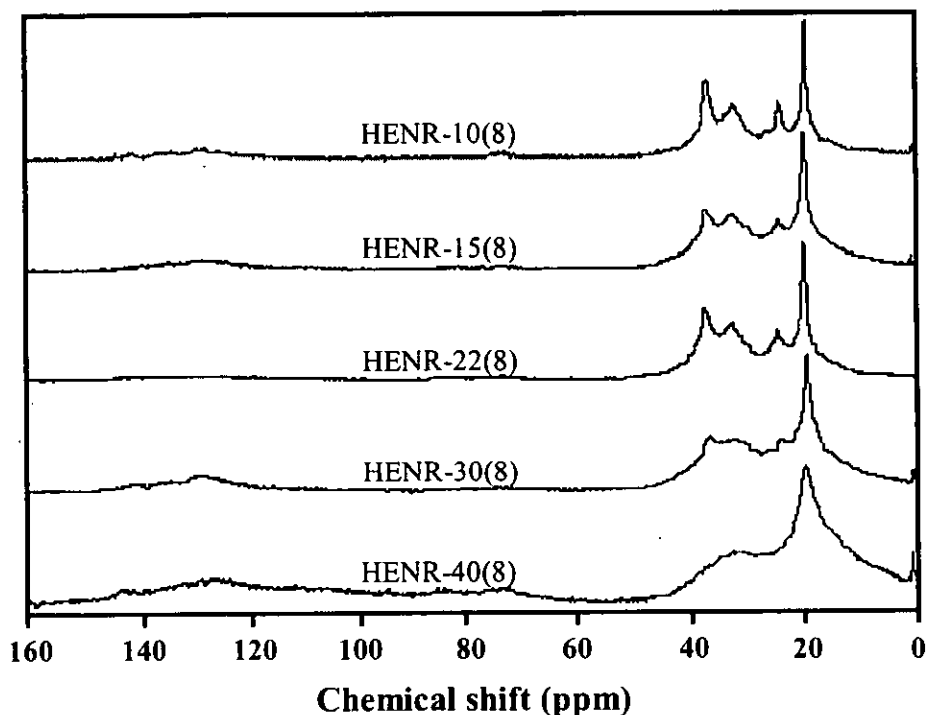


Figure 5.67 Stack plots of HD/MAS ¹³C-NMR spectra of HENR-10(8), HENR-15(8), HENR-22(8), HENR-30(8) and HENR-40(8) containing 10, 15, 22, 30 and 40 mol% epoxy content obtained at 8h of reaction time.

The HD/MAS/CP technique has been therefore applied to detect the rigid part in the hydrogenated ENRs as represented in Figure 5.68. By HD/MAS/CP technique characterization, it is interesting to note that the intensity of methine carbon peak at 33 ppm is higher than that of the use HD/MAS to detect the characteristic signals. It might be

postulated that the methine carbon of saturated unit is more rigid with respect to the other carbons atom on the molecular chains. Obviously, the peaks at 75 and 84 ppm assigning to carbon of five members ring can be seen in this technique due to the rigidity of furan structure. Additionally, the TSOH as a by product can attach to the molecular chain, which show the carbon signal at 130 and 150 ppm. The appearance of furan ring of the HENR and the fixation of TSOH on the modified rubber chains strongly affect the rigidity of the molecular chain.

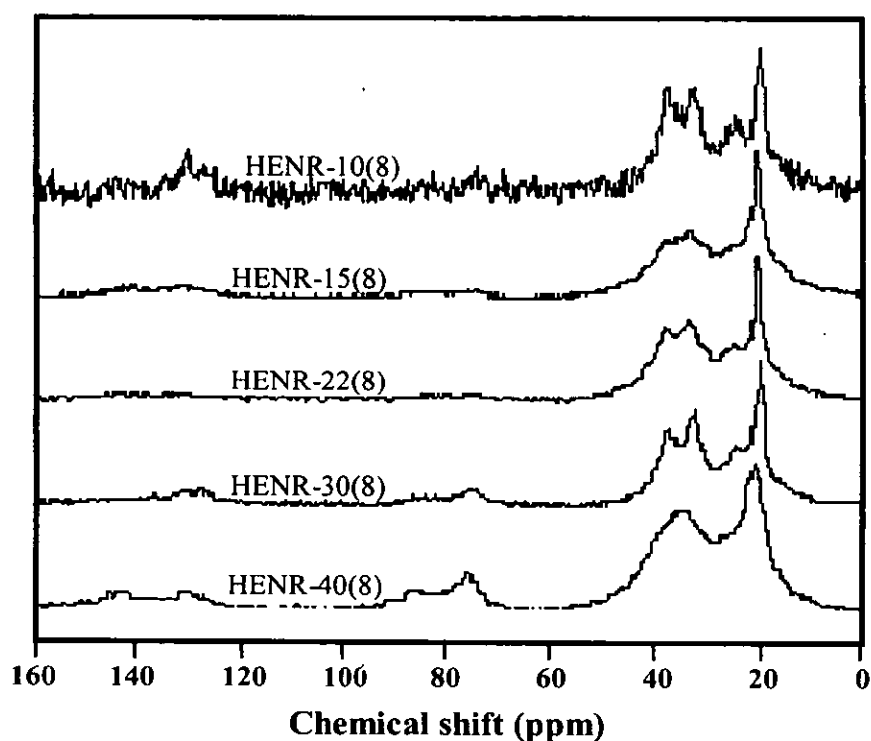


Figure 5.68 Stack plots of HD/MAS/CP ¹³C-NMR spectra of HENR-10(8), HENR-15(8), HENR-22(8), HENR-30(8) and HENR-40(8) containing 10, 15, 22, 30 and 40 mol% epoxy content obtained at 8h of reaction time.

The HD/MAS spectra of HNR(8), HENR-10(8) and HENR-30(8) in the chemical shift range of 0-45 ppm shown in Figure 5.69 are compared. It was found that in the case of the hydrogenated ENR samples, line broadening effects are very important, while the HNR one can be achieved the narrow line signal with HD/MAS technique. This is related to isotropic chemical shift distribution and residual dipolar interactions arising from the presence of components with reduced mobility on the

modified rubber chains. By comparing the line widths of HENR-10 and HENR-30, the NMR line widths of HENR-30 are broader than that of HENR-10. This may be due to the higher amount of rigid portions in the HENR-30, which depends on the content of epoxidation of ENR as characterized in section 5.3.

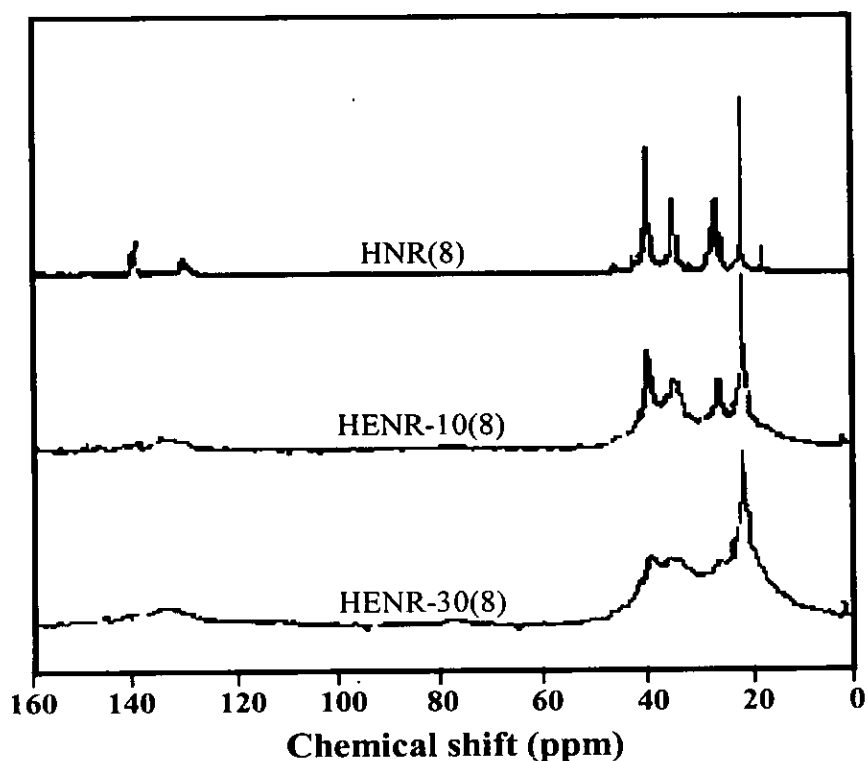


Figure 5.69 Stack plots of HD/MAS ^{13}C -NMR spectra of HNR(8), HENR-10(8) and HENR-30(8) containing 10 and 30 mol% epoxy content, respectively, obtained at 8h of reaction time.

-Dynamic of the CP experiment of the HENR-10

The cross polarization can be used to distinguish mobile components from rigid components. Figure 5.70 exhibits the stack plots of the HENR-10 spectra at different contact times. The observed carbon signals (30-40 ppm) at the shortest contact times are assigned to the carbons that have the largest dipolar ^1H - ^{13}C interactions that are the methylene and methine carbon of saturated units. The strong intensity of methyl carbon signals at 20 ppm is observed at the higher contact times due to the high mobility of methyl group on the rubber chains.

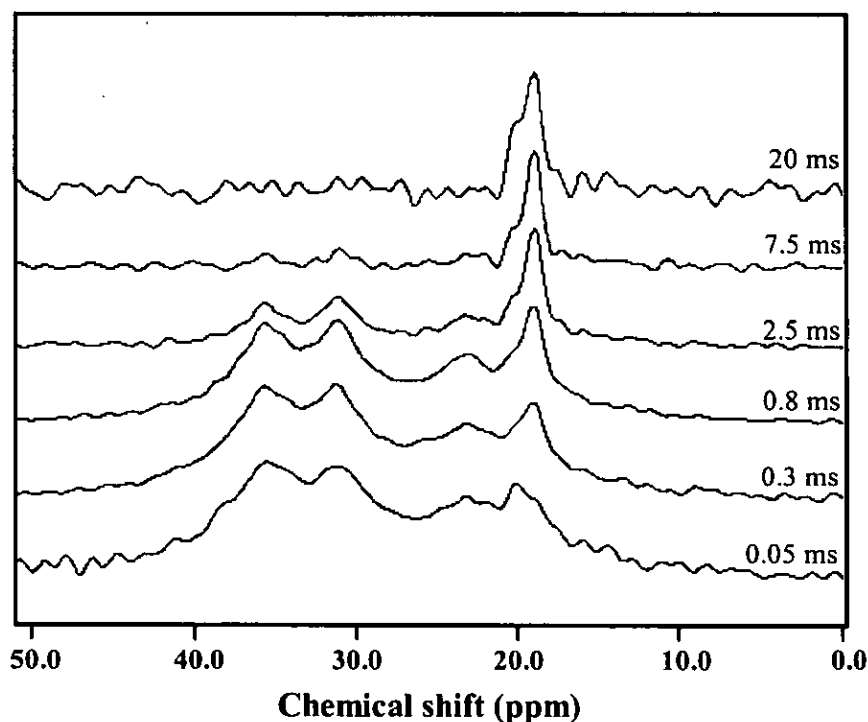


Figure 5.70 Stack plots of solid state ^{13}C -NMR spectra of HENR-10(8) at various contact times in the chemical shift range of 0-60 ppm.

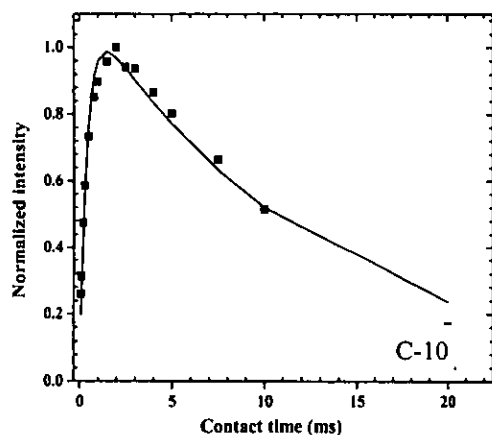
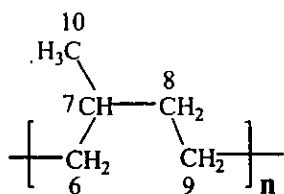
Typical variations in carbon magnetization of carbon signals in HENR-10(8) with contact time are shown in Figure 5.71. In the CP experiment, polarization is transferred from the magnetically rich protons to the magnetically poor carbons via their static dipolar interactions. By comparison with the dynamic CP curves of carbon signals in the molecular chain of HENR, it can be observed that the contact time of carbon magnetization (C-20) of saturated fraction has the highest value when are compared with other carbon signals, while the contact time of the maximum carbon magnetization of C-25, C-33 and C-38 is almost comparable. After a suitable period of the contact time, a maximum ^{13}C magnetization is reached, after which the ^{13}C signal begins to decay at a rate proportional to the inverse of the $T_{1\rho}^H$ time.

According to the dynamic CP curve also fitted with simple model as given in Equation 3.26, the $T_{1\rho}^H$ and T_{CH} can be estimated for each carbon position on the macromolecular chains as summarized in Table 5.39. It can be seen that the $T_{1\rho}^H$ of

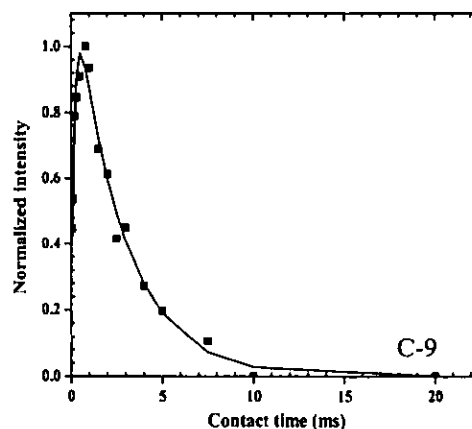
methyl carbon is the largest value, while the $T_{1\rho}^H$ of methylene (CH_2) and methine (CH) groups is comparable. This is related to the less motion of methylene and methine groups due to the appearance of rigid components i.e. furan ring and the fixation of TSOH on the molecular chain. The T_{CH} obtained from curve fitting are presented in the following order: methyl (0.41) > methylene (0.18) > methine (0.17) carbons. In the case of HENR-10, it is noted that the T_{CH} of methylene and methine groups is almost comparable. This is due to the more rigid components of molecular chain after modification. Similar to the case of the hydrogenated NR, the cross polarized time of methyl carbon is largest for mobile group.

Table 5.39 The spin-lattice relaxation time ($T_{1\rho}^H$) and cross-polarized time (T_{CH}) obtained from the simulation of kinetic CP curve of carbon signal of HENR-10(8)

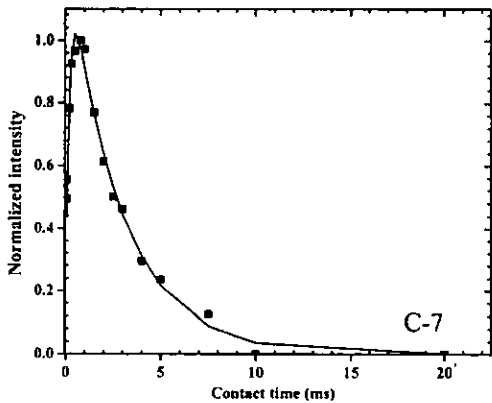
Carbon position	Group	$T_{1\rho}^H$ (ms)	T_{CH} (ms)
C-20	CH_3	12.7±1.2	0.41±0.03
C-25	CH_2	2.62±0.20	0.18±0.02
C-33	CH	2.78±0.15	0.17±0.01
C-38	CH_2	2.25±0.10	0.18±0.01



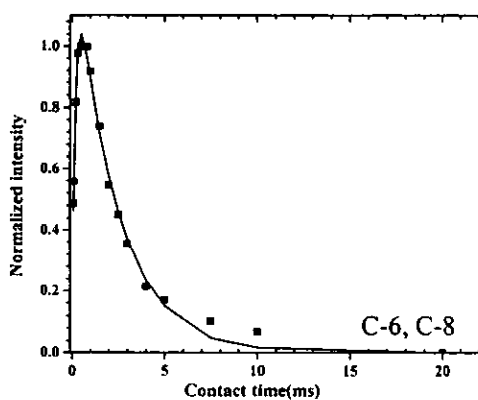
(a)



(b)



(c)



(d)

Figure 5.71 Variation of the magnetization with contact time in a CP experiment for HENR-10(8) sample of carbon positions at C-10 (a), C-9 (b), C-7 (c) and C-6, C-8 (d).



-Dynamic of the CP experiment of the HENR-30

Figure 5.72 compares the spectra of HENR-30(8) at various contact times. For the HENR-30(8) spectra, the broad line signals at the smallest contact are found similar to the HENR-10(8) spectra. Evidently, the molecular motions of these carbons cannot average the chemical shift anisotropies effectively, and the resulting lines are broad. Sharper signal emerge when the contact time is in the 0.8-4.0 ms range. The signal is assigned to the methyl carbon that experience greater motional averaging of H-C dipolar interactions and chemical shift anisotropic. In addition, the optimum condition time depends on the length of time that the proton magnetization can help in the rotating frame and so contribute to the polarization of the carbon spins.

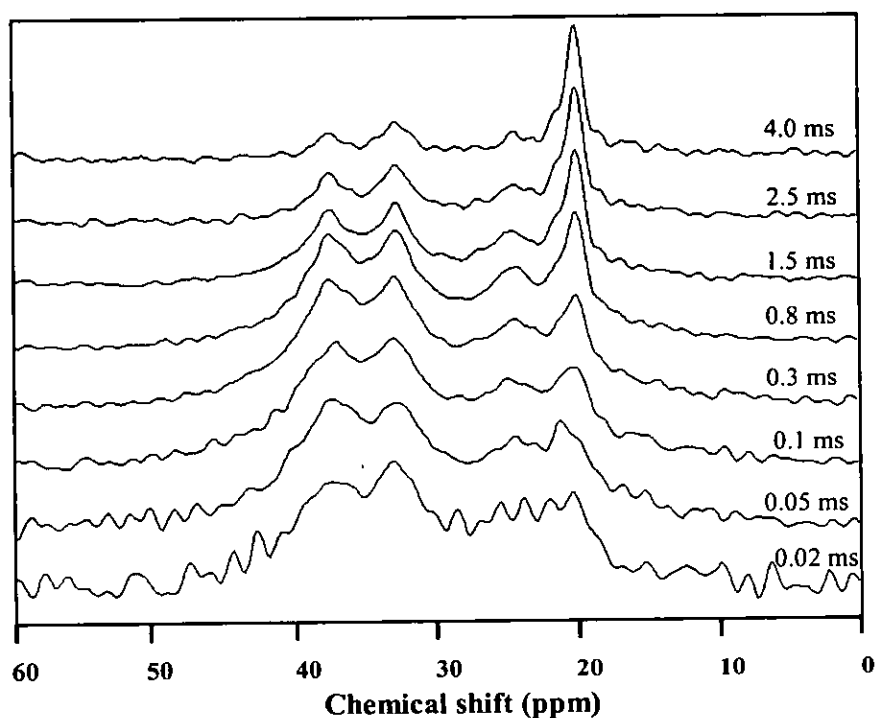


Figure 5.72 Stack plots of solid state ¹³C-NMR spectra of HENR-30(8) at various contact times in the chemical shift range of 0-60 ppm.

Figure 5.73 illustrates the CP kinetic curve of carbon signals of HENR-30(8) sample. In the case of HENR-30, the intensities of carbon signals dramatically increase at shortest contact times as comparing with the CP curve of HNR(8) and HENR-10(8).

In CP experiment of the study of molecular dynamic of HENR-30(8), it is also possible to simulate the CP kinetic curve using simple model as given in Equation 3.26. The CP kinetic curve can be fitted by double exponential function as shown in Figure 5.73 and the obtained relaxation and cross polarization time are shown in Table 5.40. It can be obviously seen that both $T_{1\rho}^H$ and T_{CH} values are short. It may be suggested that the reduced molecular motion of HENR-30(8) leads to fast transfer. By comparing the T_{CH} values in HENR-30(8) and HENR-10(8), it was found that T_{CH} of all carbon signals of HENR-30(8) are less than that of HENR-10(8) because of the more rigid fraction of the molecular chains. The literature reported that the value of T_{CH} should be less than 0.13 ms for a rigid methylene group [22]. As comparing with the values of T_{CH} in the HENR-30 sample, it can be noted that the less mobile parts appear on the rubber chains. In addition, the rate of cross-polarized time ($1/T_{CH}$) of methyl carbon in HENR-30(8) is the highest with respect to methyl carbon in HNR(8) and HENR-10(8). It is clear that the methyl carbon of HENR-30(8) is the least mobility which can relate to the more furan structure and the chemical fixation of TSOH on the rubber chain. In addition, the molecular dynamic of the hydrogenated ENR depends on the epoxidation level, and the amount of ring opening reaction. The more ring opening and the more formation of furan structure at higher epoxidation level. This result is in good agreement with the results of the ^1H -magnetization decays behavior observed in the CP experiments as reported by Kameda and Asakura [78].

Table 5.40 The spin-lattice relaxation time ($T_{1\rho}^H$) and and cross-polarized time (T_{CH}) obtained from the simulation of kinetic CP curve of carbon signal of HENR-30(8)

Carbon position	Group	$T_{1\rho}^H$ (ms)	T_{CH} (ms)
C-20	CH ₃	6.45 ±1.55	0.16±0.03
C-25	CH ₂	1.00±0.28	0.22±0.07
C-33	CH	1.63±0.16	0.066±0.01
C-38	CH ₂	1.21±0.16	0.07 ±0.01



5.7 Thermal Behaviors

The thermal behaviors of starting rubbers i.e. NR and ENR-10 and the hydrogenated rubbers i.e., HNR(6) obtained at 6h and HENR-10(4) obtained at 4h were studied by Raman spectroscopy, differential scanning calorimetry (DSC) and thermo-gravimetric analyzer (TGA).

5.7.1 By Raman Spectroscopy

In the present work, Raman spectroscopy was applied to study the change of chemical structure under vacuum at various temperatures.

(a) Chemical Characteristic of NR and the Hydrogenated NR

Figure 5.74 shows the Raman spectra of NR as a function of temperature (-160-150°C). The intensity, band shape and frequency of Raman bands were changed as a result of a change in the temperature of the samples. The low-wavenumber of the Raman bands close to 950 and 1500 cm^{-1} seems to remain at the same position as the temperature increased. In this region, the sharp bands were observed at low temperature (below T_g). The small intensities of Raman peaks at 1137 and 1207 cm^{-1} corresponding to =C-H in plane bending and -CH₂- wagging modes, respectively can be seen at low temperature (<-100°C). The higher intensity and sharp peak at 1287 cm^{-1} assigning to C-H bending mode was found at temperature around -60°C. These temperatures are associated to the glass transition from the glass to the rubber-like state. For the treatment at higher temperature, the bands became broad and weak, that is, in the rubber-like state or in the melt the chains are in relatively rapid motion, effect on the group frequencies contribution of wavenumbers. Cold treatment results in a rise in the number of bands below 1000 cm^{-1} . The new weak peaks are further seen at 544, 610, 638, 734, 809, 835, and 877 cm^{-1} under cooling (<-100°C). This may be suggested that the cold treatment induced the change of the molecular conformation of NR structure.

Figure 5.75 illustrates the temperature effect on the Raman shift at 1664 cm^{-1} , attributed to the carbon-carbon double bond stretching mode of NR. It has been known



that the NR has a less thermal stability due to the presence of carbon-carbon double bond on the rubber chains which is prone to oxidative degradation under higher temperature. There is an apparent shift of the Raman band at 1664 cm^{-1} towards lower frequency as the temperature increases. There are two extremes of interpretation of the effects of temperature. Firstly, thermal expansion affects the inherent nature of the polarizability change as a result of changes in the intermolecular forces. The other reason is the change of absorbing species concentration with temperature. The relative intensities of Raman bands slightly decrease when the temperature is above 100°C .

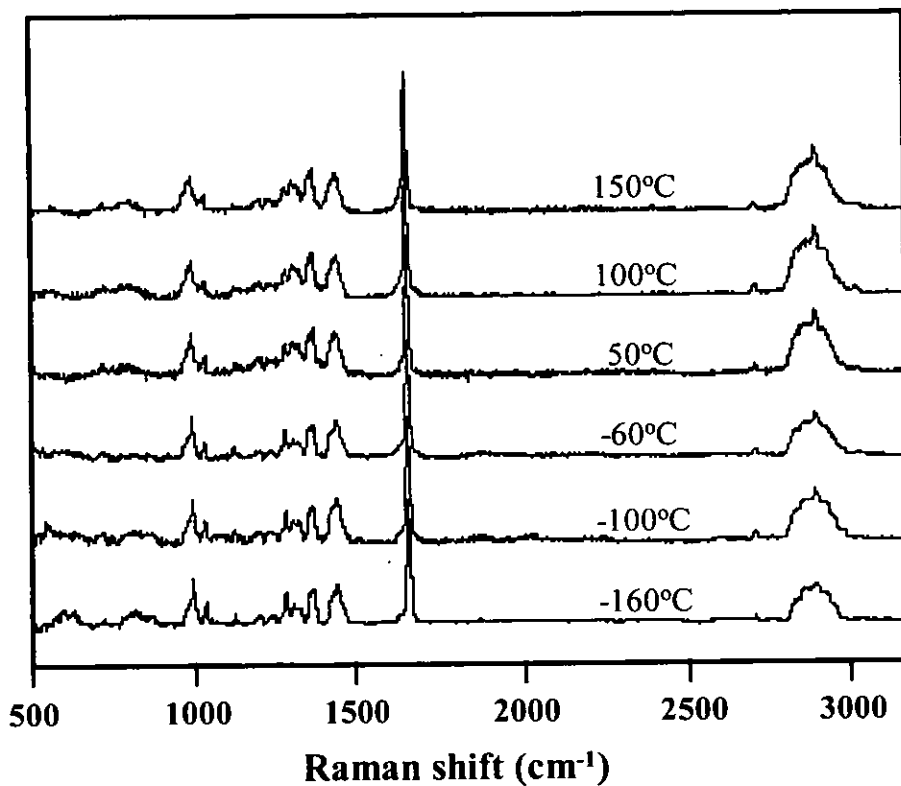


Figure 5.74 Stack plots of Raman spectra of NR as a function of temperature.

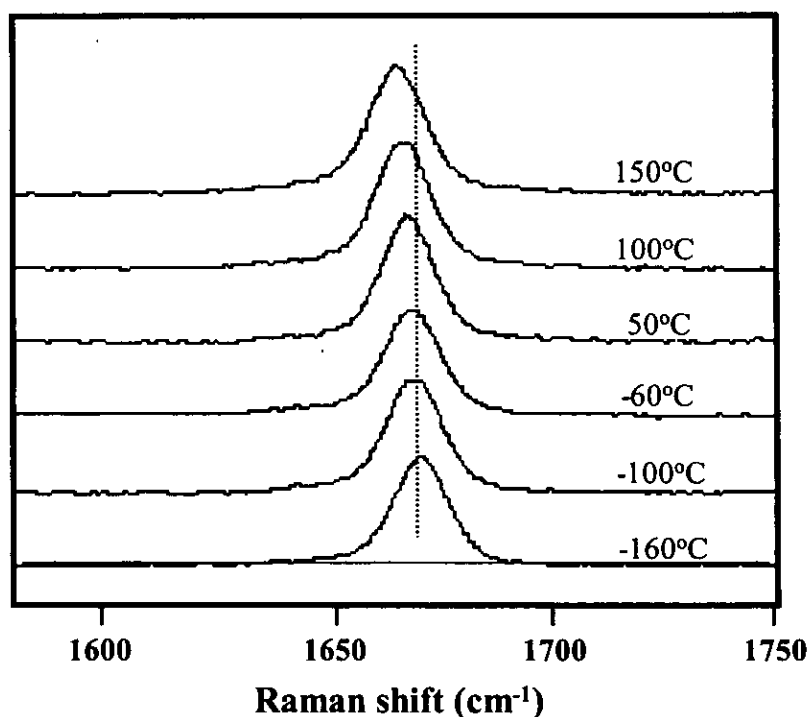


Figure 5.75 Raman shift of C=C bond of NR as a function of temperature.

After hydrogenation, the carbon-carbon double bonds of *cis*-polyisoprene unit presented in NR is converted to saturated segments. From the Raman spectra investigated at various temperatures shown in Figure 5.76, the intensity of characteristic of Raman shift at 2958 cm^{-1} corresponding to the CH stretching vibration mode of methylene groups slightly increases, while the Raman band at 1664 cm^{-1} gradually decreases with temperature. The Raman bands in the region $1000 - 1250\text{ cm}^{-1}$ can be detected which can be assigned to CH_2 wagging, rocking and C- CH_2 stretching at temperature below T_g of the HNR. Furthermore, the small bands at $530, 535, 550, 562$ and 584 cm^{-1} are found and appeared in the range of -160 to -60°C similar to NR. The relative intensity of Raman bands gradually increases and the broad Raman bands can be seen at the temperature above 50°C . The explanation is also similar as described in the case of NR. The feature at 1042 cm^{-1} assigning to CH_3 rocking motion also slightly increases in intensity when the temperature increased up to 150°C . This has been subjected to different thermal treatments to obtain samples with a wide variety of conformation in the rubber chains. In addition, the Raman signal of C=C stretching also moves toward lower wavenumber as shown in Figure

5.77 as the increasing of temperature. The relative intensity of this characteristic band slightly decreases with temperature because the degradation by heating can be occurred with the presence of residual double bonds of polyisoprene units.

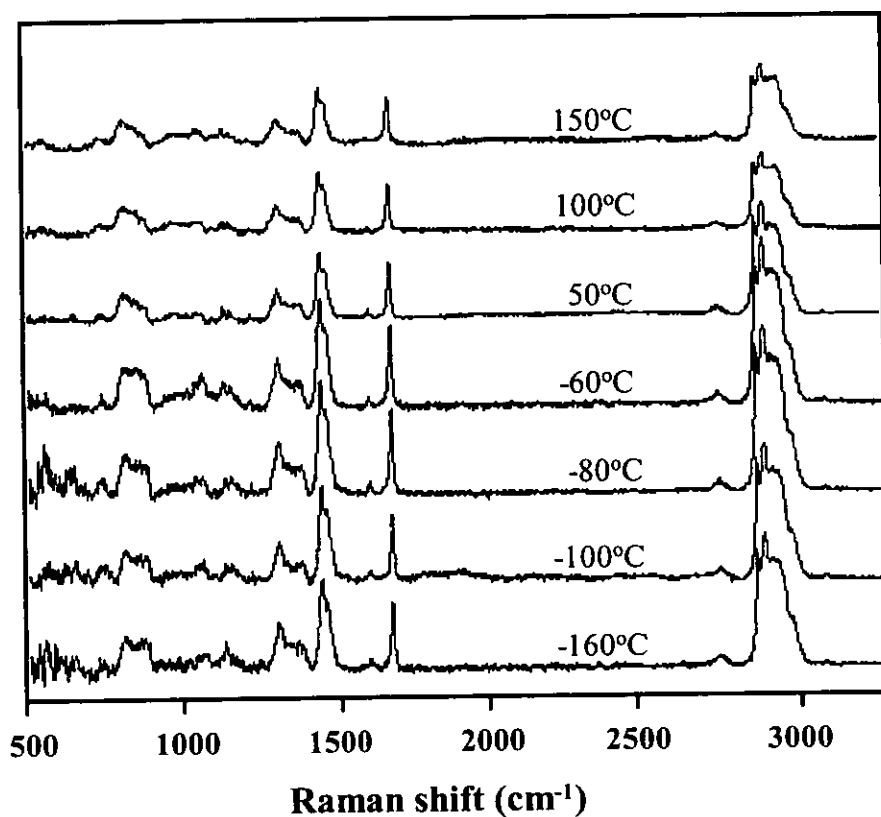


Figure 5.76 Raman spectra of partially hydrogenated NR (HNR(6)) obtained from reaction time 6h as a function of temperature.

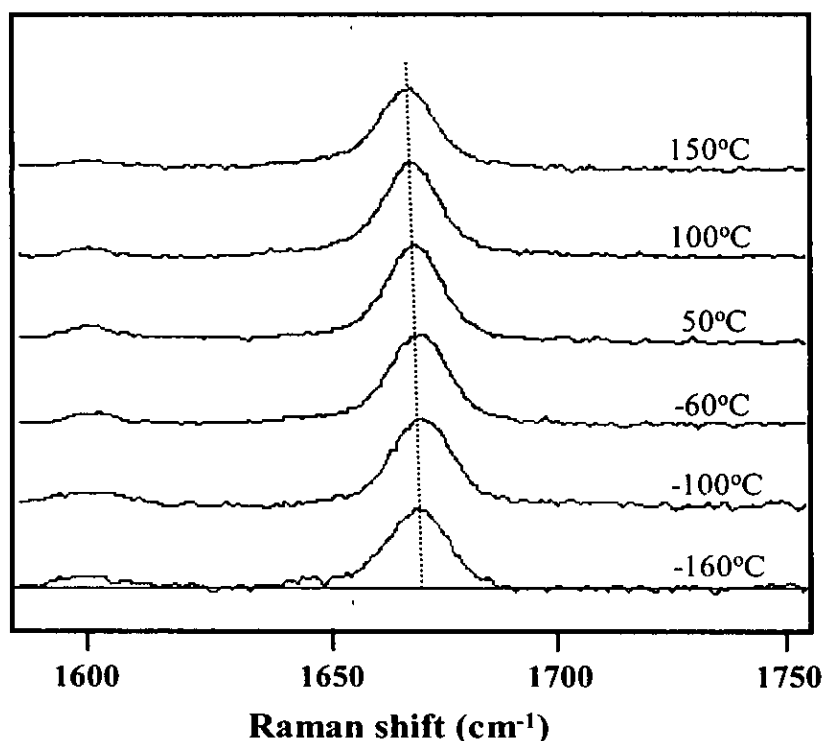


Figure 5.77 Raman shift of C=C bond of the HNR(6) as a function of temperature.

(b) Chemical Characteristic of ENR-10 and the Hydrogenated ENR

Figure 5.78 represents the stack plot of the Raman spectra of ENR-10 as a function of temperature. There is not a significant change in the characteristic of Raman spectra of ENR. However, it was found that the intensity of Raman bands increase with temperature. The broad characteristics and the increase of intensity of Raman bands are clearly observed at the temperature above 50°C. This indicated that the ENR has a better thermal resistance than the NR one. This is due to the increase of density of ENR as reported by Burfield et. al. [108] and the reduction of free volume at temperature below T_g . The slight decrease of Raman shift of the carbon-carbon double bond are also found (see Figure 5.79) similar to the recorded Raman spectra of NR and HNR(6).

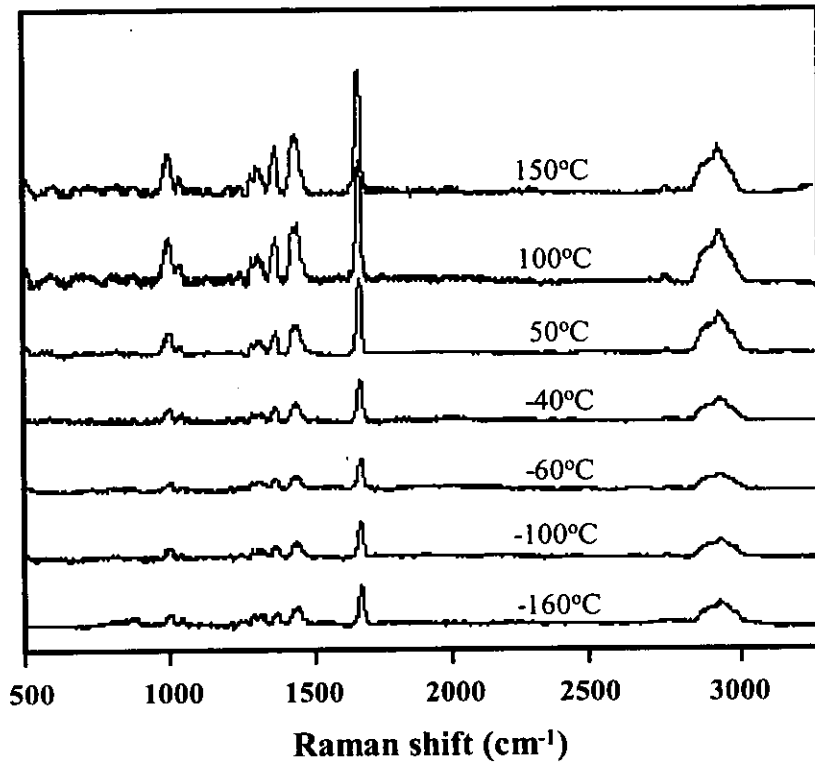


Figure 5.78 Raman shift of epoxidized NR containing 10 mol% epoxide content as a function of temperature.

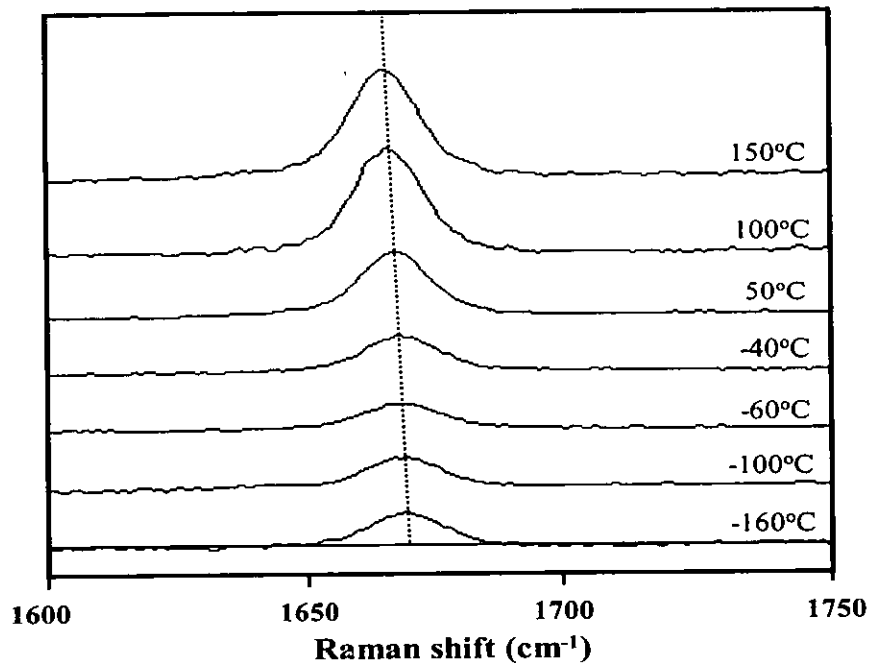


Figure 5.79 Raman shift of C=C bond of ENR-10 as a function of temperature.

For the Raman spectra of HENR-10(4) sample in Figure 5.80, the change of characteristic of Raman spectra is clearly seen at temperature range of -40 and -20°C , while in the Raman spectra of HNR(6) is found at temperature 50°C (see Figure 5.76). These temperatures are in the range of glass transition temperature of HENR-10 as will be described in the next Section. This is due to *p*-toluenesulfonic acid attached on the molecular chain of ENR after modification, which effected on the steric hindrance of chain. Therefore, the free volume between the rubber chains increases, that relates to the thermal expansion of the rubber chains.

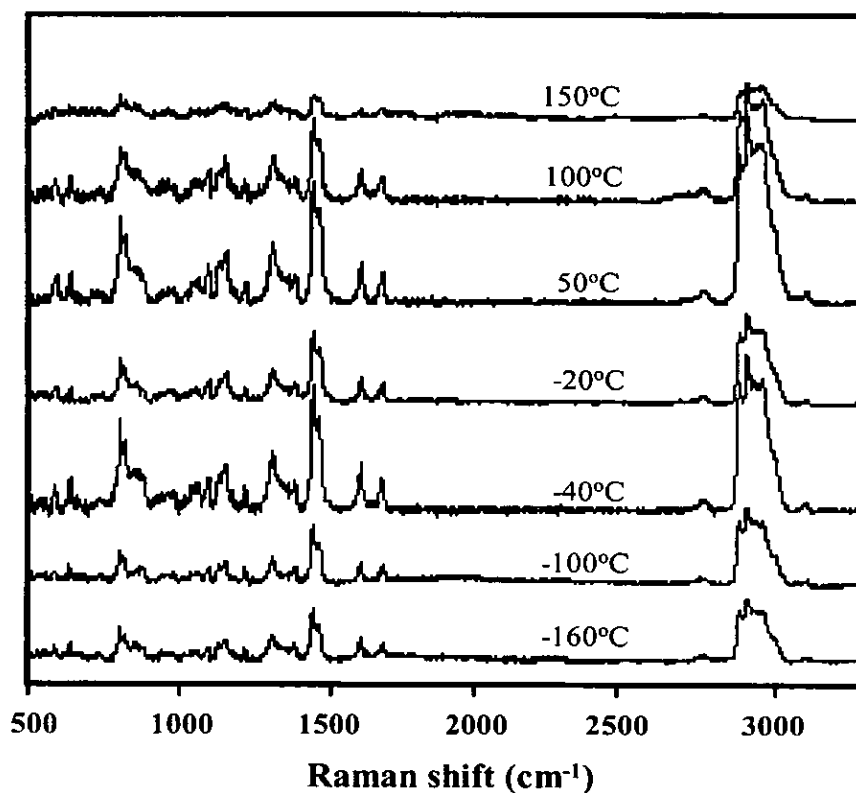


Figure 5.80 Raman shift of HENR-10(4) at 4h as a function of temperature.

5.7.2 By Differential Scanning Calorimetry

Differential scanning calorimetry (DSC) measurements were carried out as described in section 4.9. All values of thermal properties were obtained from the second heating thermogram in order to avoid the effect of thermal history. Study of the thermal transition behaviour of NR, ENR and the hydrogenated samples may provide important information concerning the rotation of bonds in the rubber chains. The transition from the glass to the rubber-like state is an important feature of NR, ENR and the hydrogenated NRs behaviour, making as it does a region where dramatic changes in the physical properties, such as hardness and elasticity.

5.7.2.1 Effect of Scanning Rate on the Thermal Transition of NR and HNR Samples

In general, the precise value of glass transition temperature (T_g) of a polymer depends on the method used. In the case of DSC measurement, the scanning rate of applied heat also affects on the segmental and molecular motions of macromolecules, hence the T_g of the studied sample. In present work, the study of varied scanning rate of DSC measurement on three rubber samples i.e. NR and HNR38, having 38 % hydrogenation and HNR97, having 97% hydrogenation. The observed onset (T_{onset}) and T_g of the samples obtained from the second heating scan of NR, HNR38 and HNR97 are listed in Table 5.41. It can be seen that the T_g of the samples slightly increases with the scanning rate. The actual glass transition temperature (T_g^0) of the samples can be determined by extrapolating to the y-axis intercept in the graph plotted between T_g and the scanning rate. The linear relationships between the T_g^0 of NR and both hydrogenated samples and the scanning rate obtained were obtained as shown in Figure 5.81. This indicated that in all experiments glass transition temperature increased with increasing of the heating scanning rate. This is in fact that the observed glass transition temperature depends very much on the time allotted to the experiment. The value generally considered for T_g is the one extrapolated data at scanning rate of $0^\circ\text{C}/\text{min}$. For NR, T_g^0 is -68.8°C , while in the HNR38 and HNR97 samples the T_g^0 are -67.0 and -64.3°C , respectively. The T_g of the hydrogenated rubber is slightly



increased with %hydrogenation, which may be implied that the modified sample did not loss its rubber behavior.

Table 5.41 Effect of scanning rate on the onset temperature and glass transition temperature of NR, HNR38 and HNR97

Scanning rate (°C/min)	NR		HNR38		HNR97	
	T _{onset} (°C)	T _g (°C)	T _{onset} (°C)	T _g (°C)	T _{onset} (°C)	T _g (°C)
5	-59.6	-68.2	-59.4	-66.3	-59.8	-63.7
10	-58.8	-67.2	-58.9	-65.4	-58.9	-62.2
15	-58.1	-66.7	-58.2	-64.6	-58	-61.7
20	-57.4	-66.0	-57.8	-64.0	-57.6	-61.0

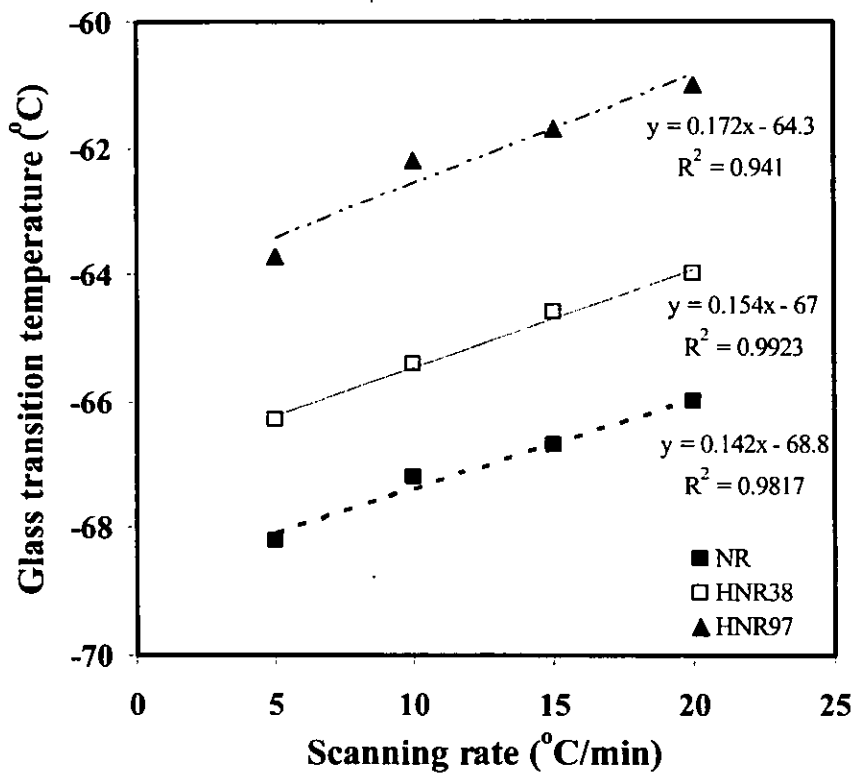


Figure 5.81 The relationship between glass transition temperature and scanning rate of NR (■), HNR38 (□) and HNR97 (▲).



5.7.2.2 Effect of Hydrogenation Content on Thermal Transition

(a) NR and the Hydrogenated NR

The values of glass transition temperature obtained from the second scan of heating (20°C/min) of NR and HNR containing various hydrogenation levels up to 97 % are listed in Table 5.42. It was found that the glass transition temperature (T_g) of the partially hydrogenated rubber is gradually increased about 2-5°C after hydrogenation. The increase of T_g value results from the increased amount of saturated units in the molecular chain, that is, the segmental mobility decreases. It is interesting to note that complete hydrogenation of *cis*-1,4 polyisoprene should form a 1:1 alternating copolymer of ethylene and propylene, having glass transition temperature, between that of polyethylene (-85°C) and polypropylene (-20°C) [11]. For the 1:1 ethylene-propylene copolymer, the calculated T_g should be approximately -52.5°, whereas the observed T_g found -61.0°C for the hydrogenated NR (97%). Mango and Lenz [11] studied the thermal transition of hydrogenated synthetic polyisoprene (HPI) by using DSC and found that the T_g of HPI is about -61°C as similar to the T_g of the our HNR sample. In addition, the *trans* microstructure obtained by *cis-trans* isomerization of residual double bonds may also result in the enhancement of T_g in the hydrogenated NR. It is interesting to note that the T_g of *cis*-PI is -73°C whereas of *trans*-PI is around -53°C [108]. It can be assumed that the *cis-trans* isomerization affects the T_g of the hydrogenated samples. The results of T_g values of all hydrogenated NR samples is lower than that of EPDM as shown in Table 5.42. It can be explained that the EPDM sample having the ethylene and propylene segment (around 91 %) on the rubber chains which can occur partially crystalline of ethylene and propylene fraction, hence, the more energy is needed to overcome the energy barrier for the segmental motion of the samples.



Table 5.42 Glass transition temperature values of NR and the HNR obtained at different percent hydrogenations with scanning rate 20°C/min

Hydrogenation (%)	T _{onset} (°C)	T _g (°C)
0	-57.9	-66.7
39.1	-57.1	-65.0
57.5	-57.5	-64.9
79.4	-57.1	-63.5
84.9	-56.5	-62.3
97	-57.6	-61.0
EPDM (%EP = 9)	-	-46.7

(b) ENR and the Hydrogenated ENR

The thermal transition of ENR-10, ENR-22, ENR-30 and ENR-40 and their hydrogenated samples, evaluated from the second heating thermograms are presented in Table 5.43. Figure 5.82(a) shows the linear relationship of epoxidation degree and T_g of the epoxide modification of NR. It was found that the introduction of epoxide function on the rubber main chain results in increasing the T_g, depending on the level of modification. These results are in accordance as has already been disclosed in several literatures that the T_g of ENR varies linearly with molar epoxy content [37, 38, 107]. Burfield et. al. reported the progressive increase in the glass transition temperature parallels a concomitant increase in polymer density [108]. This is an indicative that the increase of T_g results from a reduction in free volume of the chain segments. The presence of oxirane units on the rubber chains resulted also on the stiffness of the rubber, hence the T_g.

Table 5.43 also summarized the T_g results of different types of ENR hydrogenated during 8 h and they all have approximate equal value of hydrogenation



degree i.e. 97-99 % hydrogenation. An increased T_g of about 16°C for the HENR-10(8) as compared to that of the ENR-10 was found. The plot of the relationship between T_g of HENR and the epoxidation level of the ENR starting material shown in Figure 5.82 (b) demonstrates that the T_g of HENR progressively increased when the epoxide content of the starting rubber is increased. For instant, the T_g of HENR-40(8) based on 40 mole% of epoxide content (14.8°C) is higher than those of other types of HENR (10, 22, and 30 mole% epoxide level). This must be due to the increase in the chain stiffness after hydrogenation, which is significantly more important than in the case of hydrogenated NR. The T_g of HNR (-62°C) is lower than that of HENR (-31°C for HENR-10, -22.8°C for HENR-22, -3.9°C for HENR-30, 14.8°C for HENR-40). Two types of factors influencing the chain stiffness of HENR can be taken into account. The first one may be called the internal mobility, which reflects the ease of rotational motion of the main chain backbone. Another one is concerned with the presence of side group other than the epoxide ring i.e. the furan ring and aromatic group of TSOH attached on the chain backbone. In addition, in the case of the presence of a higher amount of epoxide group (40 mol%) the T_g of HENR-40 is very high. This is due to a higher amount of the furan ring structure, which leads to less segmental mobility of the macromolecular chains.



Table 5.43 Glass transition temperature values of ENR containing various epoxide contents and HENR obtained at 8 h of reaction time

Sample code	Hydrogenation (%)	T_{onset} (°C)	T_g (°C)
ENR-10	-	-58.9	-47.4
HENR-10(8)	97.0	-29.7	-31.0
ENR-22	-	-58.5	-40.0
HENR-22(8)	97.7	-22.4	-22.8
ENR-30	-	-41.0	-37.6
HENR-30(8)	97.4	-10.4	-3.9
ENR40	-	-34.1	-31.3
HENR-40(8)	99.3	9.0	14.8



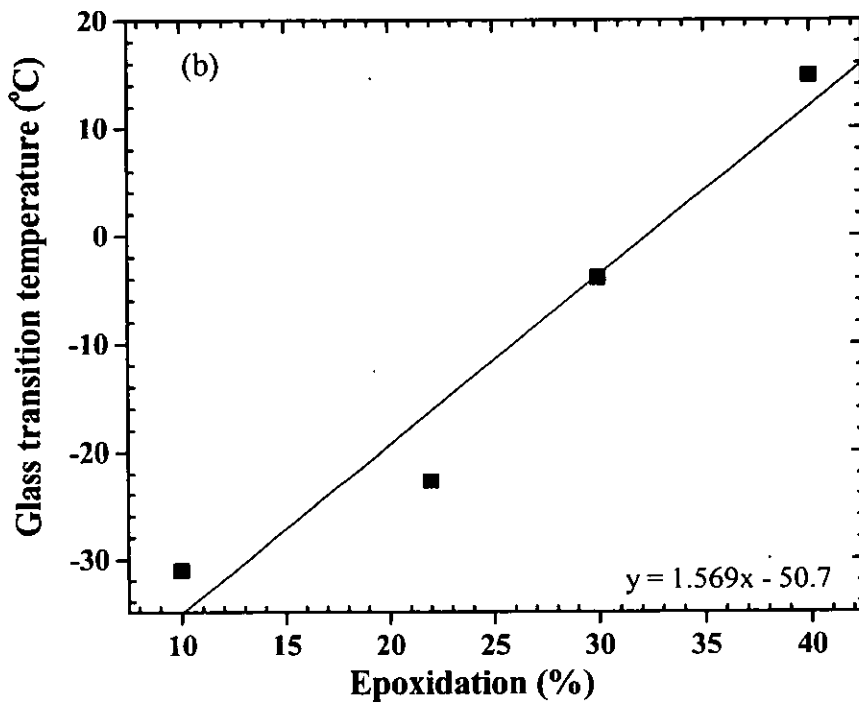
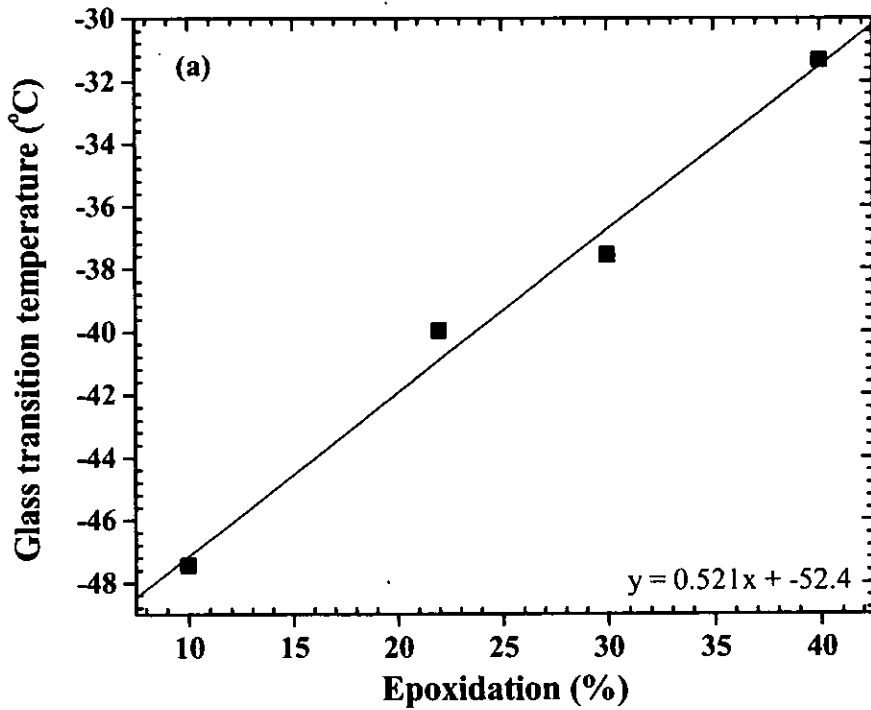


Figure 5.82 The relationship between the glass transition temperature and the epoxidation level of ENR (a) and of HENRs (b) containing 10, 22, 30 and 40 % epoxide content.



5.7.3 By Thermal Gravimetric Analysis (TGA)

The present investigation focuses on the effects of hydrogenation on the degradation behavior of HNR and HENR samples using TGA technique.

5.7.3.1 Thermal Stability of Hydrogenated NR carried out in organic media

Thermogravimetric (TG) and derivative thermogravimetric (DTG) thermograms of NR and HNR under air and nitrogen atmosphere are illustrated in Figures 5.83 and 5.84, respectively. The hydrogenated NRs exhibited the two-step weight loss curves, while the NR give a conventional weight loss curve. From the thermogram curves, shown in Figure 5.83, the data of thermal behavior was analyzed as listed in Table 5.44 and 5.45. The results show that the temperature of initial decomposition of the first step (T_1^i) of HNR samples was occurred around 230-275°C under air and 205-230°C under nitrogen atmosphere. While the second step of degradation, the T_2^i 's are in the range of 400-414°C under air and 400-432°C under nitrogen atmosphere.

It can be explained why the multi steps of TGA thermograms in Figure 5.83 of the HNR by two reasons. One reason may be the M_v of the HNR (85%) 288,000 is much lower than that of the NR ($M_v = 912,000$) due to the degradation caused by considerably high temperature of the hydrogenation. This reason supports by the observation of thermal stability of the masticated natural rubber having the weight average molecular weight about 50,000 which present the two steps of weight loss curve as shown in Table 5.45. For another reason, the HNR is the partial hydrogenation product of NR, therefore the residual unsaturated units that are located in a random manner in the molecular chain might be probably degraded in the first place, while the rigid part obtained after hydrogenation can resist to high temperature applied for a longer time.

Examining the two step of the samples, it is observed that the second decomposition temperature of the hydrogenated NRs are also higher than that of NR i.e. the maximum degradation temperatures (T_2^p) of the HNR samples are in the range 430-445°C in air and 440-460°C in nitrogen atmosphere while the degradation



temperature of NR is about 380°C in both air and nitrogen atmosphere (see Table 5.44 and 5.45). It is clearly seen that the maximum decomposition temperature shifts to higher temperature with hydrogenation level. The decomposition temperatures (T_d) of the hydrogenated products are higher than those of the starting rubbers by 60-80°C both in the air and nitrogen atmosphere. This indicates that the hydrogenation of NR could improve their thermal stability of final step.

By comparison between the thermal stability under air and nitrogen atmosphere, the decomposition temperature of HNR in air is less than that of in nitrogen atmosphere. It is well known that thermal stabilities in particularly dependent on the strength of chemical bonds in the polymer chain structure and inter-chain forces associated with them. The double bonds are very susceptible to oxidation. As a result, the presence of oxygen may cause the chemical reaction to take place generating functional groups such as $-C=O$, or $-COOH$ on the main molecular chain [80] leading to higher thermal stability in air than in nitrogen atmosphere.



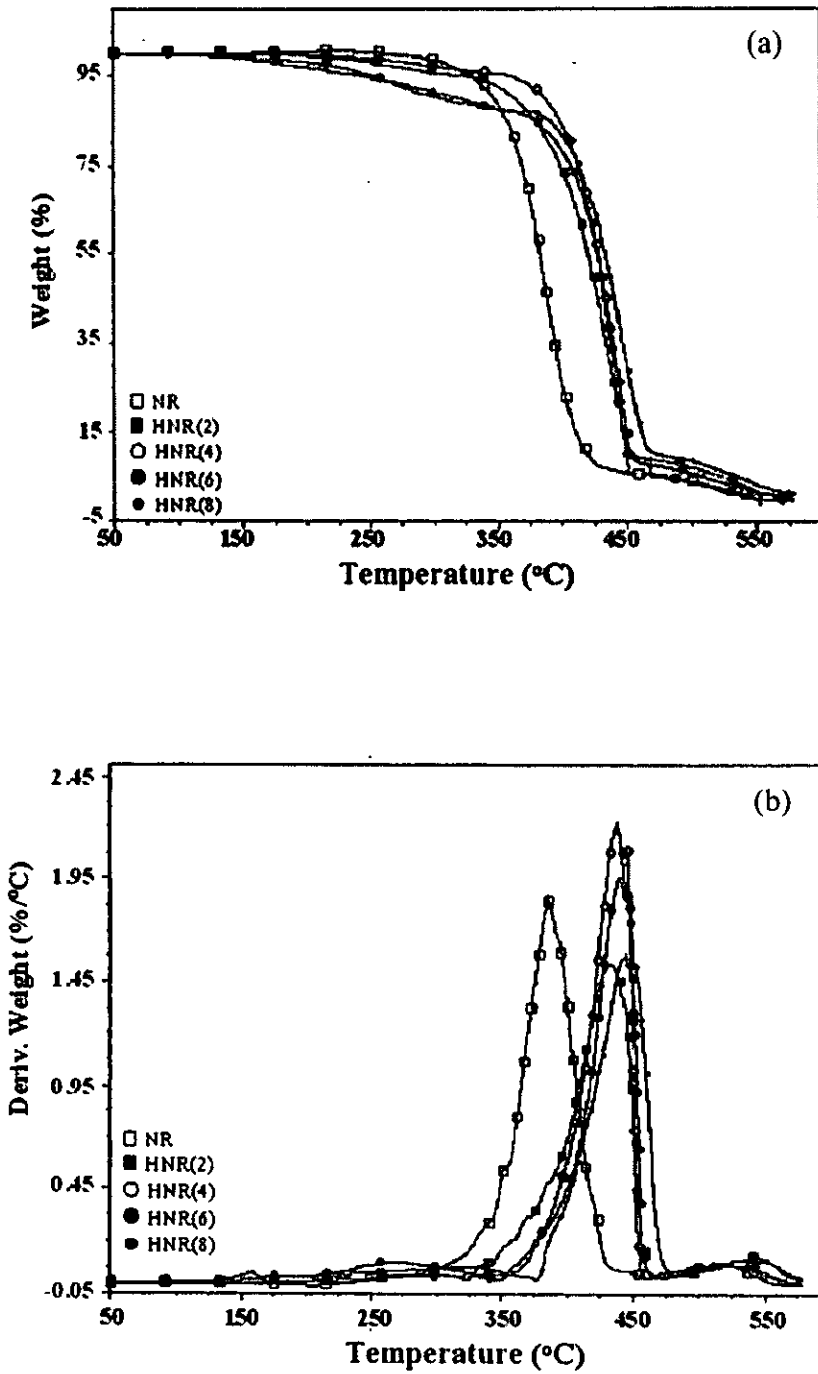


Figure 5.83 TG (a) and DTG (b) thermograms of natural rubber (NR) and their hydrogenated products (HNR) in air atmosphere.



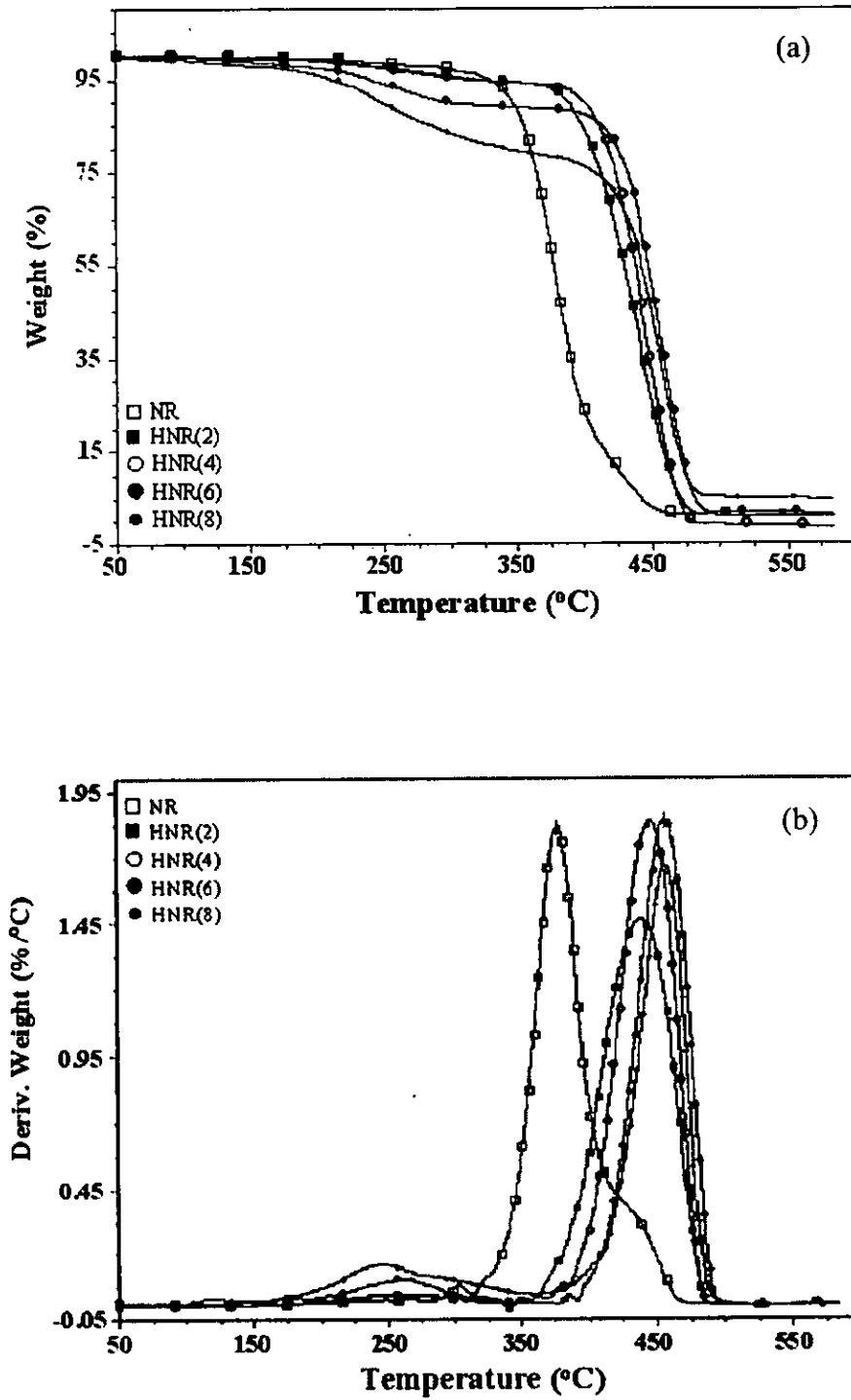


Figure 5.84 TG (a) and DTG (b) thermograms of natural rubber (NR) and their hydrogenated products (HNR) in nitrogen atmosphere.



Table 5.44 The results of TGA of NR and their hydrogenated rubbers under air atmosphere

Sample code	Hydrogenation (%)	Step 1			Step 2		
		T ₁ ⁱ (°C)	T ₁ ^f (°C)	T ₁ ^p (°C)	T ₂ ⁱ (°C)	T ₂ ^f (°C)	T ₂ ^p (°C)
NR	0	n	n	n	357.3	408.0	385.9
HNR(2)	39.1	229.8	306.6	273.1	398.6	449.5	432.8
HNR(4)	57.5	276.0	328.5	302.2	411.1	449.5	437.1
HNR(6)	79.4	233.8	301.3	271.7	413.5	451.7	440.7
HNR(8)	84.9	268.0	342.8	317.0	413.9	461.3	445.7

n = no detection

T₁ⁱ and T₂ⁱ = temperature of initial decomposition for the first and second steps,

T₁^f and T₂^f = temperature of final decomposition for the first and second steps,

T₁^p and T₂^p = temperature of maximum decomposition for the first and second steps.

Table 5.45 The results of TGA of NR and their hydrogenated rubbers under nitrogen atmosphere

Sample code	Hydrogenation (%)	Step 1			Step 2		
		T ₁ ⁱ (°C)	T ₁ ^f (°C)	T ₁ ^p (°C)	T ₂ ⁱ (°C)	T ₂ ^f (°C)	T ₂ ^p (°C)
NR	0	n	n	n	354.6	402.7	377.1
HNR(2)	39.1	227.3	300.4	268.4	403.5	465.4	438.9
HNR(4)	57.5	225.5	298.7	269.6	416.9	467.2	446.5
HNR(6)	79.4	224.3	293.9	262.2	430.4	475.5	456.7
HNR(8)	84.9	206.8	292.5	246.5	431.8	473.2	457.6
Liquid NR (M _v = 50,000)	0	208.9	260.8	249.0	398.0	470.5	446.5



5.7.3.2 Thermal Stability of HNR Carried out in Latex Form

The results of the TG and DTG analysis of all the HNRs obtained from diimide reduction in latex form are illustrated in Figure 5.85 and the characteristic temperatures of degradation are presented in Table 5.46. From the TG and DTG curves analysis, it is seen that the thermal degradation of NR and hydrogenated NR has a one step process. The results in Table 5.46 show that the temperatures of initial decomposition are in the range of 358-383°C. The maximum rate of degradation is in the range of 378-412°C, and the final decomposition temperatures are around 406-454°C. The temperature of the initial decomposition is found to increase with increase of the hydrogenation level. This indicates that the thermal stability increases with the increase of hydrogenation content in the samples. The decomposition temperatures (T_d) of the hydrogenated products are higher than those of the starting rubbers by about 20-50°C. This indicates that the hydrogenation of NR in this system could improve their thermal stability.

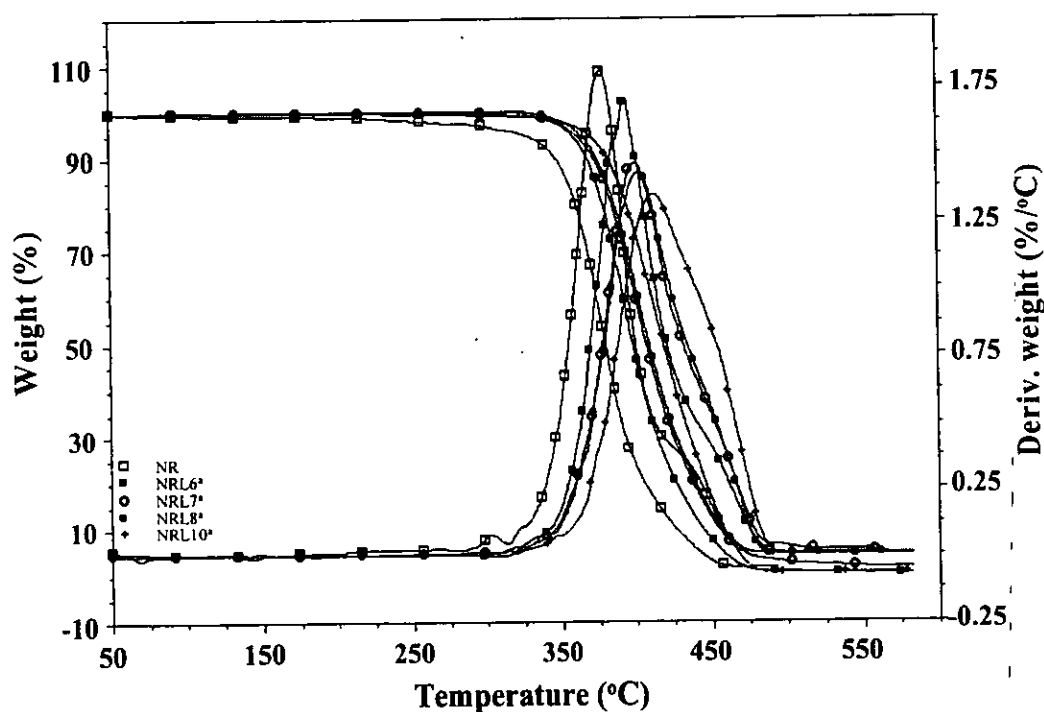


Figure 5.85 TG and DTG thermograms of natural rubber (NR) and their hydrogenated rubbers obtained in latex at various percent hydrogenations under nitrogen atmosphere.

Table 5.46 The results of TGA of NR and their hydrogenated rubbers prepared in latex stage under nitrogen atmosphere

Sample code	Hydrogenation (%)	T_1^i (°C)	T_1^f (°C)	T_1^p (°C)
NR	0	357.7	405.9	377.7
NRL6 ^a	9.6	369.3	426.6	393.5
NRL7 ^a	17.9	373.1	439.5	399.8
NRL8 ^a	21.3	374.2	439.5	402.0
NRL10 ^a	29.4	382.6	454.4	411.6

a = hydrogenated rubber taken at 24 h of reaction time

T_1^i = temperature of initial decomposition,

T_1^f = temperature of final decomposition,

T_1^p = temperature of maximum decomposition.

5.7.3.3 Thermal Stability of ENR and HENR

In the case of ENRs and their hydrogenated products, the thermal stability is also investigated by TGA technique. TGA thermograms obtained from the heating scan of ENR-10 containing 10 mol% epoxy content and the hydrogenated ENR at 2, 4, 6 and 8h of reaction time are shown in Figure 5.86 and the results of the decomposition temperature are given in Table 5.47. The result of TGA curve of ENR-10 shows the only one step of the thermal degradation that the maximum and final of degradation temperatures at 393 and 433°C are higher than in the case of NR. It is shown that the epoxidized NR form can improve the thermal stability of NR. In the case of HENR-10, the results in Table 5.47 show that the temperature of initial decomposition of the first step occurred in the range 196-230°C; for the second step of degradation, the T_2^i are in the range of 423-434°C. The maximum temperature of degradation is in the range 452-461°C. This shows that the enhancement of final thermal stability can be obtained after hydrogenation. However, the increase of percent hydrogenations did not affect on the increase of the thermal stabilities of the HENR.



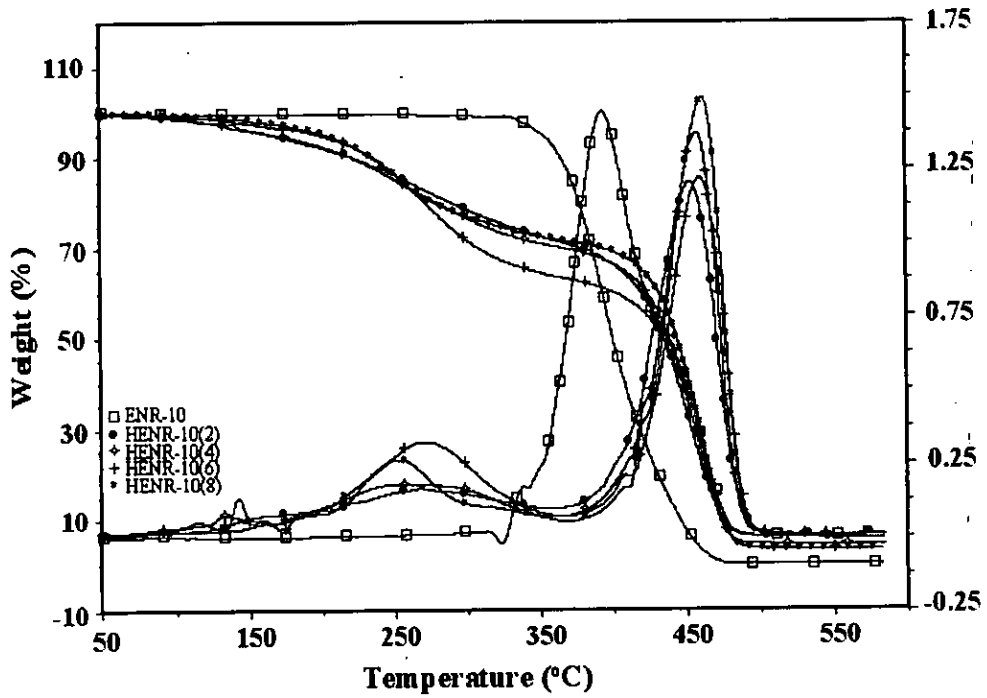


Figure 5.86 TG and DTG curves of ENR containing 10 mol% epoxy content and hydrogenated ENR obtained at 2, 4, 6 and 8h.

Table 5.47 The results of TGA of ENR-10 and their hydrogenated rubbers obtained at various reaction times under nitrogen atmosphere

Sample code	Hydrogenation (%)	Step 1			Step 2		
		T ₁ ⁱ (°C)	T ₁ ^f (°C)	T ₁ ^p (°C)	T ₂ ⁱ (°C)	T ₂ ^f (°C)	T ₂ ^p (°C)
ENR-10	0	n	n	n	365.9	433.2	392.6
HENR-10(2)	35.0	196.0	308.9	270.6	423.4	472.3	452.2
HENR-10(4)	70.0	196.8	313.9	268.8	429.6	473.7	457.6
HENR-10(6)	84.6	229.5	309.7	271.5	432.0	476.5	458.5
HENR-10(8)	93.0	212.0	288.9	252.6	433.6	476.2	461.2

n = no detection

T₁ⁱ and T₂ⁱ = temperature of initial decomposition for the first and second steps,

T₁^f and T₂^f = temperature of final decomposition for the first and second steps,

T₁^p and T₂^p = temperature of maximum decomposition for the first and second steps.



Figure 5.87 depicted the TGA and DTG curves of ENR-10, ENR-22, ENR-30 and ENR-40, containing 10, 22, 30, and 40 mol% epoxidation levels, respectively and their HENRs having around 95-97% hydrogenation, carried out under nitrogen atmosphere. It can be seen that the thermal stability slightly increases with the epoxidation level. For ENR-30 and ENR-40, the DTG curves show broad curves. This might be due to the ENR exhibited two characteristics of different structures that are isoprene units and oxiran units occurred after epoxidation reaction. The obtained TGA data of ENR and HENR are summarized in Table 5.48. For the TGA curve of all HENR samples, the two-step of degradation was found similar to the case of HNR. The maximum and final degradation temperatures of HENRs in all samples are higher than those of ENRs. It is shown that the thermal stability of the hydrogenated ENR can improve by hydrogenation (97%). In addition, it is interesting to note that in the HENR-10(8) (93 % hydrogenation) the maximum and final degradation temperatures of second step are the highest among all HENR samples. This can be explained that higher saturated fraction on the rubber chain of HENR-10 resulted on the improvement of thermal stability.



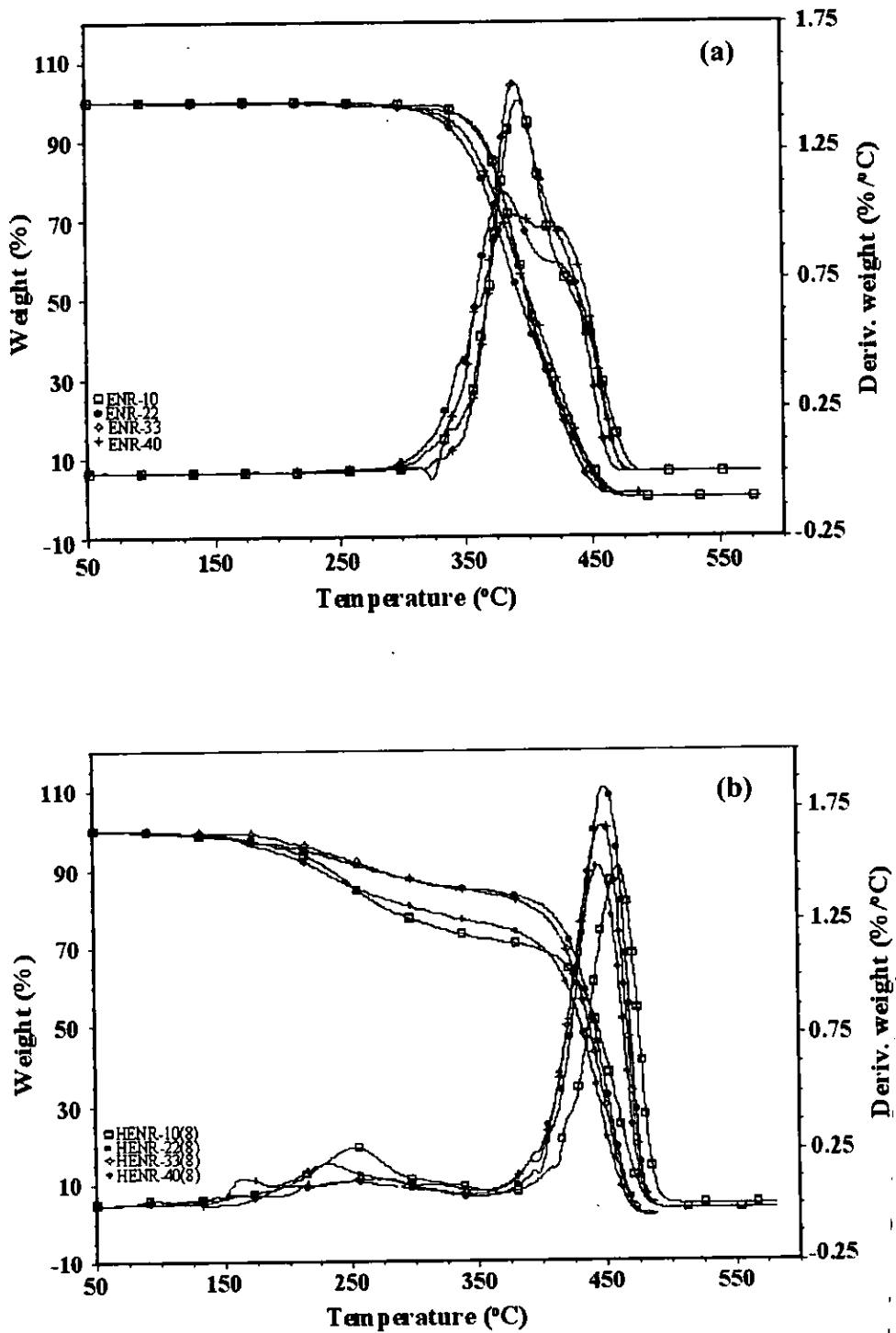


Figure 5.87 TG and DTG thermograms of ENR (a) containing 10, 22, 30 and 40 mol% epoxy content and their hydrogenated products (b) obtained at 8h.



Table 5.48 Results of TGA of ENR and their hydrogenated rubbers obtained at 8 h of reaction time in N₂ atmosphere

Sample codes	Step 1			Step 2		
	T ₁ ⁱ (°C)	T ₁ ^f (°C)	T ₁ ^p (°C)	T ₂ ⁱ (°C)	T ₂ ^f (°C)	T ₂ ^p (°C)
ENR-10	n	n	n	365.9	433.2	392.6
HENR-10(8)	212.0	288.9	252.6	433.6	476.2	461.2
ENR-22	n	n	n	349.3	432.8	381.4
HENR-22(8)	201.3	297.8	252.3	424.3	465.0	450.5
ENR-30	n	n	n	366.8	426.6	389.4
HENR-30(8)	203.2	299.1	249.1	419.3	463.9	448.2
ENR-40	n	n	n	352.7	449.1	388.4
HENR-40(8)	200.0	271.7	233.9	417.2	462.6	446.6

n = no detection

T₁ⁱ and T₂ⁱ = temperature of initial decomposition for the first and second steps,

T₁^f and T₂^f = temperature of final decomposition for the first and second steps,

T₁^p and T₂^p = temperature of maximum decomposition for the first and second steps.



5.8 Rheological Properties

This section describes rheological investigation of hydrogenated rubbers. All rheological measurements were carried out using a Rubber Process Analyzer (RPA) with an oscillatory shear at frequency 1 Hz. The temperature used for testing all the samples was fixed at 100°C. Using a modified torsional dynamic rheometer, strain and torque signals are captured and analyzed through Fourier transform. The result on the series of HNR samples with different molecular characteristics (ratio of unsaturated units per saturated units, molecular weight and MWD) were reported.

5.8.1 Results on HNR Samples using RPA

The rheology of materials is strongly dependent on its chemical and morphological structure. This section had chosen three different types of hydrogenated NR to study the relationship between the portion of saturated (ethylene-propylene) unit in the molecular structure and the rheological properties.

Figure 5.88 shows solid state NMR spectra of HNR38, HNR69 and HNR97. From the spectra, the *cis* and *trans* forms of 1,4-polyisoprene are detected at 23 and 19 ppm, respectively. It was found that the HNR38 contained *cis* and *trans* isomers of 34 and 26 % respectively with 38 %hydrogenation level. While in the case of HNR69, the % hydrogenation is 69 with the *cis* and *trans* isomers of 16 and 15%, respectively. In Figure 5.88, it is found that the dominant four peaks at 20, 27, 33 and 38 ppm are considered to be ethylene propylene copolymer according to the approximately complete hydrogenation of HNR97.



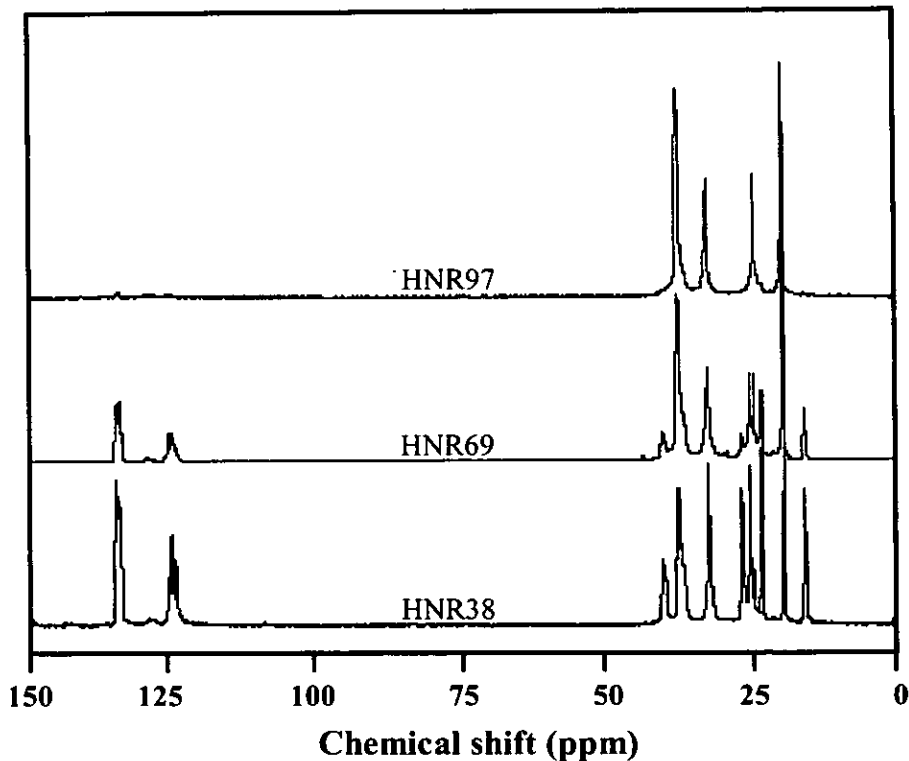


Figure 5.88 ^{13}C -NMR spectra of hydrogenated rubbers containing 38, 69 and 97 mol% hydrogenation content.

To determine how the moduli of the HNR samples change with the hydrogenation level, the rheological properties samples were investigated using RPA with the temperature of 100°C . Test results provided by the standard data treatment of the RPA of HNR38, HNR69 and HNR97 samples are shown in Figures 5.89, 5.90 and 5.91, respectively. As can be seen in Figure 5.89, there is no superposition of the two tests of the same material which indicates likely strain history effects. While in the case of HNR69 and HNR97 samples the test exhibited superposition because the same results are observed with two tests of the same material.

Significant differences are found between the three samples when considering the storage, loss and complex modulus. As can be seen, the HNR38 and HNR69 samples exhibit a linear viscoelastic plateau up to $\approx 50\%$ deformation for the dynamic storage modulus (G'), while in the case of HNR97 sample the modulus plateau shows up to $\approx 140\%$ deformation for G' . It is seen that the dynamic storage

(G') and loss (G'') moduli at 100°C of all samples decrease with increasing the % strain. According to the viscoelastic behaviour of the polymeric systems first described by Sanders et. al. [87], a logarithmic plot of dynamic moduli consists of terminal, plateau and transition zones. The time scales associated with three zones are defined to correspond to the long-range relaxation (long range entanglement of uncrosslinked polymer), the intermediate range relaxation (the region locates between the long and short entanglement), and the short-range relaxation (motion in the entanglement of the crosslinked polymer), respectively. It is seen that HNR samples reported in this work exhibit two zones: plateau (the intermediate range relaxation) and terminal zones (the short-range relaxation). From the data treatment, the samples exhibit the linear viscoelastic response by dependent on the hydrogenation level. It means that the greater hydrogenation level is observed, the larger viscoelastic region is presented. In addition to compare G' and G'' of each sample at the same strain, it is found that the G' value is higher than G'' value. This indicated that the elastic characteristic, the ability to store the energy of external forces, is a dominant factor for HNR samples under the dynamic torsion measurement. The storage and loss moduli of HNR97 sample are the highest values when compared with HNR38 and HNR69 samples. These values are remarkably increased with the hydrogenation level. For instance, the fully hydrogenated NR has a significant increment in the loss and storage moduli of the sample that is approximately 8 times of both loss and storage moduli of HNR38 sample. This means that the polymer characteristics, that is, ratio of ethylene-propylene to polyisoprene units, strongly affect on the rheological behaviour of them. The 97% hydrogenation of NR should give a new material known as ethylene-propylene diene copolymer. The viscoelastic behaviour of HNR97 sample is quite similar with EPDM as reported by Leblanc and Chapelle [109].



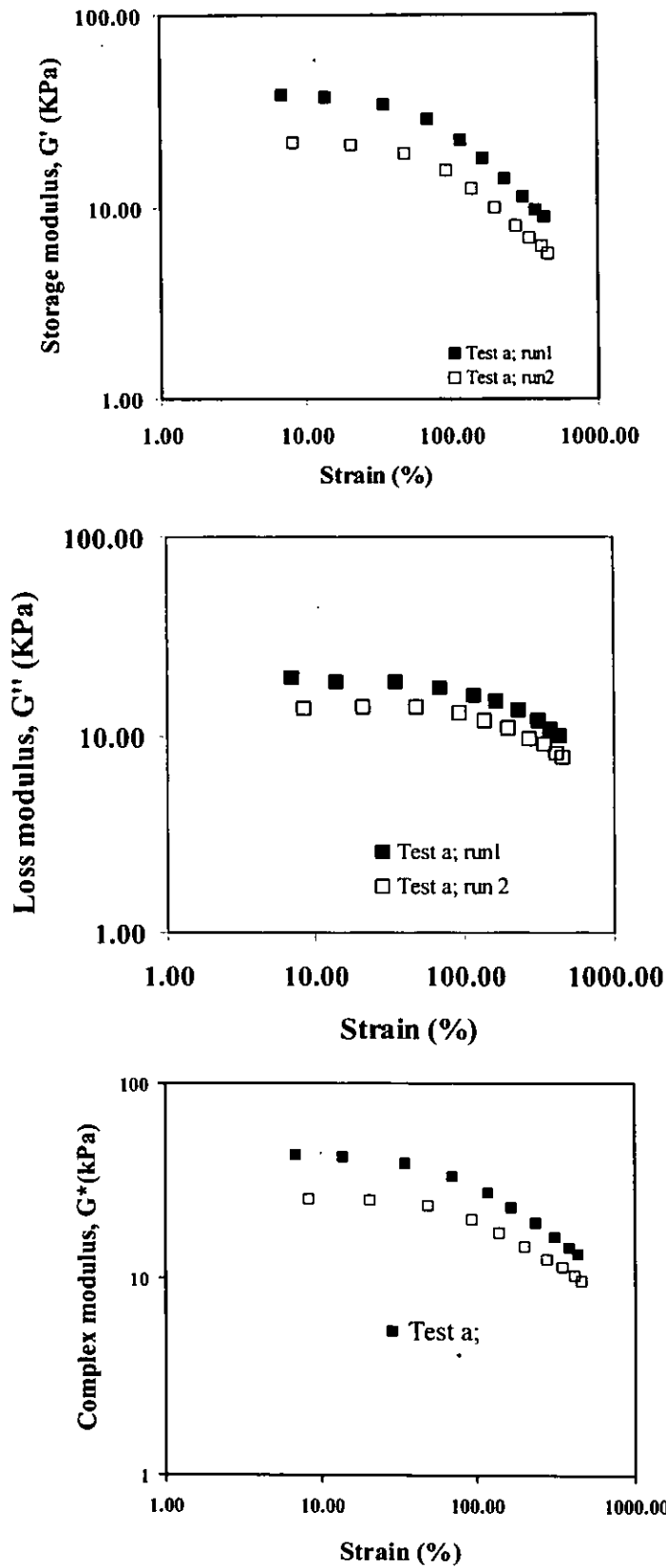


Figure 5.89 Strain sweep tests on HNR38 sample; RPA built-in data treatment.



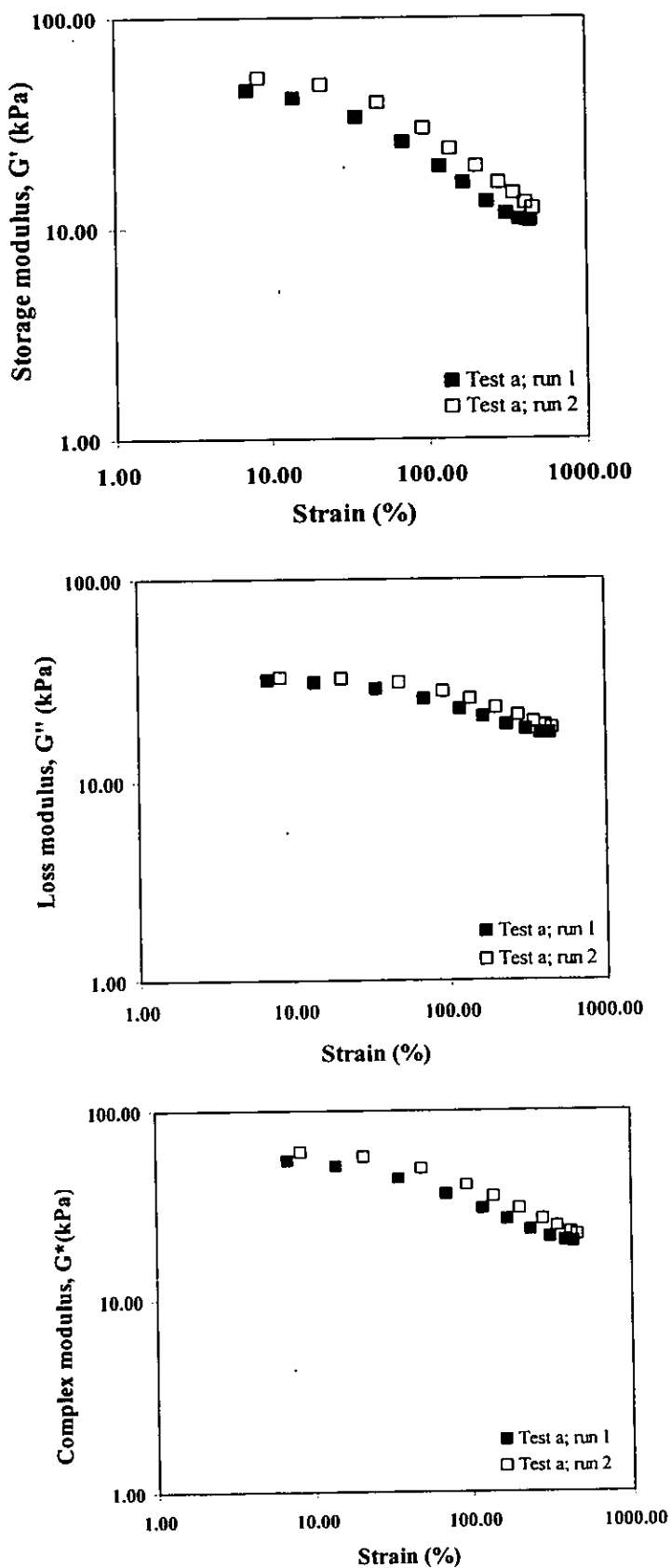


Figure 5.90 Strain sweep tests on HNR69 sample; RPA built-in data treatment.



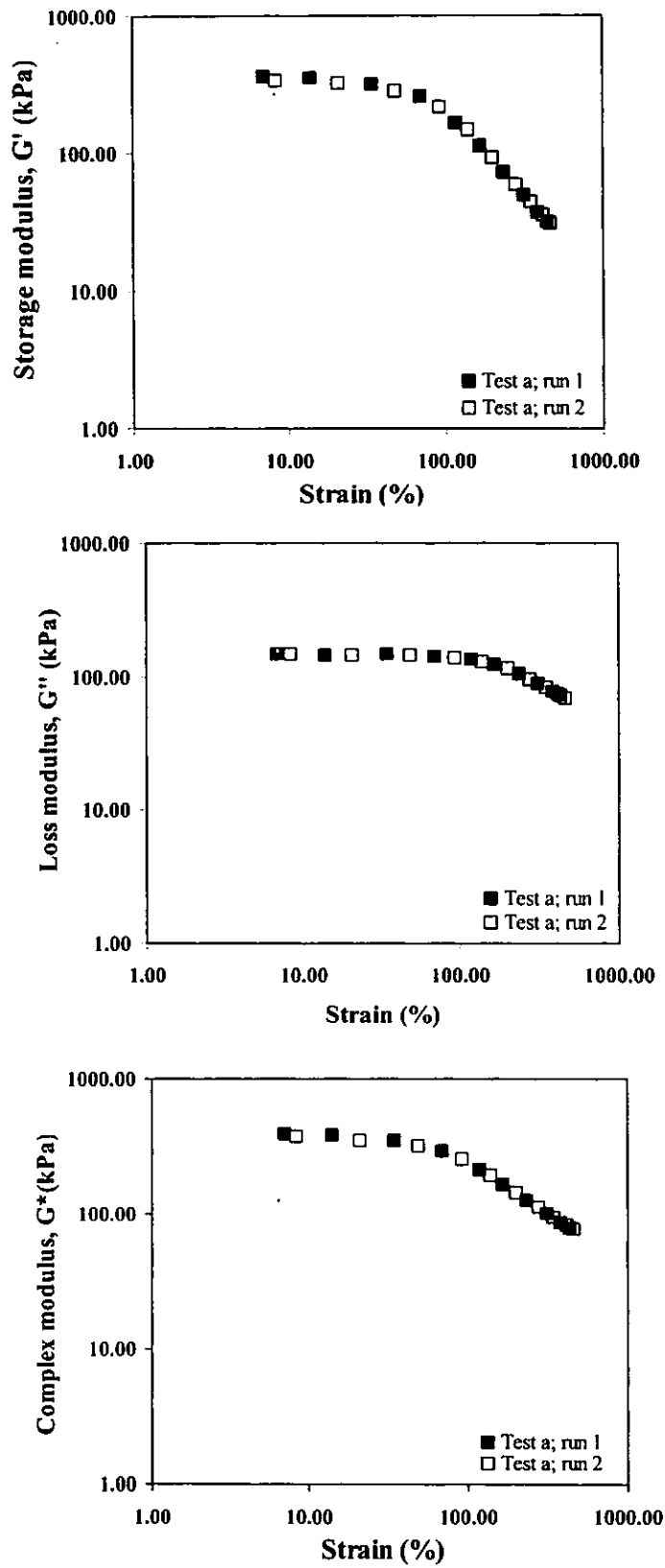


Figure 5.91 Strain sweep tests on HNR97 sample; RPA built-in data treatment.



5.8.2 Results on HNR Samples Using Fourier Transform Rheometry

In order to investigate the non-linear viscoelastic character of the samples, torsional dynamic rheometer has been modified.

Using the calculation technique described in section 3.6, Fourier transform was performed on all strain signals recorded during strain sweep tests with the data acquisition system. FT spectra were obtained from which the magnitude of the main torque component, i.e., at 1 Hz, the test frequency, and the relative odd-harmonic components, i.e., the ratio $T(n\omega_1)/T(\omega_1)$ where $n = 3, 5, 7, \dots$, were extracted. Figure 5.92 shows the main torque components from Fourier transform treatment of strain sweep tests on the HNR samples. In the HNR38 sample, a linear variation of the main torque component with the set deformation is found at very low strain ($\approx 14\%$ strain) with respect to HNR69 and HNR97 samples. Fit straight lines passes through zero and the slope depends on the materials, i.e., 3.67 for HNR70 ($r^2 = 0.9833$) and 28.41 for HNR97 ($r^2 = 0.9961$) at around 35 % deformation. In the HNR69 and HNR97 samples, the linear variation of $T(\omega_1)$ reflects clearly the linear viscoelastic behavior of this sample up to around 35 % deformation and the slope obtained by linear regression are, as expected, commensurate with G' data, as provided by built-in data treatment of the instrument while the difference of slope values in the HNR69 and HNR97 is extremely significant. It results from the structural characteristics of the samples i.e., HNR69 consists of the 69% of saturated portion and 31% of unsaturated portions whereas HNR97 is almost fully hydrogenated NR.



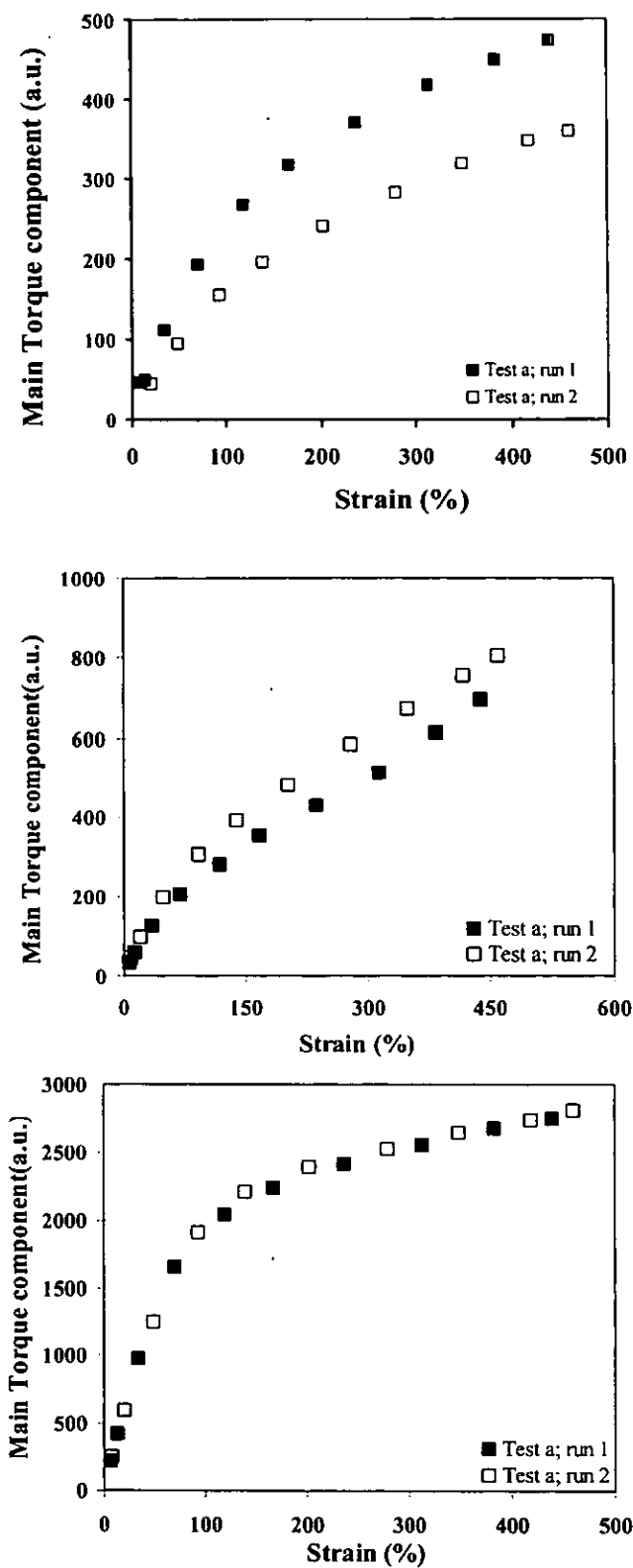


Figure 5.92 Main torque components detected from Fourier transform treatment of strain sweep tests on HNR38, HNR69 and HNR97 samples.



As described in section 3.7, the Fourier transform analysis was performed on the torque signals captured during the strain sweep tests. Wilhelm et. al. [110] have demonstrated that the envelope function for the intensity of the different harmonics decreases as $1/n\omega_1$, where $n = 3, 5, 7$. In other words, the limit of the relative torque harmonic $T(n\omega_1)/T(\omega_1)$ is expected to be equal to $1/n$, if both infinite high torques and a shear rate dependent viscosity are considered. Consequently, $T(3\omega_1)/T(\omega_1)$ is the most intense contribution compared to all other harmonics.

Figure 5.93 shows the relative third harmonic component with the set deformation as measured on HNR38, HNR69 and HNR97 samples. Lower strain angle data are scattered, in agreement with a similar study on EPDM samples [87,109]. An S-sharp variation is observed, from a (scattered) plateau value at low strain up to a maximum at high strain. Leblanc [86] attempted to describe the variation of the third harmonic component with the following equation:

$$\left[\frac{T(3\omega_1)}{T(\omega_1)} \right]_{\gamma} = \left[\frac{T(3\omega_1)}{T(\omega_1)} \right]_{\min} + \left\{ \left[\frac{T(3\omega_1)}{T(\omega_1)} \right]_{\max} - \left[\frac{T(3\omega_1)}{T(\omega_1)} \right]_{\min} \right\} x [1 - \exp(-b\gamma)]^c \quad (5.24)$$

where $\left[\frac{T(3\omega_1)}{T(\omega_1)} \right]_{\min}$ and $\left[\frac{T(3\omega_1)}{T(\omega_1)} \right]_{\max}$ are the limiting third harmonic components at very low and very high (infinite) strain, respectively. While γ is the strain amplitude, b and c are fit parameters.

Figure 5.93 obviously suggests that a sigmoidal type of equation of this model can be used to fit the experimental observations. The difference between the experimental and calculated curves is illustrated. These difference curves are quite small indicating a good quality of pattern fitting is obtained. Similar graphs are obtained with the other HNR samples, and the corresponding fit parameters are summarized in Table 5.49. From the parameters listed in Tables 5.49, it can be seen that the minimum third harmonic component appears to depend on the material tested, but this parameter describes the curve in the data range where the scatter is maximum. At the same time, the difference in the maximum third harmonic contribution of three HNR samples are seen, for instance, the HNR97 sample gives the highest value. While the values of the maximum third harmonic contribution of HNR38 and HNR69 are comparable. It might be described that the HNR97 which was completely



hydrogenation of NR resulting in ethylene-propylene copolymer that shows the increase of torque with increase of set of deformation. However, the relative third harmonic component varies with the strain amplitude is determined by the two parameters b and c . For b parameter, there is a physical meaning indicating the transition towards a strong nonlinear behavior.

Table 5.49 Effect of strain amplitude on third harmonic component; fit parameters obtained by sigmoidal model

Materials	HNR38		HNR69		HNR97	
	Run 1	Run 2	Run 1	Run 2	Run 1	Run 2
$T(3w)/T(w)_{\min}$	2.17±0.12	2.26±0.14	2.60±0.15	2.49±0.14	2.88±0.42	4.24±0.64
$T(3w)/T(w)_{\max}$	10.60±2.77	9.03±1.43	10.26±0.36	11.07±0.23	22.04±0.65	20.82±1.04
b	0.006±0.002	0.007±0.002	0.008±0.001	0.010±0.001	0.013±0.002	0.013±0.004
c	5.93±3.56	5.80±3.47	2.03±0.42	2.84±0.53	5.39±1.82	5.28±3.13
r^2	0.990	0.988	0.997	0.998	0.995	0.984



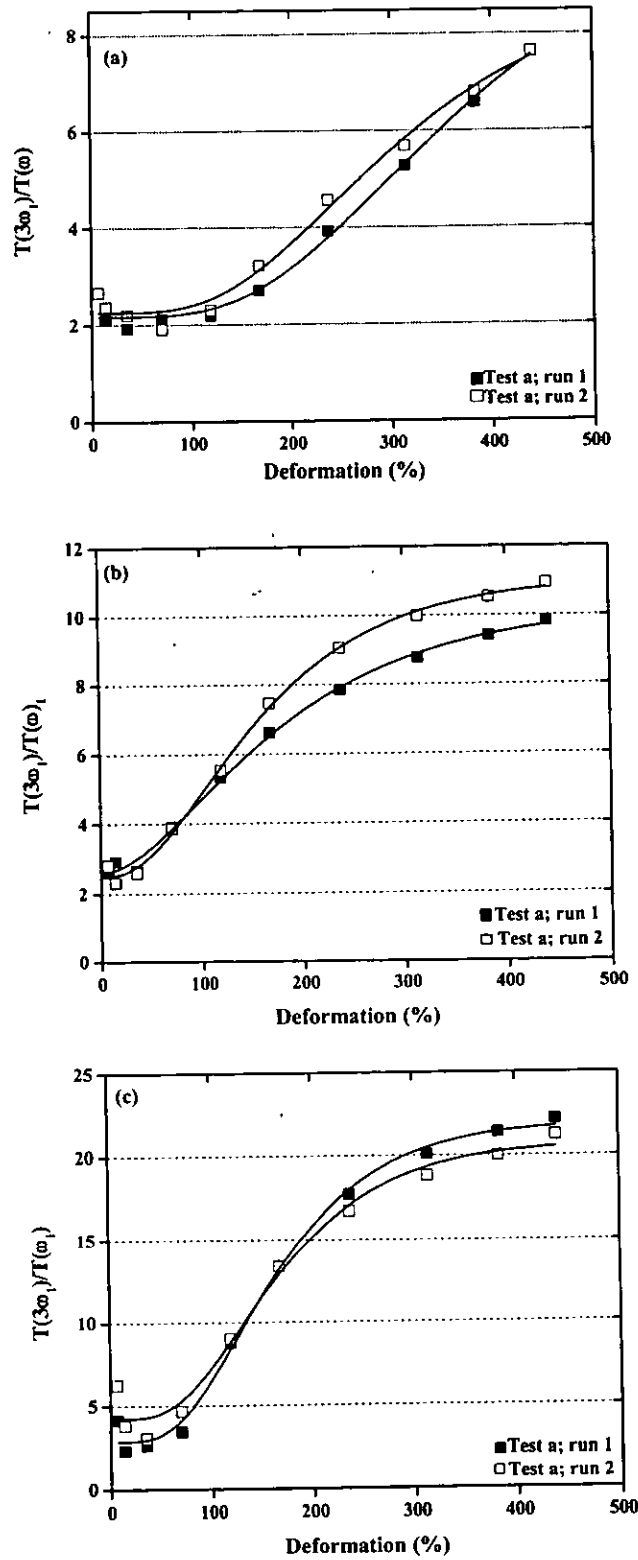


Figure 5.93 Relative third harmonic component versus strain (%) of the samples fit without constraint on parameters (a) HNR38, (b) HNR69 and (c) HNR97.



5.9 Correlation of the Molecular Characteristic with Physical Properties of NR, ENR and their Hydrogenated Samples

The physical properties of the hydrogenated rubbers are the most important for potential applications. This section will present some correlation of the physical properties of NR, ENR and their hydrogenated rubbers, such as the correlation of thermal transition with molecular characteristics of rubber chains before and after modification.

Correlation of the results from spectroscopic techniques will, it was thought, help identify the microstructure of products and determination the percent hydrogenation. The forth part is concerned with spectroscopic investigation of the molecular characteristic of the hydrogenated resulting. Both Raman and ^{13}C -NMR spectroscopies in solid state have been applied to study the molecular characteristics in order to correlate with the physical properties i.e., glass transition temperature (T_g).

The correlation results for the relative variation force constant at various hydrogenation levels of HNR samples with the glass transition temperature and maximum degradation temperature are presented in Table 5.50. There is slight increment in T_g and maximum degradation temperature (T_d) with the relative variation force constant. The possible reason to play for the gradually enhanced maximum degradation temperature with hydrogenation level is the increase in the relative variation force constant of the samples. This may result from the increase in the intermolecular force of the molecular rubber chains with reduction of unsaturated units. It has also seen that the slightly change maximum degradation temperature of HENR-10 with the relative variation force constant as tabulated in Table 5.51.



Table 5.50 Correlation between relative variation force constant, glass transition (T_g) and maximum degradation temperatures (T^P_2) of the HNR at various hydrogenation level

Hydrogenation (%)	Relative variation force constant	T_g (°C)	T^P_2 (°C)
0	0.00	-66.7	377.1
39.1	0.114	-65.0	438.9
57.5	0.186	-64.9	446.5
79.4	0.236	-63.5	456.7
84.9	0.228	-62.3	457.6

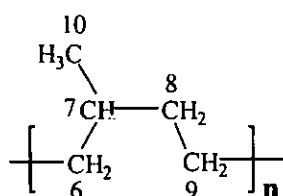
Table 5.51 Correlation between relative variation force constant and maximum degradation temperatures of the HENR-10 at various hydrogenation level.

Hydrogenation (%)	Relative variation force constant	T^P_2 (°C)
0	0.000	392.6
35.0	0.043	452.2
70.0	0.158	457.6
84.6	0.250	458.5
93.0	0.309	461.2



To investigate the correlation between the line widths of solid state NMR line at position 33 ppm (methine carbon) with thermal properties, the results are shown in Table 5.52. It is seen that the T_g gradually increases with the increasing of line widths. This is due to the T_g of HNR is independent of the line widths in the case of hydrogenated samples. The width of NMR line in solid state may be contributed to the local conformations that are *trans* isomer or saturated portions.

Table 5.52 Correlation between line widths, glass transition temperature and hydrogenation level



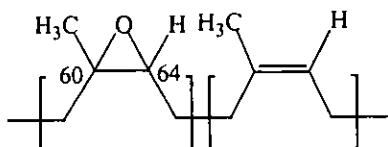
Hydrogenation (%)	Line width at C-7 (Hz)	T_g (°C)
39.1	26.42	-65.0
57.5	32.46	-65.1
79.4	34.72	-63.0
84.9	38.49	-62.4

As seen in section of characterization of ENR, the solid state NMR spectra of ENR with various oxirane units are broad line width. This is responsible for the evidence obtained from the molecular characterization that gives information about line widths of carbon signals corresponding to oxirane ring as given in Table 5.53.

It is shown that the glass transition temperatures increase with respect to the line widths of ^{13}C -resonance of oxirane units. This indicates that more rigidity of the molecular chain resulting from the epoxidation level clearly affects the glass transition temperatures of the ENR samples.



Table 5.53 Correlation between line widths and glass transition temperature of the ENR at different epoxidation levels



Epoxidation (%)	Line width at C-60 (Hz)	Line width at C-64 (Hz)	T _g (°C)
10	13.59	20.38	-47.4
15	20.38	42.27	-40.0
22	30.19	55.85	-37.3
40	43.02	111.71	-31.3

Moreover, from NMR spectra of HENR in section 5.3, it should be noted that at a higher level of epoxidation, the line width has significant influence on the onset and glass transition temperature in the HENR samples (section 5.7.2).

The possible reasons for explanation of the higher measured values for the onset and glass transition temperature is more immobility segments after hydrogenation according to the addition of TSOH by product on the rubber chains and furanization of oxirane units due to *p*-toluenesulfonic acid acting as a catalyst for this reaction.

5.10 Raman Microscopic Study of the Homogeneities of the Hydrogenated Rubbers

The micro-Raman mapping is now conveniently technique applied for point analysis and depth profiling of chemical and inhomogeneities of materials with a high spatial resolution. Therefore, this technique was chosen here to demonstrate the value of Raman imaging for the study of heterogeneities in the NR and HNR samples.

The specimen was placed on the X-Y stage and the laser beam was focused on the specimen surface through a 50x microscope objective. The specimen was moved relative to the layer spot position by steps of 0.2 μm in the xy direction. By detecting the Raman spectra at selected area, the distribution of components (homogeneities) in micro scale of the samples can be assessed in the xy direction.

The Raman spectra of the samples before and after modification in the region of interest (1300-1700 cm^{-1}) were recorded to observe the characteristics of the C=C bond, methyl and methylene groups positioned at 1664, 1452 and 1432 cm^{-1} , respectively (Figure 5.94). The calculation of [C=C]/CH₃ ratio offers the advantage of minimizing errors due to the fluctuation of laser power over the duration of the experiment (mainly as a result of errors in focusing the laser, with a resulting rapid decrease in intensity with distance from the objective focal plane). Comparing between the Raman spectra NR and HNR, it was found the intensity of the Raman band at 1664 cm^{-1} corresponding to the C=C stretching mode of polyisoprene units decreased when increase the hydrogenation time. On the other hand, the intensity of the Raman band at 1432 cm^{-1} increased, indicating the hydrogenation reaction.

The variation of unsaturated content can be determined on a relative basis by comparing the stretching vibration of the C=C (1664 cm^{-1}) to that of the CH₃ deformation mode (1450 cm^{-1}). A band should be selected as an internal reference band whose intensity does not change during hydrogenation process. The results of the distribution of the unsaturated units of NR and the hydrogenated samples in particular area are presented in Figure 5.95. Figure 5.95(a) shows the image of the ratio the area under the Raman band at 1664 cm^{-1} over that at 1452 cm^{-1} and the corresponding pseudo-3D representation. The dark shading stands (black color) for a high ratio and



thus for a high content the carbon carbon double bonds. This image is essentially comparable to those in Figure 5.95 (b) and Figure 5.95 (c) in shape of the features. The dominant soft blue color level scale appears in the case of HNR(2) sample while in the case of HNR(6) the intensity level shows the soft green scale. This means that the lowest carbon-carbon double bond content in HNR(6) is compared to that of the sample. The variation of amount of carbon-carbon double bond of *cis*-1,4 polyisoprene units within a particular map demonstrated the homogeneity of the distribution of double bonds on micron scale of NR. The recorded Raman mapping in step by step of 0.2 μm can be roughly related to the number of *cis*-1,4 polyisoprene units which is about 45 units (length of one unit of polyisoprene about 4.42 nm). The variation of error of distribution of unsaturated units in NR from one position to another which can be estimated from the relative intensity scale of Raman mapping (see Figure 5.61 (a)) is in the order of 10%. As for HNR(2), the distribution of C=C bond inside the area mapped is almost homogeneous, indeed the level of unsaturated units varies between 60-70 % with respect to that of NR assumed 100%. Moreover, the 13-18 units of polyisoprene (45 units) can react with diimide molecule within 0.2 μm step of mapping. Within 2 μm x 2 μm area of HNR(6), the distribution of double bonds is also homogeneity in a microscopic scale and the variation of the C=C bond content is approximately 30-45 % as compared to that of NR. This map shows that the distribution of the C=C bonds in microscopic scale which is in close proximity to the 25-32 units of saturated fraction. These results roughly indicate that the hydrogenation level of HNR(2) and HNR(6) samples are around 30-45 and 60-70%, respectively. It can also be seen that the standard deviations in individual maps are generally higher for the distribution of the C=C bonds of HNR(6) than for distribution of the C=C bonds of HNR(2). From the Raman mapping analysis, it becomes clear that distribution of the double bond content is almost homogeneous HNR sample around within 45 units but the variation of error depends on the hydrogenation level.



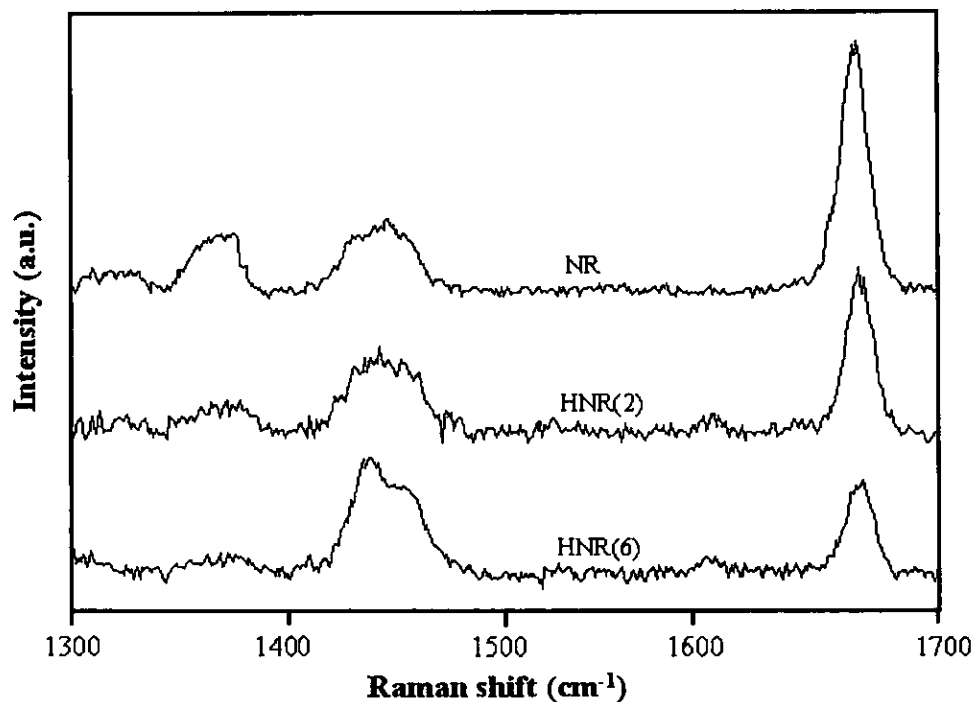


Figure 5.94 Raman spectra of NR and the hydrogenated rubbers obtained from 2 and 6h: HNR(2), and HNR(6) containing 39 and 79 % hydrogenation level.

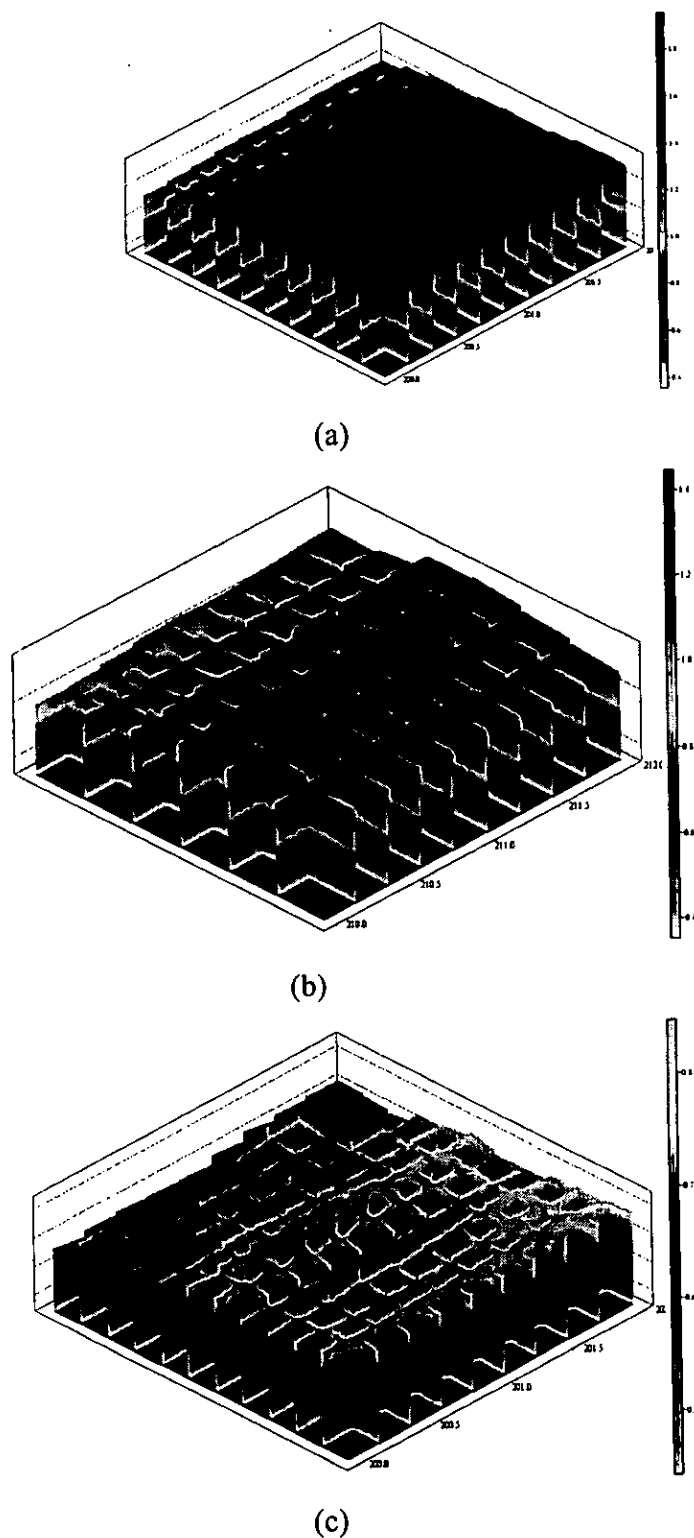


Figure 5.95 Micro-Raman mapping of NR (a), the hydrogenated rubbers obtained from 2 and 6h: HNR(2) (b), and HNR(6) (c) containing 39 and 79 % hydrogenation level at area $2 \mu\text{m} \times 2 \mu\text{m}$.

CHAPTER 6

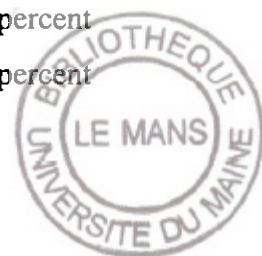
CONCLUSIONS

Hydrogenation of unsaturated rubbers was carried by non-catalytic process using diimide generated *in situ* from two types of hydrogenating agent. The first one is the use of *p*-toluenesulfonylhydrazide (TSH), which is decomposed under high temperature to form diimide molecule. The reaction had been carried out in organic media i.e. xylene. The second type is the formation of diimide from the oxidation of hydrazine by hydrogen peroxide. In this case, the reaction could be carried out in aqueous media i.e. the reaction in latex form. The microstructures of the hydrogenated products were characterized using vibration and nuclear magnetic resonance spectroscopic techniques. The molecular characteristics, thermal behavior and rheological properties were also investigated. The following conclusions could be drawn as the following.

1. The hydrogenation of NR and four different ENRs i.e. ENR-10, ENR-22, ENR-30 and ENR-40, having epoxidation level of 10, 22, 30 and 40 %, respectively, could be performed in xylene solution at 135°C using the mole ratio of [TSH]:[C=C] equal to 2. The spectroscopic techniques i.e. Raman, FT-IR, ¹H-NMR and ¹³C-NMR were used to analyze the microstructure of the resulting products after hydrogenation and it was found that partial hydrogenation was occurred.

2. The percent hydrogenation of the NR was found to be dependent on the reaction time. The maximum degree of hydrogenation of NR is about 85-89 % determined by Raman, ¹H-NMR in liquid state and ¹³C-NMR in solid state. The Raman technique was successfully used to determine the percent hydrogenation versus reaction times because the carbon-carbon double bond has a vibrational characteristic which is strongly Raman active.

3. Similar trend was observed in the case of ENRs that the percent hydrogenation increased with increasing the reaction time. The maximum percent



hydrogenation is approximately 93-98% as determined by Raman spectroscopy and $^1\text{H-NMR}$ in liquid state. The kinetic study of NR and ENRs hydrogenation reveals that the rate of hydrogenation increases when the epoxidation level of the rubber increases and is greater than that of NR.

4. *Cis-trans* isomerization was encountered during hydrogenation reaction using TSH both in the case of NR and ENRs. The percentage of transformation from *cis* to *trans* structures was quantified by $^1\text{H-NMR}$ in liquid state and $^{13}\text{C-NMR}$ in solid state. In the case of hydrogenation of ENR, the evidence of furanization and fixation of *p*-toluenesulphonic acid (TSOH) by-product on the HENR as side reactions was obviously detected by FTIR, Raman and $^{13}\text{C-NMR}$ with HD/MAS/CP technique in solid state. Another side reaction was the degradation of the modified rubber.

5. In the case of diimide reduction in latex process, various parameters affecting on the diimide reduction condition has been studied. The progress of the hydrogenation was monitored by means of NMR in liquid state as a function of reaction condition. The results indicated that percent hydrogenation increases with increasing of reaction time and temperature as well as the reactants for hydrogenation.

6. When the equimolar ratio of hydrazine, hydrogen peroxide and $\text{C}=\text{C}$ of the rubber was used, it was found that complete hydrogenation could not be obtained. This may be due to some side reactions such as the decomposition of the forming diimide into nitrogen gas and the loss of hydrogen peroxide which is decomposed into active hydroxyl radical. In addition, the diimide forming may be occurred into 2 forms i.e. *syn* and *trans* diimide and only the *syn* form can react with the $\text{C}=\text{C}$ of the rubber.

7. The effect of hydrazine and hydrogen peroxide concentration on the degree of hydrogenation revealed that the maximum hydrogenation was achieved when 1.5 mol of reagents per mole of unsaturated units were used. For the effect of dry rubber content on the hydrogenation of NR, it was found that dry rubber content has an affect on the level of hydrogenation, that is, 20% DRC gives the maximum percent hydrogenation about 23.6 when compared to 10 and 30 % DRC.

8. The investigation of various types of NR latex for hydrogenation were carried out i.e. NR latex, DPNR latex, skim NR latex. It was found that the maximum of hydrogenation degree is approximately 29% as the skim fresh NR latex was hydrogenated.



9. The molecular characteristic of NR, ENR and the hydrogenated rubbers was studied by means of Raman and ^{13}C -NMR spectroscopies in solid state.

- The relative variation force constants tend to be a linear relationship with the hydrogenation level. It might be suggested that the more stiffness part of the rubber chains appears upon hydrogenation in such a way that their relative variation force constants were probably increased.

-With solid-state NMR technique, the line widths of carbon signals i.e. methyl and methylene on the molecular chain of the NR were found to be increased as the hydrogenation level was increased. It was due to after hydrogenation, the unsaturated unit was transformed into the saturated part in which the mobility of methylene and methine carbons may be restricted as they are connected with other carbons along the rubber chains which might be in the molecular packing of saturated units. In addition, the appearance of *trans*-polyisoprene may be responsible for this evidence.

- The observed line broadenings of carbon signals of ENR significantly increased with the extent of epoxidation. The line broadenings of two carbon signals of epoxy units in ENR were related to the distributions of isotropic chemical shifts and the dipolar interactions which may not be completely averaged and arised from a variety of local conformations.

- By comparing between the resonance spectra of the HNR and the HENR, the resonance line widths of the HENR are significantly broader than that of the HNR one. It is resulted from isotropic chemical shift distribution and residual dipolar interactions arising from the presence of components with reduced mobility on the modified rubber chains.

- In CP experiment of the study of molecular dynamic of HNR, and HENR, it was found that the cross polarization time of methyl carbon in HENR-30(8) is lowest with respect to methyl carbon in HNR(8) and HENR-10(8). The methyl carbon of HENR-30(8) is clearly the least mobility due to the more furan structure and the chemical fixation of TSOH on the rubber chain.

10. The observation of Raman bands of NR, ENR and HNR under heat treatment was found broadening and the wave number of the Raman band at 1664 cm^{-1} decreased depending on temperature. This result can be explained that the inherent



nature of the polarizability change as a result of changes in the intermolecular forces arises from thermal expansion.

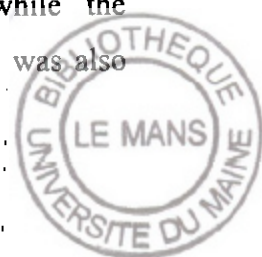
11. The DSC results for NR and all HNR samples obtained from the second heating mode revealed that with increasing hydrogenation content to 85%, the glass transition temperatures (T_g) slightly increased, whereas in HENR samples the glass transition temperatures significantly increased, due to the more rigid group on rubber chains of HENR samples. It was found that the enhancement of T_g of HENR samples tends to be dependent on the hydrogenation level.

12. Thermal stability of NR and the hydrogenated rubbers investigated by TGA was found the improvement of the samples after hydrogenation. In the case of HNRs obtained from organic solvent, thermogram of the decomposition temperatures found two step process but the thermal stability of final step of HNRs are higher than that of NR. While HNRs obtained from aqueous system give one step process of thermal stability and the decomposition temperature was enhanced as well. The results of TGA analysis of HENR also indicated the enhancement of final thermal stability after hydrogenation.

13. Rheological properties of HNR samples were measured. It was found that the storage and loss moduli of HNR97 (97% hydrogenation) sample are the highest values when compared with HNR38 (38% hydrogenation) and HNR69 (69% hydrogenation) samples and remarkably increases with the hydrogenation level. For instance, the fully hydrogenated NR has a significant increment in the loss and storage moduli of the sample.

14. The correlation results for the relative variation force constant at various hydrogenation levels of HNR samples with the T_g were examined. It was found that the T_g and maximum degradation temperature showed the increment with the relative variation force constant. The correlation between the line widths of solid state NMR with thermal properties was observed that the T_g gradually increased with the increasing of line width positioned at 33 ppm characteristic of methine carbon.

15. The investigation of variation of amount of carbon-carbon double bond of *cis*-1,4 polyisoprene units using Raman mapping technique demonstrated the homogeneity of the distribution of double bonds on micron scale of NR while the distribution of C=C bond of HNR(2) and HNR(6) inside the area mapped was also



found the homogeneity in a microscopic scale with variation of about 10-15% of error in the study area of $2\mu\text{m} \times 2\mu\text{m}$. It can be concluded that the hydrogenation of NR is a random process in micron level.



REFERENCES

1. Balkwill WJ. The history of natural rubber production in rubber ed Webster CC, Balkwill WJ. Longman 1989: 1-56.
2. Gent AN, Kawahara S, Zhao J. Crystallization and strength of natural rubber and synthetic cis-1,4 Polyisoprene. *Rubb Chem Techno* 1998; 71: 668-677.
3. Thomas AG, Whittle JM. Tensile rupture of rubber. *Rubb Chem Techno* 1970; 43: 222-228.
4. Fettes EM. Chemical reactions of polymers. New York: John Wiley and Sons; 1964.
5. Gelling IR, Porter M. Natural Rubber Science and Technology: Chemical modification of natural rubber (Chapter 10). ed Roberts AD, Oxford: University Press; 1988; 359-443.
6. Schulz DN, Turner SR, Golub MA. Recent advances in the chemical modification of unsaturated polymers. *Rubb Chem Techno* 1993; 55: 809-885.
7. Brosse JC, Campistron I, Derouet D, Hamdaoui A EL, Houdayer S, Reyx D, Ritoit-Gillier S. Chemical modifications of polydiene elastomers: a survey and some recent results. *J App Polym Sci* 2000; 78: 1461-1477.
8. Gelling IR. Epoxidised natural rubber. *J Nat Rubb Res* 1991; 6: 184-205.
9. Saelao J, Phinyocheep P. Influence of styrene on grafting efficiency of maleic anhydride onto natural rubber. *J App Polym Sci* 2005; 95: 28-38.
10. Baker CSL, Gelling IR, Newell R. Epoxidised natural rubber. *Rubb Chem Techno* 1986; 58: 67-85.
11. Mango LA, Lenz RW. Hydrogenation of unsaturated polymer with diimide. *Die Makromolekulars Chemie* 1973; 163: 13-36.
12. Singha NK, De PP, Sivaram S, Homogeneous catalytic hydrogenation of natural rubber using $\text{RhCl}(\text{PPh}_3)_3$. *J App Polym Sci* 1997; 66: 1647-1652.
13. Singha NK, Bhattacharjee S, Sivaram S. Hydrogenation of diene elastomers,



- their properties and applications: A critical review. *Rubb Chem Techno* 1997; 70: 309-367.
14. Wrana C, Reinartz K, Winkelbach HR. Therban-The high performance elastomer for the new millennium. *Macromol Mater Eng* 2001; 286: 657-662.
 15. Taha M, Frerejean V, Morphology development of LDPE-PS blend compatibilization. *J Apply Polym Sci* 1996; 61: 969-979.
 16. De SM, De PP, Bhowmick AK. New polymeric blends from hydrogenated styrene-butadiene rubber and polyethylene. *Polymer* 1998; 39: 6789-6800.
 17. Yang Y, Otsuka N, Saito H, Inoue T, Takemura Y. Morphology and elastomeric properties of isotactic polypropylene/hydrogenated poly(styrene-co-butadiene) blends: a potential for a new thermoplastic elastomer. *Polymer* 1999; 40: 559-564.
 18. Wang TY, Tsiang R C-C, Liou J-S, Wu J, Sheu H-C. Preparation and characterization of a star-shaped polystyrene-b-poly(ethylene-co-propylene) block copolymer as a viscosity index improver of lubricant. *J Apply Polym Sci* 2001; 79: 1838-1846.
 19. Gan SN, Subramaniam N, Yahya R. Hydrogenation of Natural Rubber using Nickel-2-ethylhexanoate catalyst in combination with Triisobutyl-aluminum. *J Apply Polym Sci* 1996; 59: 63-70.
 20. Bhattacharjee S, Bhowmick AK, Avasthit BN. Hydrogenation of epoxidized natural rubber in the presence of Palladium Acetate catalyst. *Polymer* 1993; 34: 5168-5173.
 21. Roy S, Bhattacharjee S, Gupta BR, Hydrogenation of epoxidized natural rubber. *J Apply Polym Sci* 1993; 49: 375-380.
 22. Koenig JL. *Spectroscopy of Polymers*. Washington: American Chemical Society: USA, 1992; 115-252.
 23. Jackson KDO, Loadman MJR, Jones CH, Ellis G. Fourier transform Raman spectroscopy of elastomers: an overview. *Spectrochim Acta* 1990; 46A: 217-226.
 24. Hendra PJ, Jackson KDO. Application of Raman spectroscopy to the analysis of natural rubber. *Spectrochim Acta* 1994; 50A: 1987-1997.



25. Poshyachinda S, Kanitthanon V. FT Raman spectroscopic study of the diimide Hydrogenation of cis-Polybutadiene: Some Evidence of cis-trans Isomerization. *Spectrochim Acta* 1994; 50A: 2011-2017.
26. Qian-Xiu Z. The significance of the structure of laticifer with relation to the exudation of latex in *Hevea brasiliensis*. *J Nat Rubb Res* 1987; 2: 94-98.
27. Witisuwannakul D, Witisuwannakul R. Biopolymers: Biochemistry of natural rubber and structure of latex (Chapter 6). Koyama T and Steinbuechel A ed. Wley-VCH, 2000; 151-179.
28. Hasma H, Subramaniam A. Composition of lipids in latex of *Hevea brasiliensis* clone RRIM 501. *J Nat Rubb Res* 1986; 1(1): 30-40.
29. Cook S, Cudby PEF, Davies RT, Morris MD. The microstructure of natural rubber latex films. *Rubb Chem Techno* 1997; 70: 549-559.
30. Gomez JB. Lutoids of *Hevea* latex: morphological considerations. *J Nat Rubb Res* 1990; 5: 231-240.
31. Gorton ADT, Pendle TD. Properties and Processability of high ammonia lattices. *J Nat Rubb Res* 1986; 1: 122-134.
32. Nakade S, Kuga A, Hayashi M, Tanaka Y. Highly purified natural rubber IV. preparation and characteristics of gloves and condoms. 1997; 12 (1): 33-42.
33. Tangpakdee J, Tanaka Y. Purification of natural rubber. *J Nat Rubb Res* 1997; 12(2): 112-119.
34. Cunneen JI, Watson WF. Bulk isomerization of polyisoprene with sulfur dioxide. *Macromolecular Syntheses* 1: 245-248.
35. Agnihotri RK, Falcon D, Fredericks EC. Cyclization of Synthetic cis-1,4 polyisoprene. *J Polym Sci: Part A-1* 1972; 10: 1839-1850.
36. Patterson DJ, Koenig JL. A Fourier transform infrared and nuclear magnetic resonance study of cyclized natural rubber. *Makromol Chem* 1987; 188: 2325-2337.
37. Scanlan J, *Chemical Reactions of Polymers: Reactions of unsaturated polymeric hydrocarbons (B) cyclization (Chapter II)*. ed Fettes EM., New york: John Wiley and Sons; 1964; 125-132.
38. Gelling IR, Modification of natural rubber latex with peracetic acid. *Rubb Chem*



Technol 1984; 58: 86-96.

39. Baker CSL, Gelling IR, Samsuri AB. Epoxidised natural rubber. *J Nat Rubb Res* 1986; 1 (2): 135-144.
40. Campbell DS, Seow PK. Graft copolymers of cis-1,4 polyisoprenes with poly(methyl methacrylate). *J Nat Rubb Res* 1990; 5: 135-143.
41. Tangpakdee J, Mizokoshi M, Endo A, Tanaka Y. Novel method for preparation of low molecular weight natural rubber latex. *Rubb Chem Techno* 1998; 71: 795-802.
42. Mohammadi NA, Rempel GL. Homogeneous catalytic hydrogenation of polybutadiene. *J Molec Catal* 1989; 50: 259-275.
43. Rao PVC, Upadhyay VK, Pillai SM. Hydrogenation of polybutadienes catalyzed by $\text{RuCl}_2(\text{PPh}_3)_3$ and a structural study. *Eur Polym J* 2001; 37: 1159-1164.
44. Bhattacharjee S, Bhowmick AK, Avasthi BN. Preparation of hydrogenated nitrile rubber using palladium acetate catalyst: Its characterization and kinetics. *J Polym Sci Part A: Polym Chem* 1992; 30: 471-484.
45. Escobar Barrios VA, Herrera Najera R., Petit A, Pla F. Selective hydrogenation of butadiene-styrene copolymers using a Ziegler-Natta type catalyst 1. Kinetic study. *Eur Polym J* 2000; 36: 1817-1834.
46. Charmondusit K, Prasassarakich P, McManus N T Rempel GL. Hydrogenation of cis-1,4-poly(isoprene) catalyzed by $\text{OsHCl}(\text{CO})(\text{O}_2)(\text{PCy}_3)_2$. *J Appl Polym Sci* 2003; 89: 142-152.
47. Squillacote M, Felippis De J, Lai YL. Hydrogenation via photochemically generated diimide. *Tetrahedron Letters* 1993; 34: 4137-4140.
48. Harwood HJ, Russell DB, Verthe JJA, Zymonas J. Diimide as a reagent for the hydrogenation of unsaturated polymers. *Die Makromolekulare Chemie* 1973; 163: 1-12.
49. Wideman LG, Process for hydrogenation of carbon-carbon double bonds in an unsaturated polymer in latex form. US Patent 4452950 The Goodyear Tire and Rubber Co. 1983.
50. Hahn SF, An improved method for the Diimide hydrogenation of butadiene and isoprene containing polymers. *J Polym Sci Part A: Polym Chem* 1992; 30: 397-408.



51. Phinyocheep P, Pasiri S, Tavichai O. Diimide Hydrogenation of Isoprene-Styrene Diblock Copolymers J. App. Polym. Sci 2003; 87: 76-82.
52. Nang TD, Katabe Y, Minoura Y. Diimide reduction of cis-1,4 polyisoprene with *p*-toluenesulfonylhydrazide. Polymer 1976; 17: 117-121.
53. Edwards HGM, Johnson AF, Lewis IR, Maitland DJ, Webb N. Vibrational and NMR spectroscopic studies of a thiosulfonate produced from the non-catalytic hydrogenation of polybutadiene. J Mole Struc 1992; 268: 363-372.
54. Parker DK, Roberts RF, Schiessl HW. The preparation, properties and potential applications of "diimide-hydrogenated" styrene-butadiene (HSBR) and polybutadiene (HBR) thermoplastic elastomers. Rubb Chem Techno 1994; 67: 288-298.
55. Sarker De M, De PP, Bhowmick AK. Thermoplastic elastomeric hydrogenated styrene-butadiene elastomer: optimization of reaction conditions, thermodynamics and kinetics. J App Polym Sci 1997; 66: 1151-1162.
56. Sarker De M, De PP, Bhowmick AK. Influence of Styrene Content on the Hydrogenation of Styrene-Butadiene Copolymer. J Apply Polym Sci 1999; 71: 1581-1595.
57. Sarker De M, De PP, Bhowmick AK. Diimide reduction of carboxylated styrene-butadiene rubber in latex stage. Polymer 2000; 41: 907-915.
58. Parker DK, Roberts RF, Schiessl HW. A new process for the preparation of highly saturated nitrile rubber in latex form. Rubb Chem Techno 1992; 65: 245-258.
59. He Y, Daniels ES, Klein A, El-Aasser MS. Hydrogenation of styrene butadiene rubber (SBR) latexes. J Appl Polym Sci 1997; 64: 2047-2056.
60. Siesler HW, Holland-Moritz K. Infrared and Raman spectroscopy of polymers. New York & Basel 1980.
61. Long DA. Raman Spectroscopy. McGraw-Hill 1977.
62. Bower DI, Maddams WF. The vibrational spectroscopy of polymers. Cambridge 1989.



63. Doi Y, Yano A, Soga K, Burfield DR. Hydrogenation of polybutadienes: Microstructure and thermal properties of hydrogenated polybutadienes. *Macromolecules* 1986; 19: 2409-2412.
64. Jones CH. A Fourier transform Raman study of the cold crystallization of natural rubber and deproteinized natural rubber. *Spectrochimica Acta*. 1991; 47A: 1313-1319.
65. Edwards HGM, Farwell DW, Johnson AF, Lewis IR, Ward NJ. Spectroscopic studies of an ambient-pressure process for the selective hydrogenation of polybutadienes. *Macromolecules* 1992; 25: 525-529.
66. Markwort L, Kip B. Micro-Raman imaging of heterogeneous polymer systems: general applications and limitations. *J Appl Polym Sci* 1996; 61: 231-254.
67. Liu H, Keen I, Rintoul L, Georage GA. Study of the degradation of polyolefins by amplifying the heterogeneous photo-oxidised sites through grafting. *Polym Degrad Stab* 2001; 72: 543-550.
68. Bovey FA, Mirau PA. *NMR of polymers*. New York Academic 1996; 1-57.
69. Laupretre F. Applications of high-resolution solid-state carbon-13 NMR to polymers. *Prog Polym Sci* 1990; 15: 425-474.
70. Harris RK. *Nuclear magnetic resonance spectroscopy A Physicochemical view*. John Wiley & Sons 1991; 144-164.
71. Patterson DJ, Koenig JL, Shelton JR. Vulcanization studies of elastomers using solid-state C-13 NMR. *Rubb Chem Techno* 1983; 56: 971-993.
72. Mori M, Koenig JL. Solid state C-13 NMR studies of vulcanized elastomers XII. TBBS accelerated, sulfurvulcanization of carbon black filled natural rubber. *Rubb Chem Techno* 1996; 68: 551-562.
73. Mori M, Koenig JL. Solid state C-13 NMR studies of vulcanized elastomers XVII. Effect of carbon black grade on the network structure in natural rubber vulcanizates. *Rubb Chem Techno* 1997; 70: 671-680.
74. Klei B, Koenig JL. Solid state ¹³C NMR analysis of vulcanized rubbers XVI. The competitive vulcanization of natural rubber and polybutadiene blends. *Rubb Chem Techno* 1997; 70: 231-242.



75. Gronski W, Hoffmann U. Structure and density of crosslinks in natural rubber vulcanizates: a combined analysis by NMR spectroscopy, Mechanical measurements and rubber-elastic theory. *Rubb Chem Techno* 1992; 65: 63-77.
76. Buzaré JY, Silly G, Emery J, Boccaccio G, Rouault E. Aging effects on vulcanized natural rubber studied by high resolution solid state ^{13}C -NMR. *Eur Polym J* 2001; 37: 85-91.
77. Kolodziejski W, Klinowski J. Kinetics of cross-polarization in solid state NMR: A guide for chemists. *Chem Rev* 2002; 102: 613-628.
78. Kameda T, Asakura T. Structure and dynamics in the amorphous region of natural rubber observed under uniaxial deformation monitored with solid-state ^{13}C -NMR. *Polymer* 2003; 44: 7539-7544.
79. Shen MC, Eisenberg A. Glass transitions in polymers. *Rubb Chem Techno* 1970; : 95-170.
80. Sarker De M, Mukunda PG, De PP, Bhowmick AK. Degradation of hydrogenated styrene-butadiene rubber at high temperature. *Rubb Chem Technol* 1997; 70: 855-870.
81. Brydson JA. Flow properties of polymer melts. London: George Godwin Limited. 2nd ed 1981.
82. Cogswell FN. Polymer melt rheology: A guide for industrial practice. John Wiley & Sons 1981.
83. Dealy JM, Wissbrun KF. Melt rheology and its role in plastics processing: theory and applications. Van Nostrand Reinhold. 1990.
84. Leblanc JL, Chapelle CDL. Updating a torsional dynamic rheometer for Fourier transform rheometry on rubber materials. *Rubb Chem Technol* 2003; 76: 287-298.
85. Pawlowski H, Dick J. Viscoelastic characterization of rubber with a new dynamic mechanical tester. *Rubb World* 1992; 206: 35-40.
86. Leblanc JL. Fourier transform rheometry on gum elastomers. *J Appl Polym Sci* 2003; 89: 1101-1115.



87. Sanders JF, Ferry JD, Valentine RH. Viscoelastic properties of 1,2-polybutadiene comparison with natural rubber and other elastomers. *J Polym Sci: Part A-2*. 1968; 6: 967-980.
88. Pearson DS, Mueller SJ, Fetters LJ, Hadjichristidis N. Comparison of the rheological properties of linear and star-branched polyisoprene in shear and elongational flows. *J Polym Sci.: Polym Phys* 1983; 21: 2287-
89. Cowie J.M.G. *Polymer chemistry & physics of modern materials* 2nd ed Blackie Academic & Professional 1997; 256-270.
90. Bhattacharjee S, Bhowmick AK, Avasthi BN. Preparation of hydrogenated nitrile rubber using Palladium acetates catalyst: its characterization and kinetic. *J Polym Sci Part A: Polym Chem* 1992; 30: 471-484.
91. Raju VR, Racha pudy H, Graessley WW. Properties of amorphous and crystallizable hydrocarbon polymers IV. Melt rheology of linear and star-branched hydrogenated polybutadiene. *J Polym Sci: Polym Phys Ed.* 1979; 17: 1223-1235.
92. Gotra JT, Graessley WW. Model hydrocarbon polymers: Rheological properties of linear polyisoprenes and hydrogenated polyisoprenes. *Macromolecule* 1984; 17: 2767-2775.
93. Phinyocheep P and Duangthong S. Ultraviolet-curable liquid natural rubber. *J Appl Polym Sci* 2000; 78: 1478-1485.
94. Massiot D, Fayon F, Capron M, King I, Le Calve S, Alonso B, Durand JO, Bujoli B, Gan Z, Hoatson G. Modelling one- and two-dimensional solid-state NMR spectra. *Magn Reson in Chem* 2002; 40: 70-76.
95. Derouet D, Brosse JC, Challioui A. Alcoholysis of epoxidized polyisoprenes by direct opening of oxirane rings with alcohol derivatives 1. Modelization of the reaction. *Eur Polym J* 2001; 37: 1315-1326.
96. Bunce SJ, Edwards HGM, Johnson AF, Lewis IR. Synthetic polyisoprene studied by Fourier transform Raman spectroscopy. *Spectrochim Acta* 1993; 49A: 775-783.
97. Lin-Vien D, Colthup NB, Fateley WG, Grasselli JG. *The Handbook of Infrared and Raman Characteristic Frequencies of Organic Molecules*; Academic Press: London,



98. Sato H, Tanaka Y. $^1\text{H-NMR}$ study of polyisoprenes. *J Polym Sci: Polym Chem Ed.* 1979; 17: 3551-3558.
99. Shahab YA, Basheer RA. Nuclear magnetic resonance spectroscopy of partially saturated diene polymers I. H-NMR spectra of partially hydrogenated and partially deuterated natural rubber, gutta percha, and cis-1,4 polybutadiene. *J Polym Sci Polym Chem Ed* 1979; 16: 2667-2670.
100. Phetphisit CW, Phinyocheep P. Kinetics and parameters affecting degradation of purified natural rubber. *J Appl Polym Sci* 2003; 90: 3546-3555.
101. Thanomsilp C. The study of non-catalytic hydrogenation of polyisoprene [M.Sc. Thesis in Polymer Science]. Bangkok: Faculty of Graduate Studies, Mahidol University, 1997.
102. Bradbury JH, Perera MCS. Epoxidation of natural rubber studied by NMR spectroscopy. *J Appl Polym Sci* 1985; 30: 3347-3364
103. Perera MCS, Elix JA, Bradbury JH. Furanized rubber studied by NMR spectroscopy. *J Polym Sci Part A: Polym Chem* 1988; 26: 637-651.
104. Nor MH, Ebdon JR. Telechelic liquid natural rubber: A review. *Prog Polym Sci* 1998; 23: 143-177.
105. Sata H, Shimoyama M, Kamiya T, Amari T, Sasic S, Ninomiya T, Siesler HW, Ozaki Y. Raman spectra of high-density, low-density, and linear low-density polyethylene pellets and prediction of their physical properties by multivariate data analysis. *J Appl Polym Sci* 2002; 86: 443-448.
106. Rodriguez-Cabello JC, Santos J, Merino JC, Pastor JM. Thermally induced structural changes in low-shrinkage poly(ethylene terephthalate) fibers. *J Polym Sci Part B: Polym Phys* 1996; 34: 1243-1255.
107. Burfield DR, Lim K-L, and Law K-S. Epoxidation of natural rubber lattices: Methods of preparation and properties of modified rubbers. *J Appl Polym Sci* 1984; 29: 1661-1673.
108. Song J-S, Huang B-C, Yu D-S. Progress of synthesis and application of *trans*-1,4-polyisoprene. *J Appl Polym Sci* 2001; 82: 81-89.
109. Leblanc JL, and Chapelle CDL. Characterizing gum elastomers by Fourier transform rheometry. *Rubb Chem Technol* 2003; 76: 979-1000.



APPENDIX A**Table 1A** Specification of high ammonia natural rubber latex (HANR)

Properties	Test Results
Total Solids Content (%)	61.8
Dry Rubber Content (%)	60.1
Non Rubber Solids (%)	1.72
pH Value	10.6
KOH number	0.4769
Volatile Fatty Acid number (VFA)	0.0147
Mechanical Stability Time @ 55% TS.Sec.	720
Specific gravity at 25°C	0.9437
Viscosity (60% TS. Spindle no.1.60 rpm) cps.	74.5
Ammonia content (on total weight, %)	0.71
Magnesium content (ppm)	37.5
Cogulum content 80 mesh	23



APPENDIX B

APPENDIX B1: HPLC Chromatogram

HPLC Chromatogram of 4-methyl-4-octene (MO) compound and Hydrogenated MO

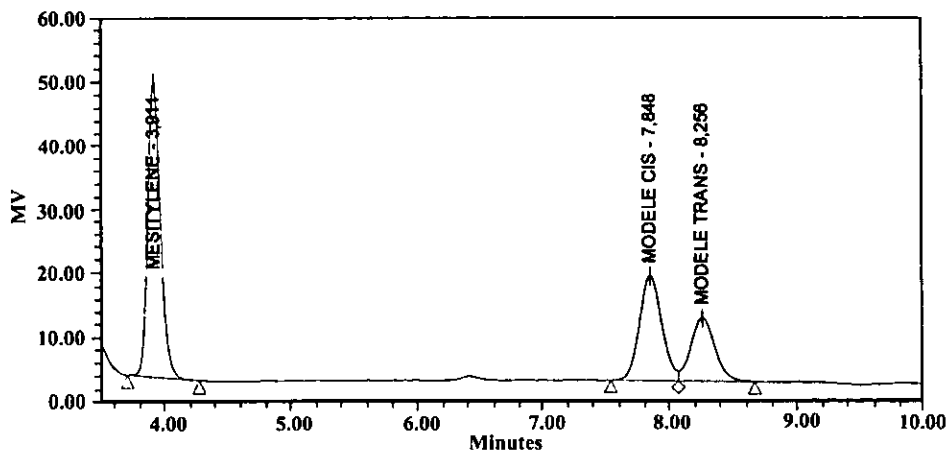


Figure 1 HPLC chromatogram of MO.

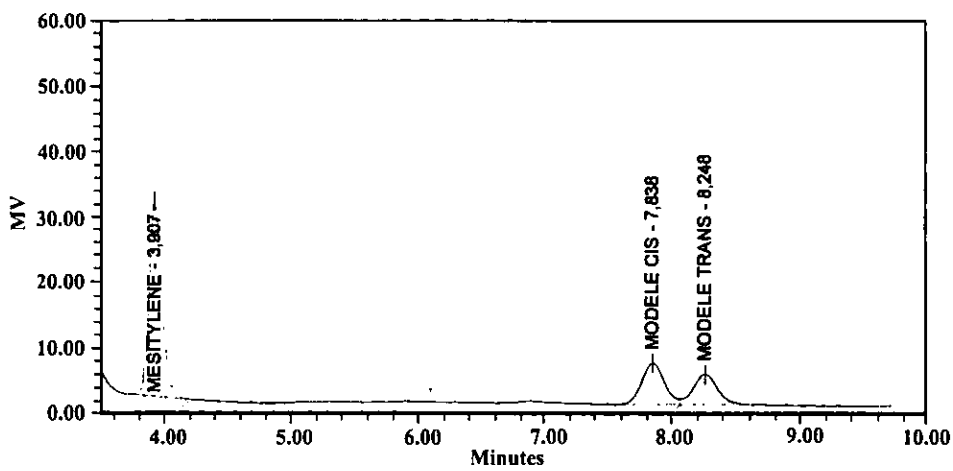


Figure 2 HPLC chromatogram of hydrogenation of MO at 30 min.



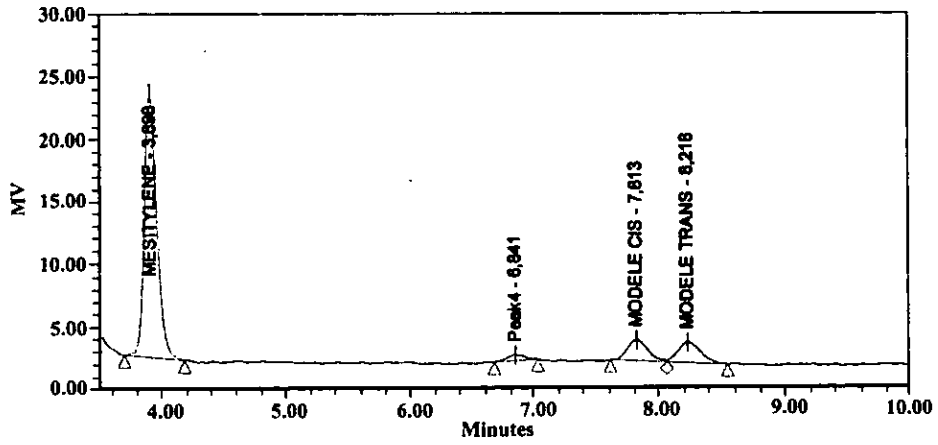


Figure 3 HPLC chromatogram of hydrogenation of MO at 120 min.

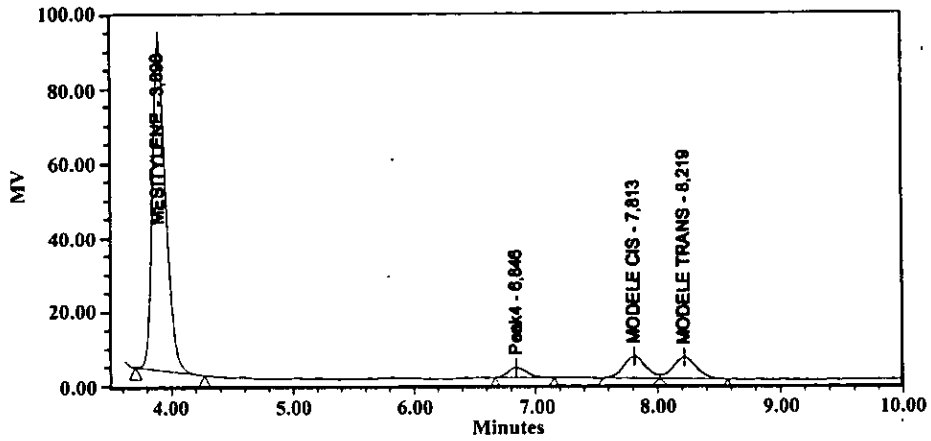


Figure 4 HPLC chromatogram of hydrogenation of MO at 180 min.

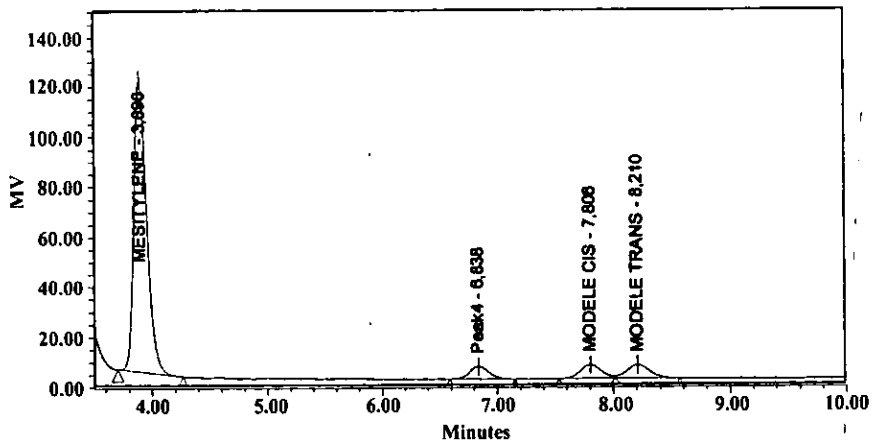


Figure 5 HPLC chromatogram of hydrogenation of MO at 240 min



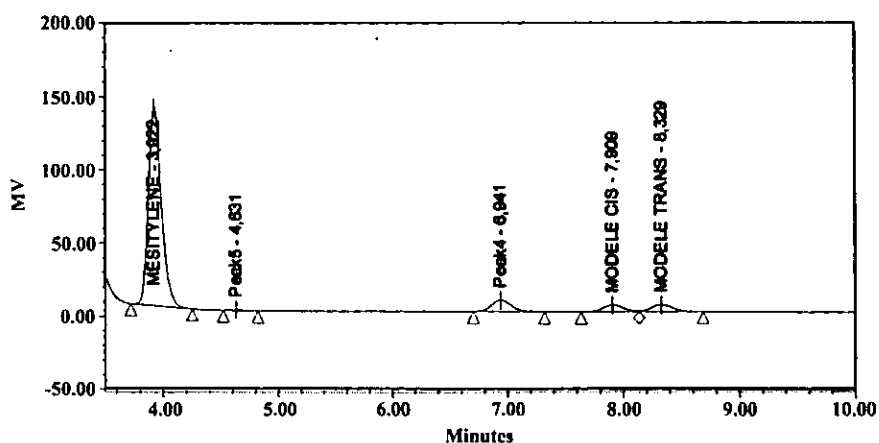


Figure 6 HPLC chromatogram of hydrogenation of MO at 360 min.

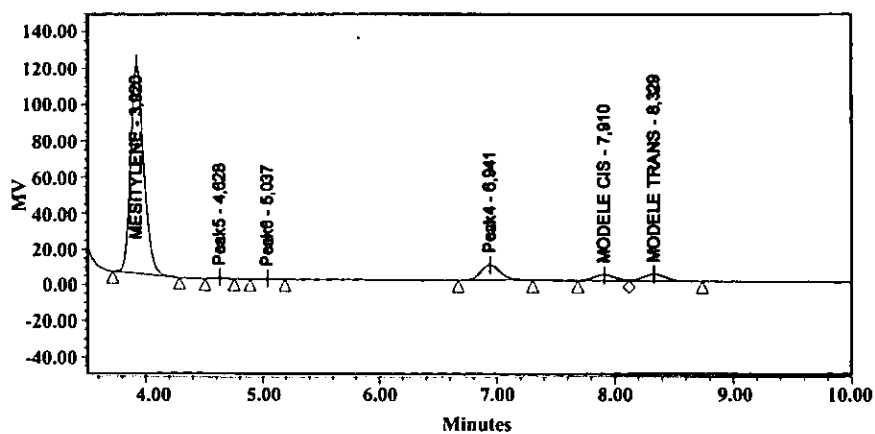


Figure 7 HPLC chromatogram of hydrogenation of MO at 480 min.

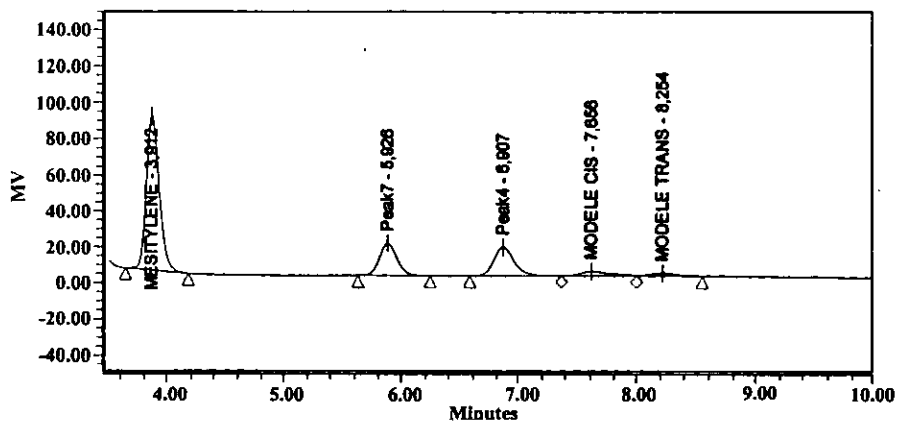


Figure 8 HPLC chromatogram of hydrogenation of MO at 24h.



APPENDIX B2

APPENDIX B2 Data of HPLC chromatogram obtained from the separation of each peak position during hydrogenation in xylene solvent.

Table 1 Area of mesitylene, *cis*-isomer, *trans*-isomer and hydrogenated MO (HMO) obtained from HPLC chromatogram.

Reaction time (h)	Area of each peak			
	Mesitylene R=3.91	<i>Cis</i> -isomer R=7.85	<i>Trans</i> -isomer R=8.25	HMO R=6.8
0	321972	131063	198824	0
0.5	205010	60383	76958	0
1	138984	29728	31684	0
2	147124	20267	18748	4704
3	677350	78450	74829	30908
4	903388	78509	73455	59105
6	1064095	64387	57947	92910
8	906142	51938	41417	102185
24	661683	49405	28217	195824



BIOGRAPHY

NAME	Miss Jareerat Samran
DATE OF BIRTH	April 25, 1972
PLACE OF BIRTH	Krabi, Thailand
INSTITUTIONS ATTENDED	Prince of Songkla University, 1991-1995: Bachelor of Science (Chemistry) Mahidol University, 1996-1998: Master of Science (Physical Chemistry) Mahidol University, (2000-2004) Doctor of Philosophy (Polymer Science and Technology) Université du Maine, (2002-2004) Docteur de l'Université du Maine (Physique-Science des Matériaux)
RESEARCH GRANTS	Commission University Development Scholarship (1996-1998) Commission University Development Scholarship (2000-2004) Institute of Science and Technology for Research and Development, Mahidol University Université du Maine au Mans (Relations Internationales)

